
# Mobile Cellular Communications with Base Station Antenna Arrays: Spectrum Efficiency, Algorithms and Propagation Models

**Per Zetterberg**

TRITA–S3–SB–9712
ISSN 1103–8039
ISRN KTH/SB/R - - 97/12 - - SE

Signal Processing
Department of Signals, Sensors and Systems
Royal Institute of Technology
Stockholm, Sweden

*Submitted to the School of Electrical Engineering, Royal Institute of Technology, in partial fulfillment of the requirements for the degree of Doctor of Philosophy.*

# Abstract

This thesis deals with the problem of increasing the spectrum efficiency of cellular systems, by the use of antenna array base stations. The focus of the thesis is on downlink transmission in frequency division duplex systems, i.e., systems with different up and downlink carrier frequency. In a short summary the thesis:

- Proposes five reasonable propagation models.
- Uses these models to design and analyze three different beamformers: The maximum desired power (MDP), the summed interference to carrier ratio minimizing (SCIR) and the generalized-SCIR beamformer.
- Introduces three capacity enhancement approaches: same sector frequency reuse (SSFR), reduced cluster size without nulling (RCS-WON) and reduced cluster size with nulling (RCS-WIN).
- Proposes channel allocation, power control, and beamforming algorithms for these approaches.
- Estimates the "outage probability" (probability of insufficient quality), for SICR-SSFR, SICR-RCS-WON and SICR-RCS-WIN, using simulations as well as analytical analysis, as a function of critical parameters.
- Investigates the capacity enhancement achieved with the base station antenna array as a function of angular spreading and the number of antennas for SICR-SSFR, SICR-RCS-WON and SICR-RCS-WIN.
- Partially verifies the system simulation assumptions using real data.

- Combines simulation and experimental results to make likely that three to tenfold capacity enhancement is realistic using $3 - 18$ antenna elements per 120-degree sector (in comparison with a system employing a single antenna per sector). The higher capacity enhancements are obtained using the more complex approaches.
- Makes a detailed proposal of a simple and robust downlink beamforming algorithm for realizing RCS-WON in GSM (the MDP beamformer) .
- Simulates this beamformer under realistic network conditions, using simulated as well as real data.

# Acknowledgment

I would like to thank my supervisor Professor Björn Ottersten, for assigning me to a very interesting and successful project : "spatial diversity in communications" and for introducing me into the field of statistical signal processing. The concept of enhancing cellular systems by the use of antenna arrays (i.e., spatial diversity) has received increasing interest, in both academia and industry, during the course of the project and it is my hope that it will continue to do so.

During the academic year 95/96 I was lucky to be a visiting researcher at the Center for PersonKommunikation (CPK) at Aalborg University which is headed by Professor Jørgen Bach Andersen. At the CPK I collaborated with the TSUNAMI(II) [1] group led by Dr. Preben Mogensen. I have been allowed to use the data, recorded using the smart antenna testbed developed by Dr Mogensen's group in this thesis. The measurement data give the thesis considerably more strength than it would have without it. Thus, I am greatly indebted to the people who built the testbed and carried out the measurements : Preben Mogensen, Frank Frederiksen, Kim Olesen, Sten Leth-Larsen, Henrik Dam, and others.

I would also like to thank NUTEK[2] and HCM[3] for their financial support, which has made this thesis possible.

During my entire time as a PhD student I have always had terrific colleges with whom I have been able to discuss research as well as all other possible issues. My colleagues have also become my friends, and we have had great fun on numerous occasions.

[1] TSUNAMI(II) stands for technology in smart antennas for universal advanced mobile infrastructure - part 2, and is a project sponsored through the European Commissions ACTS program.

[2] Närings och teknikutvecklingsverket (the National Board for Industrial and Technical Development)

[3] The European Commissions Human Capital and Mobility program

I am grateful for the support and confidence that my parents and my sister have given me.

Finally, I would also like to express my love for my fiance Linda, and my dear son Samuel who has been with us for the last eight weeks. Linda has been understandingly patient with my absent mindness and my “innovative” working schedule.

# Contents

# Chapter 1

# Introduction

## 1.1 Background

Since the early eighties a rapidly growing market for car mounted and hand held portable radio telephones[1] has evolved in the industrial countries. To support the mobile stations, networks of *base stations* have been built by several *operators*. The base stations consist of radio receivers and transmitters plus an interface to the fixed telephone infrastructure. A *network* of base stations is needed, not only to provide sufficient coverage, but also to enable reuse of the radio spectrum. The users able to access a certain base station are usually found within a radius of 0.1km to 10km from the base. Such a region is referred to as a cell. The number of users in the cell is limited by the spectrum. A number of protocols specifying the management of the spectrum (air interface) have been set up by different standardization committees. An example of such a protocol is the advanced mobile phone service (AMPS) [You79]. In the AMPS system each user needs 30kHz of spectrum. If the operator is licensing for example 6.3MHz of spectrum, then the maximum number of voice users are 210 per cell. However, since the spectrum can't be reused in adjacent cells, because of interference[2], the capacity in a cell is far less. Actually, the signal to interference ratio needed in AMPS is such that a channel can only be used in one out of 7 cells. Thus, in our example the operator is only able to provide 30 simultaneous calls per cell. The quo-

[1] from now on referred to as user terminals, mobile stations or mobiles

[2] disturbances from other cells

tient between the number of calls that can be supported by the system divided by the available bandwidth is known as the "spectrum efficiency". Since the number of mobile subscribers are increasing and the spectrum available is relatively limited, various solutions for increased spectrum efficiency are being pursued. One such solution is the introduction of the digital transmission format. With digital signaling the speech is encoded into a series of ones and zeros (bits) prior to transmission. The received bit stream is then decoded and the speech is reproduced. As opposed to analogue signaling, where the speech signal is used to modulate the carrier in a more direct fashion. Through the use of digital encoding, the bandwidth per user can be decreased and spectrum efficiency is thus increased. Other enhancement techniques are hierarchical cell structures, dynamic channel allocation, power control, and antenna array base stations. By hierarchical cell structures is meant that the area is covered by several layers of cells. The small cells provide high capacity for "hot-spots" such as malls, airports, and business centers, while the large overlaying macro-cells provide coverage and support vehicular users. Dynamic channel allocation and power control aim at distributing the spectrum and transmission power such that the interference is minimized, thereby allowing a more efficient spectrum utilization. Antenna array base stations decrease interference by electronically steering their antenna patterns so as to minimize interference, on reception as well as transmission. Antenna arrays can be implemented also at the mobile, [Vau87], however that approach has received less attention.

First generation mobile communication systems[3] are based on analogue transmission techniques, while the second generation[4] are digital. The capacity of the digital systems is about three times that of the analogue. A third generation of systems is now emerging in North America, Europe, and Japan [Cal96, Oja96, Sas96]. These systems will have higher and more flexible user data rates than the second generation, in order to better support applications such as wireless-Internet, video, and wireline quality audio. The third generation is also envisaged to be highly adapted to the aforementioned spectrum efficiency enhancement techniques.

[3] AMPS, TACS, ETACS, NMT450, NMT900, see [NMT85, Ste92, You79]

[4] DECT, PCS2000, PHS, CT2, GSM, DCS1800, PCS1900, IS54, IS136, IS95, ANSI J-STD-008, see [NM96, Hoy95, Mat95, Ste92, Tie95]

## 1.2 Thesis Topics

This thesis deals with the topic of increasing the spectrum efficiency of macro-cells[5], by the use of antenna array base stations. The focus of the thesis is on downlink[6] transmission in FDD[7] systems.

It should be noted that in comparison with the uplink problem, where a large body of work is available see e.g., [AMVW91, BS92, LP95, NEA95, ORK89, SW94, TVP94, Win84], the downlink has received relatively little attention. Transmission with antenna arrays in FDD systems is a difficult task since the knowledge at the base station, regarding the downlink channel is very limited [8], see Section 2.5. At best, the spatial distribution of power can be estimated from the uplink signals. This implies that knowledge about the distribution of the downlink channels may be available, but not the exact channel realizations. In contrast, such information can be obtained in the uplink by employing a priori information about the transmitted waveforms. For this reason the downlink performance may be anticipated to be the capacity bottleneck in interference limited systems, with base antenna arrays. This conjecture finds support in the results of the paper [Ohg94], where the downlink performance is found to be much worse than the uplink, under the assumption of a two-path model.

In TDD[9] based systems, the up- and downlink channels may be assumed to be the same, if the mobile speed is low and the receive and transmit amplifiers are appropriately calibrated. Thus, in such systems, the capacity enhancement in up- and downlink is similar, see [WMFN95]. A relevant question at this point is why downlink transmission in FDD systems is considered when the situation is much more favorable in TDD?

[5] In this thesis, a macro-cells is defined as a cell with a radius of more than one kilometer with base antenna heights significantly higher than the surrounding buildings.

[6] Transmission from base to mobile.

[7] FDD=Frequency Division Duplex. This means that the downlink transmission is performed on a different carrier frequency than the uplink.

[8] An exception to this rule may occur if mobile to base feedback is employed [Ger95]. However, the feedback rates needed seem to make this approach impractical at higher mobile speeds [Ger95]. For example, at a 25mph mobile speed, an uplink feedback rate of 13kbit/s is estimated in [Ger95] assuming a flat fading downlink channel. In addition to this a downlink overhead for transmission of probing signals is also required. Furthermore, no current or conceived cellular standard known to the author, supports this concept.

[9] In time division duplex (TDD) the uplink and downlink connections share the same carrier frequency by multiplexing the two directions in time.

One of the answers to this question is that there are a large number of operational FDD systems in the world, and there may be a need to increase the capacity of these systems. Another reason is that TDD suffers when largepropagation delays arise. In addition, TDD typically requires synchronization of the TDMA-frames of the base stations (even different operators may be required to synchronize together). Furthermore, FDD is the dominating duplex technology in first and second generation cellular and a strong candidate in third generation [Cal96, Oja96, Sas96]. Dual mode terminals supporting both duplex methods are also beginning to appear. The TDD mode is typically used when accessing small cells, while the FDD mode is used when accessing the macro-cell base stations. Thus FDD plays, and will continue to play, an important role in the cellular industry today and in the future. Therefore it is important to find out how and how much the downlink capacity of FDD systems can be increased by employing base station antenna arrays. In order to answer the question as to how much the capacity can be enhanced, it is natural to first address the issue of how the capacity should be increased. In order to do this a mathematical relation between the signals transmitted and the signals received is needed. When this relation is at hand, algorithms which improves the signal quality can be derived. The next step is to trade the quality enhancement for a capacity enhancement. This is done by employing a more aggressive spectrum allocation, by the use of a frequency reuse strategy. Thus, the main topics of the thesis are

- propagation modeling i.e., finding a mathematical relation between the signals transmitted and the signals received,
- beamforming, i.e., how the transmitted signals should be distributed over the antenna elements of the array in order to maximize performance,
- channel allocation, i.e., how to distribute the available spectrum among the mobiles in order to maximize the performance gain of the antenna array,
- capacity estimation, i.e., estimating the achieved spectrum efficiency as a function of the number of antennas employed in the arrays, and other critical parameters.

The following section describes some of the publications made by other researchers regarding these issues. The relationship between the

research presented in this thesis to the references cited is explained in the introduction to each chapter.

## 1.3 Review of the Literature

This section reviews some of the contributions made by other researchers in the field.

### 1.3.1 Channel Modeling

Channel modeling for base station antenna array systems are treated in [AFWP86, Ake91, Ebi91, Egg95a, Egg95b, Egg96, FJK+94, JLXV95, KMT+96, LR96, Mar96, MPLE+97, NEA95, SW94, TO96]. All the papers cited assume that signals received at the base can be described by a superposition of a number of rays. In [AFWP86, Ake91, Ebi91, FJK+94, TO96] a Gaussian azimuthal power distribution (as seen from the base), with mean $\theta$ and standard deviation $\sigma$, is assumed. The parameter $\sigma$ is often referred to as the "angular spread". The number of rays is assumed to be large enough for the central limit theorem to apply, and the the complex signal strength in the antenna elements (sometimes called the spatial signature or effective steering vector) is thus Gaussian distributed. This assumption is consistent with the classical Rayleigh fading model [Lee93]. The cross correlation between the signal strength in two antenna elements is obtained from $\theta$, $\sigma$, and the distance between the elements. In [AFWP86, Ake91, FJK+94, YKT91] the correlation versus antenna element separation curves is obtained from measurements and compared with those predicted using the propagation model, for various values $\sigma$. This curve fitting serves to give an indication of the validity of the model as well as an estimate of $\sigma$. In the measurement results of the cited articles, obtained in an urban and suburban environments at $1-2$km mobile to base distances and elevated base stations, the $\sigma$ parameter is estimated to be $1^o - 6^o$. Generally, the measured correlation lies below the fitted curve for small antenna separations, and above for large separations. In the paper [MPLE+97] the correlation between $\sigma$ and the shadow fading (the latter in logarithmic scale) is investigated. The correlation coefficient is found to be $-0.56$. This means that if a mobile is received with high power, the angular spread, $\sigma$, is small.

The paper [SW94] proposes a model with several clusters of scatterers where each cluster has a uniform azimuthal power distribution with

a certain width, as seen from the base. Associated with each cluster is also a time delay. A similar development is made in [Mar96]. However, in [Mar96] the width of the clusters is zero as seen from the base. In [Mar96] the power of the clusters is also Rician rather than Rayleigh distributed. The parameters of the model are estimated from data measured from a "typical macro-cell scenario" in [Mar96]. The number of clusters is estimated to be twelve, and the angles of these clusters are widely separated.

In [Egg95a] and [KMT$^+$96] the spatial distribution of power is estimated by measuring the power received using a rotating highly directional base antenna. As shown in [Egg95a], the obtained power versus angle profile is given by the circular cross-correlation function between the antenna pattern of the rotating antenna, and the power versus angle distribution of the environment. In [Egg95a] an increased sidelobe level, as compared with free-space, is reported. In free-space and rural environments the sidelobe level is estimated to be 20dB below the main lobe, whereas it increases up to around 5dB in some urban areas (at a 50 to 1000 meter range). In [KMT$^+$96] the conclusion is that : "in a lot of cases, even in many cases in urban area, the principal portion of the energy is concentrated in a single rather small interval of delay times $\tau$, and in a single rather small interval of angles of arrivals." In [Egg95b] and [Egg96] efforts are made to find well defined quantitative measures describing the spatial characteristics of propagation environments, and making analogies between the time domain entities delay spread and bandwidth and the corresponding spatial domain entities angular spreading and angular bandwidth (the latter is basically 1/beamwidth).

The propagation models described so far are based on measurements and hypotheses. In [LR96] and [NEA95] propagation models based on physical arguments were developed. In [LR96] a single-bounce model is described where the underlying assumptions are that the radiowaves propagate via a direct wave and $L$ specular reflections. The positions of the reflectors are uniformly distributed in space. The path-loss of the direct and reflected waves obeys a $\tau^{-\gamma}$ law where $\tau$ is the delay of the ray, and $\gamma$ is the path-loss exponent. If the base and mobile antenna heights are low relative to the base-mobile distance a fourth order propagation loss $\gamma = 4$ is assumed. If not, the free-space value $\gamma = 2$ is used. In [NEA95] a similar model was proposed. However, in this case, no line of sight component exist,and the path loss-law for the scatters are given by $r_1^{-\gamma_1} r_2^{-\gamma_2}$ where $r_1$ and $r_2$ are the distance to the scatterer from the base and mobile, respectively.

In [JLXV95], the variation of the spatial signature (i.e., the vector of complex signal strength) as a function of time, environmental changes, mobile movement and frequency, is investigated. In contrast to all other papers cited, [JLXV95] does not utilize any a priori assumptions on the propagation characteristics. One of the conclusions in [JLXV95] is that the spatial signature changes drastically if the frequency is changed 5MHz. The measurement environment in [JLXV95] does not appear to be representative of any real cellular environment, though.

### 1.3.2 Downlink Beamforming

The papers [CTK94, FN95, FG97, GP94, GP96, Ger95, GF96, MW96, Ohg94, RDJP95, Win94] consider multiple-antenna downlink transmission techniques for FDD systems. In all the papers cited, except [MW96, Win94], and [FG97], the vector of signals transmitted from the base to a certain user is given by a complex vector of *weights*, multiplied by the (scalar) modulated baseband waveform carrying the bit stream of the desired user. In some cases, transmission is performed to several users on the same channel. In that case the antenna signals are given by the superposition of the signals transmitted to the several users. In the papers [FN95, GP96, Ger95, GF96, RDJP95], techniques are proposed where the weights are functions of the channel correlation matrices for the desired and co-channel users at the up- or downlink frequencies. The channel correlation matrix is defined as the correlation matrix of the effective steering vector.[10] In practice, this matrix changes with time, and therefore the weights need to be updated, see Chapter 2.

In [GP96] and [Ger95] single cell scenarios with multiple co-channel users are considered. For that scenario, two algorithms which jointly optimize the weight vectors for all the users are derived. The obtained solutions are shown to maximize the minimum (mean) signal to interference ratio among the users in all the special cases considered. It is proposed in [GP96, Ger95] that the mobile estimates the downlink channel by exploiting probing signals transmitted from the base, and feeds the channel correlation matrix back to the base. Thus the channel correlation matrix will be estimated at the transmit frequency.

The paper [FN95] also treats a single cell scenario. However, in contrast to [GP96, Ger95], a known level of noise is present in each mobile receiver. A solution where the weights are chosen to minimize the total

[10] In this thesis, this matrix is frequently referred to as the multipath covariance matrix.

transmitted power, subject to a constraint on the signal to interference and noise at each receiver, is proposed. The criterion function is maximized using the Augmented-Lagrange-Algorithm or the SQP-Method [Ber82, Pow78]. This method is initialized using a less computationally complex method, "interference minimization algorithm with linear improvement". It is assumed in [FN95] that the propagation can be described by a discrete number of rays, and that the direction of arrival, and (mean) power of these rays are estimated from the uplink. With this information at hand, the channel correlation matrix at the downlink frequency can be estimated[11].

In [RDJP95] a multiple cell system, is considered. The transmit weights are chosen so as to (essentially) maximize the (mean) energy at the desired mobile divided by the sum of the interference received at all co-channel mobiles, subject to constraints on the total interference and the transmit power. Two "feasibility checks" are also employed, in order to certify that the transmit power, and the power received at the desired mobile, exceed a certain level. If either of the feasibility conditions is not fulfilled, the considered mobile is moved to another channel. The input to the weight calculation, is the channel correlation matrix for the desired mobile, and the sum of the correlation matrices for the co-channel mobiles. It is proposed in [RDJP95] that these entities are estimated at the uplink frequency from the received data. In particular, the sum of the channel correlation matrices for the co-channel mobiles is estimated directly from the data in a simple fashion. No correction, to compensate for the frequency difference between up- and downlink, is made in [RDJP95]. It is argued that this does not lead to any error if different arrays with the same "manifold," are used for up- and downlink, an approach referred to as "the matched array approach." If the same array is used for up- and downlink, the frequency difference does lead to performance degradation. The magnitude of the degradation is investigated through simulation in [RDJP95].

In [GF96], the weighting vectors maximize the (mean) energy at the desired mobile, divided by the sum of the interference received at all co-channel mobiles. The constraint employed is that unit power is delivered to the desired mobile. It is proposed that the channel correlation matrices for the desired and interfering mobiles are estimated in uplink. A truncated Fourier series approximation of the underlying spatial density of power, is fitted to the estimated covariance matrices. Thereby obtaining

[11] The results of [FN95] are formulated in terms of a square root factorization of the channel correlation matrix.

a power versus angle density estimate, which is used to form an estimate of the channel correlation matrix at the transmit frequency.

In the paper [Ohg94], a reference signal, e.g., a training sequence, is used to form a conventional least squares combining vector, $\mathbf{w} = \mathbf{R}^{-1}\mathbf{r}$, for uplink combining. The *same* vector is then normalized to unit norm, and then used for downlink transmission. The paper [Ohg94] assumes independent fast fading in the up- and downlink, as is the case in existing FDD systems, see Section 2.5. However, the analysis ignores any change in antenna pattern due to the frequency difference. The paper [CTK94], proposes a method which reduces this change.

In [Win94] and [MW96] a technique is proposed where time delayed versions of the information signal are transmitted over the antenna elements of the array. If the antenna spacings and time delays are sufficiently large to produce independent fading and uncorrelated antenna signals, the deep fades in signal strength are reduced. Assuming ideal channel estimation and maximum likelihood sequence estimation at the mobile, the performance enhancement over transmission with a single element is significant [Win94]. However, the simulations made in [MW96] using the GSM standard with frequency hopping, have shown that performance enhancement reduces to $\approx 0.5$dB in signal to interference ratio.

In [FG97] a technique is outlined where the bit stream to be transmitted from the base is divided into $m$ sub streams, which are transmitted over the $m$ antenna elements of the array. The mobile is equipped with $\geq m$ antennas and receives sub stream #1 by pointing nulls towards the $m-1$ other antenna elements. When sub stream #1 has been received and decoded it is subtracted from the received data batch. Thus when sub stream #2 is received, it is sufficient to point nulls towards $m-2$ antenna elements. The technique has mainly two drawbacks: the number of antennas at the mobile has to equal or exceed the number at the base and it fails to work if the mobile is a point source as seen from the base (unless the base has extremely large antenna spacing).

Finally, we mention the work in [GP94] and [Ger95] where it is proposed that the mobile estimates the downlink channel and feeds it back to the base. This enables the base to have instantaneous downlink channel information, and therefore achieve significant suppression of the emitted interference. It is estimated in [Ger95] that an uplink feedback rate of 13kbit/s is required, assuming a flat fading downlink and a 25mph mobile speed. In addition to this a downlink overhead for transmission of probing signals is also required. This seems to make the method impractical for vehicular users. In addition, no current or conceived cellular standard

known to the author, supports the concept.

### 1.3.3 Channel Allocation and Capacity Analysis

The channel allocation and capacity of cellular systems with base station antenna arrays are treated in [FN96, Ohg94, RDJP95, SBEM90, Tan94, Tan95]. The papers [Ohg94, RDJP95, SBEM90] assume that capacity is increased by reducing the frequency reuse cluster [12] while the papers [FN96, Tan94, Tan95] assume reuse of spectrum already allocated to cell by multiplexing users spatially.

In [SBEM90] the analysis assumes that the base can form ideal sector beams in uplink and downlink. The results indicate a capacity improvement of seven with $\approx 20^o$ beams and four with $\approx 45^o$ beams, over a system with omni directional antennas.

In [Ohg94] the capacity of a cellular system employing circular base station antenna arrays, and random channel allocation, is analyzed. The receive and transmission techniques are described in the previous section. Both one-ray and two-ray propagation models are employed. The long and short term fading in the two rays of the two-ray model are assumed independent. This implies a very small level of angular dispersion. The results in [Ohg94] indicate a sixteen-fold capacity enhancement over an omni-system using sixteen antenna elements.

In [RDJP95] eight element circular arrays are employed at the bases. The transmit method of [RDJP95] is described in the previous section. As mentioned in this description, two feasibility conditions must hold before a mobile is allocated to a certain channel. The simulation results in [RDJP95] indicate three to sixfold capacity enhancement over an omni-directional system. The propagation conditions of [RDJP95] assume a uniform distribution of energy within an angular scan of less than or equal to 30 degrees. Thirty to fifty percent of the mobiles attempting to call are not given any connection in the simulations of [RDJP95]. However, the simulation considers only one channel, and therefore this fraction may be anticipated to decrease when more channels are added to the system.

In [FG97] the Shannon capacity achieved with $m$ base and $m$ receive antennas, without knowledge of the channel at the base, is addressed. For the proposed technique, which is described in previous section, the

[12] i.e, effectively using a larger fraction of the total available spectrum allocated per cell

capacity is shown to be $\mathrm{OC}(1) + \ldots + \mathrm{OC}(m)$ where $\mathrm{OC}(k)$ is the Shannon capacity on a Rayleigh fading channel using a single transmitter, no interference and maximum ratio combining with $k$ antennas at the receiver. A scenario with a single base and a single mobile is considered and Rayleigh fading in all $m^2$ channels are assumed uncorrelated.

In [Tan94] the problem of allocating multiple users on the same channel within the same cell, such that the co-cell co-channel users are sufficiently separated in angle, is considered. An expression for the blocking probability (probability of call attempt denied) as a function of the traffic distribution in the cell, and the minimum required angular distance between co-channel users, is derived, using conventional traffic theory. As an example, it is shown that if all traffic is concentrated along a linear road going through the cell, the mean number of allocated calls is in the range of 4 through 12 (Erlang) using 8 channels, a minimum angle of 45 degrees between co-channel mobiles, and a blocking probability of 1%. The exact number in the range $4 - 12$ depends on how the road crosses the cell. As a reference, the mean number of users in a cell equipped with an omni-directional antenna, is 4 in the considered example. Thus the "spatial multiplex gain" is $0 - 200\%$.

Due to the nature of radio propagation in urban environments, the ratio of the power of the strongest user to the weakest user, in the same cell, may be in the order of 100dB. This makes is it reasonable not to allocate the weakest and strongest mobile on the same channel, since uplink reception of the weaker mobile would require extremely accurate mobiles, base station receive amplifiers, and A/D converters. In order to avoid this problem it is proposed in [Tan95] to group the mobiles into power classes. A power class is defined by a maximum and a minimum power level. The levels can be static or dynamic. Mobiles from different power classes are not allocated to the same channel. The reduction of the carried traffic due to the grouping is estimated to be around 20%.

In [FN96] five channel allocation algorithms for the downlink beamforming technique of [FN95] (described in previous section), are proposed and compared. The objective is to group several mobiles on the same channel within the same cell, such that the total power employed is minimized and a given signal to interference ratio obtained. The propagation model employed is general. All five channel allocation algorithms proposed work by successively allocating more users onto the available channels, without any re-allocations. A new mobile is allocated to the channel with the smallest "separability" index. Five such indices are proposed yielding five different channel allocation algorithms. Index number

one is defined as the increase in total transmit power needed, if the new user is allocated to the considered channel. In order to calculate this index it is necessary to calculate the transmit vectors for the new user and re-calculate it for the users already allocated to the channel, assuming that the new user is allocated to the considered channel. This is computationally complex. Since index number one is closely related to the employed performance criterion, it is regarded as the optimal solution. Of the other four computationally less expensive solutions, number five has almost the same performance as number one. Using eight channels and an eight element base station, the simulation results indicate a spatial multiplex gain of 2 to 3. The propagation model employed has high angular dispersion.

## 1.4 Contributions and Thesis Outline

As mentioned in Section 1.2 this thesis deals with propagation modeling, beamforming, channel allocation and capacity estimation for cellular systems employing base station antenna arrays. The focus is on downlink (i.e., the base to mobile link) in FDD (frequency division duplex) systems. In a short summary, the thesis :

- Proposes five reasonable propagation models.
- Uses these models to design and analyze three different beamformers: The maximum desired power (MDP), the summed interference to carrier ratio minimizing (SICR) and the generalized-SICR beamformer.
- Introduces three capacity enhancement approaches: same sector frequency reuse (SSFR), reduced cluster size without nulling (RCS-WON) and reduced cluster size with nulling (RCS-WIN).
- Proposes channel allocation, power control, and beamforming algorithms for these approaches.
- Estimates the "outage probability" ( probability of insufficient quality), for SICR-SSFR, SICR-RCS-WON and SICR-RCS-WIN, using simulations as well as analytical analysis, as a function of critical parameters.

- Investigates the capacity enhancement achieved with the base station antenna array as a function of angular spreading and the number of antennas for SICR-SSFR, SICR-RCS-WON and SICR-RCS-WIN.
- Partially verifies the system simulation assumptions using real data.
- Combines simulation and experimental results to make likely that three to tenfold capacity enhancement is realistic using around $5-18$ antenna elements per 120-degree sector (in comparison with a system employing a single antenna per sector). The higher capacity enhancements are obtained using the more complex approaches.
- Makes a detailed proposal of a simple and robust downlink beamforming algorithm for realizing RCS-WON in GSM (the MDP beamformer).
- Simulates this beamformer under realistic network conditions, using simulated as well as real data.

The content of each chapter is described in more detail below. The descriptions also contain recommendations on what sections that should be read before the chapter in question. The reader is recommended to read through the sections below in order to find chapters and sections of particular interest to him or her.

## Chapter 2: Propagation Modeling

In this chapter five propagation models are derived: Gaussian Wide Sense Stationary Uncorrelated Scattering (GWSSUS), Gaussian Angle of Arrival (GAA), Gaussian Angle of Arrival One Cluster (GAAO), Typical Urban (TU) and Bad Urban (BU). The GWSSUS model is a generalization of the well-known wideband statistical multipath model [PB82, Pro89] to the multiple antenna case. This generalization does not impose any restrictions on the spatial distribution of power. The GAA model, which is a special case of the GWSSUS model, does however impose such restrictions.

A special case of the GAA model referred to as GAAO is developed further in Section 2.3.1. The GAAO model assumes that all energy received at the base from a certain mobile is Gaussian distributed in azimuth, with a certain (optionally distance dependent) angular spreading

$\sigma$. The results of Chapter 7 indicate that such a model yields realistic performance predictions using $\sigma = 3^o$ to $6^o$.

When analyzing GSM systems, a frequently adopted model for the temporal-domain power distribution is the typical urban (TU) model defined in [GSM92], which is frequently employed when making GSM radio-link simulations. In this thesis we introduce a propagation model which has (almost) the same temporal domain properties as this model (exponentially decaying with an rms-delay spread of $\approx 1\mu$s), and similar spatial domain properties as the GAAO model. The TU model shows that an exponential decaying power delay profile is consistent with a single cluster of scatterers with a azimuthal power distribution similar to the GAAO model. Another similar model is also introduced: bad urban (BU).

Part of the material in this chapter has previously been published in the report [MZD+96], and the conference articles [ZE96, ZEM96, ZDF+96].

## Chapter 3: Techniques for Downlink Capacity Enhancement of FDD Systems

In this chapter, three capacity enhancement approaches for use with adaptive arrays are introduced: same sector frequency reuse (SSFR), reduced cluster size without nulling (RCS-WON), and reduced cluster size with nulling (RCS-WIN). In the SSFR approach, several mobiles are allocated to the same channel within the same 120-degree sector, while in the RCS approach, a larger fraction of the total spectral resources are allocated to each cell. In some cases a combination of the two approaches is applied. However, we define all approaches with more than one mobile within the same sector as SSFR. Both RCS and SSFR lead to increased interference levels which have to be compensated for using adaptive antenna patterns.

The two variants of RCS distinguish weather nulls are steered in the direction of strong users in adjacent cells or not. The term "nulling" is to be broadly interpreted, and denotes that the antenna pattern is synthesized in order to have a low gain in the direction of a certain mobile, but not necessarily zero gain. A beamformer called SICR is derived from the GAAO model introduced in Section 2.3.1. The chapter also describes how this beamformer is applied in the three cases RCS-WIN, RCS-WON and SSFR. Channel allocation and uplink power control algorithms to take care of the inter-cell cross-talk and dynamic range problems for

the three systems, are proposed. The resulting systems are referred to as SICR-RCS-WIN, SICR-RCS-WON and SICR-SSFR. How the SICR-beamformer should be applied in practice is treated in Chapter 7. *A prerequisite for reading this chapter is Section 2.3.1.*

The chapter is partially based on work published in the journal article [ZO95], on the submitted article [Zet95a], and the conference articles [Zet95b] and [Zet97].

## Chapter 4: Capacity Results

In this chapter, the previously introduced systems SICR-RCS-WIN, SICR-RCS-WON and SICR-SSFR are simulated and analyzed in order to find their capacity enhancement potential, as a function of critical parameters such as the number of antennas, the mobile power control range, and the angular spreading, $\sigma$, of the environment.

Closed form expressions for the "outage probability", i.e., the probability of insufficient transmission quality is also derived and found to agree well with simulation results under certain conditions. The main findings of the chapter are

- A large *uplink* power control range is necessary to make the *downlink* inter-cell nulling feature of the SICR-RCS-WIN system effective.
- The uplink near-far ratio, defined as the ratio of the power of the strongest user to the weakest desired user (averaged over fast fading), allocated to the same timeslot (but sometimes different carrier), is typically less than 25dB, for all investigated systems. For the SICR-RCS system with $e = 1$ and fast handover, it is typically less than 4dB.
- The SICR-SSFR system requires around 16 channels (per power group and sector) in order to be able to allocate channels with spatially well separated users.
- The SICR-SSFR system increases capacity more than SICR-RCS-WIN and SICR-RCS-WON systems in most of the investigated cases.
- The capacity enhancement achieved using SICR-RCS-WIN is larger than or equal to that obtained using SICR-RCS-WON.

- The experimental results of Chapter 7 suggest that $\sigma_0 = 3^o$ to $6^o$, $r_0 = \infty$ (the framework is introduced in Section 2.3.1) is a realistic model. Combining this information with the results of Chapter 4, yields the following capacity predictions in the more optimistic case $\sigma_0 = 3^o$: Threefold capacity enhancement is achieved using the SICR-RCS-WIN and SICR-RCS-WON systems with three and five antenna elements per 120-degree sector, respectively (in comparison with a reference system employing a single element per 120-degree sector). Four and tenfold capacity enhancement is achieved with SICR-SSFR using five and eighteen antenna elements respectively. Using SICR-RCS-WIN or SICR-SSFR, eight antenna elements per sector, and an improved handover, a ninefold capacity enhancement is obtained. However, it is unclear how much of the ninefold capacity enhancement should be attributed to the improved handover in this case.

- The derived analytical expression for the outage probability agrees well with simulation results in the SICR-SSFR case if sixteen (or more) channels per group are employed, in the SICR-RCS-WIN case if $e = 1$ is employed, and in the SICR-RCS-WON case if slow handover is assumed.

*Prerequisites for reading this chapter are Section 2.3.1 and Chapter 3.* The chapter is partially based on work published in the journal article [ZO95], on the submitted article [Zet95a], and the conference articles [Zet95b] and [Zet97].

## Chapter 5: The Generalized SICR Beamformer

In Chapters 3 and 4, the SICR-beamformer is applied to calculate the transmit weights. This beamformer is based on the assumption that the energy received from each mobile is Gaussian distributed in azimuth (as seen from the base), and that the mean direction and angular spreading of this distribution are known (without any estimation error) for the desired and the identified interfering users (the GAAO model). The generalized-beamformer introduced in this section, relaxes the propagation assumption and treats general GWSSUS channels. The obtained algorithm is applied to real data in Chapter 7. The results therein indicate that the algorithm is able to reduce the interference level by 11.9dB using an eight antenna linear array for 120-degree coverage (as compared

to using a single antenna element per sector). *Prerequisites for reading this chapter are Sections 2.1-2.3.1 and 3.2.1*

The main ideas behind the generalized SICR beamformer is published in the conference paper [Zet97].

## Chapter 6: A Downlink Beam Steering Algorithm for GSM

In this chapter a simple beamforming algorithm for implementation of the RCS-WON approach[13] in GSM is proposed. Consideration of approaches without nulling is motivated by their less demanding requirements on channel allocation, power control, synchronization, and hardware. Furthermore, approaches without nulling are generally very robust with respect to angular dispersion and calibration errors.

It is argued in the chapter that almost the same performance is obtained by transmission with a single beam i.e., $\mathbf{w} = \text{constant} \times \mathbf{a}(\theta_0)$, as with the vector obtained from the complex generalized-SICR beamformer of Chapter 5 (in the case without nulling). A simple algorithm which estimates $\theta_0$ in the case of a GSM system is derived and simulated. The simulation results indicate that the proposed technique generates at most 0.9dB more interference than the generalized-SICR algorithm, under some assumptions. In the case of frequency hopping, this result is obtained even at a $-8$dB uplink signal to interference ratio. Simulation results using the TU and BU model, as well as using the data collected in downtown Aalborg (Section 7.1), indicate that the algorithm is capable of reducing the downlink interference level approximately $6-8$dB in urban environments using linear arrays of eight antenna elements per sector (as compared to using a single antenna element per sector). *Prerequisites for reading this chapter are Sections 2.1-2.3.1 and Chapter 5.*

Parts of the material in this chapter have previously been published in the report [MZD+96], and the conference articles [ZE96, ZEM96, ZDF+96]. The GSM algorithm described will be employed in a large DCS1800 field-trial conducted by the partners of TSUNAMI(II) [14].

[13] i.e., capacity enhancement by means of increasing the fraction of the total spectra used in a cell without employing co-channel nulling, see above

[14] TSUNAMI(II) is one of the projects of the EU commission ACTS program. The TSUNAMI(II) consortium consists of Motorola ECID, Orange PCS, Robert Bosch, France Telecom CNET, DETyCOM, University of Bristol, University of Aalborg, Orange PCS and University of Polytechnic of Catalunya

### Chapter 7: Experimental Performance Results

The nulling performance of the SICR and generalized-SICR beamformers, are estimated by applying them to data measured in a macro-cellular environment. The parameters needed in the SICR beamformer are estimated using the least-squares algorithm introduced in [TO96], while the input matrices needed in the generalized-SICR algorithm are estimated directly from the data. It is concluded that the angular dispersion is basically independent of the base-mobile distance in the available data. The performance of the SICR and generalized-SICR beamformer is estimated from the measurement data and compared with that obtained from the GAAO model introduced in Section 2.3.1. It is found that the average performance of the SICR and generalized SICR beamformers is close that obtained on the GAAO model using $\sigma = 6^o$, $r_0 = \infty$ and $\sigma = 3^o$, $r_0 = \infty$ respectively . From this result, the conclusion is drawn, that $\sigma_0 = 3^o$ to $6^o$ is a good first assumption for predicting the performance of downlink beamforming approaches involving nulling. However, further investigations are needed to evaluate the system impact of the deviation between the actual and predicted performance in particular situations. *Prerequisites for reading this chapter are Sections 2.1-2.3.1, 3.2.1 and Chapter 5.*

The results of the chapter are previously unpublished.

## 1.5 Mathematical Notation

The table lists some of the notational conventions used in the thesis. The naming of signals, variables and parameters, are introduced successively in the text.

| Notation | Description |
|---|---|
| $\mathbf{Y}^c$ | Complex conjugate of the matrix $\mathbf{Y}$ |
| $\mathbf{Y}^T$ | Transpose of the matrix $\mathbf{Y}$ |
| $\mathbf{Y}^*$ | Complex conjugate transpose of the matrix $\mathbf{Y}$ |
| Trace $\{\mathbf{Y}\}$ | The sum of the diagonal elements of $\mathbf{Y}$ |
| $[\mathbf{Y}]_{k,l}$ | Element $k, l$ of the matrix $\mathbf{Y}$ |
| $[y]_k$ | Element $k$ of the vector $\mathbf{y}$ |
| $\text{diag}(\mathbf{y})$ | Diagonal matrix which has the vector $\mathbf{y}$ as its diagonal components |
| $\|\mathbf{y}\|$ | The norm of the vector $\mathbf{y}$: $= \sqrt{\sum_{k=1}^{m} \|[y]_k\|^2}$ where $m$ is the dimension of $\mathbf{y}$. |
| $(y)_{2\pi}$ | Modulo $2\pi$ of the real number $y$ |
| $x \overset{\text{dist}}{=} y$ | The stochastic variables, $x$ and $y$ have the same distribution function |
| $x \times y$ | The product of $x$ and $y$. |

## 1.6 Abbreviations

The following table lists some of the abbreviations used in the thesis.

| Abbreviation | Description |
|---|---|
| *Propagation models* | |
| GWSSUS | Gaussian wide sense stationary uncorrelated scattering |
| GAA | Gaussian angle of arrival |
| GAAO | Gaussian angle of arrival one cluster |
| TU | Typical urban |
| BU | Bad urban |
| *Capacity enhancement approaches* | |
| RCS | Reduced cluster size |
| RCS-WIN | RCS with nulling |
| RCS-WON | RCS without nulling |
| SSFR | Same sector frequency reuse |
| *Beamformers* | |
| SICR | Summed interference to carrier ratio minimizing |
| MDP | Maximum desired power |
| *Systems* | |
| SICR-SSFR | SICR beamforming with SSFR |
| SICR-RCS-WIN | SICR beamforming and RCS-WIN |
| SICR-RCS-WON | SICR beamforming and RCS-WON |

# Chapter 2

# Propagation Modeling

Propagation models are used for three purposes in the thesis: to derive algorithms, analytically analyze the performance of algorithms and systems, and to perform simulations. In this chapter we define five propagation models: Gaussian Wide Sense Stationary Uncorrelated Scattering (GWSSUS), Gaussian Angle of Arrival (GAA), Gaussian Angle of Arrival One cluster (GAAO), Typical Urban (TU), and Bad Urban (BU). All five proposed models start by assuming that the propagation can be described by a superposition of plane waves, reflected by so-called scatterers. In the GWSSUS model the scatterers are grouped into $d$ clusters where it is assumed that each cluster is flat Rayleigh fading (no time dispersion), with an arbitrary power distribution in azimuth. However, a time delay is associated with each cluster and the combined channel may thus not be flat fading. The GAA model, which is a special case of the GWSSUS model, assumes that the azimuth distribution of power from each cluster is Gaussian distributed with some mean and standard deviation as seen from the base. A special case of the GAA model employing a single cluster of scatterers is developed further to account for path-loss and shadowing effects. This model is referred to as GAAO. The TU model consists of 120 scatterers with certain amplitudes and positions. An important feature of this channel model is that its temporal properties are similar to the typical urban (TU) model defined in [GSM92], which is frequently employed in GSM simulations. The azimuth power distribution (as seen from the base) of the proposed TU model is approximately Gaussian with mean in the direction of the mobile, and with a standard deviation of ten degrees at a 1km base-mobile distance. The standard

deviation is inversely proportional to the base-mobile distance. The BU model consists of a superposition of two TU clusters. Hence the number of rays in the BU model is $2 \times 120 = 240$. One of these clusters is located at the mobile and the other is located 45 degrees from the mobile but at the same distance from the base. The two clusters undergo independent log-normal shadow fading, with the second cluster being 5dB weaker than the first, on average.

The TU and BU models are made for simulation of algorithms and systems while the GAA, GAAO and GWSSUS models are also for analytical derivations and analysis. This fact is reflected by the number of parameters required by the models. The TU and BU models only require the base to mobile distance, while the GAA and GWSSUS models need the number of cluster of scatterers as well as several parameters characterizing the clusters.

The GWSSUS model is basically a straight-forward generalization of the widely accepted wide-band statistical multipath model [PB82, Pro89] without imposing any information about the spatial distribution of power. For the narrow band case, equivalent models have been used in [GP96, Ger95, RDJP95]. The generalization to the wide band case herein, is useful when analyzing wideband systems.

The GAA model does impose some spatial information by letting the power of each cluster of scatterers be Gaussian distributed in azimuth. A similar model has also been proposed in [SW94], but there a uniform azimuth power distribution is assumed for the clusters. The paper [Mar96], also proposes a similar model, but assumes that each cluster can be approximated by a point source. Propagation data are employed in [Mar96] to motivate a model with twelve clusters. An advantage of the GAA over the model of [SW94], is that the parameters of the Gaussian scattering model have been estimated from real data in the papers [AFWP86, Ake91, FJK$^+$94, TO96, YKT91, Zet95c].

The TU model and the GAAO model described in Section 2.3.1 employ a single cluster of scatters. The energy from that cluster is assumed to distributed in a narrow sector centered at the mobile. This assumption is frequently adopted in the simulation of base station antenna array systems, [AFWP86, AMVW91, FN96, GP96, Ger95, RDJP95, Lee73], although it is generally not used when deriving the applied algorithms. The results of Chapters 6 and 7 suggest that a single cluster model yields reasonable performance predictions for the urban macro-cellular environment we consider. Some additional support for the use of single cluster models can be found in [KMT$^+$96]. It is reasonable to believe that a sin-

gle cluster model can be used in environments where the base antenna is high in comparison with the surrounding buildings and hills, and where there are relatively few distinct high buildings and hills at longer distances from the base. If the former of these conditions are not met, the signal will arrive from virtually all angles at the base, while multiple clusters of scatterers has to be considered in the latter.

In the temporal domain, the TU model defined here is similar to the TU model defined in [GSM92], which is frequently employed in GSM simulations. In this model the power delay profile, Section 2.D.1, is assumed to be exponentially decaying with an rms-delay spread of $\approx 1\mu$s, which agrees well with the propagation measurements in [Cox75, SJD94]. The TU model proposed herein is unique in that it exhibits some temporal dispersion within a single cluster of scatterers in the vicinity of the mobile. It is also useful in that it shows that an exponential decaying power delay profile is consistent with a single cluster of scatterers with an azimuthal power distribution similar to the GAAO model.

The BU model proposed in this thesis does not really fall in to either of the two categories, single cluster, or multiple cluster models. This is because the two clusters undergo independent log-normal shadowing. This means that most of the time, one of the two clusters is too weak to make any noticeable contribution to the impulse response. The model is useful when investigating the ability of a beam-steering algorithm, to switch the transmit power between the two clusters. The results of Example 2 of chapter 7 in the report [MZD+96] indicate that such situations can arise in reality.

As is shown in Section 2.5, the proposed models induce independent fast fading (short term channel variations), in up- and downlink, in frequency division duplex (FFD) systems[1] with a duplex distance of more than 10MHz. This implies that the instantaneous downlink channel is unknown. In Section 2.5 it is therefore proposed that the downlink beam synthesis is based on average downlink information in the form of the "summed multipath covariance matrix", for the desired and co-channel users. Methods to obtain that matrix from the corresponding uplink entity are listed.

The chapter is organized as follows: In Section 2.1 the basic assumptions which form the starting point for all five models are stated. Then Section 2.2, 2.3 and 2.4 introduce the GWSSUS, GAA, TU/BU models respectively. In Section 2.5, the differences between downlink beamform-

[1] FDD=Frequency Division Duplex. This means that the downlink transmission takes part a different frequency than the uplink

ing in TDD (time division duplex) and FDD (frequency division duplex) systems are discussed. The proposed models assume a linear digital modulation. However, they are also applicable for other modulation formats if some re-interpretations are made. This and other issues are discussed in Section 2.6. The connection between the GAA model and the model usually used in analysis of angle of arrival estimation using antenna arrays, is explained in Section 2.A. Appendix 2.B contains a more in-depth introduction and derivation of the assumptions stated in Section 2.1. Appendix 2.C fully defines the TU and BU propagation models, with all the necessary details. Appendix 2.D shows the properties of the TU model claimed in Section 2.4. Appendix 2.E finally, shows how the TU and BU models can be used in simulations where some of the signals are simulated and some have been recorded during field-trials.

## 2.1 Basic Assumptions

In this section generic assumptions about propagation are made. The assumptions basically state that the impulse response between the multiple antennas at the base, and the single antenna at the mobile, is given by a superposition of rays, where each ray has a distinct angle of arrival and delay. The angle of arrival together with the spatial distribution of the antenna elements, their antenna patterns and the carrier frequency determine the spatial response of each ray, while the delay together with the modulation pulse-shaping and receiver filters forms the temporal response. The model is true if the propagation can be described as a superposition of rays and the receive and transmit circuitry is linear.

### 2.1.1 Uplink

The discrete time baseband signal sampled at symbol rate at the base, is defined by

$$\mathbf{x}_q^{\mathrm{RX}} = [x_1^{\mathrm{RX}}(qT_{\mathrm{b}} + \Delta T^{\mathrm{RX}}), \ldots, x_m^{\mathrm{RX}}(qT_{\mathrm{b}} + \Delta T^{\mathrm{RX}})]^T, \qquad (2.1)$$

where $x_1^{\mathrm{RX}}(t), \ldots, x_m^{\mathrm{RX}}(t)$ are the antenna signals, $m$ is the number of antenna elements, $q$ is the sample number, $T_{\mathrm{b}}$ is the symbol time and $\Delta T^{\mathrm{RX}}$ is the sampling phase. The information to be sent from the mobile to the base is encoded into a stream of complex symbols, $I_q$, which are transmitted using a linear modulation. The signal received at the base is given by

$$\mathbf{x}_q^{\mathrm{RX}} = \sum_{l \geq 0} \mathbf{h}_l^{RX} I_{q-l}, \tag{2.2}$$

where $\mathbf{h}_l^{RX}$ is the $l$th coefficient of the discrete-time multi-dimensional uplink impulse response. The radio wave propagates via $N$ *scatterers*, as illustrated in Figure 2.1. Scatterer $n$ has complex amplitude[2] $\tilde{h}_n$, propagation distance $l_n = \hat{l}_n + \check{l}_n$ (the total propagation distance from the mobile to antenna element number 1), and azimuth angle $\theta_n$ (as seen from the base). The $l$th tap is given by

$$\mathbf{h}_l^{\mathrm{RX}} = \sum_{n=1}^{N} \tilde{h}_n \exp(-j2\pi f^{\mathrm{RX}} \frac{l_n}{c} + \beta^{\mathrm{RX}}) \times \mathrm{pr}(lT_{\mathrm{b}} + \Delta T^{\mathrm{RX}} - T_{\mathrm{b}} - \frac{l_n}{c}) \mathbf{a}^{\mathrm{RX}}(\theta_n, f^{\mathrm{RX}}), \tag{2.3}$$

where $f^{\mathrm{RX}}$ is the (receive) carrier frequency, $c$ is the speed of light, $\mathrm{pr}(\tau)$ is the convolution of the modulation pulse shape and the receiver filter impulse response, $\beta^{\mathrm{RX}}$ is the receiver-transmitter phase-offset, and $\mathbf{a}^{\mathrm{RX}}(\theta_n, f^{\mathrm{RX}})$ is the vector of receive antenna element gains and phases in azimuth direction $\theta_n$ at frequency $f^{\mathrm{RX}}$, for the receive antenna array.

For linear array configurations with uniformly spaced antenna elements (ULAs) and identical antenna patterns, $\mathbf{a}^{\mathrm{RX}}(\theta, f)$ is given by

$$\mathbf{a}^{\mathrm{RX}}(\theta, f) = p(\theta, f) \times [1, \exp(-j2\pi f \Delta \sin(\theta)/c), \ldots, \exp(-j2(m-1)\pi f \Delta \sin(\theta)/c)]^T, \tag{2.4}$$

where $m$ is the number of antenna elements, $\Delta$ is the inter-element spacing, and $p(\theta, f)$ is the element pattern of the identical elements, see Figure 2.2. Equation (2.4) also requires the antenna elements to be uncoupled and identically directed. The requirement of uncoupled antennas can be relaxed if a sufficient number of dummy elements are added on each end of the array, so that elements are identically coupled.

When the mobile moves, the distance between the mobile and the scatterers (i.e., $\check{l}_n$ in Figure 2.1) changes. The position and amplitudes

[2] The amplitude $\tilde{h}_n$ is treated as real-valued in the derivations of Appendix 2.B, for simplicity.

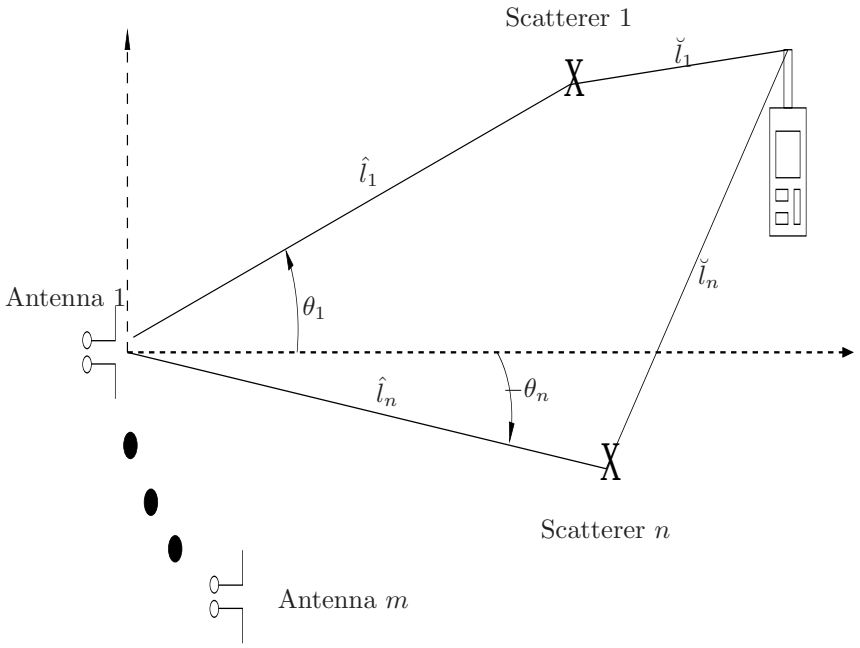


Figure 2.1: *Schematic illustration of multipath model. Note that the scatterers are assumed to be in the far field.*

of the effective scatterers will of course also change. However, they are assumed to be practically fixed during the time the mobile moves a couple of wavelengths. Thus, within a couple of wavelengths the following relationship may be considered valid

$$l_n = l_{n,0} - v\cos(\phi_n)t, \tag{2.5}$$

where $l_{n,0}$ is the propagation distance at time zero, $v$ is the speed of the mobile, $\phi_n$ is the angle between the speed vector of the mobile and the $n$th scatterer, and $t$ is time. Combining (2.3) and (2.5) yields

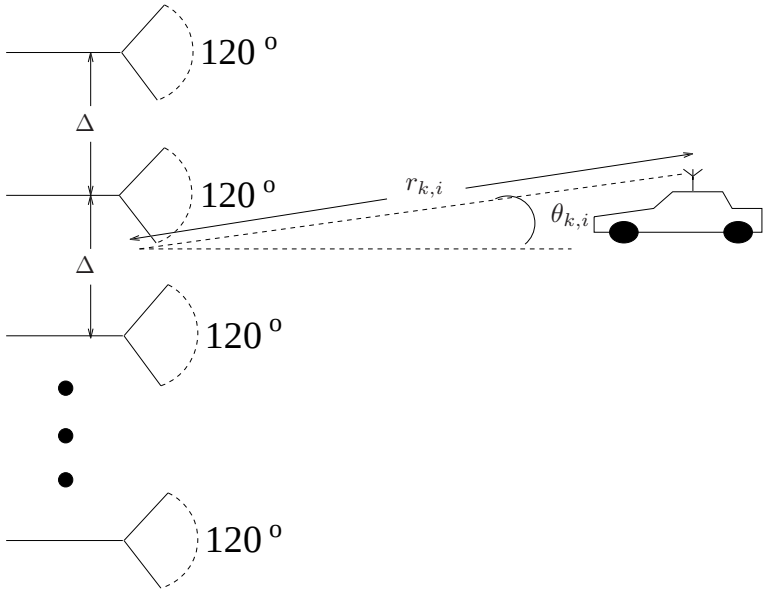


Figure 2.2: *The Uniform Linear Array (ULA) and a polar coordinate system, with reference to the considered base station.*

$$\mathbf{h}_l^{\mathrm{RX}} = \sum_{n=1}^{N} \tilde{h}_n \exp(-j2\pi f^{\mathrm{RX}} \frac{l_{n,0} - v\cos(\phi_n)t}{c} + \beta^{\mathrm{RX}}) \times \mathrm{pr}(lT_{\mathrm{b}} + \Delta T^{\mathrm{RX}} - T_{\mathrm{b}} - \frac{l_{n,0}}{c}) \mathbf{a}^{\mathrm{RX}}(\theta_n, f^{\mathrm{RX}}), \quad (2.6)$$

where we have assumed that

$$\mathrm{pr}(lT_{\mathrm{b}} + \Delta T^{\mathrm{RX}} - T_{\mathrm{b}} - \frac{l_{n,0}}{c}) \approx \mathrm{pr}(lT + \Delta T^{\mathrm{RX}} - T_{\mathrm{b}} - \frac{l_n}{c}), \quad (2.7)$$

which is, for all practical purposes, a good approximation. From (2.6) it is clear that for each scatterer, there is an associated *Doppler frequency*, $f^{\mathrm{RX}} v\cos(\phi_n)/c$. When the contributions from all scatterers are added, the sum in (2.6), alternates between constructive and destructive sum-

mation, due to the fast phase changes induced by the Doppler frequencies. These fast channel variations will be referred to as Doppler fading, Rayleigh fading, or fast fading.[3] In addition to the channel variations due to the Doppler fading, the channel also changes due to changes in the ray parameters $N$, $\tilde{h}_n$, $\theta_n$, $\phi_n$, $l_{n,0}$. However, as already mentioned, these variations are assumed to be much slower than those imposed by the fast fading. The slow changes in the ray parameters will be referred to as shadow fading or slow fading, since buildings and hills between the mobile and base determine the effective scatterers. *Hence several of the entities in (2.3) are time dependent, although this is not explicitly indicated.*

### 2.1.2 Downlink

Already at this point we fix the (equivalent baseband) signal transmitted on each element of the transmit antenna array to be a complex scalar times the modulated waveform. This is ad-hoc and other choices have appeared in the literature [MW96, Win94, FG97], see Section 1.3.2. Let us denote the weight vector applied to the $m$ antenna elements as $\mathbf{w} = [w_1, \ldots, w_m]^T$. The baseband signal sampled at the mobile, $u_q$, will then be given by

$$u_q = \sum_{l \geq 0} (\mathbf{w}^* \mathbf{h}_l^{\mathrm{TX}}) I_{q-l}, \tag{2.8}$$

where $(\cdot)^*$ denotes complex conjugate (Hermitian) transpose and $\mathbf{h}_l^{\mathrm{TX}}$ is given by

$$\mathbf{h}_l^{\mathrm{TX}} = \sum_{n=1}^{N} \tilde{h}_n \exp(-j2\pi f^{\mathrm{TX}} \frac{l_n}{c} + \beta^{\mathrm{TX}}) \times \mathrm{pr}(lT_{\mathrm{b}} + \Delta T^{\mathrm{TX}} - T_{\mathrm{b}} - \frac{l_n}{c}) \mathbf{a}^{\mathrm{TX}}(\theta_n, f^{\mathrm{TX}}). \tag{2.9}$$

Doppler fading and shadow fading applies (of course) to the uplink taps $\mathbf{h}_l^{\mathrm{TX}}$ in the same way as to the downlink taps $\mathbf{h}_l^{\mathrm{RX}}$. However, the fast

[3] The word Rayleigh fading is only used when the amplitude distribution is Rayleigh, while the wording Doppler fading is used when we want remind the reader of the underlying phenomena. The wording fast fading is used when we refer to the fast channel changes (as opposed to the slow shadow fading) without emphasizing on the underlying mechanisms

fading processes in the two links are uncorrelated in many systems, see Section 2.5 below. In the remainder of this thesis, the up- and downlink superscript RX/TX will be omitted in equations which are valid for both links, or if it is evident from the context which link is considered.

## 2.2 Gaussian Wide Sense Stationary Uncorrelated Scattering (GWSSUS)

In the GWSSUS model, the scatterers are grouped into $d$ clusters. Let $\Omega_r$ be the indices of the scatters in the $r$th cluster. The delay differences within the $r$th cluster are assumed to be such that

$$\mathrm{pr}(\tau - \frac{l_n}{c}) \approx \mathrm{pr}(\tau - \tau_r), \text{ where } n \in \Omega_r. \tag{2.10}$$

Combing (2.6) or (2.9) and (2.10) yields

$$\mathbf{h}_l = \sum_{k=1}^{d} \mathbf{v}_k \,\mathrm{pr}(lT_\mathrm{b} + \Delta T - T_\mathrm{b} - \tau_r), \tag{2.11}$$

where the *effective steering vector* $\mathbf{v}_k$ is given by the superposition of the scatterers, $n \in \Omega_r$, which belong to the $r$th cluster i.e.,

$$\mathbf{v}_r = \sum_{n \in \Omega_r} \tilde{h}_n \exp(-j2\pi f \frac{l_n}{c} + \beta)\mathbf{a}(\theta_n, f). \tag{2.12}$$

The vectors $\mathbf{v}_r$ are functions of time which change with the Doppler fading rate, while the delays $\tau_r$ change at the much slower shadowing rate. Assuming that $\tilde{h}_n \exp(-j2\pi f \frac{l_n}{c})$ are independent identically distributed random variables with finite mean and finite non-zero variance, and that the number of scatterers within each cluster is large, it follows from the central limit theorem, [GS92], that the vectors $\mathbf{v}_k$ converge to complex Gaussian distributed random variables. Since the vectors $\mathbf{v}_k$ change with time they are considered as Gaussian wide sense stationary random processes (in time, although the time independence is suppressed). In order to find the mean and covariance of $\mathbf{v}_r$, a deterministic view is taken. Consider the following integrals

$$\mathrm{Int}_1 = \frac{1}{T}\int_{t=0}^{T} \mathbf{v}_r \mathrm{d}t \tag{2.13}$$

$$\mathrm{Int}_2 = \frac{1}{T}\int_{t=0}^{T} \mathbf{v}_r \mathbf{v}_r^T \mathrm{d}t, \tag{2.14}$$

$$\mathrm{Int}_3 = \frac{1}{T}\int_{t=0}^{T} \mathbf{v}_r \mathbf{v}_r^* \mathrm{d}t. \tag{2.15}$$

Using (2.5), (2.12) and assuming that the Doppler frequencies,

$$f v \cos(\phi_n)/c, \tag{2.16}$$

are distinct the following limits are obtained

$$\lim_{T \longrightarrow \infty} \mathrm{Int}_1 = \mathbf{0} \tag{2.17}$$

$$\lim_{T \longrightarrow \infty} \mathrm{Int}_2 = \mathbf{0} \tag{2.18}$$

$$\lim_{T \longrightarrow \infty} \mathrm{Int}_3 = \mathbf{R}_r, \tag{2.19}$$

where $\mathbf{R}_r$ is given by

$$\mathbf{R}_r = \sum_{n \in \Omega_r} |\tilde{h}_n|^2 \mathbf{a}(\theta_n, f)\mathbf{a}^*(\theta_n, f). \tag{2.20}$$

Turning back to a stochastic view, the properties (2.17-2.23) are modeled by defining the following statistical expectations

$$\mathrm{E}\{\mathbf{v}_r\} = \mathbf{0} \tag{2.21}$$

$$\mathrm{E}\{\mathbf{v}_r \mathbf{v}_r^T\} = \mathbf{0} \tag{2.22}$$

$$\mathrm{E}\{\mathbf{v}_k \mathbf{v}_k^*\} = \mathbf{R}_r. \tag{2.23}$$

The expectation in (2.21-2.23) is over the Doppler fading only. The delays, $\tau_r$, and covariance matrices, $\mathbf{R}_r$, change at the slower shadow fading rate. If there is just a single cluster, i.e., $d = 1$, the channel is said to be flat Rayleigh fading. This is because the physical channel, i.e., the channel excluding the effects of the receiver filter and modulation pulse-shaping, becomes independent of frequency, and therefore the amplitude on each antenna element is Rayleigh distributed.

## 2.3 Gaussian Angle of Arrival (GAA)

In the GAA model, which is a special case of the GWSSUS model, it is assumed that the power of the $r$th cluster is $P_r$, and the distribution of this power, with respect to azimuth $\theta$, is Gaussian with mean $\theta_r$ and standard deviation $\sigma_r$. The number of scatterers within a cluster is assumed infinite, therefore, the summation (2.20) turns into an integral. For linear array configurations with uniformly spaced antenna elements (ULAs) the row=$k$,column=$e$ element of the multipath covariance matrices $\mathbf{R}_r$ is obtained from (2.20) as

$$
\begin{aligned}
[\mathbf{R}_r]_{k,e} &= P_r \int_{-\infty}^{\infty} \frac{1}{\sqrt{2\pi}\sigma_r} \exp(-\nu^2/(2\sigma_r^2))[\mathbf{a}(\theta_r+\nu,f)\mathbf{a}^*(\theta_r+\nu,f)]_{k,e} \\
&= P_r \int_{-\infty}^{\infty} \frac{1}{\sqrt{2\pi}\sigma_r} \exp(-\nu^2/(2\sigma_r^2))|p(\theta_r+\nu,f)|^2 \\
&\times \exp(j(e-k)\frac{2\pi\Delta f}{c}\sin(\theta_r+\nu))\mathrm{d}\nu \qquad (2.24) \\
&\approx P_r|p(\theta_r,f)|^2 \int_{-\infty}^{\infty} \frac{1}{\sqrt{2\pi}\sigma_r} \exp(-\nu^2/(2\sigma_r^2)) \\
&\times \exp(j(e-k)\frac{2\pi\Delta f}{c}\sin(\theta_r+\nu))\mathrm{d}\nu \qquad (2.25) \\
&\approx G_r \exp(-\frac{1}{2}\tilde{\sigma}_r^2(e-k)^2)\exp(j(e-k)\frac{2\pi\Delta f}{c}\sin(\theta_r)) \qquad (2.26)
\end{aligned}
$$

where

$$
\tilde{\sigma}_r = \frac{\pi^2\Delta f}{90^o c}\cos(\theta_r)\sigma_r, \qquad (2.27)
$$

and $G_r = P_r|p(\theta_r,f)|^2$ is the power received from the cluster, $\Delta$ is the spacing between the $m$ antenna elements and $p(\theta_r,f)$ is the antenna pattern of the identical antenna elements. The angular spread, $\sigma_r$, is assumed to be in degrees in (2.27). Approximation (2.25) assumes that the gain of the antenna pattern varies little within say $[\theta_r-3\sigma,\theta_r+3\sigma]$. The approximation (2.26) is obtained by linearizing $\sin(\theta_r+\nu)$ around $\theta_r$ and applying formula 15.73 of [Spi90] which reads

$$
\int_{x=0}^{\infty} \exp(-ax^2)\times\cos(bx)\mathrm{d}x = \frac{1}{2}\sqrt{\frac{\pi}{a}}\exp(\frac{-b^2}{4a}). \qquad (2.28)
$$

The parameter $\tilde{\sigma}_r$ which is related to the angular spread, $\sigma_r$, through (2.27) is proportional to the angular spread divided by the beamwidth of the array. Since the beamwidth of a linear array increases with $\theta_r$, $\tilde{\sigma}_r$ decreases with $\theta_r$. The parameters associated with a cluster are $G_r$, $\theta_r$ and $\sigma_r$. These parameters are assumed to change at the shadow fading rate which is assumed to be much slower than the variations in $\mathbf{v}_r$. The cluster parameters are assumed the same in both up- and downlink. However, the up- and downlink channels are conditioned on the cluster parameters i.e., $(\mathbf{v}_r^{\mathrm{RX}}|G_r, \theta_r, \sigma_r)$ and $(\mathbf{v}_r^{\mathrm{TX}}|G_r, \theta_r, \sigma_r)$ respectively, are assumed independent in FDD systems with $|f^{\mathrm{RX}} - f^{\mathrm{TX}}| > 10\mathrm{MHz}$, see Section 2.5 below.

### 2.3.1 The GAAO model

In this section a special case of the GAA model is developed further in order to include path loss and shadowing effects. The notations introduced here are used in Chapters 3 and 4. The section is written such that it should be possible to follow without having read the previous sections of this chapter. The material therefore overlaps somewhat with that of previous sections.

The special case considered is the GAA model described above, with a single cluster of scatterers (per mobile) i.e., $d = 1$. The model is referred to as GAAO where the letter 'O' stands for "one cluster". In this section we restrict ourselves to linear arrays of identical uniformly distributed antenna elements (ULAs), see Figure 2.2. Such an array is applied to cover a 120-degree sector. The three arrays covering the three sectors of a cell are seen as three different base stations, see Chapter 3.

In this model the physical downlink channel from the $m$ antennas of the $k$th base station and the single antenna at the $i$th mobile can can be described by an $m$ dimensional complex vector $\mathbf{v}_{k,i}^{\mathrm{TX}}$. Correspondingly, the physical uplink channel from the single antenna at the $i$th mobile to the multiple antennas at the $k$th base, can be described by another $m$ dimensional vector $\mathbf{v}_{k,i}^{\mathrm{RX}}$. In the following description, the up/downlink indications RX/TX will be suppressed, since the properties are assumed valid for both links.

Since $\mathbf{v}_{k,i}$ is just a vector of complex numbers, there is no delay spread in the channel [Lee93]. However, the vector $\mathbf{v}_{k,i}$ only models the physical channel and not the influence of the pulse-shaping of the transmitter and the receiver filters (i.e., $\mathrm{pr}(\tau)$ is the previous sections). These effects, however, are assumed to be the same on all antennas, and for both the

desired and interfering signals. The vector $\mathbf{v}_{k,i}$ changes with the motion of the mobile. These changes are referred to as Doppler fading, Rayleigh fading or fast fading, and are modeled by treating $\mathbf{v}_{k,i}$ as a random process in time (where the dependence on time is suppressed). The elements of the vector $\mathbf{v}_{k,i}$ are assumed to be zero-mean, complex, and circular symmetric, jointly Gaussian random variables i.e.,

$$\mathrm{E}\{\mathbf{v}_{k,i}\} = \mathbf{0} \tag{2.29}$$

$$\mathrm{E}\{\mathbf{v}_{k,i}\mathbf{v}_{k,i}^T\} = \mathbf{0}. \tag{2.30}$$

The covariance matrix of $\mathbf{v}_{k,i}$ is defined by

$$\mathbf{R}_{k,i} = \mathrm{E}\{\mathbf{v}_{k,i}\mathbf{v}_{k,i}^*\}. \tag{2.31}$$

This is a generalization of the flat Rayleigh fading model from the single antenna case to the multiple antenna case. The Rayleigh channel model is frequently used in the analysis of mobile communication systems see e.g., [Lee93]. The power received from the mobile (by the base) is assumed Gaussian distributed in azimuthal angle. The mean and standard deviation of the Gaussian distribution are $\theta_{k,i}$ and $\sigma_{k,i}$, respectively. Under this assumption $\mathbf{R}_{k,i}$, may be approximated by

$$\mathbf{R}_{k,i} = G_{k,i}\mathbf{R}(\theta_{k,i}, \sigma_{k,i}), \tag{2.32}$$

where $G_{k,i}$ is a real-valued scalar, and $\mathbf{R}(\theta, \sigma)$ is a complex-matrix valued function of $\theta$ and $\sigma$. The scalar $G_{k,i}$ will be referred to as the path-gain between base $k$ and mobile $i$. Element $[\cdot]_{r,e}$ of the matrix $\mathbf{R}(\theta, \sigma)$ is defined as

$$[\mathbf{R}(\theta, \sigma)]_{r,e} = \exp(-\frac{1}{2}\tilde{\sigma}^2(e-r)^2)\exp(j(e-r)\frac{2\pi\Delta}{\lambda}\sin(\theta_r)), \tag{2.33}$$

where

$$\tilde{\sigma} = \frac{\pi^2\Delta}{90^o\lambda}\cos(\theta)\sigma. \tag{2.34}$$

Note that $\mathbf{R}_{k,i}$ is the correlation of the complex signal strengths between the antenna elements of the array. From (2.32-2.34) it is deduced that this correlation decreases with the "angular spread", $\sigma$, and the antenna spacing $\Delta$. The rank of the matrix also reduces with increasing angular

spread. In the special case $\sigma = 0^o$ the rank is one, which corresponds to a conventional point source model. The path gain $G_{k,i}$ is modeled as

$$G_{k,i} = (\frac{1}{r_{k,i}})^{\gamma} |p(\theta_{k,i}, f)|^2 L_{k,i}, \tag{2.35}$$

where $r_{k,i}$ is the base-mobile distance, $\gamma$ is the path loss exponent, $p(\theta, f)$ is the element patterns of the identical antenna elements in direction $\theta$, and $L_{k,i}$ is a log-normally distributed random variable. This means that $10\log(L_{k,i})$ is a normally distributed random variable with mean zero and standard deviation $\sigma_{\mathrm{L}}$ (dB). These parameters vary with time and are therefore considered to be random processes. The "angular spread", $\sigma_{k,i}$, is assumed to vary with distance as

$$\sigma_{k,i}(r_{k,i}) = \begin{cases} \frac{r_0}{r_{k,i}}\sigma_0, \text{ when } r_{k,i} > r_0 \\ \sigma_0 \text{ when } r_{k,i} < r_0 \end{cases} \tag{2.36}$$

The motivation for this distance dependence is that that the distance from the mobile to the scatterers should basically be independent of base-mobile distance which yields an inverse relationship between the angular spreading and distance at larger distances. However, the results of chapter 7 suggest that $r_0 = \infty$ $\sigma_0 = 3^o$ to $96o$ is reasonable model for performance prediction, thereby effectively yielding a distance independent angular spreading.

In a strict sense $\mathbf{v}_{k,i}$ is a complex Gaussian random vector only when it is conditioned on the random variables $G_{k,i}, \theta_{k,i}, \sigma_{k,i}$. This be can be formulated mathematically as

$$(\mathbf{v}_{k,i} | G_{k,i}, \theta_{k,i}, \sigma_{k,i}) \in \mathrm{N}(\mathbf{0}, G_{k,i}\mathbf{R}(\theta_{k,i}, \sigma_{k,i})). \tag{2.37}$$

The rate of change in the stochastic process $\mathbf{v}_{k,i}$, is assumed much higher than in the distribution parameters $G_{k,i}, \theta_{k,i}, \sigma_{k,i}$. The properties described are assumed valid for both the up- and downlink channels i.e., both $\mathbf{v}_{k,i}^{\mathrm{RX}}$ and $\mathbf{v}_{k,i}^{\mathrm{TX}}$. They are thus distributed according to (2.37), where the parameters $G_{k,i}, \theta_{k,i}, \sigma_{k,i}$ are assumed the same for both processes. However, in FDD systems with a carrier frequency difference of more than 10MHz, the two conditioned processes $(\mathbf{v}_{k,i}^{\mathrm{RX}} | G_{k,i}, \theta_{k,i}, \sigma_{k,i})$ and $(\mathbf{v}_{k,i}^{\mathrm{TX}} | G_{k,i}, \theta_{k,i}, \sigma_{k,i})$ respectively, are practically independent, see Section 2.5 below. Assume that base $k$, transmits using the weights of the vector $\mathbf{w}_k$. Then from (2.8) and (2.11), the (continuous time) signal received at the $i$th mobile is given by

$$u_i(t) = \mathbf{w}_k^* \mathbf{v}_{k,i} s(t - \tau_{k,i}), \tag{2.38}$$

where $s(t)$ is the signal transmitted by the $k$th base convolved with the impulse response of the receiver filter at the mobile, and $\tau_{k,i}$ is the propagation delay between the $k$th base and the $i$th mobile. Thus in the framework of Section 2.1,

$$s(t) = \sum_p I_p \,\mathrm{pr}(t - pT_\mathrm{b}), \tag{2.39}$$

where $I_p$ are the transmitted symbols, $pr(\tau)$ is the convolution of the modulation pulse shape and the receiver filters, $T_\mathrm{b}$ is the symbol time. The signal $u(t)$ is sampled at time, $t = qT + \Delta T_{k,i} - T$ where $q$ is the sample number (integer).

Without loss of generality, assume that the average power per symbol (averaged over all symbols in the alphabet) is unity i.e.,

$$\mathrm{E}\{|I_p|^2\} = 1, \tag{2.40}$$

and assume that the power of the pulse $\mathrm{pr}(\tau)$ is normalized as

$$\int_{-\infty}^{\infty} |\,\mathrm{pr}(\tau)|^2 \mathrm{d}t = 1. \tag{2.41}$$

The power (per symbol) averaged over the fast fading and the chosen symbol (but conditioned on $G_{k,i}, \theta_{k,i}, \sigma_{k,i}$) of the received signal is then given by

$$\begin{aligned} P_{k,i} &= \mathrm{E}\{\|\mathbf{w}_k^* \mathbf{v}_{k,i}\|^2 \mathrm{E}\{|I_p|^2\}\} \\ &= \mathrm{E}\{\mathbf{w}_k^* \mathbf{v}_{k,i} \mathbf{v}_{k,i}^* \mathbf{w}_k\} \\ &= \mathbf{w}_k^* \mathrm{E}\{\mathbf{v}_{k,i} \mathbf{v}_{k,i}^*\} \mathbf{w}_k \\ &= G_{k,i} \mathbf{w}_k^* \mathbf{R}(\theta_{k,i}, \sigma_{k,i}) \mathbf{w}_k, \end{aligned} \tag{2.42}$$

where the weights $\mathbf{w}_k$ may be functions of $G_{k,i}, \theta_{k,i}$ and $\sigma_{k,i}$ but not of $\mathbf{v}_{k,i}$.

## 2.4 The Typical Urban (TU) and Bad Urban (BU) Simulation Models

In the temporal domain, the TU model defined here is similar to the TU model defined in [GSM92], which is frequently employed in GSM simulations. The TU model of [GSM92] has a temporal distribution of power, which is a discretized version of an exponentially decaying power versus delay distribution, [Fai89]. This agrees well with the propagation measurements in [Cox75, SJD94]. In the azimuth domain (as seen from the base) the power is approximately Gaussian distributed as in the GAA model using $d = 1$ and with an angular spreading of $\sigma_1 = 10^o/r$ where $r$ is the base to mobile distance in kilometers. This is shown in Appendix 2.D. The TU model is generated in the following way: (a more complete description is given in Appendix 2.C.1) There are $N = 120$ scatterers pseudo randomly distributed within a radius of 1km from the mobile. The power decays exponentially with the distance from the mobile. The positions of all the scatterers are held fixed during the time the mobile moves five meters. For each considered mobile position the impulse response is calculated by brute force using (2.3) and/or (2.6). When the mobile has moved five meters all the scatterers are reoriented to their original positions with respect to the new mobile position, except for a small random offset. The random offset is introduced in order to generate different fading realizations during different five meter sections. In order to take the effect of shadowing and path loss into account, the gains of all scatterers are multiplied with a common factor $-35\log(r) + L$ (dB) where $r$ is the base to mobile distance and $L$ is normally distributed with zero-mean and standard deviation 8dB. The shadowing factor is held constant during five meters of mobile motion, and is re-randomized with some correlation between five meter sections. In the BU model we add the contribution of two clusters of the type described above: one at the mobile and one at the same distance as the mobile but with an angular offset of 45 degrees from the desired mobile. The multipath cluster is given an appropriate delay and the clusters are weighted such that the cluster at the mobile is 5dB stronger than the multipath cluster averaged over fast and slow fading. Obviously the BU is approximately a GAA model with two clusters $d = 2$, and powers $P_k$ varying according to the log-normal fading.

## 2.5 Implications of the Proposed Models for TDD and FDD Systems

Mobile communication standards can be divided into two classes, time division duplex (TDD) and frequency division duplex (FDD). In TDD the uplink and downlink connections share the same carrier frequency (i.e., $f^{\mathrm{RX}} = f^{\mathrm{TX}}$ in the framework above) by multiplexing the two links in time. In FDD, the uplink and downlink transmission is performed at different frequencies (i.e., $f^{\mathrm{RX}} \neq f^{\mathrm{TX}}$). The standards DECT, PCS2000, PHS, CT1 and CT2 are based on TDD while TACS, AMPS, GSM, DCS1800, PCS1900, IS54, IS136, IS95 and ANSI J-STD-008 are based on FDD [Hoy95, Mat95, NM96, Ste92, Tie95]. As we will now explain, there is a fundamental difference between FDD and TDD concerning downlink beamforming. The difference is that the *instantaneous* downlink channel information may be available in TDD but not in FDD systems.[4] This means that $\mathbf{h}_l^{\mathrm{TX}}$ may be considered observable in TDD systems but not in FDD systems, as is shown in Sections 2.5.1 and 2.5.2 below. Therefore the downlink beamforming in FDD systems has to be based on other information. Under the GWSSUS and GAA models, one such source of information, is the "summed multipath covariance matrix" defined by

$$\mathbf{R}^{\mathrm{TX}} = \sum_{r=1}^{d} \mathbf{R}_r^{\mathrm{TX}}. \tag{2.43}$$

This matrix is used as input to the generalized SICR-beamformer introduced in Chapter 5. It should be noted that $\mathbf{R}^{\mathrm{TX}}$ cannot be estimated directly from the uplink data. In order to obtain an estimate of this matrix, we propose that the corresponding uplink matrix i.e., $\mathbf{R}^{\mathrm{RX}} = \sum_{k=1}^{d} \mathbf{R}_r^{\mathrm{RX}}$, is estimated first. Then one of the four methods listed below may be used to make the transformation from $\mathbf{R}^{\mathrm{RX}}$ to $\mathbf{R}^{\mathrm{TX}}$.

1. If a uniform linear array is used in the uplink, i.e., $\mathbf{a}(\theta, f)$ is given by (2.4), and the GAA model applies, then the method of [TO96] may be employed to estimate $\theta_r$ and $\sigma_r$. With these estimates at hand, the transmit matrix $\mathbf{R}^{\mathrm{TX}}$ may be explicitly calculated.

2. If the up- and downlink manifolds are the same i.e.,

[4] An exception to this rule may occur if mobile to base feedback is employed [Ger95].

$$\mathbf{a}^{\mathrm{RX}}(\theta_n, f^{\mathrm{RX}}) = \mathbf{a}^{\mathrm{TX}}(\theta_n, f^{\mathrm{TX}}). \tag{2.44}$$

it follows from (2.20) that the up- and downlink multipath covariance matrices are the same i.e., $\mathbf{R}^{\mathrm{TX}} = \mathbf{R}^{\mathrm{RX}}$. This requires two different antenna arrays for up- and downlink. The two arrays should have the same structure but with scaled to their respective wavelength. This idea was first proposed in [RDJP95], and is referred to as "the matched array approach", in that paper.

3. The same array is used in up- and downlink, i.e.,

$$\mathbf{a}^{\mathrm{RX}}(\theta, f) = \mathbf{a}^{\mathrm{TX}}(\theta, f) = \mathbf{a}(\theta, f), \tag{2.45}$$

and the relative duplex separation $2(f^{\mathrm{RX}} - f^{\mathrm{TX}})/(f^{\mathrm{RX}} + f^{\mathrm{TX}})$ is small. Then there may exist a compensation matrix $\mathbf{A}_{\mathrm{compensate}}$ such that

$$\mathbf{A}_{\mathrm{compensate}}\mathbf{a}^{\mathrm{RX}}(\theta_n, f^{\mathrm{RX}}) \approx \mathbf{a}^{\mathrm{TX}}(\theta_n, f^{\mathrm{TX}}), \tag{2.46}$$

see Example 2.1 below. If (2.46) is valid $\mathbf{R}^{\mathrm{TX}}$ may be approximated as

$$\mathbf{R}^{\mathrm{TX}} \approx \mathbf{A}_{\mathrm{compensate}}\mathbf{R}^{\mathrm{RX}}\mathbf{A}^{*}_{\mathrm{compensate}}. \tag{2.47}$$

4. If the spatial distribution of power is well approximated by a number of rays (less than the number of antenna elements), i.e.,

$$\mathbf{R}^{\mathrm{RX}}_{k,i} \approx |\tilde{h}_n|^2 \mathbf{a}^{\mathrm{RX}}(\theta_n, f^{\mathrm{RX}})(\mathbf{a}^{\mathrm{RX}}(\theta_n, f^{\mathrm{RX}}))^*, \tag{2.48}$$

then the powers $|h_n|^2$ and directions $\theta_n$ of these rays can be estimated from $\mathbf{R}^{\mathrm{RX}}_{k,i}$, using a conventional direction finding technique, e.g. [BM86, Orf90, OVK92, RPK86, Sch79]. These estimates may then be used to calculate $\mathbf{R}^{\mathrm{TX}}$ using

$$\mathbf{R}^{\mathrm{TX}}_{k,i} \approx |\tilde{h}_n|^2 \mathbf{a}^{\mathrm{TX}}(\theta_n, f^{\mathrm{TX}})(\mathbf{a}^{\mathrm{TX}}(\theta_n, f^{\mathrm{TX}}))^*, \tag{2.49}$$

**Example 2.1**

Let the up- and downlink frequency be the lowest possible in GSM i.e., $f^{\mathrm{RX}} = 890\mathrm{MHz}$ and $f^{\mathrm{TX}} = 935\mathrm{MHz}$. Let the manifold be given

by (2.4) i.e., a uniform linear array. The antenna element patterns are assumed independent of frequency i.e.,

$$p(\theta) = p(\theta, f^{\mathrm{RX}}) = p(\theta, f^{\mathrm{TX}}) \tag{2.50}$$

Let the antenna spacing be 0.4 wavelengths at 960MHz which is the highest possible frequency in GSM. The compensation matrix $\mathbf{A}_{\mathrm{compensate}}$ is defined by

$$\begin{aligned}\mathbf{A}_{\mathrm{compensate}} = (&\int_{\theta=-180^o}^{180^o} \frac{1}{|p(\theta)|^2)} \mathbf{a}(\theta, f^{\mathrm{TX}})\mathbf{a}^*(\theta, f^{\mathrm{RX}})\mathrm{d}\theta)\times \\ &(\int_{\theta=-180^o}^{180^o} \frac{1}{|p(\theta)|^2} \mathbf{a}(\theta, f^{\mathrm{RX}})\mathbf{a}^*(\theta, f^{\mathrm{RX}})\mathrm{d}\theta)^{-1}\end{aligned} \tag{2.51}$$

The approximation error is defined as

$$\epsilon = \max_{\theta}\{\frac{\|\mathbf{A}_{\mathrm{compensate}}\mathbf{a}(\theta, f^{\mathrm{RX}}) - \mathbf{a}(\theta, f^{\mathrm{TX}})\|^2}{\|\mathbf{a}(\theta, f^{\mathrm{TX}})\|^2}\}. \tag{2.52}$$

Using (2.4) and (2.50- 2.51) it is apparent that (2.52) is independent of the element pattern $p(\theta, f)$. The error $\epsilon$ is evaluated using between two and twenty antennas i.e., $m = 2, \ldots, 20$. The largest error obtained was $\epsilon = 0.83\%$. This value is obtained using $m = 4$. Combining (2.50),(2.45), (2.52) and (2.20) yields

$$\begin{aligned}&\mathbf{A}_{\mathrm{compensate}}\mathbf{R}^{\mathrm{RX}}\mathbf{A}^*_{\mathrm{compensate}} = \\ &\sum_n |\tilde{h}_n|^2 \mathbf{A}_{\mathrm{compensate}}\mathbf{a}(\theta, f^{\mathrm{RX}})\mathbf{a}(\theta, f^{\mathrm{RX}})\mathbf{A}_{\mathrm{compensate},*} = \\ &\sum_n |\tilde{h}_n|^2 (\mathbf{a}(\theta, f^{\mathrm{TX}}) + \mathbf{e}(\theta))(\mathbf{a}(\theta, f^{\mathrm{TX}}) + \mathbf{e}(\theta))^* \approx \mathbf{R}^{\mathrm{TX}} = \\ &\sum_n |\tilde{h}_n|^2 \mathbf{a}(\theta, f^{\mathrm{TX}})\mathbf{a}^*(\theta, f^{\mathrm{TX}})\end{aligned} \tag{2.53}$$

where $\|\mathbf{e}(\theta)\|^2 \leq 0.0083 \times \|\mathbf{a}(\theta, f^{\mathrm{TX}})\|^2$ . This error is probably to small to have any noticable effect on performance.

### 2.5.1 Conditions Under Which the Up- and Downlink Impulse Response are Equal in TDD

In TDD systems the channel is divided into time slots (small intervals of time) where the up- and downlink signaling alternates. If the mobile motion between the uplink timeslot and the subsequent downlink timeslot is sufficiently small (typically a small fraction of a wavelength), then the delays $l_n/c$ and DOAs $\theta_n$ of the arriving wave fields may be considered the same in both time slots. From (2.3) and (2.9) we thus obtain that the receive and transmit impulse responses in the two slots will be the same (i.e., $\mathbf{h}_l^{\mathrm{RX}} = \mathbf{h}_l^{\mathrm{TX}}$) if the same array is applied both in up- and downlink and the sampling phase is the same i.e., $\Delta T^{\mathrm{RX}} = \Delta T^{\mathrm{TX}}$. In practice the up- and downlink impulse responses will differ due to the motion of the mobile, calibration errors in the receive and transmit amplifiers and filters, and since $\Delta T^{\mathrm{RX}} \neq \Delta T^{\mathrm{TX}}$. Of these "errors" the last one is generally unimportant.

### 2.5.2 The Fast Fading in Up- and Downlink is Independent in FDD

In the FDD case, the fast fading can be considered independent in up- and downlink. Since the downlink channel is unobservable, the instantaneous downlink channel is unknown. This is motivated as follows: Consider a time interval small enough for the gains $\tilde{h}_n$ and angle of arrivals $\theta_n$ (in the framework of Section 2.1) to be considered constant, but where the propagation path lengths varies as in (2.5). During this interval the continuous time multi-dimensional impulse response between the multiple antennas at the base and the single antenna at the mobile, is derived from (2.6) and (2.9) as

$$\mathbf{h}^{\mathrm{RX}}(\tau) = \sum_{n=1}^{N} \tilde{h}_n \exp(-j2\pi f^{\mathrm{RX}} \frac{l_{n,0} - v\cos(\phi_n)t}{c} + \beta^{\mathrm{RX}}) \times \delta(\tau - \frac{l_{n,0}}{c}) \mathbf{a}^{\mathrm{RX}}(\theta_n, f^{\mathrm{RX}}), \quad (2.54)$$

in the uplink and

$$\mathbf{h}^{\mathrm{TX}}(\tau) = \sum_{n=1}^{N} \tilde{h}_n \exp(-j2\pi f^{\mathrm{TX}} \frac{l_{n,0} - v\cos(\phi_n)t}{c} + \beta^{\mathrm{TX}}) \times \delta(\tau - \frac{l_{n,0}}{c})\mathbf{a}^{\mathrm{TX}}(\theta_n, f^{\mathrm{TX}}), \quad (2.55)$$

in the downlink. Equations (2.54) and (2.55) only model the physical channel i.e., the influence of the receiver-modulation pulse-shaping, $\mathrm{pr}(\tau)$, is excluded. Taking the Fourier transform of $\mathbf{h}^{\mathrm{RX}}(\tau)$ and $\mathbf{h}^{\mathrm{TX}}(\tau)$ with respect to $\tau$, and letting $f \to f + f^{\mathrm{RX}}$ and $f \to f + f^{\mathrm{TX}}$, respectively, yields

$$\mathbf{H}^{\mathrm{RX}}(f,t) = \sum_{n=1}^{N} \tilde{h}_n \exp(-j2\pi \frac{l_{n,0} - v\cos(\phi_n)t}{c} f + \beta^{\mathrm{RX}})\mathbf{a}^{\mathrm{RX}}(\theta_n, f) \quad (2.56)$$

and

$$\mathbf{H}^{\mathrm{TX}}(f,t) = \sum_{n=1}^{N} \tilde{h}_n \exp(-j2\pi \frac{l_{n,0} - v\cos(\phi_n)t}{c} f + \beta^{\mathrm{TX}})\mathbf{a}^{\mathrm{TX}}(\theta_n, f) \quad (2.57)$$

respectively, where the time dependence has been made explicit momentarily. In Appendix 2.D.3 and Appendix 2.F below it is simulations show that $\mathbf{H}^{\mathrm{RX}}(f_1,t)$ and $\mathbf{H}^{\mathrm{TX}}(f_2,t)$ are practically uncorrelated functions if $|f_1 - f_2| \geq 10$MHz, using the GAA and TU model respectively. By this we mean that the correlation coefficient $c_{r,e}$ defined by

$$c_{r,e}(\Delta t, t, f_1, f_2) = \frac{\frac{1}{T}\int_{t=0}^{T}[\mathbf{H}^{\mathrm{RX}}(f_1, t+\Delta t)]_r[\mathbf{H}^{\mathrm{TX},*}(f_2,t)]_e \mathrm{d}t}{\sqrt{(\frac{1}{T}\int_{t=0}^{T}|[\mathbf{H}^{\mathrm{RX}}(f_1,t+\Delta t)]_r|^2\mathrm{d}t)(\frac{1}{T}\int_{t=0}^{T}|[\mathbf{H}^{\mathrm{TX}}(f_2,t)]_e|^2\mathrm{d}t)}}, \quad (2.58)$$

is practically zero for all $\Delta t$, $1 \leq e \leq m$, $1 \leq r \leq m$ using $f_1 = f^{\mathrm{RX}}$ and $f_2 = f^{\mathrm{TX}}$. The time interval $T$ in (2.58) should be chosen short enough for

the position and gain of the scatterers to be considered fixed, and long enough to make $c_{r,e}$ converge. In the GAA and GWSSUS models the integration $\frac{1}{T}\int_{t=0}^{T}(\cdot)\mathrm{d}t$, corresponds to the (statistical) expectation over fast fading. It should be noted that the simulations of Appendix 2.D.3 and Appendix 2.F assume that position of the scatterers are independent of frequency, and thereby the absolute carrier frequency unimportant. This is only valid over limited frequency range. If the position of the active scatterers move with frequency, the correlation is probably even lower.

Since all FDD standards listed in Section 2.5 have a duplex distance, i.e., $|f^{\mathrm{TX}} - f^{\mathrm{RX}}|$, larger than 10MHz, we claim that the up- and downlink transfer functions are uncorrelated in FDD systems. If the number of scatterers $N$ is large, then $\mathbf{H}^{\mathrm{RX}}(f_1, t)$ and $\mathbf{H}^{\mathrm{TX}}(f_2, t)$ may be seen as complex Gaussian distributed random processes. In fact, all models proposed in this thesis possess this property, see Section 2.2, 2.3 and 2.D.2. Since the up- and downlink transfer functions are uncorrelated and Gaussian, they are also statistically independent. This property pertains also to the impulse response coefficients, $\mathbf{h}_l^{\mathrm{RX}}$ and $\mathbf{h}_l^{\mathrm{TX}}$, since they are linear functions of the channel transfer functions $\mathbf{H}(f + f^{\mathrm{RX}})$ and $\mathbf{H}(f + f^{\mathrm{TX}})$. In fact, they can be obtained through the formulas

$$\mathbf{h}_l^{\mathrm{RX}} = \int_{-\infty}^{\infty} \mathbf{H}(f + f^{\mathrm{RX}})\,\mathrm{PR}(f) \times \exp(j2\pi f((l-1)T_{\mathrm{b}} + \Delta^{\mathrm{RX}}T)\mathrm{d}f \quad (2.59)$$

and

$$\mathbf{h}_l^{\mathrm{TX}} = \int_{-\infty}^{\infty} \mathbf{H}(f + f^{\mathrm{TX}})\,\mathrm{PR}(f) \times \exp(j2\pi f((l-1)T_{\mathrm{b}} + \Delta^{\mathrm{RX}}T)\mathrm{d}f \quad (2.60)$$

respectively (where $\mathrm{PR}(f)$ is the Fourier transform of $\mathrm{pr}(\tau)$).

## 2.6 Remarks

All four proposed models : GWSSUS, GAA, TU and BU were derived from a generic model which assumed that all received wave fields are reflected ones on their way between the mobile and the base, see Section

2.1. This assumption introduces a complicated dependence between the Doppler frequencies and the angle of arrivals, $\theta_n$, of the wave fields, which in turn makes it difficult to derive the Doppler spectrums of the GWSSUS and GAA models. With two reflections per ray, the Doppler frequencies can be assumed independent of the angle of arrivals, which makes it feasible to derive the Doppler spectrum, see e.g. [RDNP94, Mar96]. However, the statistics of *snapshots* of the channel are not necessarily affected by the number of reflections for each ray. In the cases where the GAA and GWSSUS models are used in the thesis, only the channel statistics and not the variations are used, and therefore the distinction is not important.

The GWSSUS model defined in [Mar96], allows for a dominant ray per cluster. In the framework of the GWSSUS model herein, this can be modeled by letting $\mathbf{v}_r$ have a deterministic mean i.e.,

$$\mathrm{E}\{\mathbf{v}_r\} = \text{ constant} \times \exp(-j2\pi f_r t)\mathbf{a}(\breve{\theta}_r, f), \tag{2.61}$$

where $f_r$ and $\breve{\theta}_r$ are the Doppler frequency and angle of arrival of the direct wave, respectively. However, situations where such terms exist are generally favorable for the approaches taken in this thesis, and they have therefore not been considered.

The derivations in this chapter assume a linear digital modulation, where the (complex) baseband signal can be described as

$$u(t) = \sum_i I_i p(t - iT_\mathrm{b}), \tag{2.62}$$

where $i$ is the symbol index, $I_i$ is the complex symbols, and $p(t)$ is the modulation pulse shape. Many standards utilize linear modulations e.g. IS54, IS136, PHS, IS95 and ANSI J-STD-008. The GSM standard and its derivatives DCS1800 and PCS1900, utilize a GMSK modulation which can be well approximated by a linear modulation. In other cases the results of this section can be used by assuming that the modulation is band limited $|f| \leq 1/(2T_\mathrm{b})$, and letting $\mathrm{pr}(t)$ be an ideal band limited pulse shape i.e.,

$$\mathrm{pr}(t) = \frac{sin(\frac{\pi t}{2T_\mathrm{b}})}{(\frac{\pi t}{2T_\mathrm{b}})}. \tag{2.63}$$

The sequence $I_i$, will then represent the modulated signal sampled at rate $1/T_\mathrm{b}$. Therefore $I_i$ will no longer be confined to a discrete set of symbols, but can attain any complex value.

# Appendix 2.A Connection Between the GAA Model and the Conventional Sensor Array Model

Assume a GAA model with one cluster i.e., $d = 1$. Let us denote the steering vector of that cluster $\mathbf{v}$ rather than $\mathbf{v}_1$ for simplicity. If $\sigma$ is reasonably small, then $\mathbf{v}$ can be approximated by a small number of manifold vectors i.e.,

$$\mathbf{v} \approx \sum_{n=1}^{\breve{d}} \varrho_n \mathbf{a}(\breve{\theta}_n, f) \tag{2.64}$$

where $\breve{\theta}_n$ is in the vicinity of the nominal direction $\theta$, see Example 2.2, and $\varrho_n$ are the complex amplitude of the steering vectors. Define the *signal waveforms* (SW) $s_{n,q}$ as

$$s_{n,q} = \sum_{l \geq 0} \varrho_n \operatorname{pr}(lT_{\mathrm{b}} + \Delta T - T_{\mathrm{b}} - \tau_r) I_{q-l} \tag{2.65}$$

Combining (2.64), (2.65), (2.2) and (2.11) yields

$$\mathbf{x}_q = \sum_{n=1}^{\breve{d}} \mathbf{a}(\breve{\theta}_n) s_{n,q} + \mathbf{n}_q, \tag{2.66}$$

where additive noise $\mathbf{n}_q$ has been introduced. Of course (2.66) can be extended with signals from multiple mobiles, and multiple clusters per mobile by adding more terms. The model (2.66) is the model frequently used in the literature on direction estimation, see e.g. [Orf90, OVK92, RPK86, Sch79, SS90]. Equation (2.66) can be written in a more compact form as

$$\mathbf{x}_q = \mathbf{A}(\breve{\theta}) \mathbf{s}_{n,q} + \mathbf{n}_q \tag{2.67}$$

where

$$\breve{\boldsymbol{\theta}} = [\breve{\theta}_1, \ldots, \breve{\theta}_{\breve{d}}] \tag{2.68}$$

$$\mathbf{A}(\breve{\boldsymbol{\theta}}) = [\mathbf{a}(\breve{\theta}_1), \ldots, \mathbf{a}(\breve{\theta}_{\breve{d}})] \tag{2.69}$$

$$\mathbf{s}_q = [s_{q,1}, \ldots, s_{q,\breve{d}}]^T. \tag{2.70}$$

It is commonly assumed that the noise is zero-mean, circular symmetric spatially white i.e. and independent of $s_{n,q}$ i.e

$$\begin{aligned} \mathrm{E}\{n_{k,q}n_{l,q}^*\} &= \sigma_n^2\delta_{kl} \\ \mathrm{E}\{n_{k,q}n_{l,q}^T\} &= 0 \\ \mathrm{E}\{\mathbf{s}_q\mathbf{n}_q^*\} &= \mathbf{0} \\ \mathrm{E}\{\mathbf{s}_q\mathbf{n}_q^T\} &= \mathbf{0} \end{aligned} \tag{2.71}$$

With these assumptions, the covariance matrix of $\mathbf{x}_q$ can be written

$$\mathbf{R}_{xx} = \mathrm{E}\{\mathbf{x}_q\mathbf{x}_q^*\} \tag{2.72}$$

$$= \mathbf{A}(\breve{\boldsymbol{\theta}})\mathbf{S}\mathbf{A}^*(\breve{\boldsymbol{\theta}}) + \sigma_n^2\mathbf{I} \tag{2.73}$$

where $\mathbf{I}$ is an $m \times m$ identity matrix and $\mathbf{S}$ is the signal waveform covariance matrix defined by

$$\mathbf{S} = \mathrm{E}\{\mathbf{s}_q\mathbf{s}_q^*\}. \tag{2.74}$$

The expectations in (2.72) and (2.74) are over the realizations of the signals $\mathbf{s}_q$ only and *not* over the fast or slow fading.

**Example 2.2**

In order to quantify the error in the approximation (2.64) the measure

$$\frac{\epsilon}{\|\mathbf{v}\|^2} \tag{2.75}$$

where $\epsilon$ is given by

$$\epsilon^2 = \min_{\varrho_n, \breve{\theta}_n} \|\mathbf{v} - \sum_{n=1}^{\breve{d}} \varrho_n \mathbf{a}(\breve{\theta}_n)\|^2, \tag{2.76}$$

and $\|\cdot\|^2$ denotes the Frobenius norm, will be used. It is possible to minimize $\epsilon^2$ explicitly over $\varrho_n$, yielding

$$\epsilon^2 = \min_{\breve{\boldsymbol{\theta}}} \mathrm{Trace}\{\mathbf{P}_{\mathbf{A}}^{\perp}(\breve{\boldsymbol{\theta}})\mathbf{v}\mathbf{v}^*\} \tag{2.77}$$

where $\mathbf{P}_{\mathbf{A}}^{\perp}(\breve{\boldsymbol{\theta}})$ is given by

$$\mathbf{P}_{\mathbf{A}}^{\perp}(\breve{\boldsymbol{\theta}}) = \mathbf{I} - \mathbf{A}(\breve{\boldsymbol{\theta}})(\mathbf{A}^{*}(\breve{\boldsymbol{\theta}})\mathbf{A}(\breve{\boldsymbol{\theta}}))^{-1}\mathbf{A}(\breve{\boldsymbol{\theta}}). \tag{2.78}$$

For uniform linear arrays i.e., arrays for which $\mathbf{a}(\theta, f)$ is given by (2.4) the minimization in (2.77) can be solved efficiently using the IQML technique introduced in [BM86]. In Figure 2.3 below, the probability that

$$\epsilon^2/|\mathbf{v}|^2 < 0.01, \tag{2.79}$$

is been plotted as a function of of the number of rays, $d$. The probabilities are obtained from 200 Monte-Carlo runs in each case. The number of antennas used in the simulation is nine, $m = 9$, the antenna spacing is 0.4 wavelengths, and mobile is located at broadside i.e., $\theta$=0$^o$. The plot shows that a two ray model is sufficient to model 99% of the energy in more than 80% of the cases if $\sigma \leq 3^o$.

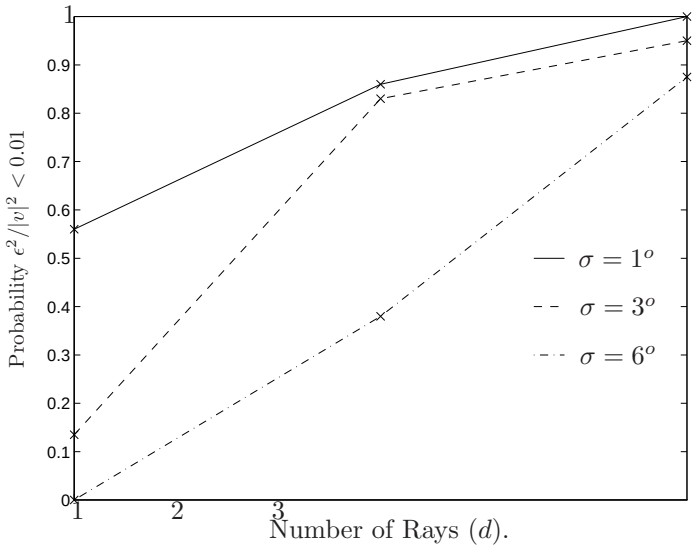


Figure 2.3: *Approximation with a finite number of rays.*

# Appendix 2.B Thorough Development of the Basic Assumptions

This section contains a more in-depth derivation of the basic assumptions introduced in Section 2.1.

## 2.B.1 Uplink

We assume that the radio wave propagation between the $m$ base station antennas with the single mobile antenna is propagating via $N$ scatterers, see Figure 2.4.

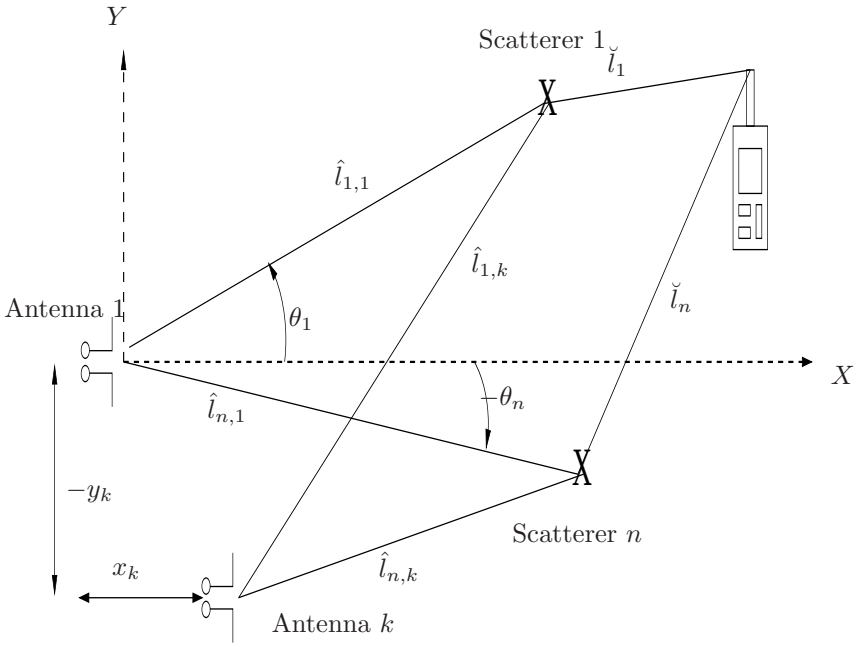


Figure 2.4: *Schematic illustration of multipath model. Note that the scatterers are assumed to be in the far field.*

It is further assumed that if the signal $\tilde{u}^{\mathrm{TX}}(t)$ is applied to the mobile antenna, the signal received in the $k$th base antenna is

$$\tilde{x}_k^{\mathrm{RX}}(t) = \sum_{n=1}^{N} \tilde{h}_n \tilde{u}^{\mathrm{TX}}(t - \frac{l_{n,k}}{c}) * \tilde{a}_k(\theta_n, t) \tag{2.80}$$

where $N$ is the number of scatterers, $\tilde{h}_n$ is a reflection gain, $c$ is the speed of light $\approx 3 \times 10^8$m/s, $l_{n,k} = \hat{l}_{n,k} + \breve{l}_n$ is the propagation distance between the mobile and base station antenna $k$ for the $n$th ray, $\theta_n$ is the azimuth angle of the $n$th ray, $\tilde{a}_k(\theta, t)$ is the impulse response of the $k$th antenna element in azimuth direction $\theta$, and $*$ is the convolution operator. The geometry of the considered situation is illustrated in Figure 2.4. The modulated signal (the signal transmitted over the air) transmitted from the mobile is assumed to be given by

$$\begin{aligned}\tilde{u}^{\mathrm{TX}}(t) &= Re\{\exp(j2\pi f^{\mathrm{RX}} t + \beta^{\mathrm{RX}}) \sum_i I_i p(t - iT_{\mathrm{b}})\} \\ &= |\sum_i I_i p(t - iT_{\mathrm{b}})| \cos(2\pi f^{\mathrm{RX}} t + \beta^{\mathrm{RX}} + \angle(\sum_i I_i p(t - iT_{\mathrm{b}}))) \end{aligned} \tag{2.81}$$

where $f^{\mathrm{RX}}$ is the uplink frequency, $i$ is the symbol/bit index, $I_i$ is the $i$th symbol drawn from some discrete set of complex numbers, $p(t)$ is the modulation pulse shape, $T_{\mathrm{b}}$ is the inter-symbol time and $\beta$ is some unknown phase offset. At the base the received signals are multiplied by $\exp(-j2\pi f^{\mathrm{RX}} t)$ followed by low pass filtering and sampling at symbol rate. Assuming sampling at $t = (q-1)T + \Delta T^{\mathrm{RX}}$, $\Delta T^{\mathrm{RX}} \in [0, T_{\mathrm{b}})$ equation (2.80) and (2.81) yield (after extensive derivations)

$$\begin{aligned} x_k^{\mathrm{RX}}(qT_{\mathrm{b}} + \Delta T^{\mathrm{RX}} - T_{\mathrm{b}}) &= (\tilde{x}_k^{\mathrm{RX}}(t) \exp(-j2\pi f^{\mathrm{RX}} t)) * h_r(t) \\ &\qquad \text{where } t = (q-1)T_{\mathrm{b}} + \Delta T^{\mathrm{RX}} \\ &= \sum_{i,n} \tilde{h}_n a_k^{\mathrm{RX}}(\theta, f^{\mathrm{RX}}) \exp(-j2\pi f^{\mathrm{RX}} \frac{l_{n,k}}{c} + \beta^{\mathrm{RX}}) \\ &\qquad \times \mathrm{pr}(qT_{\mathrm{b}} + \Delta T^{\mathrm{RX}} - T_{\mathrm{b}} - \frac{l_{n,k}}{c} - iT_{\mathrm{b}}) I_i \end{aligned} \tag{2.82}$$

where $\mathrm{pr}(t)$ is the convolution of the pulse shape $p(t)$ and the receiver filter $h_r(t)$, and $a(\theta, f)$ is the Fourier transform of the antenna transfer function $\tilde{a}_k(\theta, t)$. Since the distance between the antennas is only a few wavelengths $\mathrm{pr}((q-1)T_{\mathrm{b}} + \Delta T^{\mathrm{RX}} - \frac{l_{n,k}}{c} - iT_{\mathrm{b}}) = \mathrm{pr}((q-1)T_{\mathrm{b}} + \Delta T^{\mathrm{RX}} - \frac{l_{n,1}}{c} - iT_{\mathrm{b}})$ and we may write

$$x_k^{\mathrm{RX}}(qT_\mathrm{b} + \Delta T^{\mathrm{RX}} - T_\mathrm{b}) = \sum_{l,n} \tilde{h}_n a_k(\theta, f^{\mathrm{RX}}) \exp(-j2\pi f^{\mathrm{RX}} \frac{l_{n,k}}{c} + \beta^{\mathrm{RX}})$$
$$\times \mathrm{pr}(lT_\mathrm{b} + \Delta T^{\mathrm{RX}} - T_\mathrm{b} - \frac{l_{n,1}}{c}) I_{q-l} \quad (2.83)$$
$$= \sum_{l \geq 0} h_k(lT_\mathrm{b} + \Delta T^{\mathrm{RX}} - T_\mathrm{b}) I_{q-l} \quad (2.84)$$

where

$$h_k(\tau) =$$
$$\sum_n \tilde{h}_n a_k(\theta_n, f^{\mathrm{RX}}) \exp(-j2\pi f^{\mathrm{RX}} \frac{l_{n,k}}{c} + \beta^{\mathrm{RX}}) \,\mathrm{pr}(\tau - \frac{l_{n,1}}{c}). \quad (2.85)$$

Since the position of the $k$th antenna is $(x_k, y_k)$ relative to antenna 1, and all scatterers are in the far field, the relationship

$$l_{n,k} = l_{n,1} - y_k \sin(\theta_n) - x_k \cos(\theta_n) \quad (2.86)$$

is valid. Using (2.86) and defining

$$\mathbf{x}_q^{\mathrm{RX}} = [x_1^{\mathrm{RX}}(qT_\mathrm{b} + \Delta T - T_\mathrm{b}), \ldots, x_m^{\mathrm{RX}}(qT_\mathrm{b} + \Delta T - T_\mathrm{b})]^T \quad (2.87)$$
$$\mathbf{a}^{\mathrm{RX}}(\theta, f) = [a_1(\theta, f), \ldots \exp(j2\pi f(y_2 \sin(\theta) + x_2 \cos(\theta))/c) a_2(\theta, f), \ldots,$$
$$\exp(j2\pi f(y_m \sin(\theta) + x_m \cos(\theta))/c) a_m(\theta, f)]^T \quad (2.88)$$

(2.84) and (2.85) may be given in vector notation as

$$\mathbf{x}_q^{\mathrm{RX}} = \sum_{l \geq 0} \mathbf{h}_l^{\mathrm{RX}} I_{q-l} \quad (2.89)$$

where $q$ is the sample number, $T_\mathrm{b}$ is the symbol time, $\Delta T^{\mathrm{RX}}$ is the sampling phase and the multidimensional impulse response $\mathbf{h}_l^{\mathrm{RX}}$ is given by

$$\mathbf{h}_l^{\mathrm{RX}} = \sum_n \tilde{h}_n \exp(-j2\pi f^{\mathrm{RX}} \frac{l_n}{c} + \beta^{\mathrm{RX}}) \times$$
$$\mathrm{pr}(lT_\mathrm{b} + \Delta T^{\mathrm{RX}} - T_\mathrm{b} - \frac{l_n}{c}) \mathbf{a}(\theta_n, f^{\mathrm{RX}}), \quad (2.90)$$

where $l_n = l_{n,1}$.

### 2.B.2 Downlink

In the downlink the base transmits signals of the form (2.81) on each of the antenna inputs. However, each antenna element is given an individual complex weight $w_k$ i.e., the signal transmitted on the $k$th element is given by

$$\tilde{x}_k^{\mathrm{TX}}(t) = Re\{w_k^c \exp(j2\pi f^{\mathrm{RX}} t) \sum_i I_i p(t - iT_{\mathrm{b}})\} \tag{2.91}$$

where the complex conjugate $(\cdot)^c$, is introduced for notational convenience later. Assuming reciprocity the signal obtained at the mobile after low-pass filtering and sampling is given by

$$u_q^{\mathrm{RX}} = \mathbf{w}^*(\sum_{l\geq 0} \mathbf{h}_l^{\mathrm{TX}} I_{q-l}) \tag{2.92}$$

where $\mathbf{w} = [w_1, \ldots, w_m]^T$ and $\mathbf{h}_l^{\mathrm{TX}}$ is given by (2.90), with RX replaced by TX in all places.

### 2.B.3 Influence of Mutual Coupling

The derivations above assumed no mutual coupling. However, it is easily shown that (2.90) and (2.92) are valid also with mutual coupling. However, in that case the expression for $\mathbf{a}(\theta, f)$ (equation (2.88)) should be changed to

$$\begin{aligned}\mathbf{a}(\theta, f) = \mathbf{Z}^{\mathrm{RX}}(\theta, f)[a_1(\theta, f), \exp(j2\pi f(y_2 \sin(\theta) + x_2 \cos(\theta))/c) a_2(\theta, f),\\ \ldots, \exp(j2\pi f(y_m \sin(\theta) + x_m \cos(\theta))/c) a_m(\theta, f)]^T,\end{aligned} \tag{2.93}$$

where $\mathbf{Z}^{\mathrm{RX}}(\theta, f)$ is the mutual coupling matrix. Element $k, l =$ ( row , column ) of this matrix contains the coupling from antenna $l$ to antenna $k$ at frequency $f$. This applies both to the up- and down link of course, although the mutual coupling matrices may be different for the two links.

# Appendix 2.C Thorough Derivation of the Proposed TU and BU Models

This section defines the TU and BU models using the framework of the previous section. A briefer description is given in Section 2.4. The first model is aimed to be consistent with the typical urban GSM-TU model defined in [GSM92]. The second model is aimed at modeling environments with reflectors such as towers, large buildings and hills, and other obstacles which are not in the vicinity of the mobile.

## 2.C.1 The Typical Urban (TU) Model

The propagation is assumed to be built up by 120 paths (i.e., $N = 120$ in the framework of previous section). The position of these paths are assumed constant during the time over which the mobile moves five meters. The starting point of the five meter journey defines the origin of a coordinate system $(x\prime, y\prime)$. The $x\prime$-axis of this coordinate system is oriented in the radial direction seen from the base station, as illustrated in Figure 2.5.

The positions of the scatterers are oriented with respect to the $(x\prime, y\prime)$ coordinate system and their positions are listed in Table 2.1 of the Appendix 2.G. The positions of the scatterers relative to the mobile are also illustrated in Figure 2.6 below. After the mobile has moved five meters the $x\prime, y\prime$ coordinate system is redefined according to the starting point of the next five meter section, and the scatterers are moved accordingly. However, in order not to experience the same fast fading realization in each five meter section, the scatterers are given a random displacement in a two by two meter area (in $x\prime$ and $y\prime$ coordinates) from the position listed in Table 2.1. This displacement is re-randomized for each five meter journey. The amplitude of the scatterers ($\tilde{h}_n$ in the framework of Section 2.B), are decomposed into three factors: path loss, shadowing, and reflection gain. The path loss and the shadowing are common to all the scatterers. The path loss is modeled as $(1/r)^{\gamma/2}$ where $\gamma$ is the path loss exponent $\gamma = 3.5$, and $r$ is the distance between the base and the mobile, see Figure 2.5. The shadowing is modeled by a factor $L^{1/2}$ which has log-normal distribution . This means that $10\log(L)$ is normally distributed with mean zero and standard deviation $\sigma_{\mathrm{L}} = 8\mathrm{dB}$. The reflection gain $\breve{h}_n^2$ are used to distribute the energy among the scatterers. This parameter is listed in Table 2.1 for each reflection. The reflection gains are normalized such that

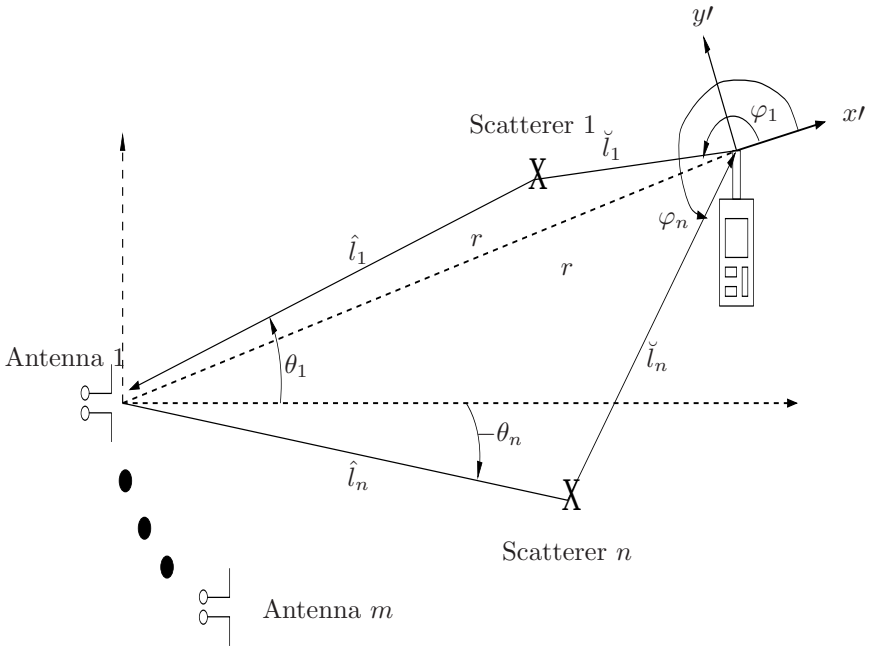


Figure 2.5: *Schematic illustration of multipath model. Note that the scatterers are assumed to be in the far field.*

$$\sum_{n=1}^{N} \breve{h}_n^2 = 1. \tag{2.94}$$

Thus, we have

$$\tilde{h}_n = G^{1/2} \breve{h}_n. \tag{2.95}$$

where

$$G = (1/r)^{\gamma} L. \tag{2.96}$$

The shadowing is held fixed during the five meters of motion. At the next five meter journey, the shadowing is updated as

$$[10\log(L)]_{\text{new}} = \exp(-di/dc)[10\log(L)]_{\text{old}} + \sqrt{1-\exp(-2di/dc)}\xi \quad (2.97)$$

where $di$ is the distance between the starting point of the two five meter sections, $dc$ is the so-called correlation distance, and $\xi$ is an independent normally distributed random variable with mean zero and standard deviation $\sigma_{\text{L}}$.

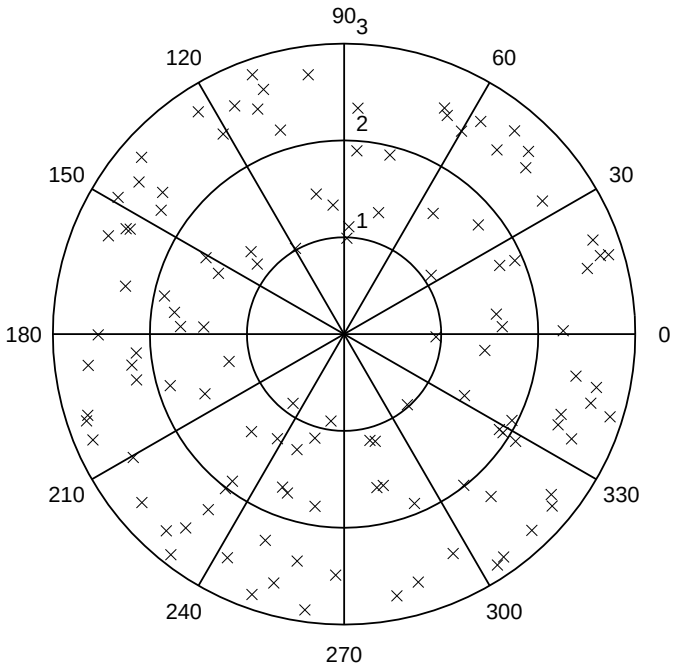


Figure 2.6: *Position of the scatterers relative to the mobile. The zero and ninety degree direction in the plot correspond to the x′ and y′ axis respectively. The radial distances are logarithmic. The radius of the inner circle is* $10m$*, the radius of middle circle is* $100m$ *and the radius of the outer circle is* $1000m$*.*

### 2.C.2 The Bad Urban (BU) Propagation Model

The bad urban (BU) model is generated similar to the (TU) model, i.e., the positions of the scatterers are assumed constant for the time during which the mobile moves five meters. A difference is that while in the TU case, the starting point of the five meter journey defines *one* coordinate system, the starting point now defines *two* coordinate systems, $(x'_1, y'_1)$ and $(x'_2, y'_2)$. Coordinate system 1 is identical to the coordinate system in the TU case while the other is rotated 45 degrees with respect to the base. This means that the origin of the second coordinate systems is at the same distance from the base as the first but with a 45 degree offset counter-clock-wise, as illustrated in Figure 2.C.2. The positions of scatterers are distributed according to Table 2.1 of the Appendix, in *both* coordinate systems, yielding at total of $N = 240$ scatterers in the framework of Section 2.B. As in the TU case, the two coordinate systems and the scatterers are moved when the mobile has moved five meters and starts a new five meter section. The scatterers are also given a random displacement in a two by two meter area from their nominal position listed in Table 2.1, as in the TU case. This displacement is re-randomized for each five meter journey, and is independent for all $N = 240$ scatterers. The gains of the scatterers in the two clusters $\tilde{h}_{1,n}$ and $\tilde{h}_{2,n}$ are given by

$$\tilde{h}_{i,n} = G_i^{1/2} \breve{h}_n, \tag{2.98}$$

where

$$G_i = (1/r)^{\gamma} L_i g_i \tag{2.99}$$

and $i = 1, 2$. The factor $(1/r)^{\gamma}$ is defined as in the TU case. The shadowing of the two clusters ($L_1$ and $L_2$) are both log-normally distributed, independent and updated according to (2.97). The factors $g_1$ and $g_2$ distribute the total power among the two clusters. There are no measurements available (known to the author) of typical $g_1$ and $g_2$ values. We have therefore arbitrarily chosen $g_1 = 1$ and $g_2 = 10^{-0.5}$ i.e., the second cluster is 5dB weaker than the cluster at the mobile (in average). This in implies that the probability of the second cluster being stronger than the first is 30%. The probability of $10\log(L_1 g_1) - 10\log(L_2 g_2)$ being in the range $[-5, 5] dB$ is 31%.

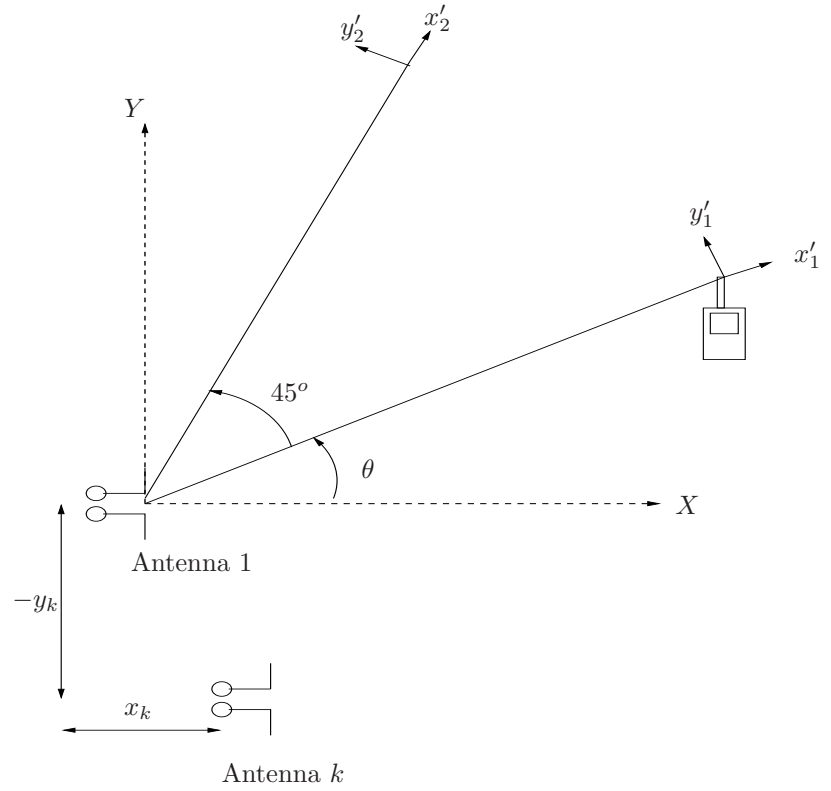


Figure 2.7: *Schematic illustration of the coordinate systems involved in the BU model.*

### 2.C.3 Implementation

The following section describes an implementation of the TU and BU models for the DCS1800 standard, [MP92, Ste92]. This implementation is utilized in the simulations in Chapter 6 The mobile is assumed to make a circumferential route in a sector specified as input to the routine. The route is divided into five meter sections interleaved by "jumps" with a length specified as input to the routine. The path loss exponent used is $\gamma = 3.5$, the log-normal standard deviation is $\sigma_{\mathrm{L}} = 8dB$ and the correlation distance $dc$ is 110 meter.

Of the eight timeslots of the TDMA frame of GSM the mobile is

active in two, one downlink and one uplink timeslot. The delay between the downlink timeslot and the subsequent uplink timeslot is two timeslots. The implementation uses a spacing between the bursts of 4cm for both up- and downlink i.e., the mobile is assumed to travel 4cm between two consecutive uplink timeslots. The time between two uplink timeslots is 4.6ms. Thus the mobile speed is assumed to be $4/0.46 * 3.6 =\approx 30$km/h. The delay between an uplink and the corresponding downlink timeslot is 2.8ms, which corresponds to a spacing of 2.5cm. With the position of the mobile known the distance to each scatterer (120 scatters in the TU case and 240 in the BU case) $l_{n,1}$ is calculated. The direct path delay $r/c$ is subtracted from each path to remove unnecessary delay. The phase offset of the carrier $\beta$ is randomized uniformally $[0, 2\pi]$. The frequency of the up- and downlink are specified by the input. If multiple frequencies are provided for up- and downlink, one of them is chosen randomly for each timeslot. This option is used when frequency hopping is considered. With these quantities determined, the multidimensional impulse response is calculated using (2.90) and (2.95) for the up- and downlink frequencies. The function $\mathrm{pr}(t)$ is calculated using a lookup table, with a resolution of ten times the bit rate. The error introduced by the time quantization is less than $-20$dB. The estimated impulse response is stored in a file. The number of taps stored is chosen to capture at least 99% of the total energy. The process described is repeated for each timeslot until the mobile has moved five meter. Then the mobile moves a distance specified by the "jump" parameter. The jump is made circumferentially. After this the log-normal fading is updated and another five meters can be generated.

# Appendix 2.D Properties of the Proposed TU and BU Propagation Models

By means of simulations it is shown that the proposed TU model is similar to the GSM-TU model with respect to power-delay-profile (exponential), short-term-narrow-band-power-distribution
(Rayleigh), and Doppler spectrum (Classical). We believe that this is sufficient to state that the temporal properties of the proposed TU and the GSM-TU model are equivalent for practical purposes . An example in section 2.D.3 also shows the reasonable frequency correlation properties of the proposed model. Finally, an example in section 2.D.5 shows that the azimuth power distribution of the model is approximately Gaussian as seen from the base. The properties derived for the TU model are valid also for the BU model with obvious modifications.

## 2.D.1 Temporal Properties

One of the goals with the TU model is that it should have properties similar to the GSM-TU model defined in [GSM92]. A commonly used entity when investigating the temporal properties of fading channels is the power delay profile. This entity is defined as

$$P(\tau) = \mathrm{E}\{|h(\tau)|^2\}, \tag{2.100}$$

where the expectation theoretically should be over the fast fading. We restrict $h(\tau)$ in (2.100), to be the response of the physical channel between the mobile antenna and a single omni-directional antenna at the base. Thus $h(\tau)$ is given by (2.54) or (2.55) with $\mathbf{a}(\theta_n, f^{\mathrm{RX}}) = 1$ Thus $h(\tau)$ is a scalar. In Figure 2.8 below the power delay profile is plotted for the proposed model (upper) and the GSM-TU profile (lower) respectively. For both models the impulse response of the channel has been convolved with an ideal bandlimited 1MHz pulse: $\mathrm{pr}(\tau) = sin(\pi B\tau)/(B\pi\tau), B =$ 1MHz. Thus the curves shown represent the convolution of $P(\tau)$ with $|\,\mathrm{pr}(\tau)|^2$. As can be seen in Figure 2.8 the profiles of the two models are very similar. Furthermore, the average rms delay spread is defined as

$$\sigma_\tau = \int_{\tau=0}^{\infty} \frac{P(\tau)}{P_{\mathrm{tot}}} (\tau - \bar{\tau})^2 \tag{2.101}$$

where

$$P_{\text{tot}} = \int_{\tau=0}^{\infty} P_{\text{tot}}(\tau) \tag{2.102}$$

$$\bar{\tau} = \int_{\tau=0}^{\infty} \frac{P(\tau)}{P_{\text{tot}}} \tau \tag{2.103}$$

is 1.071$\mu$s in the proposed model, while it is 1.026$\mu$s in the TU model of [GSM92], i.e., very close.

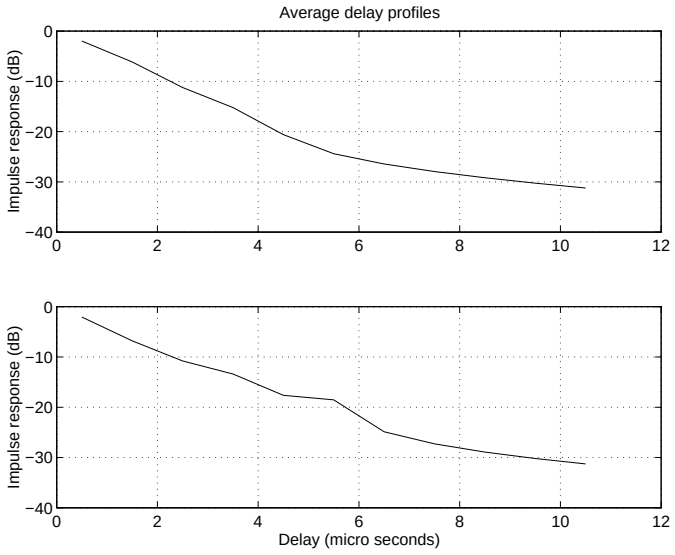


Figure 2.8: *The temporal distribution of power: Average delay profile. Upper: proposed Typical Urban (TU). Lower: GSM typical urban (GSM-TU).*

### 2.D.2 Amplitude Distributions

Due to the many scatterers, the proposed model produces a Rayleigh fading channel if a narrow frequency interval is considered. This is illustrated in Figure 2.9 below, where a histogram of the $|H(f,t)|$ (See Section 2.5.2) values obtained from simulations using $f = 1710$MHz are shown. In these simulations the mobile is moved two times five meters.

However, the path loss and shadowing is removed and thus the average power is 1, due to the normalization (2.94). The simulations also assume a 2km distance between the base and the mobile, a carrier frequency of 1710MHz, and a single omni directional antenna at the base.

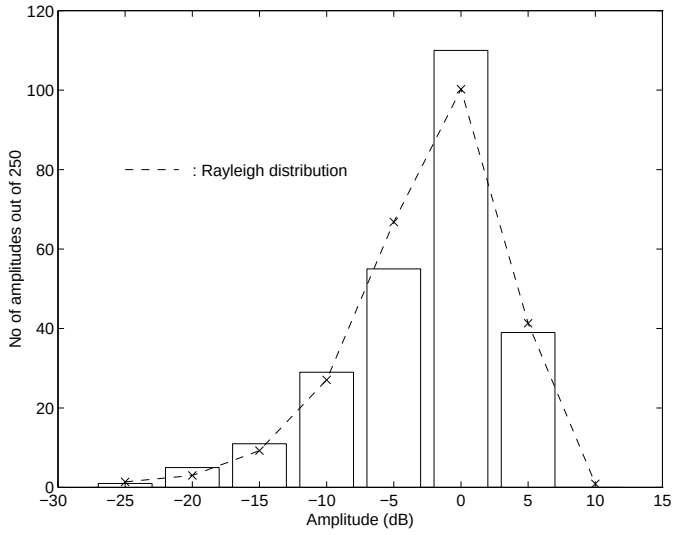


Figure 2.9: *Amplitude distribution on a carrier frequency*

### 2.D.3 Frequency Correlation

In Section 2.5.2, the correlation coefficient $c_{r,e}(\Delta t, f_1, f_2)$ was introduced. A very similar entity, we refer to as "envelope correlation coefficient", may be defined as

$$rc_{r,e}(\Delta t, f_1, f_2) = \frac{\frac{1}{T}\int_{t=0}^{T}(|[\mathbf{H}^{\mathrm{RX}}(f_1, t+\Delta t)]_r| - m_1)(|[\mathbf{H}^{\mathrm{TX},*}(f_2, t)]_e| - m_2)\mathrm{d}t}{\sqrt{v_1 v_2}}, \quad (2.104)$$

where

$$m_1 = \frac{1}{T}\int_{t=0}^{T} |[\mathbf{H}^{\mathrm{RX}}(f_1, t+\Delta t)]_r| \mathrm{d}t \tag{2.105}$$

$$m_2 = \frac{1}{T}\int_{t=0}^{T} |[\mathbf{H}^{\mathrm{TX}}(f_2, t)]| \mathrm{d}t \tag{2.106}$$

$$v_1 = (\frac{1}{T}\int_{t=0}^{T} (|[\mathbf{H}^{\mathrm{RX}}(f_1, t+\Delta t)]_r| - m_1)^2 \mathrm{d}t \tag{2.107}$$

$$v_2 = \frac{1}{T}\int_{t=0}^{T} (|[\mathbf{H}^{\mathrm{TX}}(f_2, t)]_e|^2 - m_2) \mathrm{d}t \tag{2.108}$$

and $T$ is chosen correspondingly as in (2.58).

The coefficient $rc_{r,e}(\Delta t, f_1, f_2)$ has been estimated from a simulation of two times five meter mobile movement using different values of $f_2$. The results are shown in Figure 2.10. In fact, the frequencies investigated correspond to the carrier frequencies defined in DCS1800. Both antennas are assumed omni directional. The upper and lower subfigures are obtained by processing the first and the second five meters sections separately. It should be noted that the results here are not directly comparable to those of Appendix 2.F, since the complex correlation coefficient defined by (2.58) is used there. However the following approximate relationship is valid between $rc_{r,e}(\Delta t, f_1, f_2)$ and $c_{r,e}(\Delta t, f_1, f_2)$

$$|rc_{r,e}(\Delta t, f_1, f_2)| \approx |c_{r,e}(\Delta t, f_1, f_2)|^2, \tag{2.109}$$

see [Cla68]. Thus, the $|c_{r,e}(\Delta t, f_1, f_2)| = 0.3$ threshold used as a rule of thumb for independence in Appendic 2.F, implies an equivalent threshold of $|rc_{r,e}(\Delta t, f_1, f_2)| = 0.09$. The mean level of $|rc_{r,e}(\Delta t, f_1, f_2)| = 0.09$ between 9 and 11MHz, in Figure 2.10, is 0.08 and thus below the threshold. For larger frequency differences, similar values are obtained. It is therefore concluded that the up- and downlink carriers are practically uncorrelated when the frequency distance is larger that 10MHz.

### 2.D.4 Doppler Spectrums

The so-called Doppler spectrum may be defined as

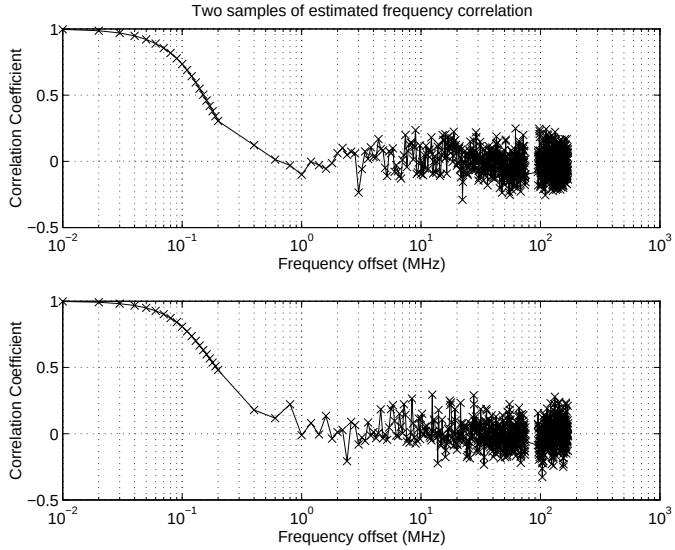


Figure 2.10: *Envelope correlation coefficient between carriers. The real correlation coefficient* $rc_{r,e}(\Delta t, f_1, f_2)$*, as a function of* $f_2 - f_1$ *using* $f_1 = 1710MHz$ *and* $\Delta t = 0$*. The frequencies investigated correspond to the carrier frequencies of DCS1800.*

$$\text{Doppler}(f_d) = \int_{\Delta x=-\infty}^{\infty} \text{E}\{H(f,x)H^*(f,x+\Delta x)\}\exp(-j2\pi f_d \Delta x)\text{d}\Delta x \quad (2.110)$$

where $H(f,x)$ is the transfer function of a single omni-directional antenna when the mobile is in location $x$, and the expectation is over the fast fading. Thus, with this definition $f_d$ is a spatial, rather than temporal frequency. The Doppler spectrum is estimated from the same simulation as in Section 2.D.2. Since $H(f,x)$ is a function of the mobile position, $x$, the frequency of $f_d$ is meter$^{-1}$. In theory, the highest possible frequency is $f_d = f/c$ where $f$ is the carrier frequency (Hz), and $c$ is the speed of light $\approx 3 \times 10^8$m/s. In Figure 2.11 two Doppler spectra estimates are shown in the upper and lower part of the figure. The two spectra correspond to the two five meter sections simulated. The spectras was cal-

culated from samples of the channel $H(f, x)$ spaced 4cm. The frequency unit (on the x-axis) has been normalized to the theoretical maximum Doppler frequency. The figure also shows the classical Doppler spectrum $(1 - (f_d(\frac{c}{f}))^2)^{-1/2}$, $|f_d| \leq \frac{c}{f}$, which is used in the GSM-TU propagation model, see [GSM92]. The figure indicates that the two spectra are close enough so that the short-term channel variations of the proposed model for practical purposes are the same as those obtained with the classical Doppler spectrum.

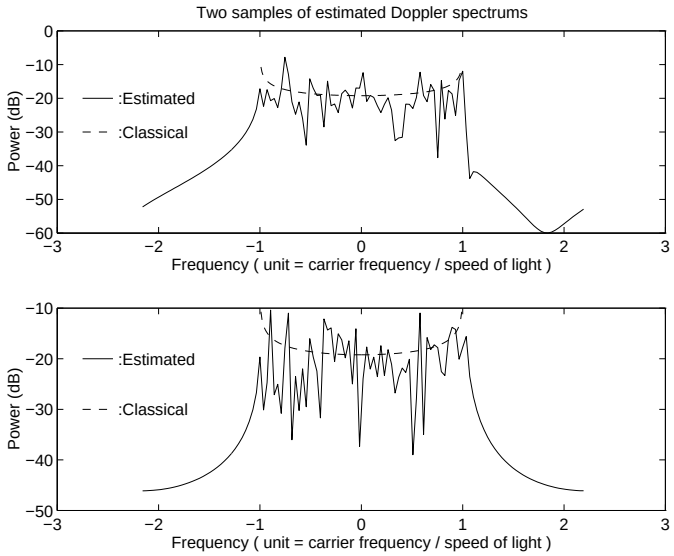


Figure 2.11: *Doppler spectrum induced by the proposed model.*

### 2.D.5 Angle of Arrival Spectrum

The performance gain of a smart antenna system is heavily dependent on the angular distribution of the energy received at the base. In order to investigate the angular power distribution of the proposed model, the scatterers are divided into groups with azimuth angles within [ $-40^o$, $30^o$], [$-30^o$, $20^o$], ..., [$-30^o$,$40^o$] respectively. The power of the scatterers within group each group is calculated as

$$\sum_{n \in \text{considered group}} \breve{h}_n^2, \tag{2.111}$$

where $\breve{h}_n^2$ is defined in Section 2.C.1. The results of two such calculations are shown in Figure 2.12 below, where base to mobile distances of 1km and 2km are applied in the upper and lower subfigure, respectively. The value on the x-axis is the center point of the angular scan of the corresponding group, and the y-axis is the fraction of the total power within the group. For comparison a Gaussian distribution has been plotted in the upper and lower subfigure. In the upper case a five degree standard deviation is applied while the lower uses ten degrees. The Gaussian distribution is plotted such that the points in the plot correspond to the integral of the Gaussian distribution corresponding to the angular scan of the group.

From Figure 2.12 we deduce that the Gaussian distribution is a good approximation of the proposed model using ten degrees resolution. With finer resolution the Gaussian model fits worse. However, it should be possible to compare results obtained with the proposed TU model with results obtained using a Gaussian scattering model, provided that the beamwidth of the antenna array is ten degrees or more.

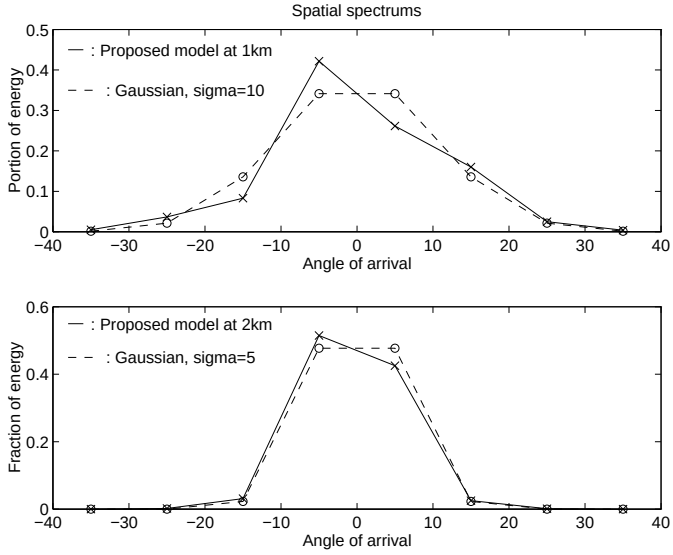


Figure 2.12: *Comparison of angle of arrival distribution of the proposed model and the Gaussian model.*

# Appendix 2.E Mixing Model and Measurement Data

In Chapter 6 simulations are performed where some signals are generated using measured impulse responses, and others are generated using the TU propagation model. In these simulations there is a problem of choosing the constant with which to multiply the measured impulses, in order to obtain compatible scaling. In order to select this factor the assumption that the received power (per symbol) averaged over fast fading (typically estimated as an average over ten wavelengths of mobile motion) is given by

$$\mathrm{E}\{\int_{\tau=0}^{\infty} \|\mathbf{h}(\tau)\|^2 \mathrm{d}\tau\} = b(1/r)^{\tilde{\gamma}} \tilde{L} \|\mathbf{a}(\theta, f)\|^2 \tag{2.112}$$

where $b$ and $\tilde{\gamma}$ are generally unknown constants. The shadowing factor $\tilde{L}$ is assumed to be zero mean in the log-domain i.e., $\mathrm{E}\{\log(\tilde{L})\} = 0$. The factor $\|\mathbf{a}(\theta, f)\|^2$ is a factor resulting from the directivity of the base an-

tennas in the direction $\theta$ of the mobile. For the TU model the parameters $\tilde{\gamma} = \gamma$ and $c = 1$ apply. When adding the TU model with measured data the measured data impulse responses may be multiplied with the factor $b^{-1/2} r^{(\tilde{\gamma}-\gamma)/2}$ which makes the measured data compatible with the TU data. This however, requires $c$ and $\tilde{\gamma}$ to be known. These constants are estimated as follows: The route driven by the mobile is divided into sections of length corresponding to ten wavelengths and the mean received power (i.e., the left hand side of (2.112) is estimated repeatedly. The distance $r$ and angle $\theta$ are logged for each section. The constants $\tilde{\gamma}$ and $c$ are then estimated by using a linear least squares fit in the logarithmic domain.

When BU and TU models are mixed, the BU data may be treated as measured data, in order to make it compatible with the TU model.

## Appendix 2.F Frequency Separation for Uncorrelated Up- and Downlink

In this section the frequency corrrelation coefficient defined by (2.58) is investigated as a function of $|f_1 - f_2|$ and $\Delta t$, assuming the GAAO model. The coefficient is shown to be smaller than 0.3 if $|f_1 - f_2| >$ 10Mhz. We regard this correlation as negligable. Applying (2.56-2.57) in the nominator of (2.58) yields

$$\begin{aligned}
&\frac{1}{T}\int_{t=0}^{T}[\mathbf{H}^{\mathrm{RX}}(f_1, t+\Delta t)]_r[\mathbf{H}^{\mathrm{TX},*}(f_2,t)]_e \mathrm{d}t = \\
&\sum_{n=1}^{N}\sum_{\tilde{n}=1}^{N}(\tilde{h}_n\tilde{h}_{\tilde{n}}\exp(-j2\pi\frac{l_{n,0}f_1 - l_{\tilde{n},0}f_2}{c})[\mathbf{a}^{\mathrm{RX}}(\theta_n,f_1)]_r[\mathbf{a}^{\mathrm{TX},*}(\theta_{\tilde{n}},f_2)]_e \\
&\qquad\qquad \times \exp(+j2\pi\frac{v}{c}\cos(\phi_n)\Delta t f_1 + \beta^{\mathrm{RX}} - \beta^{\mathrm{TX}}) \\
&\qquad\qquad \times \frac{1}{T}\int_{t=0}^{T}\exp(j2\pi\frac{v}{c}(\cos(\phi_n)f_1 - \cos(\phi_{\tilde{n}})f_2)t)\mathrm{d}t). \quad (2.113)
\end{aligned}$$

Assuming that the angles $\phi_n$ are distinct yields

$$\frac{1}{T}\int_{t=0}^{T}\exp(j2\pi\frac{v}{c}(\cos(\phi_n)f_1 - \cos(\phi_{\tilde{n}})f_2)t)\mathrm{d}t \approx 0, \quad (2.114)$$

when $n \neq \tilde{n}$. Inserting (2.114) into (2.113) yields

$$\begin{aligned}
&\frac{1}{T}\int_{t=0}^{T}[\mathbf{H}^{\mathrm{RX}}(f_1, t+\Delta t)]_r[\mathbf{H}^{\mathrm{TX},*}(f_2,t)]_e \mathrm{d}t \\
&\quad = \sum_{n=1}^{N}(|\tilde{h}_n|^2\exp(-j2\pi\frac{l_{n,0}(f_1 - f_2)}{c})[\mathbf{a}^{\mathrm{RX}}(\theta_n,f_1)]_r[\mathbf{a}^{\mathrm{TX},*}(\theta_n,f_2)]_e \\
&\qquad\qquad \times \exp(j2\pi\frac{v}{c}\cos(\phi_n)\Delta t f_1 + \beta^{\mathrm{RX}} - \beta^{\mathrm{TX}})). \quad (2.115)
\end{aligned}$$

We now assume propagation according to the GAA model with $d = 1$. In this model the number of rays is assumed infinite, and the power Gaussian distributed with respect to the azimuth angle $\theta$. This distribution is consistent with the following stochastic model on the scatterer positions (if the angular spread is small in comparison to the base-mobile

distance): Let $\breve{l}_n$ be Rayleigh distributed with mean $l_0\sqrt{\frac{\pi}{2}}$, and $\varphi_n$ uniform distributed $[0, 2\pi]$ (see Figure 2.5). Assume further that the gain of all scatterers is $\tilde{h}_n = \sqrt{\frac{P}{N}}$. Let $N$ go to infinity.

The relationship between the standard deviation of the Gaussian angle distribution with respect to $\theta$, and the mean of the $l_n$ distribution is

$$\sigma = \frac{180^o \times l_0}{\pi r}, \tag{2.116}$$

where $r$ is the base-mobile distance. Using (2.116) and the experimental results of [AFWP86] and [ZO94], it can be deduced that $l_0$ should be at least in the range 20-100 meter. Thus using this stochastic model, the correlation may be evaluated using Monte-Carlo simulations. Since $\sigma/r$ is small, $l_{n,0}$ may be approximated by

$$l_{n,0} - r = \breve{l}_n + \breve{l}_n \cos(\varphi_n). \tag{2.117}$$

Inserting (2.117) in (2.115) yields

$$\begin{aligned}\frac{1}{T}\int_{t=0}^{T}[\mathbf{H}^{\mathrm{RX}}(f_1, t+\Delta t)]_r[\mathbf{H}^{\mathrm{TX},*}(f_2,t)]_e \mathrm{d}t = \exp(-j2\pi\frac{r}{c}(f_1-f_2)) \\ \times [\mathbf{a}^{\mathrm{RX}}(\theta_n, f_1)]_r[\mathbf{a}^{\mathrm{TX},*}(\theta_n, f_2)]_e \\ \times \sum_{n=1}^{N}(\frac{P}{N}\exp(-j2\pi\frac{(\breve{l}_n + \breve{l}_n\cos(\varphi_n))(f_1-f_2)}{c}) \\ \times \exp(j2\pi\frac{v}{c}\cos(\phi_n)\Delta t f_1 + \beta^{\mathrm{RX}} - \beta^{\mathrm{TX}})),\end{aligned} \tag{2.118}$$

where it is assumed that the antenna element transfer functions vary only negligibly in say $[\theta - 3\sigma, \theta + 3\sigma]$. The two angles $\varphi_n$ and $\phi_n$ are related as

$$\phi_n = \varphi_n - \Delta\varphi, \tag{2.119}$$

where $\Delta\varphi$ is the mobile direction in the $\varphi$-coordinate system (see Figure 2.5). Using (2.119) in (2.118) yields

$$\begin{aligned}c_{r,e}(\Delta t, f_1, f_2) = \frac{1}{N}\sum_{n=1}^{N}(\exp(-j2\pi\frac{(\breve{l}_n + \breve{l}_n\cos(\varphi_n))(f_1-f_2)}{c}) \\ \times \exp(j2\pi\frac{v}{c}\cos(\varphi_n - \Delta\varphi)\Delta t f_1 + \beta^{\mathrm{RX}} - \beta^{\mathrm{TX}})).\end{aligned} \tag{2.120}$$

The $|c_{r,e}(\Delta t, f_1, f_2)|$ has been evaluated using $\Delta\tau = 0$, as a function of $f_1 - f_2$ and $l_0$. The result of this simulation is shown in Figure 2.13 below. The highest correlation is obtained with $l_0 = 20$m. At $|f_1 - f_2| > 10$MHz the correlation is less than 0.2. Extensive simulations we have made using $l_0 = 20$m have shown that that $|c_{r,e}(\Delta t, f_1, f_2)|$ can increase up to 0.3 using $\Delta\varphi = 0^o$ and the maximizing $\tau$ (!). However, in all other cases investigated, $c_{r,e}(\Delta t, f_1, f_2)$ attains its maximum when $\Delta t = 0$. From these results it is concluded that the up- and downlink channels are practically uncorrelated when $|f_1 - f_2| > 10$MHz.

If $N$ is large then $[\mathbf{H}^{\mathrm{RX}}(f_1, t+\Delta t)]_r$ and $[\mathbf{H}^{\mathrm{TX},*}(f_2, t)]_e$ may be seen as Gaussian random variables. If $[\mathbf{H}^{\mathrm{RX}}(f_1, t+\Delta t)]_r$ is used as the input to an estimate of $[\mathbf{H}^{\mathrm{TX},*}(f_2, t)]_e$, the Gaussian theory then yields a minimum *mean* square error in the estimate of $\mathrm{VAR}\{[\mathbf{H}^{\mathrm{RX}}(f_1, t+\Delta t)]_r\}(1 - 0.3^2)$, using $c_{r,e}(\Delta t, f_1, f_2) = 0.3$. Thus, just guessing $[\mathbf{H}^{\mathrm{TX},*}(f_2, t)]_e = 0$ is almost as good in a mean square error sense.

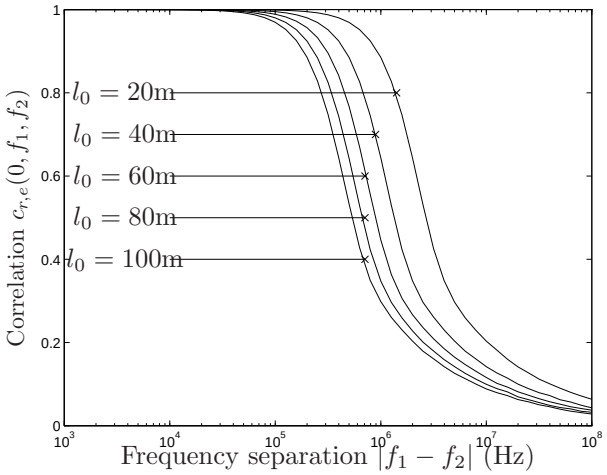


Figure 2.13: *Frequency correlation properties of the steering vectors.*

# Appendix 2.G The Positions and Gains of the Scatterers in the TU Model

Table 2.1: The positions and gains of the scatterers

| $n$ | $x'_n$ (m), | $y'_n$ (m) | $h'_n$ |
|---|---|---|---|
| 1 | 6.347 | -7.09 | 0.04526 |
| 2 | -3.515 | -12.57 | 0.04524 |
| 3 | -1.207 | -8.014 | 0.04526 |
| 4 | 8.861 | -0.2597 | 0.04526 |
| 5 | -10.98 | 8.876 | 0.04524 |
| 6 | 3.18 | -13.09 | 0.04524 |
| 7 | -4.575 | -6.226 | 0.04526 |
| 8 | 0.2897 | 9.775 | 0.04526 |
| 9 | 10.03 | 6.793 | 0.04525 |
| 10 | -5.117 | 9.063 | 0.04525 |
| 11 | 3.953 | -13.64 | 0.04524 |
| 12 | 0.5791 | 12.87 | 0.04524 |
| 13 | -16.77 | -17.73 | 0.06388 |
| 14 | -24.66 | 11.98 | 0.06384 |
| 15 | -14.29 | 12.69 | 0.06393 |
| 16 | -7.298 | -17.96 | 0.06393 |
| 17 | -16.04 | -3.834 | 0.06396 |
| 18 | -1.83 | 21.67 | 0.06391 |
| 19 | 28.63 | -3.329 | 0.06382 |
| 20 | -27.95 | 1.426 | 0.06383 |
| 21 | 5.495 | 19.37 | 0.06392 |
| 22 | -10.23 | -16.08 | 0.06393 |
| 23 | -5.785 | 29.24 | 0.0638 |
| 24 | 22.05 | -11.3 | 0.06387 |
| 25 | 51.83 | 22.89 | 0.08939 |
| 26 | 37.85 | 4.984 | 0.09002 |
| 27 | 8.737 | -40.89 | 0.08992 |
| 28 | -18.77 | -46.8 | 0.08963 |
| 29 | -48.42 | 2.253 | 0.0897 |
| 30 | -57.31 | 7.378 | 0.08935 |
| 31 | 42.83 | 2.029 | 0.08989 |

| $n$ | $x'_n$ (m), | $y'_n$ (m) | $h'_n$ |
|---|---|---|---|
| 32 | 20.94 | 28.46 | 0.0901 |
| 33 | -36.96 | 20.52 | 0.0899 |
| 34 | -18.5 | -52.05 | 0.08945 |
| 35 | -33.4 | -14.39 | 0.09007 |
| 36 | 10.32 | -39.92 | 0.08993 |
| 37 | 47.22 | 38.47 | 0.08922 |
| 38 | -76.08 | 16.17 | 0.08838 |
| 39 | 30.07 | -72.46 | 0.08835 |
| 40 | -10.56 | -62.78 | 0.08909 |
| 41 | -70.71 | -21.07 | 0.0886 |
| 42 | 20 | 78.35 | 0.08821 |
| 43 | 5.488 | 78.89 | 0.08831 |
| 44 | 75.65 | 32.67 | 0.08812 |
| 45 | -48.55 | -64.14 | 0.08824 |
| 46 | 71.91 | -44.74 | 0.08799 |
| 47 | 78.47 | -40.44 | 0.08777 |
| 48 | 64.58 | -39.79 | 0.08849 |
| 49 | 181 | 2.728 | 0.1521 |
| 50 | -150.8 | -33.41 | 0.1576 |
| 51 | -156.9 | 106.5 | 0.1502 |
| 52 | -160.1 | -23.49 | 0.1562 |
| 53 | -62.17 | -81.17 | 0.1663 |
| 54 | 103 | -64.6 | 0.1634 |
| 55 | -67.7 | -177.8 | 0.15 |
| 56 | -119 | -154.2 | 0.149 |
| 57 | 122 | -135.1 | 0.1519 |
| 58 | -140.3 | -12.76 | 0.1602 |
| 59 | -47.76 | 153.5 | 0.1564 |
| 60 | 60.52 | -76.67 | 0.1669 |
| 61 | 240.7 | 162 | 0.118 |
| 62 | -197.5 | 43.47 | 0.1404 |
| 63 | 13.33 | 217 | 0.1368 |
| 64 | -133.7 | 221.7 | 0.1264 |
| 65 | 263.9 | -47.98 | 0.124 |
| 66 | 228.5 | -97.15 | 0.1292 |

| $n$ | $x'_n$ (m), | $y'_n$ (m) | $h'_n$ |
|---|---|---|---|
| 67 | -186.3 | 145.9 | 0.1322 |
| 68 | 131.4 | 227.5 | 0.1254 |
| 69 | -256.3 | 126.1 | 0.1193 |
| 70 | 227.4 | -84.37 | 0.1306 |
| 71 | -49.92 | -242.1 | 0.1295 |
| 72 | 187.8 | 226.9 | 0.1168 |
| 73 | -10.82 | -309.5 | 0.1126 |
| 74 | 150.1 | -302.6 | 0.1047 |
| 75 | 380.7 | 103 | 0.08874 |
| 76 | 145 | 327 | 0.09911 |
| 77 | -110.1 | 287.4 | 0.1132 |
| 78 | -341.2 | -1.096 | 0.1038 |
| 79 | 346.3 | -159.9 | 0.09239 |
| 80 | -241.5 | -296.4 | 0.09212 |
| 81 | -281 | 136.2 | 0.1119 |
| 82 | 255.6 | 234.7 | 0.1021 |
| 83 | -284.1 | -166.8 | 0.1071 |
| 84 | 133.5 | 283.5 | 0.1116 |
| 85 | -185.3 | -355.9 | 0.08683 |
| 86 | 420.8 | -118 | 0.077 |
| 87 | 134.6 | -451.3 | 0.06808 |
| 88 | -344.1 | 255.9 | 0.07923 |
| 89 | 219.2 | 342 | 0.08544 |
| 90 | -126.6 | -450 | 0.06898 |
| 91 | -142.5 | 434.1 | 0.07173 |
| 92 | 444.5 | -94.21 | 0.0724 |
| 93 | -449.5 | -55.15 | 0.07278 |
| 94 | -395.4 | 165.3 | 0.07929 |
| 95 | 337.1 | 334.7 | 0.06704 |
| 96 | -176.6 | 369.2 | 0.0846 |
| 97 | -69.16 | 501.6 | 0.05929 |
| 98 | 515.9 | 195.5 | 0.04894 |
| 99 | -303.6 | 464.1 | 0.04831 |
| 100 | -364.6 | -404.5 | 0.05049 |
| 101 | -561.3 | -178.3 | 0.04129 |

| $n$ | $x'_n$ (m), | $y'_n$ (m) | $h'_n$ |
|---|---|---|---|
| 102 | 113 | -560.4 | 0.04473 |
| 103 | 552.1 | 169.6 | 0.04354 |
| 104 | -445.1 | 389.6 | 0.04078 |
| 105 | 397.3 | -308.4 | 0.0601 |
| 106 | -451.9 | 274 | 0.0541 |
| 107 | -397.1 | -331.6 | 0.05668 |
| 108 | 350.4 | 418.9 | 0.05015 |
| 109 | 400.3 | -604.4 | 0.02856 |
| 110 | 437.1 | -458.3 | 0.04699 |
| 111 | -105.7 | -747.1 | 0.02398 |
| 112 | 468.4 | -388 | 0.05323 |
| 113 | -229.9 | 652.6 | 0.03446 |
| 114 | -483.4 | -617.4 | 0.01999 |
| 115 | -592.6 | -250.5 | 0.04464 |
| 116 | 707.3 | -220.5 | 0.02602 |
| 117 | -236.7 | -671 | 0.03087 |
| 118 | 670.6 | 201.8 | 0.03288 |
| 119 | 391.3 | -547.9 | 0.03813 |
| 120 | -598.5 | -202.1 | 0.04737 |

# Chapter 3

# Techniques for Downlink Capacity Enhancement of FDD Systems

The basic *conceptual* steps for capacity improvement with base station antenna arrays are: 1) improve the signal to interference ratio using adaptive antenna patterns 2) trade this improvement for capacity. One of the main issues addressed in this thesis is whether step 2) should be made by reducing the cluster size i.e., increase the fraction of the total spectrum employed at a base stations, or by allocating multiple users to the spectrum already available in the cell. The former of these approaches is referred to as the *reduced cluster size (RCS) approach* while the latter will be called the *same sector frequency reuse (SSFR) approach* . Herein, two versions of the RCS approach are investigated: RCS with nulling (RCS-WIN) and RCS without nulling (RCS-WON). In the former version, the antenna pattern is synthesized to have a low gain in the direction of identified co-channel users (co-channel users for which propagation parameters are known), while this is not the case in RCS-WON. An algorithm called the summed interference to carrier ratio (SICR) minimizing beamformer is also introduced in the chapter. The SICR beamformer minimizes the sum of the interference to carrier ratio at the co-channel users in the own and adjacent co-channel cells subject to the constraint of unit array gain towards the desired mobile. Three systems called SICR-SSFR, SICR-RCS-WIN and SICR-RCS-WON, based on the SICR beamformer are

also defined in the chapter. These systems specify beamforming, channel allocation, and uplink power control. The channel allocation and uplink power control aims at solving the uplink near-far problem and separate same-sector co-channel users. In the next chapter the approaches are analyzed in order to assess their performance. The idea is that this comparison should not only be representative for the considered implementations SICR-SSFR, SICR-RCS-WIN and SICR-RCS-WON, but also serve to give an indication on the underlying capacity enhancement principle i.e., SSFR, RCS-WIN and RCS-WON respectively. The propagation model used in the design and analysis is the GAAO model of Section 2.3.1. As shown in Chapter 7, this model is capable of delivering reasonable performance predictions for at least the investigated macro-cellular environment.

Previous work on capacity with antenna arrays has considered the RCS-WIN approach, [Ohg94, RDJP95], or channel allocation and capacity for SSFR, [FN95, FN96, Tan94, Tan95]. An exception is the paper [SBEM90] which investigates the RCS approach assuming that ideal sector beams can be formed. There are two ways of interpreting this assumption: nulls are steered towards co-channel users outside the ideal sector beam *or* the sidelobes outside the sector are negligible. Thus, it is unclear weather the analysis in [SBEM90] represents RCS-WIN or RCS-WON. The work in this and the next chapter differs from the aforementioned references (and to all references known by the author), in that

- The SSFR, RCS-WIN and RCS-WON approaches are compared using the same assumptions.
- Critical issues such as the uplink near-far ratio, uplink dynamic power-control range, and downlink outage probability are treated simultaneously for the different solutions.
- The capacity enhancement is estimated as a function of the number of antennas, as compared with a three sector solution.
- Closed form solutions for the outage probability (probability of insufficient transmission quality) are provided for the SSFR, RCS-WIN and RCS-WON approaches, as a function of the number of antennas, angular spreading and frequency reuse.
- The analytical calculations are combined with experimental results to form capacity predictions.

The main conclusions are:

- A large *uplink* power control range is necessary to make the *downlink* inter-cell nulling feature of the SICR-RCS-WIN system effective.

- The uplink near-far ratio, defined as the ratio of the power of the strongest user to the weakest desired user (averaged over fast fading), allocated to the same timeslot (but sometimes different carrier), is typically less than 25dB, for all investigated systems. For the SICR-RCS system with $e = 1$ and fast handover, it is typically less than 4dB.

- The SICR-SSFR system requires around 16 channels (per power group and sector) in order to be able to allocate channels with spatially well separated users.

- The SICR-SSFR system increases capacity more than SICR-RCS-WIN and SICR-RCS-WON systems in most of the investigated cases.

- The capacity enhancement achieved using SICR-RCS-WIN is larger than or equal to that obtained using SICR-RCS-WON.

- The experimental results of Chapter 7 suggest that $\sigma_0 = 3^o$ to $6^o$, $r_0 = \infty$ (the framework is introduced in Section 2.3.1) is a realistic model. Combining this information with the results of Chapter 4, yields the following capacity predictions in the more optimistic case $\sigma_0 = 3^o$: Threefold capacity enhancement is achieved using the SICR-RCS-WIN and SICR-RCS-WON systems with three and five antenna elements per 120-degree sector, respectively (in comparison with a reference system employing a single element per 120-degree sector). Four and tenfold capacity enhancement is achieved with SICR-SSFR using five and eighteen antenna elements respectively. Using SICR-RCS-WIN or SICR-SSFR, eight antenna elements per sector, and an improved handover, a ninefold capacity enhancement is obtained. However, it is unclear how much of the ninefold capacity enhancement should be attributed to the improved handover in this case.

- The derived analytical expression for the outage probability agrees well with simulation results in the SICR-SSFR case if sixteen (or

more) channels per group are employed, in the SICR-RCS-WIN case if $e = 1$ is employed, and in the SICR-RCS-WON case if slow handover is assumed.

The SICR beamformer proposed in the chapter resembles the algorithms previously proposed in [FN95, GP96, RDJP95]. In particular the "subspace beamformer" introduced in [GP96]. In conformity with the subspace beamformer the SICR beamformer tries to maximize the sum of the inverse signal to interference ratio at the mobiles. The major difference between the two algorithms is that users in other cells are treated by the SICR algorithm but not by the subspace beamformer.

In comparison with the "co-operative algorithm" introduced in [RDJP95], the main difference is that hard bounds on transmitted energy, generated interference and desired signal power are imposed by that algorithm but not in the SICR beamformer (if these can not be met, the paper [RDJP95] suggests a channel re-allocation). The propagation model applied in the chapter is more restrictive than those in the papers [FN95, RDJP95, GP96]. However, a generalization of the proposed beamformer to the more general GWSSUS model is provided in Chapter 5.

The chapter is organized as follows: Section 3.1 introduces the cellular systems the geometries, and the three capacity enhancement approaches "reduced cluster size with inter-cell nulling" (RCS-WIN), "reduced cluster size without inter-cell nulling" (RCS-WON) and "same sector frequency reuse" (SSFR). In Section 3.2, the SICR beamformer is derived. Three system proposals employing the SICR method are also defined in Section 3.2. The three systems are based on the RCS-WIN, RCS-WON and SSFR approaches respectively and are referred to as the SICR-RCS-WIN, SICR-RCS-WON and SICR-SSFR. The three systems specify power control, channel allocation, parameter estimation and beamforming. Finally, a summary of the chapter is given in Section 3.4.

## 3.1 Frequency Reuse

### 3.1.1 Cellular Geometry and Frequency Allocations

The coverage area of a mobile radio system is divided into a network of cells, where each cell is covered by a base station site. In the theoretical analysis of such systems it is common to assume hexagonal cells

with the base station site in the center of the cell, as depicted in Figure 3.1 below, see [Mac79]. The cells are then assigned a subset of the available spectrum such that the same frequency cells are sufficiently spatially separated. The spectrum is divided into $K$ disjunct subsets, and each cells is assigned among these subsets. If $K$ is one of the numbers {1,3,4,7,9,12,13,16,19,21,...}, then the spectrum can be distributed in such a fashion that every cell has a first tier of six *co-channel cells* (cells using the same channel set) at the distance $D_c$ given by

$$D_c = \sqrt{3K}R, \tag{3.1}$$

where $D_c$ is measured between the cell centers and $R$ is the cell radius, see [Mac79]. In the analysis of this thesis such a spectrum allocation is assumed. However, the cells are further divided into three $120^o$-sector subcells or sectors as is common in operational macro-cells. These sectors are covered by one or several directional antenna elements. The sectors may use all the spectrum, allocated to the cell, *or* a fixed third of the spectrum. In the former case the bandwidth per sector is three times higher than in the latter (assuming the same cluster size). To distinguish between the two cases the parameter $S$ will be used. When $S = 3$, the three sectors of a site use non-overlapping frequency spectra while when $S = 1$ all three sectors use the same spectrum. *The product of $K$ and $S$ will be denoted by $C$, and referred to as the cluster size.* This wording reflects the fact that each sector uses one out of $C = K \times S$ channel sets, and that the whole cellular network can be divided into identical contiguous clusters of $K$ cells, where all cells in a cluster use disjoint spectrums. The sector orientation and frequency allocation of two cells (in the same network) using the same spectrum are assumed identical.

Figure 3.1 below illustrates a cellular system. Contrary to the usual procedure, the cell labeling in Figure 3.1 does not refer to the spectra used in the the cell. The three sectors of a cell are labeled with the cell number as prefix and “a”,”b”, or “c” as suffix. The “a”,”b”, and “c” subcells are always oriented upwards, to the right and to the left, respectively.

Table 3.1, lists the dominant interfering sectors in the downlink (base to mobile) in sector 1a, using different frequency reuse patterns. The list of interfering sectors takes into account that the sectors cannot be ideal, and thus interference is generated outside the 120-degree sector of coverage. Symmetry yields that the situation only has to be analyzed from the viewpoint of sector 1a.

| Reuse Pattern | Interfering Bases/Sectors |
|---|---|
| $K = 1, S = 1$ | 1b,1c,2b,2c,3b,7c,4a,5a,6a |
| $K = 3, S = 1$ | 8b,9b,10a,11a,12c,13c |
| $K = 4, S = 1$ | 14b,14c,15b,16a,16b,17a,18a,18c,19c |
| $K = 7, S = 1$ | 20b,22b,24a,26a,28c,30c |
| $K = 12, S = 1$ | Outside of figure |
| $K = 1, S = 3$ | 4a,5a,6a |
| $K = 3, S = 3$ | 9a,10a,11a,12a |
| $K = 4, S = 3$ | 16a,17a,18a |
| $K = 7, S = 3$ | 24a, 27a, 28a |

Table 3.1: Interfering base stations in the downlink seen from subcell 1a

### 3.1.2 Same Sector Frequency Reuse (SSFR)

By using antenna arrays at the base stations, it may be possible to have several mobiles allocated to the *same* channel within the *same* sector. We will refer to this concept as same sector frequency reuse (SSFR). The formal difference between employing SSFR within a sector as compared to subdividing the sector into even smaller sectors (according to our definition) is in the channel allocation. In sectorization multiple users may share the same channel (at the same base station site) if the positions of the users fall into different (fixed) sectors. In SSFR, the allocation of multiple users on the same channel is based on more complex criteria. SSFR channel allocation algorithms are introduced in Section 3.3.1.1 below and in the paper [FN96]. The number of users on the same channel within the same sector is denoted $D$. In a practical implementation of SSFR, the channel allocation algorithm should not always assign new mobiles until all channels are filled with $D$ mobiles. For instance, if all mobiles are in the same azimuth direction as seen from the base, only a single mobile per channel may be allocated. Thus, by letting the channel allocator block mobiles (i.e., no line allocated), even though not all channels have $D$ mobiles allocated, blocking is traded for quality (see also discussion in Appendix 3.A below). In order to simplify simulations and comparisons, this possibility has been disregarded in this thesis. As a consequence, a bad distribution of users leads to outages (calls lost due to insufficient call quality), rather than blocking.

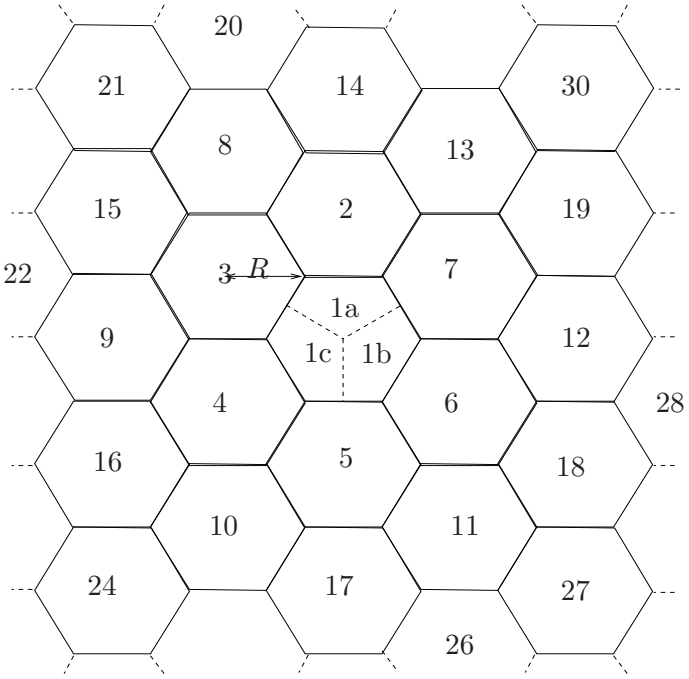


Figure 3.1: *Part of a cellular system.*

### 3.1.3 The SSFR, RCS-WIN and RCS-WON Approaches

For each of the frequency reuse strategies listed in Table 3.1, a corresponding capacity is assigned. In order to do this, it is assumed that the same amount of spectrum is allocated to each cell. It is further assumed that the number of traffic channels in each sector is proportional to the amount of spectrum allocated to the sector. It should also be noted that conventionally, a Poisson model for the traffic is assumed, and the capacity is defined as the carried traffic at a certain blocking probability (probability of all lines busy). This introduces a progressive dependence between the number of channels in a cell and the capacity (this is further discussed in Appendix 3.A below). Such effects are disregarded. Furthermore it is assumed that $D$ mobiles share the same sector by SSFR,

without restrictions, as described in the previous section. With these assumptions the capacity (or spectrum efficiency), $E$, of the channel reuse scheme may be defined as

$$E = \frac{D}{C} = \frac{D}{K \times S}. \tag{3.2}$$

One of the problems investigated in this thesis is, how to optimize a system with respect to $S$, $K$ and $D$. The objective is capacity at a certain minimum quality of service. Of particular interest is the capacity gain when going from a solution with three conventional 120-degree sector antennas per site, to a solution with antenna arrays covering the sectors. The basic *conceptual* steps for capacity improvement with antenna arrays are: 1) improve the signal to interference ratio using adaptive antenna patterns 2) trade this improvement for capacity. One of main issues addressed in Chapter 4 , is whether step 2) should be made by reducing the cluster size, $C$, or by allocating multiple mobiles on the same channel within the same sector (SSFR), i.e., increase $D$. The former of these approaches will be referred to as the reduced cluster size (RCS) approach while the latter will be called the same sector frequency reuse approach (SSFR). Of course, the optimal solution may be a combination of the two.

We will distinguish between two variants of the RCS approach: reduced cluster size with inter-cell nulling (RCS-WIN) and reduced cluster size without inter-cell nulling (RCS-WON). In the RCS-WIN approach nulling is performed towards co-channel users in other cells while with RCS-WON nulling is not applied. In the SSFR approach, nulls are directed towards the co-channel users within the sector cell but not outside of it. Nulling is here used in a wide-sense, denoting that the antenna pattern is synthesized in order to have low gain in the direction of a certain mobile, but not necessarily zero gain.

## 3.2 Three Downlink Proposals for FDD Cellular Systems

In Section 3.2.1 below the SICR-beamformer is introduced. This beamformer is based on the GAAO model described in Section 2.3.1. It is assumed that the base stations employ linear arrays of uniform distributed (directional) antenna elements (ULAs), see Figure 2.2. One ULA is employed to cover a 120-degree sector. The three sectors of a cell-site are

regarded as three different base stations.

### 3.2.1 The Summed Inverse Interference to Carrier Ratio Minimizing Beamformer (SICR)

Consider the situation where $Q$ base stations are transmitting simultaneously (at the same frequency) to $Q$ mobiles[1]. The three sectors of a cell-site are regarded as three different base stations. Let the $k$th mobile be connected to the $k$ base station. The desired signal energy received at mobile $k$ is obtained from (2.35) as

$$P_{k,k} = G_{k,k}\mathbf{w}_k^*\mathbf{R}(\theta_{k,k}, \sigma_{k,k})\mathbf{w}_k. \tag{3.3}$$

Before giving a criterion function for the choice of $\mathbf{w}_k$ the ad-hoc restriction is made that the "antenna array gain", in the direction of the desired mobile should be unity i.e.,

$$\mathbf{w}_k^*\mathbf{R}(\theta_{k,k}, \sigma_{k,k})\mathbf{w}_k = 1. \tag{3.4}$$

Note that $P_{k,k} = G_{k,k}$ is the desired energy received if a single antenna element is used to transmit and unity energy is employed. Simulations have indicated that the constraint (3.4) is a good choice although no optimality is claimed. Assume for a moment that no other base station than base station $k$ creates interference. Then the (mean) desired signal (or carrier) power to the (mean) interference signal power, $\widetilde{\mathrm{CIR}}_i$, at the $i$th mobile, is given by

$$\begin{aligned}\widetilde{\mathrm{CIR}}_i &= \frac{P_{i,i}}{P_{k,i}} \\ &= \frac{G_{i,i}\mathbf{w}_i^*\mathbf{R}(\theta_{i,i}, \sigma_{i,i})\mathbf{w}_i}{G_{k,i}\mathbf{w}_k^*\mathbf{R}(\theta_{k,i}, \sigma_{k,i})\mathbf{w}_k} \\ &= \frac{G_{i,i}}{G_{k,i}\mathbf{w}_k^*\mathbf{R}(\theta_{k,i}, \sigma_{k,i})\mathbf{w}_k},\end{aligned} \tag{3.5}$$

where the last equality follows since the $i$th base station also has a unity antenna array gain towards its desired mobile (all base stations employ

[1]This assumption seems to be inconsistent with the SSFR approach, since there are more mobiles than base stations in that case. However, by interpreting the results of the section pragmatically, the obtained algorithm can be used also in the SSFR case, see Section 3.3.1.2.

the same transmission algorithm). Now, the criterion function for chosing $\mathbf{w}_k$ is

$$\mathbf{w}_k = \arg_{\mathbf{w}} \min\{ \sum_{i=1,\neq k}^{Q} \widetilde{\mathrm{CIR}}_i^{-1} \}. \tag{3.6}$$

Thus, in a sense, $\mathbf{w}_k$ is chosen to minimize *the sum of the inverse of the signal to interference ratios of the mobiles in the system. This is the reason for calling the algorithm the summed interference to carrier ratio minimizing beamformer (SICR).* Combining (3.5) and (3.6) yields

$$\mathbf{w}_k = \arg_{\mathbf{w}} \min\{\mathbf{w}_k^* \mathbf{M} \mathbf{w}_k\}, \tag{3.7}$$

where the matrix, $\mathbf{M}$, is given by

$$\mathbf{M} = \sum_{i=1,\neq k}^{Q} \frac{G_{k,i}}{G_{i,i}} \mathbf{R}(\theta_{k,i}, \sigma_{k,i}). \tag{3.8}$$

In practice, the interference at the $i$th mobile will of course not only come from base $k$, but from all bases. However, the criterion (3.7), which was derived ignoring such interference, is used anyway. The solution to (3.8), subject to the constraint (3.3), is given by

$$\mathbf{w} = \frac{\mathbf{e}}{\sqrt{\mathbf{e}^* \mathbf{R}(\theta_{k,k}, \sigma_{k,k}) \mathbf{e}}}. \tag{3.9}$$

where $\mathbf{e}$ maximizes

$$\frac{\mathbf{e}^* \mathbf{R}(\theta_{k,k}, \sigma_{k,k}) \mathbf{e}}{\mathbf{e}^* \mathbf{M} \mathbf{e}}. \tag{3.10}$$

It can be shown that $\mathbf{e}$ is the generalized eigenvector associated with the matrix pair $(\mathbf{R}(\theta_{k,k}, \sigma_{k,k}), \mathbf{M})$, corresponding to the largest eigenvalue, [Par80]. Methods to compute $\mathbf{e}$ may be found in [GL83], where it should be noted that $\mathbf{R}(\theta_{k,k}, \sigma_{k,k})$ is Hermitian and positive semi-definite and $\mathbf{M}$ is Hermitian and positive definite (from the assumptions below). The parameters required to compute $\mathbf{w}_k$, are $G_{k,i}/G_{i,i}$, $\theta_{k,i}$ and $\sigma_{k,i}$ for all (co-channel) mobiles in the system. In practice, the necessary parameters will be known for only a subset of the interfering mobiles, say mobile $1, \ldots, p$. These mobiles will be referred to as the *identified* interfered mobiles. In order to account for the remaining mobiles the approximation

$$\sum_{i=p+1,\neq k}^{Q} \frac{G_{k,i}}{G_{i,i}} \mathbf{R}(\theta_{k,i}, \sigma_{k,i}) \approx \text{constant} \times \mathbf{I} \tag{3.11}$$

is made, i.e., the sum of the interference to carrier ration at these mobiles is assumed to be proportional to $\|\mathbf{w}_k\|^2$. This approximation is reasonable if the angles $\theta_{k,i}$ are well separated. The constant in (3.11) will be obtained from *loose* reasoning and will vary between systems. In summary, the vector $\mathbf{w}_k$ is obtained from (3.9), where $\mathbf{e}$ is the solution to the generalized eigenvector problem

$$\mathbf{R}(\theta_{k,k}, \sigma_{k,k})\mathbf{e} = \mu \mathbf{M}\mathbf{e} \tag{3.12}$$

corresponding to the largest eigenvalue $\mu$, with $\mathbf{M}$ given by

$$\mathbf{M} = \sum_{i=1}^{p} \frac{G_{k,i}}{G_{i,i}} \mathbf{R}(\theta_{k,i}, \sigma_{k,i}) + \text{constant} \times \mathbf{I}. \tag{3.13}$$

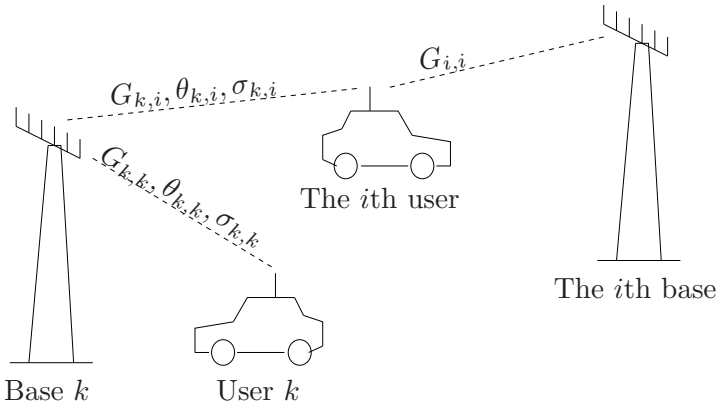


Figure 3.2: *Illustration of the considered situation.*

## 3.3 The SICR-SSFR, SICR-RCS-WIN and SICR-RCS-WON Systems

In this section three systems based on the SICR beamformer are proposed. The systems differ in terms of channel allocation, power control,

synchronization requirements, and identification of interfered users.

### 3.3.1 The SICR-SSFR System

In this approach several mobiles are allocated to the same channel within the same sector as was described in Sections 3.1.2 and 3.1.3. Although the main idea with the system is to obtain capacity enhancement through increased channel utilization within a sector, we will also investigate cases where the cluster size is simultaneously reduced. To make multiple mobiles on the same channel feasible, dynamic channel allocation is applied to separate the co-channel users in the cell (with respect to azimuth angle as seen from the base). In principle, the deployment of the SSFR approach in the downlink does not imply that the same capacity enhancement strategy has to be used in the uplink. However, if it is used, channel allocation and power control must be employed to combat near far effects in the uplink processing. Since most cellular standards dictate a one to one relation between uplink and downlink channels, e.g in GSM, it is assumed that the mobiles simultaneously accessing the same channel in the downlink also do so in the uplink.

#### 3.3.1.1 Channel Allocation and Power Control

The parameters $G$, $\theta$, and $\sigma$ are estimated for all mobiles in the sector. The mobiles in the same sector are sorted with respect to their path gain $G$, to their desired base. Note that this entity is assumed reciprocal in the up and downlink. Then, they are divided into power groups say $\Gamma_1, \Gamma_2, \ldots$ such that all the mobiles in $\Gamma_1$ are stronger than all the mobiles in $\Gamma_2$ and so on. The power groups are allocated to different channel subsets out of the total number of channels available in the sector. The exact implementation of this allocation depends on the standard considered, and the bandwidth available. The objective of this allocation is to reduce the requirements on the uplink processing, in terms of adjacent channel interference and dynamic range requirements. In order to distribute the mobiles within a power group, on the channels available for that power group, the azimuth positions $\theta$ of these mobiles are sorted. Assuming that the sorted list of angular positions is $\eta_1, \ldots, \eta_{n_c \times D}$, the mobiles with angles $\eta_i, \eta_{i+n_c}, \ldots, \eta_{i+(D-1)n_c}$ will be allocated to the same channel. This operation is illustrated by Example 3.1 below. If frequency hopping is applied, the same channel users hop according to the same pattern. Finally, power control is applied such that all mobiles on the same channel

are received equally strongly (averaged over fast fading). The common power level is given by $0.5G_{\max} + 0.5G_{\text{in}}$, where $G_{\max}$ and $G_{\min}$ are the maximum and minimum path gain among the mobiles in a dB scale.

**Example 3.1**

Assume that there are 48 users in a sector allocated to 16 channels i.e., $D = 3$. These 48 users are divided into four power groups with twelve mobiles in each group. Each group uses four channels. Assume further that the angular positions of the mobiles in group one are given by [$-60^o$,$-50^o$,$-40^o$,$-30^o$, $-20^o$,$-10^o$,$0^o$,$10^o$,$20^o$,$30^o$,$40^o$,$50^o$]. Then the mobiles with positions [$-60^o$,$-20^o$,$20^o$], are allocated to channel number one, $-50^o$,$-10^o$,$30^o$ to channel number two, $-40^o$,$0^o$,$40^o$, to channel three, and $-30^o$,$10^o$,$50^o$ to channel four.

#### 3.3.1.2 User Tracking and Nulling

The users on the same channel within the same sector are considered as the identified interfered users in the framework of Section 3.2.1. Since the considered base station and the base station of the identified interfered user is the same base, it follows that $G_{k,i} = G_{i,i}$. Thus, the factors $G_{k,i}/G_{i,i}$ in (3.13) are equal to one. The constant in (3.13) is chosen using the following crude reasoning: Assume that only mobiles in the first tier of co-channel cells are interfered with. Assume that the path gains to these mobiles are given by $G_{k,i} = (1/D_c)^\gamma$ where $D_c$ is the distance between the $k$th base and the first tier of co-channel base stations, see Section 3.1.1. Note that $(1/D_c)^\gamma$ is the median signal strength at the distance $D_c$, assuming $|p(\theta, f)|^2 = 1$, from (2.35). Assume further that these mobiles have received desired power $G_{i,i} = (1/R)^\gamma$ (which is the median signal strength on the cell border assuming $|p(\theta, f)|^2 = 1$). Geometrical arguments yield that the number of unidentified co-channel mobiles in the first tier of co-channels cells is $Q - p - 1 = D \times l$ where $l$ is equal to 11 when $S = 1$, and 3 when $S = 3$. Using these assumptions in (3.11) yields

$$\sum_{i=p+1, i\neq k}^{Q} \text{SIR}_i^{-1} = (1/D_c)^\gamma \sum_{i=p+1}^{p+lD} \mathbf{R}_{vv}(\theta_{k,i}, \sigma_{k,i}) \approx (R/D_c)^\gamma lD\mathbf{I}. \quad (3.14)$$

Thus the constant in (3.13) is chosen as

$$\text{constant} = (R/D_c)^{\gamma} lD. \tag{3.15}$$

### 3.3.2 The SICR-RCS-WIN/WON Systems

In this section we describe the two RCS based systems SICR-RCS-WIN and SICR-RCS-WON. The description leaves the uplink power control parameter, $e$, unspecified. The development below assumes that uplink co-channel mobiles are downlink co-channel mobiles, i.e., mobiles that are interferers as seen from a certain base station in the uplink, are interfered with by that base station in the downlink. For TDMA systems this implies that the timeslots of the base stations need to be synchronized. In large cells the desired and interfering TDMA slots will arrive unaligned at the mobile anyway, due to propagation delays. However, this will typically only degrade performance on the first bits of a burst. The development in Sections 3.3.2.1 to 3.3.2.3 assumes for simplicity that frequency hopping is not applied. How the systems should be implemented in a frequency hopping system is described in Section 3.3.2.4.

#### 3.3.2.1 Power Control

Consider the situation depicted in Figure 3.2 again. Assume for a moment that no other base or mobiles than the two present in the plot exist. The uplink (mean) carrier to (mean) interference ratio at base $k$ in a *single antenna element* is then given by

$$\text{CIR}_k^{\text{up}} = \frac{G_{k,k} P_k^{\text{up}}}{G_{k,i} P_i^{\text{up}}}, \tag{3.16}$$

where $P_k^{\text{up}}$ and $P_i^{\text{up}}$ are the power transmitted by user $k$ and user $i$ respectively. Similarly, the downlink signal to interference ratio at the $i$th interfered mobile is given by

$$\text{CIR}_i^{\text{down}} = \frac{G_{i,i}}{G_{k,i}}, \tag{3.17}$$

if only a single antenna element is employed in the transmission and the transmitted energy is unity. Herein, the power control law

$$P_i^{\text{up}} = G_{i,i}^{-e}. \tag{3.18}$$

is employed, where $e$ is a design parameter. If $e = 1$ then $\mathrm{CIR}_k^{\mathrm{up}} = \mathrm{CIR}_i^{\mathrm{down}}$, from (3.16-3.18). Thus if the $i$th mobile is interfering significantly at base $k$ in the uplink, it will be equally interfered with by base $k$ in the downlink. This is a desirable property , since it implies that base will have a good chance of identifying mobiles with poor downlink CIR, since those mobiles will be interfering strongly in the uplink. Another advantage with $e = 1$ is that all mobiles within the cell are received equally strong at the base and therefore, the uplink adjacent channel interference can be kept small. In practice the use of $e = 1$, may be prohibited by the dynamic range of power control range for the mobiles. In that case a smaller $e$ has to be employed.

#### 3.3.2.2 Dynamic Channel Allocation

When $e \neq 1$ the power of the mobiles may vary significantly which causes adjacent channel interference problems. We propose that this problem is solved using dynamic channel allocation as follows: Sort the mobiles in the subcell with respect to their path gain to the base $G_{k,k}$. Divide the mobiles into power groups say $\Gamma_1, \Gamma_2, \ldots$ such that all the mobiles in $\Gamma_1$ are stronger than all the mobiles in $\Gamma_2$ and so on. Finally, allocate the groups in channels such that the dissimilar power of the groups does not negatively influence the uplink processing. If $e = 1$ is used, random channel allocation is simply employed.

#### 3.3.2.3 User Tracking and Nulling

This is where the difference between the SICR-RCS-WIN and SICR-RCS-WON arises. The two cases are described below.

**SICR-RCS-WIN**: The required entities of identified interfering users in (3.11) are $G_{k,i}/G_{i,i}, \theta_{k,i}$ and $\sigma_{k,i}$. When power control with $e = 1$ is used, $G_{k,i}/G_{i,i}$ is the (mean) power received in the uplink from the $i$th user (in a single antenna element) and thus all the parameters can be derived from the uplink data. When $e \neq 1$ however, the $i$th base must inform base $k$ about the value of $G_{i,i}$. This in turn requires that the base $k$ is able to identify which base the interfered user is connected to. In order to choose the constant in (3.11) it is assumed that the base is able to identify interfering users stronger than $P_{\min}$, and that the value of $P_{\min}$ is known by the base. Since the power of the desired user differs among the channels $P_{\min}$ will be channel dependent. Thus, seen from the

view point of base $k$, the interfering users that satisfy

$$G_{k,i}G_{i,i}^{-e} \leq P_{\min} \tag{3.19}$$

are *not* identified. Combining (3.19) in (3.11) yields

$$\begin{aligned}
\sum_{i=p+2}^{Q} \mathrm{CIR}_i^{-1} &= \sum_{i=p+2}^{Q} G_{k,i}G_{i,i}^{-1}\mathbf{R}_{vv}(\theta_{k,i},\sigma_{k,i}) \\
&\leq \sum_{i=p+2}^{Q} P_{\min}G_{i,i}^{e-1}\mathbf{R}_{vv}(\theta_{k,i},\sigma_{k,i}) \\
&\approx (0.1)^{e-1}P_{\min}(r-p)\mathbf{I} \qquad (3.20) \\
&= \text{const} \times \mathbf{I} \qquad (3.21)
\end{aligned}$$

where approximation (3.20) is based on the assumption $G_{i,i} = \frac{0.1}{R^{\gamma}}$ which from (2.35) is a pessimistic assumption (assuming $|p(\theta,f)|^2 \approx 1$). Based on geometry, the parameter $r$ is set to 11 when $S = 1$ and 3 when $S = 3$.

**SICR-RCS-WON**: In this case no interfering mobiles are identified in the framework of Section 3.2.1, i.e., $p = 0$. It follows that the constant in (3.11) can be chosen arbitrarily. With this approach synchronized bases are not a requirement.

#### 3.3.2.4 Influence of Frequency Hopping

Let us consider the GSM system [MP92] with frequency hopping. In this system a user occupies the same time slot in each TDMA frame but changes frequency according to a pseudo-random pattern. The time and frequency of the uplink timeslot are given by the downlink timeslot with a delay of two burst periods and a frequency translation of 45MHz respectively. The frequency hopping implies that a user "meets" different interferers in each TDMA frame. Let us for a moment regard all frequency channels multiplexed on the same time slot in the TDMA frame as a single wideband channel. With this channel definition we may say that uplink co-channel mobiles are downlink co-channel mobiles. The idea is to track the users (i.e., estimate $G_{k,i}, G_{i,i}$, $\theta_{k,i}$ and $\sigma_{k,i}$ in the framework of Section 3.2.1) as they switch from frequency to frequency. This is possible if the base is able to determine the home cell of the interfering users, which in turn will enable the infrastructure to inform the base

of the frequency hopping pattern of the interfering mobile. The base transmits with nulls in the direction of the identified interfered users which are using the same frequency in the particular timeslot. Note that the minimum power enabling identification of interfering users, $P_{\min}$, will depend on the power of all the users that are using the same time slot.

## 3.4 Summary

In this chapter the concepts of capacity enhancement by means of same sector frequency reuse (SSFR), and reduced cluster size with (RCS-WIN) and without nulling RCS-WON, have been introduced. A beamformer called SICR, has also be defined. Three systems referred to as SICR-SSFR, SICR-RCS-WIN and SICR-RCS-WON have been proposed. All systems, except the SICR-RCS system with $e = 1$ (see Section 3.3.2.1), divide the mobiles into groups with similar power levels, and allocates them to channels such that the dissimilar power between the different groups can be handled. The channel allocation of the SICR-SSFR also tries to make the channel allocation such that the same channel users have large azimuthal separation. In Section 3.3.2.1 a conjecture is stated. This conjecture says that the SICR-RCS-WIN system will be able to identify and null the mobiles that are in trouble in the downlink, if $e = 1$ is employed. This conjecture will be investigated in the following chapter.

# Appendix 3.A Blocking Considerations

The *maximum* number of mobiles that may be served simultaneously by the base, is a function of the spectrum allocated to the cell minus the spectrum needed for control-channels. In the literature on mobile cellular systems, a frequently assumed traffic model is one where the incoming calls are Poisson distributed in time, and where the duration of each call is exponentially distributed, [Sch87]. Furthermore, it is assumed that users who do not get a line, are cleared (no queuing) and that their attempts to re-call, do not alter the distribution of incoming calls. For such systems, the probability, $B$, of a call blocking (i.e., all lines busy), is given by the so-called Erlang-B formula [Kle75] as

$$B = \frac{\rho^{N_c}/N_c!}{\sum_{k=0}^{N_c} \rho^k/k!}, \tag{3.22}$$

where $N_c$ is the number of available channels in the sector and $\rho$ is the ratio of the mean call hold time and the mean call inter-arrival time. The mean number of users, $\bar{A}$, in the system (the carried traffic), is given by

$$\bar{A} = \rho(1 - B). \tag{3.23}$$

In the upper part of Figure 3.3, the mean number of users, $\bar{A}$, is plotted as a function of the number of channels, $N_c$, at a $B = 2\%$ blocking probability. The lower part of the figure, shows $\bar{A}/N_c$ as a function of $N_c$. From these results it is deduced that the capacity measured as the carried traffic at a certain blocking probability is a function with a positive second derivative. As an example, consider a GSM system with 36 carriers, and thereby $N_c = 36 \times 8 = 288$ channels. If $C = 1, S = 3, D = 1$ reuse is employed, the number of channels per sector is 96, while only 32 channels are obtained per sector if $C = 3, S = 3, D = 1$ reuse is employed. Thus, in the former case there are three times more channels available per sector. However, using the results of Figure 3.3, the difference in carried traffic between the two is 354%, at a 2% blocking probability. In the thesis, the impact of blocking is neglected and the capacity of $C = 1, S = 3, D = 1$ will be regarded as three times that of $C = 3, S = 3, D = 1$, thereby introducing a relative error of $(354/3) - 100 = 18\%$ in this special case. However, the effect of this assumption on the results in the thesis, is only an under-estimation of the capacity enhancement achieved by introducing base station antenna arrays.

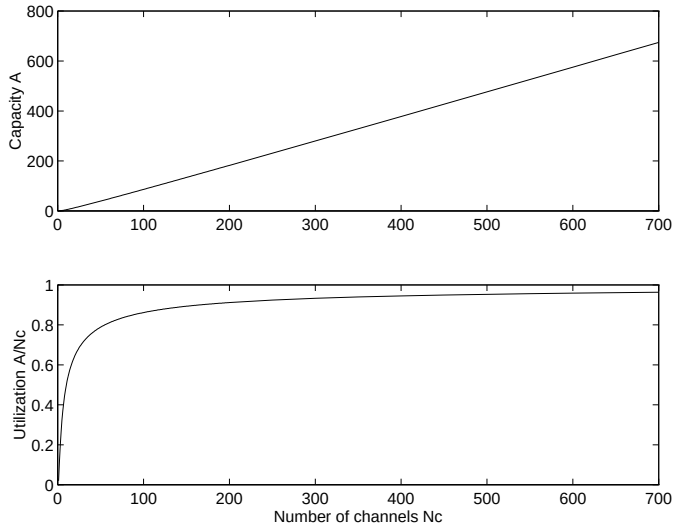


Figure 3.3: *Upper: Carried traffic, $\bar{A}$, as a function of the number of channels, $N_c$ at a $B = 2\%$ blocking probability. Lower: $\bar{A}/N_c$ as a function of the number of channels, $N_c$ at a $B = 2\%$ blocking probability.*

# Chapter 4

# Capacity Results

In the previous chapter, two main capacity enhancement approaches are identified: reduced cluster size (RCS) and same sector frequency reuse (SSFR). In the former approach the capacity is enhanced by increasing the fraction of the total spectrum used in a sector, while the capacity is enhanced by allocating more mobiles on the spectrum already available in the cell in the latter. In the case of the SSFR approach, nulls are steered towards co-channel users within the same sector. In the RCS approach, nulls may or may not be steered towards co-channel users in other cells. The two cases are referred to as RCS-WIN and RCS-WON where WIN and WON stands for "with nulling" and "without nulling", respectively. A beamformer called the "summed interference to carrier ratio minizing" (SICR) beamformer is also introduced in the previous chapter. This beamformer basically steers a main beam towards the desired user and nulls towards a number of co-channel users. Three systems referred to as SICR-SSFR, SICR-RCS-WIN and SICR-RCS-WON employing the SICR beamformer and the three capacity enhancement approaches are also defined in the previous chapter. These three systems are also defined in terms of dynamic channel allocation and uplink power control.

In this chapter, the three systems SICR-RCS-WIN, SICR-RCS-WON and SICR-SSFR are simulated and analyzed in order to find their capacity enhancement potential as a function of critical parameters such as the number of antennas, the mobile power control range, and the angular spreading, $\sigma$, of the environment. Closed form expressions for the "outage probability" i.e., the probability of insufficient transmission quality is also derived and found to agree well with simulation results under certain

conditions. The main findings of this chapter are listed below.

- A large *uplink* power control range is necessary to make the *downlink* inter-cell nulling feature of the SICR-RCS-WIN system effective.
- The uplink near-far ratio, defined as the ratio of the power of the strongest user to the weakest desired user (averaged over fast fading), allocated to the same timeslot (but sometimes different carrier), is typically less than 25dB, for all investigated systems. For the SICR-RCS system with $e = 1$ and fast handover, it is typically less than 4dB.
- The SICR-SSFR system requires around 16 channels (per power group and sector) in order to be able to allocate channels with spatially well separated users.
- The SICR-SSFR system increases capacity more than SICR-RCS-WIN and SICR-RCS-WON systems in most of the investigated cases.
- The capacity enhancement achieved using SICR-RCS-WIN is larger than or equal to that obtained using SICR-RCS-WON.
- The experimental results of Chapter 7 suggest that $\sigma_0 = 3^o$ to $6^o$, $r_0 = \infty$ (the framework is introduced in Section 2.3.1) is a realistic model. Combining this information with the results of Chapter 4, yields the following capacity predictions in the more optimistic case $\sigma_0 = 3^o$: Threefold capacity enhancement is achieved using the SICR-RCS-WIN and SICR-RCS-WON systems with three and five antenna elements per 120-degree sector, respectively (in comparison with a reference system employing a single element per 120-degree sector). Four and tenfold capacity enhancement is achieved with SICR-SSFR using five and eighteen antenna elements respectively. Using SICR-RCS-WIN or SICR-SSFR, eight antenna elements per sector, and an improved handover, a ninefold capacity enhancement is obtained. However, it is unclear how much of the ninefold capacity enhancement should be attributed to the improved handover in this case.
- The derived analytical expression for the outage probability agrees well with simulation results in the SICR-SSFR case if sixteen (or

more) channels per group are employed, in the SICR-RCS-WIN case if $e = 1$ is employed, and in the SICR-RCS-WON case if slow handover is assumed.

The details of this chapter are as follows: In Examples 4.1 and 4.2, the performance of a SICR-SSFR system using $K = 1, S = 3, D = 3$ is compared with that of four SICR-RCS systems employing $K = 1, S = 1$, as a function of the angular spreading $\sigma_0$ assuming $r_0 = \infty$, (definition see Section 2.3.1). The comparison is made by simulations and considers both downlink outage probability (probability of unacceptable transmission performance), uplink power control requirements and so-called uplink near-far ratios. The system considered has an air interface similar to GSM with frequency hopping. The difference between Example 4.1 and 4.2 is in the assumption on the performance of the handover. In Example 4.1, the handover is assumed to be slower than in Example 4.2. This is explained in more detail in Section 4.1 below.

Example 4.3, is a comparison of four versions of the SICR-SSFR systems. This example reveals that the SICR-SSFR system needs power-groups (see Section 3.3.1.1) with more than four channels to achieve the same performance as predicted by the analytical analysis. The simulations of Example 4.4 are identical to those of Example 4.1 except that the propagation parameter $r_0 = 0.35R$ is used rather that $r_0 = \infty$.

Example 4.5 uses the analytical expressions to investigate the influence of channel reuse scheme (i.e., $K, S, D$), angular spreading, $\sigma_0$, and the number of antennas, $m$, on the outage probability.

The chapter is divided into two sections, where the first section introduces assumptions common for all examples, and the second contains the actual results. Some conclusions are drawn in Section 4.3. Two Appendices, 4.B and 4.C, which detail the simulation method and the derivation of the analytical performance expressions, respectively, are also included.

## 4.1 Preliminaries

The comparisons in this chapter assume the GAAO propagation model of Section 2.3.1, with a path loss slope of $\gamma = 3.5$ and a standard deviation in the log-normal fading of $\sigma_L = 8dB$. However, the log-normal fading between a mobile and two base stations are correlated with correlation coefficient 0.5 i.e., $\mathrm{E}\{10\log(L_{i_1,i})10\log(L_{i_2,i})\} = \sigma_{\mathrm{L}}^2/2$, which is in reasonable agreement with the results of [Maw92].

Linear antenna arrays of $m$, antenna elements are employed to cover the 120-degree sector cells. The element patterns $p(x, f)$ of the elements are assumed to to be given by

$$|p(\theta, f)|^2 = \begin{cases} \cos^2(\theta) & \text{if } |\theta| < 90^o, \\ 0 & \text{otherwise,} \end{cases} \tag{4.1}$$

which closely fits the element pattern of the prototype linear array presented in [Joh95]. In the simulations, the antenna spacing is assumed to be half a wavelength at the transmit frequency, i.e., $\Delta = \frac{c}{2f^{\text{TX}}}$, while they are increased to $\Delta = \frac{c}{\sqrt{3}f^{\text{TX}}}$ in the analytical investigations of Appendix 4.C. Half a wavelength antenna spacing is used in the simulations since the results of [MZD+96] has shown that it yields slightly better performance than the larger antenna spacing. The larger antenna spacing is used only to simplify the derivation of the analytical results.

All investigations assume a F/TDMA system with slow pseudo random frequency hopping. Thus the frequency carrier employed by the mobile is chosen pseudo-randomly in each time slot, but remains fixed during the time slot. The frequency-hopping patterns of all mobiles in a cell contain no collisions (except for the same sector and channel mobiles in the SICR-SSFR system which all use the same pattern). It is also assumed that discontinuous transmission is employed, i.e., the base is only transmitting when the user in the fixed network is talking. The probability of this event is assumed to be 50% (this assumption is not important for the qualitative results).

Two types of handover are considered: geometry, and signal strength based. In the first type, the mobile is connected to the base with the strongest gain averaged over both the log-normal *and* the Rayleigh fading. From (2.35), the mobile is thus connected to the base which maximizes

$$\left(\frac{1}{r_{k,i}}\right)^{\gamma} |p(\theta_{k,i}, f)|^2. \tag{4.2}$$

Thus in the geometry based case, the base selection is based on the geometric entities $r_{k,i}$ and $\theta_{k,i}$. In the signal strength case, the base selection is based on the signal strength averaged over the Rayleigh fading *but not* the log-normal fading. As a consequence, the relevant entity is $G_{k,i}$ which is given by (2.35). In the signal strength handover case the mobile starts by connecting to the strongest base. It then makes a handover when one of the neighboring base stations is two times (= 3dB) stronger than the desired base. This introduces a "hysteresis" in the

handover process of 6dB. The geometrical handover case can be seen as a slow-handover assumption while the signal strength based handover can be seen as a fast-handover assumption, since the handover is based on a "more averaged" signal strength measurement in the former case than in the latter. The spatial distribution of the users is assumed uniform.

From (2.37-2.38) it is evident that the signal strength conditioned on $\mathbf{w}_k$, $G_{k,i}$, $r_{k,i}$, $\theta_{k,i}$, $\sigma_{k,i}$ is Rayleigh distributed, for both the desired and interfering users [Lee93]. The mean (over Rayleigh fading) carrier to interference ratio at mobile $i$ is given by

$$\begin{aligned} \mathrm{CIR}_i &= \frac{P_{i,i}}{\sum_{k\neq i} P_{k,i}} \\ &= \frac{G_{i,i}}{\sum_{k\neq i} P_{k,i}}, \end{aligned} \tag{4.3}$$

where $P_{k,i}$ is given by (2.42) and the second equality follows from (3.4). Previous results have shown that 9dB average carrier to interference ratio is sufficient to provide reasonable speech quality in GSM on Rayleigh fading channels, [RU91]. We assume that the crucial factor for the receiver is the probability that the *instantaneous* carrier to interference is less than 3dB. In the case of a single interfering signal (uncorrelated) this probability can be computed using the formula (see [PK91])

$$\Pr\{\mathrm{CIR}_{\text{instantaneous}} \leq \mathrm{CIR}_{\mathrm{t}}\} = \frac{1}{1+\mathrm{CIR}_i/\mathrm{CIR}_t}, \tag{4.4}$$

with $\mathrm{CIR}_t = 10^{0.3}$ and $\mathrm{CIR}_i = 10^{0.9}$ which yields $\Pr\{\mathrm{CIR}_{\text{instantaneous}} \leq \mathrm{CIR}_{\mathrm{t}}\} = 0.2$. The choice of a 3dB "receiver threshold" is justified by simulations, [Wig95], which have shown that CIR = 3dB on a *static channel* (no fading and no time dispersion) is sufficient to obtain a 0.9% frame error rate. In the simulations made below the probability of an instantaneous carrier to interference ratio smaller than 3dB (i.e., $\mathrm{CIR}_{\text{instantaneous}} \leq$ 3dB) are calculated for several mobiles in a simulated cellular system. The fraction of mobiles for which this probability exceeds 20% is seen as an estimate of the so-called *outage probability*.

## 4.2 Results

**Example 4.1**

**Assumptions**

A $K = 1, S = 3, D = 3$ SICR-SSFR system is compared with four SICR-RCS systems employing $K = 1, S = 1$ reuse. Equation (3.2) tells us that the capacity of all these systems are equal. The propagation parameter $r_0$ introduced in Section 2.3.1, is $r_0 = \infty$ which implies that the angular spreading is given by $\sigma_{k,i} = \sigma_0$ independently of the base-mobile distance. All sectors are covered by linear antenna arrays with ten elements and half wavelength inter-element spacing. Two different power control parameters, $e$, are considered for the SICR-RCS systems : $e = 0.3$ and $e = 1$ (see Section 3.3.2.1). A total of six carriers with eight timeslots multiplexed on each is assumed. This yields a total of 48 channels in the system. The simulation considers 48 users in each sector. The SICR-SSFR system uses four power groups with twelve mobiles each. Group 1 uses the first and second time slot, group 2 the third and fourth and so on (see Section 3.3.1.1). The SICR-RCS-WIN systems use a $P_{\min}$ (see Section 3.3.2.3) which is half of the mean power of the six desired users in a TDMA time slot. When $e = 1$ is used in the RCS systems, random channel allocation is employed, whereas the channel allocation of Section 3.3.2.2 is used when $e = 0.3$. In the latter case, eight power groups with six mobiles each are assumed where group number 1 is allocated to the first time slot in the TDMA frame, group 2 to the second and so on.

**Figures**

Simulations for the described systems are made 40 times according to the simulation method described in Appendix 4.B. Histograms of the power transmitted from the mobiles using the power control methods described in Section 3.3.1.1 and 3.3.2.1, are shown in Figure 4.1. The upper, middle, and lower subplots consider the SICR-SSFR system, the SICR-RCS systems with $e = 1$ and the SICR-RCS systems with $e = 0.3$ respectively. The powers are in all three cases normalized such that the mean power transmitted from a mobile is 0dB.

Figure 4.2 shows a histogram of the ratio of the power of the strongest signal to the weakest desired signal in a time slot (all six carriers), in terms of $G_{k,i}$ (see Section 2.3.1), as seen from base $k$. The upper, middle and lower subplot considers the SICR-SSFR system, the SICR-RCS systems with $e = 1$ and the SICR-RCS systems with $e = 0.3$ respectively.

In Figure 4.3 the simulated outage probability (definition see Section 4.1 above), is plotted as s function of the angular spread, $\sigma_0$, see Section

2.3.1. The standard deviation of the estimated outage probabilities is approximately 0.7% and 0.3% at a 10% and 2% true outage probability respectively. In Appendix 4.C approximative analytical expressions of the outage probability are derived for the SICR-SSFR system, the SICR-RCS-WIN system (only the case $e = 1$), and the SICR-RCS-WON (independent of $e$). Results using these expressions are also displayed in Figure 4.3.

**Observations**

From the results of Figure 4.1, it is estimated that 99% of the users have a power control setting within [−15,+14]dB, [−32,29]dB, and [−10,9]dB, in the SICR-SSFR, SICR-RCS($e = 1$), and SICR-RCS($e = 0.3$) case, respectively.

This indicates that a power control range of 30dB, 62dB and 20dB, is required in the three cases respectively. However, in the SICR-RCS cases, this number assumes a perfect choice of the reference level towards which the power is controlled (common reference in all cells). Thus, in practice some extra margin will be needed for these systems.

Figure 4.2 indicates that the uplink processing must be able to suppress interferers that are about 25dB stronger than the desired signal in all three cases. To achieve this the base may exploit frequency selective filtering (when the interference is using another frequency) and array gain selectivity.

The simulations results in Figure 4.3 indicate that the SCIR-SSFR system and the SICR-RCS-WIN system with $e = 1$ has similar performance. However the performance of the SICR-RCS-WIN system with $e = 0.3$ is significantly worse. The SICR-RCS-WON system has approximately the same performance using the two values $e = 1$ and $e = 0.3$. This indicates that the difference in performance between $e = 0.3$ and $e = 1$, in the SICR-RCS-WIN case, is due to a better nulling performance. Thus the conjecture that the base will be able to identify exactly the mobile it needs when $e = 1$, stated in Section 3.3.2.1, appears valid. Note that $e = 1$ implies that the uplink power control completely compensates for the path-loss and shadowing.

The agreement between the simulation results and the corresponding analytical results is found to be reasonable, except for the SICR-SSFR system at $\sigma_0 = 6^o$, where the analytical results are optimistic. In the SICR-SSFR cases, this is because the analytical result assumes that the same sector users are well separated in angle which becomes critical at large angular spreads, as is shown by Example 4.3 below.

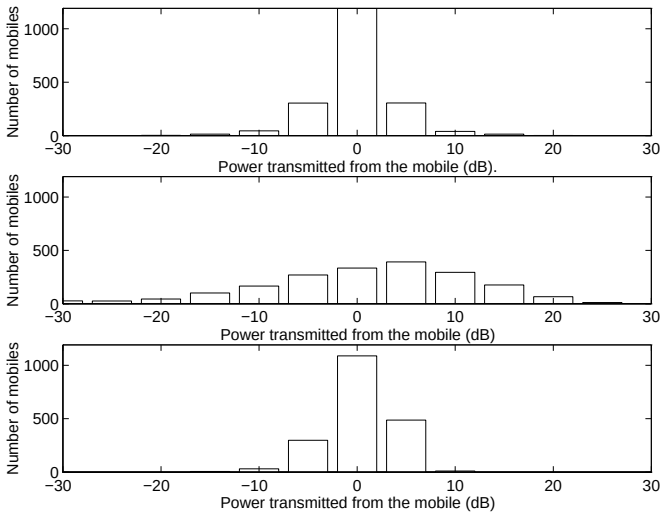


Figure 4.1: *Distribution of the power control settings; upper: SSFR, middle: RCS with* $e = 1$*, lower: RCS with* $e = 0.3$*.*

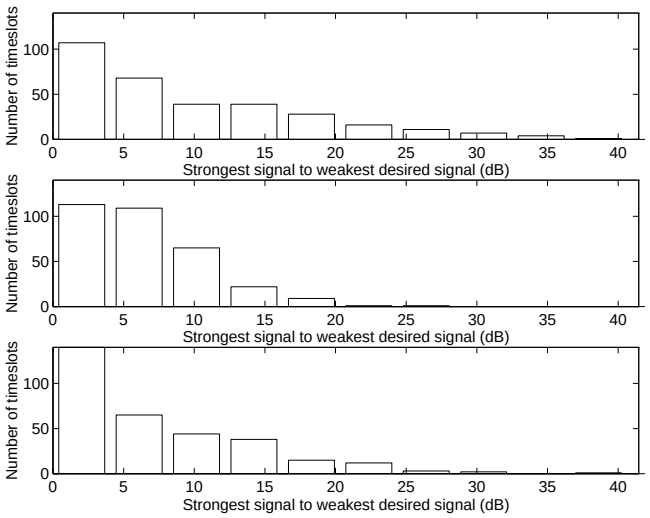


Figure 4.2: *"Near-far" ratios in the* $6 \times 200kHz$ *spectrum; upper: SSFR, middle: RCS with* $(e = 1)$*, lower: RCS with* $e = 0.3$*.*

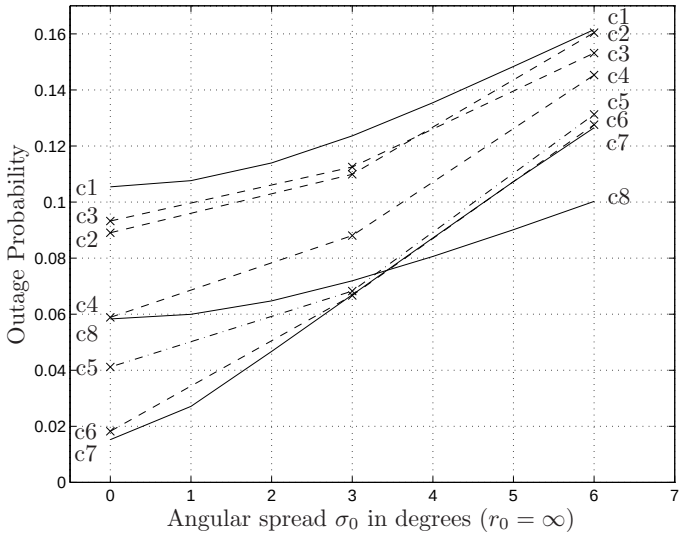


Figure 4.3: *Outage probability as a function of* $\sigma_0$ *with* $r_0 = \infty$*, and geometric based handover.*

| | | | |
|---|---|---|---|
| c1: | SICR-RCS-WON, | $K = 1, S = 1,$ | analytical. |
| c2: | SICR-RCS-WON, | $K = 1, S = 1, e = 1,$ | simulation. |
| c3: | SICR-RCS-WON, | $K = 1, S = 1, e = 0.3,$ | simulation. |
| c4: | SICR-RCS-WIN, | $K = 1, S = 1, e = 0.3,$ | simulation. |
| c5: | SICR-SSFR, | $K = 1, S = 3, D = 3,$ | simulation. |
| c6: | SICR-RCS-WIN, | $K = 1, S = 1, e = 1,$ | simulation |
| c7: | SICR-RCS-WIN, | $K = 1, S = 1, e = 1,$ | analytical. |
| c8: | SICR-SSFR, | $K = 1, S = 3, D = 3,$ | analytical. |

**Example 4.2**

**Assumptions and Figures**

All the simulations and computations performed in Example 1, are repeated but assuming signal-strength based handover, see Section 4.1 above. Figures 4.4, 4.5 and 4.6 are the counterparts of Figure 4.1, 4.2 and 4.3 respectively.

**Observations**

From the results of Figure 4.4, it is estimated that 99% of the users have a power control setting within [−10,+10] dB, [−30,23] dB, and [−9,7] dB , in the SICR-SSFR, SICR-RCS($e = 1$), and SICR-RCS($e = 0.3$) case

respectively. This indicates that a power control range of 21dB, 37dB and 17dB, is required in the three cases respectively

Figure 4.5 shows that the uplink processing has to be able to supress interferers that are about 25dB stronger than the desired signal in the SICR-SSFR and and SICR-RCS($e = 0.3$) cases. However in the SICR-RCS($e = 1$) case, only 4dB is required. This makes this system more suited for a digitalization of the entire receive bandwidth, than the other systems, [Mit95, Wep95].

A comparison of Figure 4.3 and 4.6 reveals that the outage probability of all systems has decreased significantly with the introduction of signal strength handover. The improvement is particularly large for the RCS systems. The highest performance is obtained with SICR-RCS-WON and $e = 1$. The outage probability of SICR-RCS-WIN is only slightly smaller than that of SICR-RCS-WON when $e = 0.3$, but significantly smaller when $e = 1$. This again confirms the conjecture of Section 3.3.2.1. The agreement between analytical and simulation results is reasonable for the SICR-RCS-WIN ($e = 1$) system, although the analytical result is somewhat pessimistic. In the SICR-SSFR case the agreement is good except when $\sigma = 6^o$. The reason being the same as in the previous example, i.e., that the same-sector co-channel users become very close due to the very small number of channels. This interpretation finds support in the results of Example 4.3 below. The reason for the pessimtic predictions of the closed form expressions in the RCS cases is probably that with $(K, S) = (1, 1)$ and signal strength handover, both the distribution of the path-gain to the desired and the interfering bases improve (as compared to geometric handover), while only the improvement of the path-loss to the desired base is modeled by the closed form expressions.

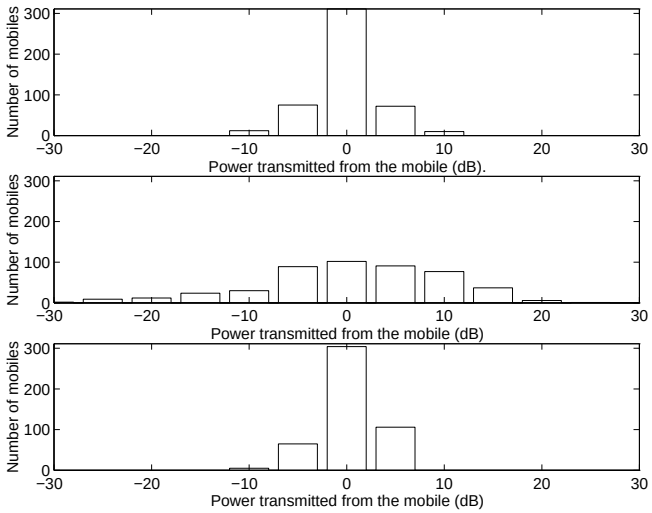


Figure 4.4: *Distribution of the power control settings; upper: SSFR, middle: RCS with* $e = 1$*, lower: RCS with* $e = 0.3$*.*

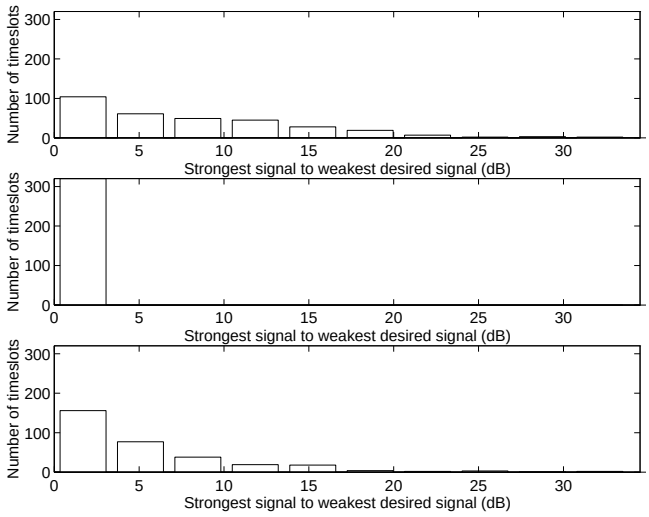


Figure 4.5: *"Near-far" ratios in the* $6 \times 200kHz$ *spectrum; upper: SSFR, middle: RCS with* $e = 1$*, lower: RCS with* $e = 0.3$*.*

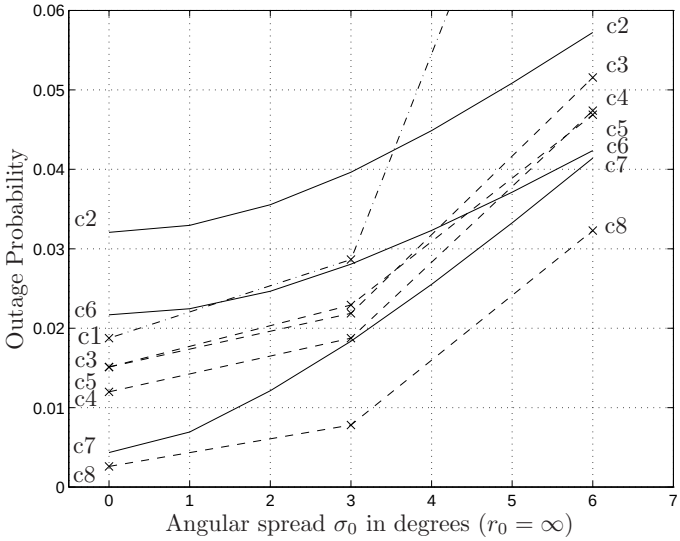


Figure 4.6: *Outage probability as a function of* $\sigma_0$ *with* $r_0 = \infty$*, and signal-strength based handover.*

| | | | |
|---|---|---|---|
| c1: | SICR-SSFR, | $K = 1, S = 3, D = 3,$ | simulation. |
| c2: | SICR-RCS-WON, | $K = 1, S = 1,$ | analytical. |
| c3: | SICR-RCS-WON, | $K = 1, S = 1, e = 0.3,$ | simulation. |
| c4: | SICR-RCS-WIN, | $K = 1, S = 1, e = 0.3,$ | simulation. |
| c5: | SICR-RCS-WON, | $K = 1, S = 1, e = 1,$ | simulation. |
| c6: | SICR-SSFR, | $K = 1, S = 3, D = 3,$ | analytical. |
| c7: | SICR-RCS-WIN, | $K = 1, S = 1, e = 1,$ | analytical. |
| c8: | SICR-RCS-WIN, | $K = 1, S = 1, e = 1,$ | simulation. |

**Example 4.3**

**Assumptions**

The performances of four SICR-SSFR systems all using $K = 1, S = 3, D = 3$ are compared. The difference between the four SICR-SSFR systems is in the channel allocation, power control and handover. Two of the systems uses four power groups as in previous examples, while the other two uses only one power group (no grouping). Thus in the latter

case, a larger uplink power control range is needed. The simulations and computations performed in Example 4.1 and Example 4.2 are repeated.

**Figures**

In Figure 4.7, the performance of the four systems is plotted as a function of the multipath angular spread.

**Observations**

The performance with only one power group, is very close to the analytical performance curve, under both handover assumptions, while the performance of the four-groups system is worse at large angle spreads. The reason for this behaviour is that the one-group system is capable of separating same channel users more in angle than the four-group system. This in turn is due to the fact that there are 16 channels per group in the one-group case, while there are only 4 channels per group in case of four power groups.

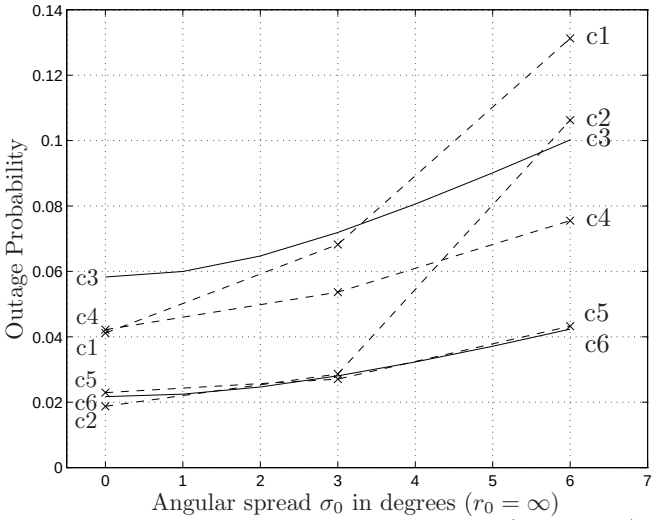


Figure 4.7: *Outage probability as a function of $\sigma_0$ (in degrees) with $r_0 = \infty$, and signal strength as well as geometric based handover.*

| | | |
|---|---|---|
| c1: SICR-SSFR, | geometric HO | four power groups, simulation. |
| c2: SICR-SSFR, | signal HO | four power groups, simulation. |
| c3: SICR-SSFR, | geometric HO | analytical. |
| c4: SICR-SSFR, | geometric HO | one power group, simulation |
| c5: SICR-SSFR, | signal HO | one power group, simulation. |
| c6: SICR-SSFR, | signal HO | analytical. |

HO = Handover

**Example 4.4**

**Assumptions and Figures**

All the simulations and computations performed in Example 4.1, are repeated but using $r_0 = 0.35R$ (where $R$ is the cell radius) rather than $r_0 = \infty$. Thus, the angular spreading starts to decrease at base-mobile distances larger than $r_0 = 0.35R$. Note that only $\approx 15\%$ of the users are camping inside $r_0 = 0.35R$.

In Figure 4.8 the estimated outage probability (definition see Section 4.1 above), is plotted as s function of the multipath angular spread $\sigma_0$, see Section 2.3.1.

**Observations**

The results in Figure 4.8 show that the SICR-RCS-WIN system has the lowest outage probability, of all five systems, if $e = 1$ is applied. How-

ever, this superiority is lost, at small $\sigma_0$, if $e = 0.3$ is used. In contrast to Example 4.1 and 4.2, the performance of the SICR-RCS-WIN, $e = 1$ system, is pessimistic at large angular spreading. The reason is probably because the analytical expression assumes that the angular spreading of the desired user is estimated (erronously) by all bases to be zero. When the angular spreading of the desired user is large, and the angular spreading of the identified interfered users is small, this assumption becomes pessimistic.

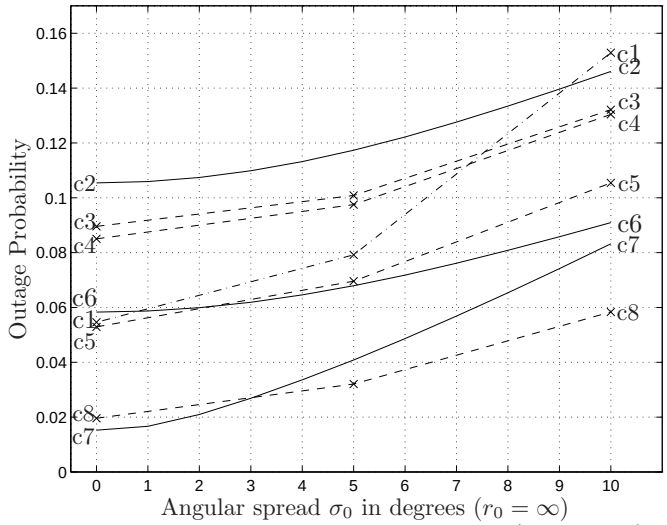


Figure 4.8: *Outage probability as a function of $\sigma_0$ (in degrees) with $r_0 = 0.35R$, and geometric based handover.*

| | | | |
|---|---|---|---|
| c1: | SICR-SSFR, | $K = 1, S = 3, D = 3,$ | simulation. |
| c2: | SICR-RCS-WON, | $K = 1, S = 1,$ | analytical. |
| c3: | SICR-RCS-WON, | $K = 1, S = 1, e = 0.3,$ | simulation. |
| c4: | SICR-RCS-WON, | $K = 1, S = 1, e = 1,$ | simulation. |
| c5: | SICR-RCS-WIN, | $K = 1, S = 1, e = 0.3,$ | simulation. |
| c6: | SICR-SSFR, | $K = 1, S = 3, D = 3,$ | analytical. |
| c7: | SICR-RCS-WIN, | $K = 1, S = 1, e = 1,$ | analytical. |
| c8: | SICR-RCS-WIN, | $K = 1, S = 1, e = 1,$ | simulation. |

In the next example, our goal is to estimate the capacity enhancement

achieved using the proposed systems as a function of the channel reuse scheme, number of antennas, and angular spreading. The parameter $r_0$ is set to $r_0 = \infty$, since this value has support in the experimental results of Chapter 7. To do this evaluation by means of the simulation procedure described in Appendix 4.B, would require months of simulation time. Therefore we resort to the use of the analytical expressions of Appendix 4.C. The results of Example 4.1, and 4.3 inidicate that these espressions are accurate for all systems in the geometric handover case. In the signal-strenght handover case, the expressions are only accurate for the SICR-SSFR system and the SICR-RCS-WIN ($e = 1$) system, see Example 4.2 and 4.3. Note that for $\sigma_0$ larger than three degrees, Example 4.3 indicates that, the SICR-SSFR system achieves the analytical performance if more than sixteen channels are available per group. In practical applications, it is likely that this is the case even if several power groups are employed.

**Example 4.5**

**Assumptions**

This example investigates the impact of the number of antennas $m$, the angular spread $\sigma_0$, ($r_0 = \infty$) on the performance of the systems for which the analytical expressions agree with simulation results (see above). As a reference, a $K = 3, S = 3$ system with one antenna per sector, i.e., $m = 1$, employing geometric handover is used. The outage probability for this system is estimated to be 2.2% (using the analytical expression for the SICR-RCS-WON system). For the SICR-SSFR system the channel reuses $(K, S) =$\{(3, 3),(3, 1),(4, 1),(1, 3),(1, 1)\} are considered with $D = 2, \ldots, 9$, $\sigma_0 = \{0^o, 3^o, 6^o\}$, $m = 1, \ldots, 20$ and geometric as well as signal strength based handover. The SICR-RCS-WON and the SICR-RCS-WIN($e$=1) systems are considered using $(K, S) = \{(4, 1),(1, 3),(3, 1),(1, 1),\ (1.5, 1),(2, 1)\}$. The channel reuse schemes $(K, S) = (1.5, 1)$ and $(K, S) = (2, 1)$ were not introduced in Section 3.1.1. However, they are defined in Appendix 4.A below.

**Results:**

In Figure 4.9 and 4.10 below, the number of antennas required to achieve an outage probability less than 2.2% is plotted as a function of the (relative) spectrum efficiency $9E$, (note that for the reference system $E = 1/9$) for the SICR-SSFR system, assuming geometric and signal-strength handover, respectively (only the most favorable frequency reuses in terms of $K$ and $S$ are shown). In Figure 4.11 and 4.12 the number of antennas required to achieve the target performance is plotted as a function of

the spectrum efficiency $9E$, for the SICR-RCS-WIN system, assuming geometric and signal-strength handover, respectively. The corresponding results for the SICR-RCS-WON systems are shown in Figure 4.13.

**Observations**

The highest capacity is always achieved with SICR-SSFR with a few exceptions. In these exceptional cases, the SICR-SSFR system requires an additional antenna (per sector) to achieve the same capacity as SICR-RCS-WIN. The SICR-SSFR system achieves its performance by a combination of a reduced cluster size and multiple mobiles per channel. An important feature of the SICR-SSFR system, especially when signal-strength handover is employed, is its ability of delivering capacity larger than one (in terms of $E$ defined in (3.2)).

At a given number of antenna elements per sector, the capacity of SICR-RCS-WIN is always higher than that of SICR-RCS-WON, except when three antennas per sector, and geometric handover is applied. In this case the capacity of the SICR-RCS-WIN and SICR-RCS-WON are equal.

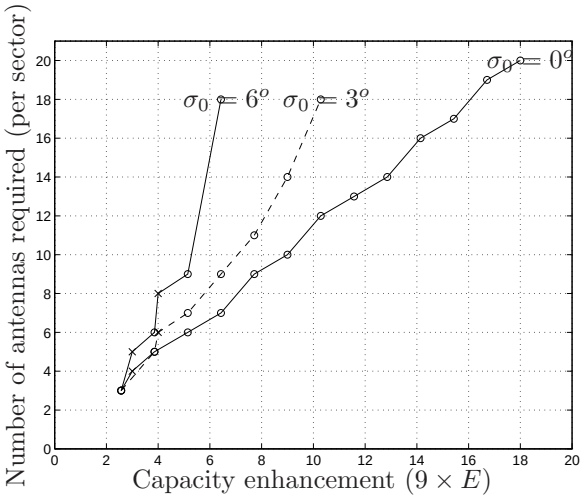


Figure 4.9: *Number of antennas required as a function of capacity for the SICR-SSFR system, in the geometric handover case. The points in the plot correspond to 'x': $K = 3, S = 3$, $D = 2, 3$ 'o': $K = 7, S = 1, D = 2, \ldots, 9$.*

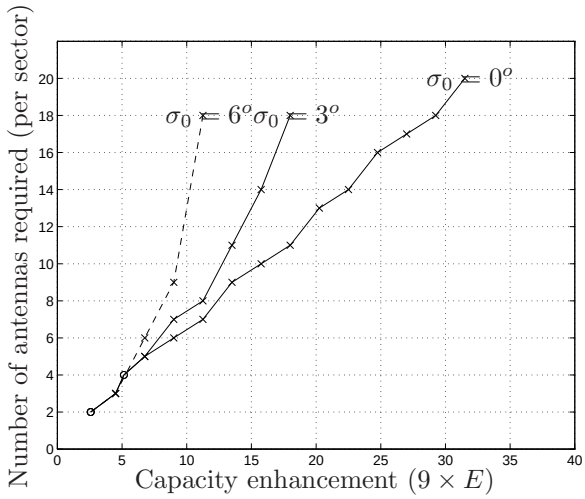


Figure 4.10: *Number of antennas required as a function of capacity for the SICR-SSFR system, in the signal-strength handover case. The points in the plot correspond to 'x':* $K = 4, S = 1,\ D = 2, 3, \ldots, 14$ *'o':* $K = 7, S = 1, D = 2, 4$.

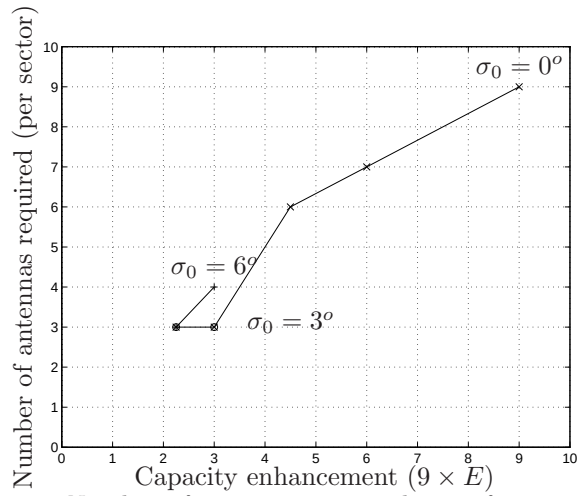


Figure 4.11: *Number of antennas required as a function of capacity, for the SICR-RCS-WIN system (using* $e = 1$*) assuming geometric handover. The points in the plot correspond to 'x':* $\sigma_0 = 0^o$*, 'o':* $\sigma_0 = 3^o$*, and '+':* $\sigma_0 = 6^o$*. The frequency reuses employed are* $(K,S) = \{(4,1),(1,3),(2,1),(1.5,1),\ (1,1)\}$.

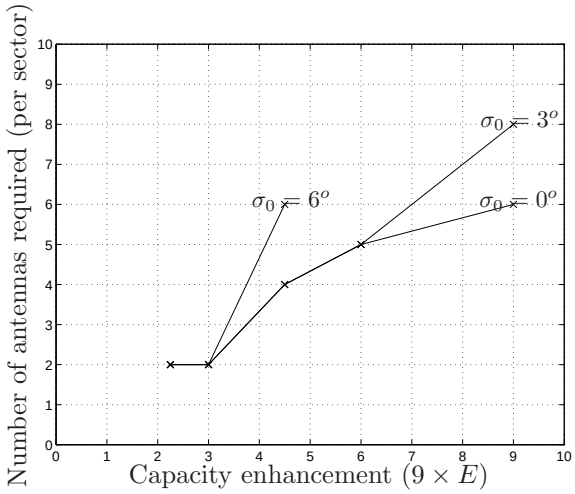


Figure 4.12: *Number of antennas required as a function of capacity, for the SICR-RCS-WIN system (using* $e = 1$*) assuming signal-strength handover. The points in the plot correspond to* $(K, S) = \{(4,1),(1,3),(2,1),(1.5,1),(1,1)\}$.

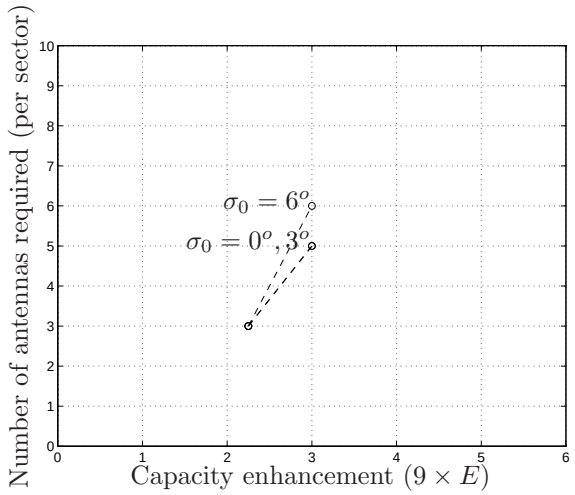


Figure 4.13: *Number of antennas required as a function of capacity, for the SICR-RCS-WON system assuming geometric handover. The points in the plot correspond to* $(K, S) = \{(4,1),(3,1)\}$.

## 4.3 Conclusions and Discussion

The following sections list conclusions drawn from the observations made above, and discuss critical assumptions.

### 4.3.1 Uplink Near-Far Effects and Power Control

In Examples 4.1 and 4.2 the near-far ratio, defined as the quotient of the power of the strongest user to the power of the weakest desired user allocated to the same time-slot (averaged over the fast fading), is investigated for the different systems. The results show that this ratios up to 25dB occurs for all systems except one. This system is SICR-RCS with $e = 1$ and signal-strength handover. For this system the near-far ratio is typically less than 4dB. We believe that the near-far ratio 25dB is manageable, although 4dB is of course more favorable. For instance a smaller number of bits is required in the analogue to digital converters. This makes the SICR-RCS with $e = 1$ and signal-strength handover *more* suited for a completely digital uplink solution[1], than the other investigated alternatives.

The results of Examples 4.1 and 4.2 also show that the dynamic power control range in the mobiles must be larger than 50dB in the $e = 1$ case, while $\approx$ 30dB is sufficient in the $e = 0.3$ and SICR-SSFR case. As a reference, the GSM standard supports a power control range of 30dB, [MP92].

Critical for the conclusions in this section regarding the SICR-RCS system with $e = 0.3$ is that the speed of the intra-cell channel allocation is fast enough to follow the shadow fading. With $e = 1$, the critical assumption is that the power control is fast enough to follow the shadow fading. For the SICR-SSFR system both requirements are critical.

It is concluded that the uplink near-far problem can be managed if a sufficiently fast power-control or intra-cell handover is available. The smallest uplink near-far ratios are obtained if a fast inter-cell handover and power control with $e = 1$ is employed.

[1] by this we mean that the entire receive bandwidth is digitized at once [Mit95, Wep95]

### 4.3.2 Uplink Power Control Downlink Performance Dependence

The results of Examples 4.1, 4.2, and 4.5 show that the uplink power control is critical for the downlink performance of systems with downlink inter-cell nulling. In particular, the results show that the power control parameter $e = 1$ yields much better results than $e = 0.3$. Thus the conjecture of Section 3.3.2.1, which stated that the base will be able to identify and null the mobiles with poor downlink quality if $e = 1$ is applied, appears correct.

Is this result general ? If the identification threshold $P_{\min}$ is made sufficiently small (i.e., the base can identify very weak mobiles), then $e = 0.3$ will perform equally well. The conclusion may thus not be true for any system. However, the result indicates the importance of an issue which is typically overlooked. It should also be noted that the SICR beamformer takes the desired signal strength at identified interfering mobiles into account in the criterion function (in order to achieve this, information has to be transmitted between the bases in the $e = 0.3$ case but not in the $e = 1$ case, Section 3.3.2.3). If this is not the case, the effect may be worse since deep nulls can point towards users with already good signal to interference ratio. This problem does not arise in systems with only two users and two base stations, and analysis and experiments under such conditions can therefore be misleading. The issues raised here apply equally to TDD systems as to FDD systems.

### 4.3.3 Agreement Between Simulation and Analytical Results

An investigation of Examples 4.1, 4.2, 4.3 and 4.4 reveals that the closed form expressions for the outage probabilities of the SICR-SSFR, SICR-RCS-WIN($e = 1$) and SICR-RCS-WON systems are accurate or pessimistic in all cases but one. The exception is SICR-SSFR with large angular spread and a small number of channels, and thereby not well separated same-channel users, see Example 4.3. From this discussion it is concluded that the analytical expressions can be used to obtain an initial pessimistic estimate of the performance of a given approach, although it should be kept in mind that the SICR-SSFR system needs well separated same-sector co-channel users to achieve its analytical performance at high angular spread values.

The accuracy of the closed form expression is found to be good in the

SICR-SSFR case if sixteen (or more) channels per group are employed, see Example 4.3. In the SICR-RCS-WIN case good agreement is found if $e = 1$ is employed, see Examples 4.1,4.2 and 4.4. In the SICR-RCS-WON case finally, slow handover has to be assumed to achieve good agreement, see Example 4.1 and 4.2.

The critical assumptions for the closed-form solutions are the same as for the simulations and are treated in Section 4.3.4, below.

### 4.3.4 Capacity Estimates

Based on Example 4.3 the following conclusions are drawn: The highest capacity enhancement is achieved with SICR-SSFR with a few exceptions. In these exceptional cases, the SICR-SSFR system requires an additional antenna (per sector) to achieve the same capacity as SICR-RCS-WIN. The SICR-SSFR system achieves its optimal performance by a combination of a reduced cluster size and multiple mobiles per channel. An important feature of the SICR-SSFR system, especially when signal-strength handover is employed, is its ability to deliver a capacity larger than one (in terms of $E$ defined in (3.2)).

At a given number of antenna elements per sector, the capacity of SICR-RCS-WIN is always higher than or equal to that of SICR-RCS-WON.

The results of Chapter 7 show that reasonable performance predictions are obtained using the parameter setting $r_0 = \infty$ and $\sigma_0 = 3^o$ to $6^o$. Using the more optimistic value $\sigma_0 = 3^o$, and the results of Example 4.3 the following performance predictions are made:

Using five antenna elements per sector and the SICR-RCS-WON approach, a threefold capacity enhancement is achieved. Using SICR-RCS-WIN($e = 1$) threefold capacity enhancement is achieved using only three antennas. Using SICR-SSFR and five or eighteen antennas per sector, four and tenfold capacity enhancement is achieved respectively. With an improved handover, ninefold capacity enhancement is achieved with SICR-RCS-WIN($e = 1$) and SICR-SSFR using seven and eight antenna elements per sector, respectively. However, it is unclear how much of the ninefold capacity enhancement should be attributed to the improved handover in this case.

A critical assumption for the SICR-SSFR systems is the user distribution. As illustrated by Example 4.3, the system needs same-cell users with good spatial separation. As is also shown by Example 4.3, this can probably be achieved if a reasonable number channels are available, *and*

the users are uniformly distributed in the cell. The latter condition is one of the critical issues of SSFR approaches. In the RCS cases, there is no immediate reason to expect degradation in the overall performance of the network if the user distribution is not uniform.

The results of Chapter 7 indicated that $\sigma_0 = 3^o$ to $6^o$, $r_0 = \infty$ yields good average performance predictions, although significant deviations occur in particular instances. In the RCS approaches there is good hope that these deviations do not effect performance negatively. This is because the RCS approaches herein do not attempt to allocate users in a fashion that maximizes the interference suppression of the adaptive antenna pattern. In contrast, the SSFR system allocates the users such that desired and interfering signal directions have disjunct angular power distributions. This means that the performance deviations (between the performance predicted by the model and the actually obtained performance), may cause degradation in the SSFR case.

In conclusion, the SICR-SSFR system provides the highest capacity in most investigated cases, under the uniform user distribution and the GAAO propagation model. The capacity of SICR-RCS-WIN($e = 1$) only matches or exceeds the SICR-SSFR system for a few parameter settings. On the other hand, the SICR-RCS-WIN($e = 1$) system appears to be more robust with respect to the propagation and user distributions. For this reason, the SICR-RCS-WIN($e = 1$) is the system of choice, in the cases when the capacity of the two systems are equal. In the remaining very large number of cases, the impact of the performance deviations between predicted and actually obtained performance in Chapter 4, has to be evaluated. There is thus no clear "winner" between SICR-RCS-WIN($e = 1$) and SICR-SSFR. The capacity of the SICR-RCS-WIN($e = 1$) equals or exceeds that of the SICR-RCS-WON, at a given number of antenna elements per sector.

There is no reason to believe that the conclusions drawn here for the SICR-SSFR, SICR-RCS-WIN($e = 1$) and SICR-RCS-WON systems, should not be representative to the more general class systems based on the SSFR, RCS-WIN and RCS-WON principles, Section 3.1.3.

## Appendix 4.A Frequency Reuse $(K, S)$=$(1.5, 1)$ and $(K, S) = (2, 1)$

In Section 3.1.1 different frequency planning schemes in terms of $K$ and $S$ are introduced. The capacity of the schemes under the RCS approach is given by

$$E = \frac{1}{K \times S}, \tag{4.5}$$

see Section 3.1.3. A problem is that there is no reuse scheme in Section 3.1.1 with capacity between $E = 1/3$ and $E = 1$. However, two such schemes are introduced here, for the case that frequency hopping is applied. Under both introduced schemes frequency planning is first done according to $(K, S) = (1, 1)$. Thus the entire spectrum is allocated to all sectors. However, in the $(K, S) = (1.5, 1)$ case only $1/1.5 = 0.66\%$ of the channels available in a sector are allowed to be used at the same time. This is implemented such that the mobiles hop on all the frequencies available, but only $1/1.5 = 0.66\%$ of the possible collision free hopping patterns are used at the same time. The outage probability of the reuse scheme is obtained by using the results of Section 4.C.1 and 4.C.2 using the geometric of the $(K, S) = (1, 1)$ system, but with a reduced voice activity factor. The voice activity factor is reduced from DTX $= 0.5$ to DTX $= 0.5 \times 0.66$. The reason being that in order to obtain interference from a certain base station in a certain point in time, there must be a user allocated to the same frequency in the interfering base station (probability 66%) and that user must be active (probability 50%). The $(K, S) = (2, 1)$ reuse scheme is generated the same way, using at most 50% of the channels available. Obviously, this is modeled by reducing the DTX factor to DTX $= 0.5 \times 0.5$.

# Appendix 4.B Simulation Procedure

The enumeration below describes the simulation procedure used in the paper.

1. The positions of the $11 \times 3 \times 48$ users in cells 1-9,12-13, are generated as follows: The position of user $i$ is randomized with equal probability in the area

$$(\frac{cos(30^o)}{\cos(\theta_{i,i})})^{2/\gamma}(\frac{r_{i,i}}{R}) \leq 2,\ |\theta_{i,i}| \leq 60^o. \tag{4.6}$$

   The log-normal fading to each neighboring base station is randomized and the corresponding path gain is calculated. The position of the user and the log-normal fading are regenerated (randomized) if a "failure" is detected. In the slow-handover case a failure has occurred if the average path-gain defined by (4.2) is larger for some base other than base $i$. In the fast-handover case a failure has occurred if the strongest path gain i.e., $\max_k G_{k,i}$ is more than 3dB stronger than the desired-base path gain $G_{i,i}$. If there are $n$ base stations which are stronger then $0.5G_{i,i}$ (including the $i$th base), then a "failure" is generated with probability $(n-1)/n$. Thus a random number is drawn to determine if a "failure" has occurred or not.

2. The channel allocation algorithms are invoked (Sections 3.3.1.1 and 3.3.2.2). All simulations assume that the TDMA slots of the base stations are synchronized, although this is critical only for the reduced cluster size approach with directed nulls. However, the TDMA frames are desynchronized in the sense of each base having a random offset of 1-8 eight bursts.

3. Weighting vectors (Chapter 3) are calculated for all users in sectors 1a-c, 2b-c, 3b, 4a, 5a, 6a, 7c in the 1/1 reuse case and 1a, 4a, 5a, 6a in the 1/3 reuse case. In the SSFR approach only one weighting vector per user is necessary. This applies also to the reduced cluster size approach if nulling is not applied. With nulling however, multiple weighting vectors per user must be calculated. This is due to the fact that frequency hopping is applied and thereby different co-channel users appear in different time slots. In order to calculate the weighting vectors it is therefore necessary to determine which

users are identified by the base. This requires the power control settings to be calculated. Thus the power control at the mobiles are calculated first. Then it is determined which of the interfered users are stronger than $P_{\min}$, (and thus identified, see Section 3.3.2.3). Only users in neighboring cells are candidates.

4. For each of the 48 users in subcell 1a, it is investigated whether they are experiencing acceptable speech quality or not. Based on the reasoning in Section 4.1, we assume that this is the case if the *instantaneous* signal to interference ratio exceeds 3dB in at least 80% of the time slots. The fraction is calculated as follows: The mean desired power averaged over fading $G_{i,i}$ for the considered user is calculated using (2.35). A random frequency hopping pattern is simulated by randomizing the co-channel user in cells $1-7$ with neighboring cells 10000 times. For each of the 10000 hops the co-channel users are drawn with equal probability among the mobiles allocated in the time slot. The mean interference (averaged over fading) at user $i$, is calculated for each hop using the formula

$$I_i = \sum_{k \neq i} \eta_k G_{k,i} \mathbf{w}_k^* \mathbf{R}(\theta_{k,i}, \sigma_{k,i}) \mathbf{w}_k, \tag{4.7}$$

where $\mathbf{w}_k$ is the weighting vector of the $k$th user and $G_{k,i}, \theta_{k,i}$, and $\sigma_{k,i}$ are the propagation parameters between the $i$th user and the $k$th users desired base (can be the same base in the SSFR case), see Figure 4.14 below. The sectors selected in the sum of (4.7) are the co-channel users in cell 1b, 1c, 2b, 2c, 3b, 4a, 5a, 6a, 7c in the $K = 1$,$S = 1$ case, and 1a, 4a, 5a, 6a in the $K = 1$,$S = 3$ case. Notice that with SSFR, there are $D$ co-channel users per sector (Section 3.3.1).

To simulate discontinuous transmission the factor $\eta_k$ is randomized independently for each hop ($\Pr\{\eta_k = 1\} = 1 - \Pr\{\eta_k = 0\} = \mathrm{DTX} = 0.5$), except the same sector co-channel users which are assumed to be active all the time. Note that the users who use the same channel within the same sector are the same in each time slot (Section 3.3.1.1). When the mean desired and interfering signals have been calculated the probability for the instantaneous signal to interference ratio to exceed 3dB is calculated using (4.4) (for the concider hop) This probability is averaged over the hops to obtain the fraction of time which the considered user has a signal to interference ratio better than 3dB.

Finally, the number of users with acceptable speech quality are counted and the outage probability is estimated as the fraction of users in sub-cell 1a with unacceptable quality.

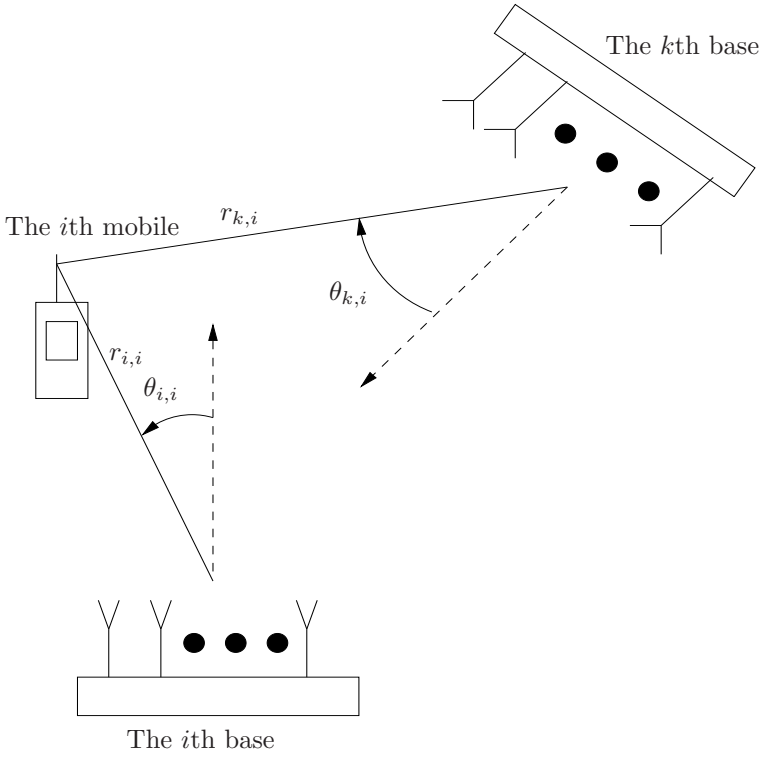


Figure 4.14: *Illustration of the downlink geometry*

## Appendix 4.C Analytical Results

In this section, we derive analytical approximations of the outage probability for the SICR-SSFR system, the SICR-RCS-WIN (only in the $e = 1$ case) and the SICR-RCS-WON (independent of $e$). In order to obtain analytical expressions we make some assumptions which are different from the assumptions used in the simulations. Among those assumptions are the antenna spacing, the number of users in the system and the spatial distribution of the users. The antenna spacing is slightly increased to

$$\Delta = \lambda/\sqrt{3}, \tag{4.8}$$

and the number of users is assumed large (infinite). The spatial probability density of the user positions (seen from the desired base) is assumed to be given by

$$f(r_{i,i}, \theta_{i,i}) = \text{constant} \times \begin{cases} r_{i,i} \cos^{(1-4/\gamma)}(\theta_{i,i}) & \text{if } r \le r_0 g(\theta), |\theta| \le 60^o \\ 0 & \text{elsewhere,} \end{cases} \tag{4.9}$$

where $g(\theta)$ is given by

$$g(\theta) = R(\frac{\cos(\theta_{i,i})}{\cos(30^o)})^{2/\gamma}, \tag{4.10}$$

and the choice of $r_0$ is defined by the handover algorithm assumed. In Sections 4.C.3-4.C.2 below approximative expressions for the outage probability (probability of unacceptable speech quality) conditioned on the user position are obtained for the three cases. In order to obtain the unconditioned outage probability, the sub-cells are divided into "elements", $\Omega(i_1, i_2)$ , defined by

$$\Omega(i_1, i_2) = \{0.05i_1 \le (\frac{\cos(30^o)}{\cos(\theta_{i,i})})^{2/\gamma}(r_{i,i}/R) \le 0.05 + 0.05i_1, \text{ and } 5i_2 - 60 \le \theta \le 5i_2 - 55\}. \tag{4.11}$$

This partitioning is illustrated in Figure 4.15 using $i_1$=0,...,17, $i_2$ = 0,...,23, i.e., $r_0 = 0.9$. The outage probability is calculated for a central

point in each element. Then, the unconditioned outage probability is obtained as the sum of the central point outage probabilities weighted by the fraction of users in the element. These fractions are calculated using the formula

$$\int_{\Omega(i_1,i_2)} f(r,\theta)\mathrm{d}r\mathrm{d}\theta = \frac{((0.4+0.05i_1)^2-(0.35+0.05i_1)^2)}{\sqrt{3}r_0^2}\times (\sin(5i_2-55)-\sin(5i_2-60)). \quad (4.12)$$

The intuition behind the approach is that the elements should be small enough that the outage probability is approximately constant within an element.

It is easily shown that the mean downlink desired signal strength along the borders of the "annular elements" (where annular element $i_1$ is defined as $\bigcup_{i_2}\Omega(i_1,i_2)$) are constant. If the user distributions of all subcells in the system are added, only small spots are left "empty" if $r_0 = 0.9$ is used. Thus $r_0 = 0.9$ will be used when "geometric based handover" is assumed. Previous results, [MP92], have shown that the gain of mobile assisted over geometric based handover is about 4dB. We model this effect by choosing $r_0 = 0.7$, and thereby moving the mobiles (a distance corresponding to 4dB, using $\gamma = 3.5$), closer to the base. In Sections 4.C.1, 4.C.2 and 4.C.3 below, SICR-RCS-WIN, SICR-RCS-WON and SICR-SSFR are treated respectively. The SICR-RCS-WIN system is only investigated in the case $e = 1$. ($e$ is defined in Section 3.3.2.1).

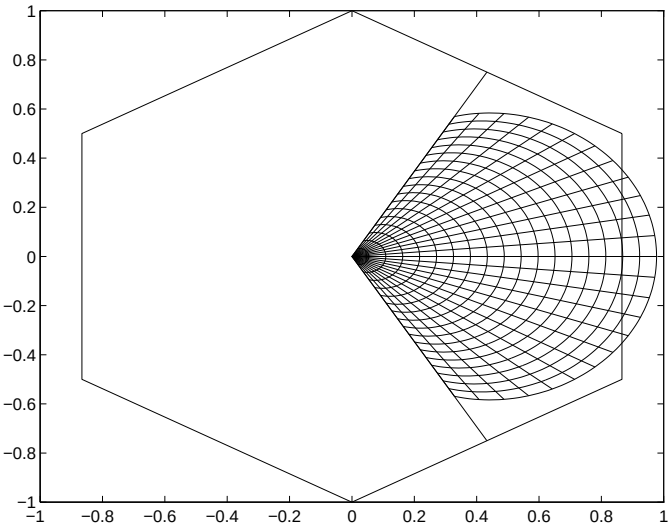


Figure 4.15: *The division of the subcell*

### 4.C.1 SICR-RCS-WIN with $e = 1$

Consider the speech quality experienced by the $i$th user. We assume that all bases erroneously believe that their desired mobile has zero angular spread i.e., $\sigma_{k,k} = 0^o$ for all $k$. Using the equations of Section 3.2.1 and

$$\mathbf{R}(\theta_{k,k}, 0) = \tilde{\mathbf{a}}(\theta_{k,k})\tilde{\mathbf{a}}^*(\theta_{k,k}), \tag{4.13}$$

where $\tilde{\mathbf{a}}(\theta)$ is defined by

$$\tilde{\mathbf{a}}(\theta) = [1, \exp(-j2\pi \sin(\theta)/\sqrt{3}), \ldots, \exp(-j2\pi(m-1)\sin(\theta)/\sqrt{3})]^T. \tag{4.14}$$

yields the following expression for the weighting vector at the $k$th base

$$\mathbf{w}_k = \mathbf{M}^{-1}\tilde{\mathbf{a}}(\theta_{k,k})/(\tilde{\mathbf{a}}^*(\theta_{k,k})\mathbf{M}^{-1}\tilde{\mathbf{a}}(\theta_{k,k})). \tag{4.15}$$

Assuming that base $k$ has identified the $i$th mobile (i.e., the parameters $G_{k,i}/G_{i,i}$,$\theta_{k,i}$ and $\sigma_{k,i}$ are known by the $k$th base) and no other co-channel mobile yields

$$\mathbf{M} = \mathbf{B}((2\pi/\sqrt{3})\sin(\theta_{k,i}))\mathbf{D}_{k,i}\mathbf{B}^*((2\pi/\sqrt{3})\sin(\theta_{k,i})) \tag{4.16}$$

where

$$\mathbf{D}_{k,i} = \frac{G_{k,i}}{G_{i,i}}\mathbf{R}(0, \sigma_{k,i}\cos(\theta_{k,i})) + (r-1)P_{\min}\mathbf{I}, \tag{4.17}$$

and

$$\mathbf{B}(x) = \mathrm{diag}(1, \exp(-jx), \ldots, \exp(-j(m-1)x)). \tag{4.18}$$

Using (3.3) and (4.15) we obtain that the undesired power (averaged over the fast fading) at the identified interfered user is given by

$$G_{k,i}\mathbf{w}_k^*\mathbf{R}(\theta_{k,i}, \sigma_{k,i})\mathbf{w}_k = \frac{G_{k,i}\tilde{\mathbf{a}}^*(\theta_{k,k})\mathbf{M}^{-1}\mathbf{R}(\theta_{k,i}, \sigma_{k,i})\mathbf{M}^{-1}\tilde{\mathbf{a}}(\theta_{k,k})}{(\tilde{\mathbf{a}}^*(\theta_{k,k})\mathbf{M}^{-1}\tilde{\mathbf{a}}(\theta_{k,k}))^2}. \tag{4.19}$$

Using

$$\mathbf{M}^{-1} = \mathbf{B}((2\pi/\sqrt{3})\sin(\theta_{k,i}))\mathbf{D}_{k,i}^{-1}\mathbf{B}^*((2\pi/\sqrt{3})\sin(\theta_{k,i})) \tag{4.20}$$

and

$$\tilde{\mathbf{a}}(x) = \mathbf{B}((2\pi/\sqrt{3})\sin(x))\tilde{\mathbf{a}}(0) \tag{4.21}$$

in (4.19) yields

$$G_{k,i}\mathbf{w}_k^*\mathbf{R}(\theta_{k,i}, \sigma_{k,i})\mathbf{w}_k = \frac{G_{k,i}\tilde{\mathbf{a}}^*(0)\mathbf{B}^*(\tilde{\alpha}_k)\mathbf{D}_{k,i}^{-1}\mathbf{R}(0, \sigma_{k,i}\cos(\theta_{k,i}))\mathbf{D}_{k,i}^{-1}\mathbf{B}(\tilde{\alpha}_k)\tilde{\mathbf{a}}(0)}{(\tilde{\mathbf{a}}^*(0)\mathbf{B}^*(\tilde{\alpha}_k)\mathbf{D}_{k,i}^{-1}\mathbf{B}(\tilde{\alpha}_k)\tilde{\mathbf{a}}(0))^2} \tag{4.22}$$

where

$$\tilde{\alpha}_k = ((2\pi/\sqrt{3})\sin(\theta_{k,k}) - (2\pi/\sqrt{3})\sin(\theta_{k,i}))_{2\pi}. \tag{4.23}$$

Thus with multiple interfering base stations (which all have identified the $i$th mobile but no other mobile) the interference to signal ratio at the $i$th mobile is given by

$$\mathrm{SIR}^{-1} = \sum_{k\neq i} \eta_k \frac{G_{k,i}\tilde{\mathbf{a}}^*(0)\mathbf{B}^*(\tilde{\alpha}_k)\mathbf{D}_{k,i}^{-1}\mathbf{R}(0,\sigma_{k,i}\cos(\theta_{k,i}))\mathbf{D}_{k,i}^{-1}\mathbf{B}(\tilde{\alpha}_k)\tilde{\mathbf{a}}(0)}{P_{\mathrm{d}}(\tilde{\mathbf{a}}^*(0)\mathbf{B}^*(\tilde{\alpha}_k)\mathbf{D}_{k,i}^{-1}\mathbf{B}(\tilde{\alpha}_k)\tilde{\mathbf{a}}(0))^2}. \quad (4.24)$$

where $\eta_k$ is the voice activity factor ($\Pr\{\eta_k = 1\} = 1 - \Pr\{\eta_k = 0\} =$ DTX) and $P_{\mathrm{d}}$ is the desired power. Assuming that base $i$ has not identified any co-channel mobile, $P_{\mathrm{d}}$ is given by

$$P_{\mathrm{d}} = \frac{G_{i,i}}{m^2}\tilde{\mathbf{a}}^*(\theta_{i,i})\mathbf{R}(\theta_{i,i},\sigma_{i,i})\tilde{\mathbf{a}}(\theta_{i,i}). \quad (4.25)$$

From Appendix 4.D we have the approximation

$$\Pr\{\mathrm{SIR}_{\mathrm{instantaneous}} \leq \mathrm{SIR}_{\mathrm{t}}\} = \frac{\mathrm{SIR}_0}{(1+\mathrm{SIR}_0/\mathrm{SIR}_{\mathrm{t}})\mathrm{SIR}}. \quad (4.26)$$

Combining (4.24), (4.26) and (4.25) yields

$$\Pr\{\mathrm{SIR}_{\mathrm{instantaneous}} \leq \mathrm{SIR}_0\} = \sum_{k\neq i} \eta_k \frac{m^2 G_{k,i}\tilde{\mathbf{a}}^*(0)\mathbf{B}^*(\tilde{\alpha}_k)\mathbf{D}_{k,i}^{-1}\mathbf{R}(0,\sigma_{k,i}\cos(\theta_{k,i}))\mathbf{D}_{k,i}^{-1}\mathbf{B}(\tilde{\alpha}_k)\tilde{\mathbf{a}}(0)}{G_{i,i}\tilde{\mathbf{a}}^*(\theta_{i,i})\mathbf{R}(\theta_{i,i},\sigma_{i,i})\tilde{\mathbf{a}}(\theta_{i,i})(\tilde{\mathbf{a}}^*(0)\mathbf{B}^*(\tilde{\alpha}_k)\mathbf{D}_{k,i}^{-1}\mathbf{B}(\tilde{\alpha}_k)\tilde{\mathbf{a}}(0))^2} \times \frac{\mathrm{SIR}_0}{(1+\mathrm{SIR}_0/\mathrm{SIR}_{\mathrm{t}})}. \quad (4.27)$$

The impact of frequency hopping and discontinuous transmission is now appropriately modeled by averaging over the distribution of $\eta_k$ and $\tilde{\alpha}_k$, since infinitely many co-channel users and infinitely many channels to hop on are assumed. It follows from the results of Appendix 4.E that $\tilde{\alpha}_k$ is uniformly distributed $[0, 2\pi]$ and independent of $\theta_{k,i}$. Thus (4.27) can be rewritten

$$\Pr\{\mathrm{SIR}_{\mathrm{instantaneous}} \leq \mathrm{SIR}_t\} = (\sum_{k\neq i} \int_{\tilde{\alpha}=0}^{2\pi} \frac{m^2 G_{k,i}\tilde{\mathbf{a}}^*(0)\mathbf{B}^*(\tilde{\alpha})\mathbf{D}_{k,i}^{-1}\mathbf{R}(0,\sigma_{k,i}\cos(\theta_{k,i}))\mathbf{D}_{k,i}^{-1}\mathbf{B}(\tilde{\alpha})\tilde{\mathbf{a}}(0)}{G_{i,i}\tilde{\mathbf{a}}^*(\theta_{i,i})\mathbf{R}(\theta_{i,i},\sigma_{i,i})\tilde{\mathbf{a}}(\theta_{i,i})(\tilde{\mathbf{a}}^*(0)\mathbf{B}^*(\tilde{\alpha})\mathbf{D}_{k,i}^{-1}\mathbf{B}(\tilde{\alpha})\tilde{\mathbf{a}}(0))^2}\mathrm{d}\tilde{\alpha}) \times \frac{\mathrm{SIR}_0}{(1+\mathrm{SIR}_0/\mathrm{SIR}_{\mathrm{t}})}\mathrm{DTX} \quad (4.28)$$

Let us define $f(x, y)$ as

$$f(x,y) = x \int_{\tilde{\alpha}=0}^{2\pi} \frac{\tilde{\mathbf{a}}^*(0)\mathbf{B}^*(\tilde{\alpha})\breve{\mathbf{D}}^{-1}(x,y)\mathbf{R}(0,y)\breve{\mathbf{D}}^{-1}(x,y)\mathbf{B}(\tilde{\alpha})\tilde{\mathbf{a}}(0)}{(\tilde{\mathbf{a}}^*(0)\mathbf{B}^*(\tilde{\alpha})\breve{\mathbf{D}}^{-1}(x,y)\mathbf{B}(\tilde{\alpha})\tilde{\mathbf{a}}(0))^2} \mathrm{d}\tilde{\alpha} \quad (4.29)$$

where

$$\breve{\mathbf{D}}(x,y) = x\mathbf{R}(0,y) + \mathbf{I}. \quad (4.30)$$

Then the availability can be written as

$$\Pr\{\mathrm{SIR}_{\mathrm{instantaneous}} \leq \mathrm{SIR}_t\} = \frac{m^2(r-1)P_{\min}\mathrm{SIR}_0}{\tilde{\mathbf{a}}^*(\theta_{i,i})\mathbf{R}(\theta_{i,i},\sigma_{i,i})\tilde{\mathbf{a}}(\theta_{i,i})(1+\mathrm{SIR}_0/\mathrm{SIR}_\mathrm{t})}(\mathrm{DTX})\times \sum_{k\neq i} f(G_{k,i}/(G_{i,i}(r-1)P_{\min}), \sigma_{k,i}\cos(\theta_{k,i})). \quad (4.31)$$

The function $f(x, y)$ is plotted in Figure 4.16 below using $m = 10$, i.e., with ten antenna elements.

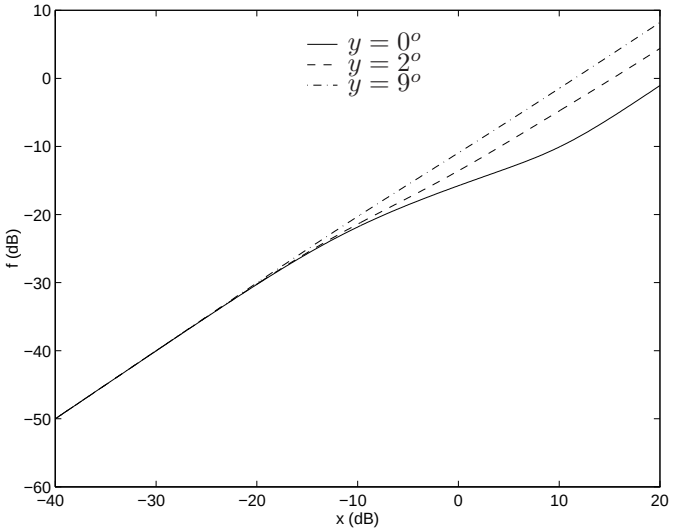


Figure 4.16: *Illustration of the function* $f(x, y)$.

Define $g(z, y)$ as

$$g(z, y) = \max_x \{f(x, y) \leq z\}. \tag{4.32}$$

Assume that adequate transmission quality is obtained if the instantaneous signal to interference ratio is larger than $\mathrm{SIR}_t$ in at least a fraction $t$ of time slots. Then the probability of outage (inadequate speech quality) can be approximated as

$$
\begin{aligned}
1-\Pr\{\text{Outage}\} = \\
&\Pr\{\frac{m^2(r-1)P_{\min}\text{SIR}_0}{\tilde{\mathbf{a}}^*(\theta_{i,i})\mathbf{R}(\theta_{i,i},\sigma_{i,i})\tilde{\mathbf{a}}(\theta_{i,i})(1+\text{SIR}_0/\text{SIR}_\text{t})}\text{DTX}\times \\
&\sum_i f(G_{k,i}/(G_{i,i}(r-1)P_{\min}),\sigma_{k,i}\cos(\theta_{k,i}))\le t\} \\
&\approx \Pr\{G_{k,i}/(m^2(r-1)P_{\min}G_{i,i}) \\
&\le g((\text{DTX})^{-1}\tilde{\mathbf{a}}^*(\theta_{i,i})\mathbf{R}(\theta_{i,i},\sigma_{i,i})\tilde{\mathbf{a}}(\theta_{i,i})(\frac{(1+\text{SIR}_0/\text{SIR}_\text{t})}{(r-1)m^2P_{\min}\text{SIR}_0}t), \\
&\sigma_{k,i}\cos(\theta_{k,i})),\ \forall i\} \\
&= \Pr\{10\log(G_{k,i})-10\log(G_{i,i})-10\log((r-1)P_{\min}) \\
&\le 10\log(g((\text{DTX})^{-1}\tilde{\mathbf{a}}^*(\theta_{i,i})\mathbf{R}(\theta_{i,i},\sigma_{i,i})\tilde{\mathbf{a}}(\theta_{i,i})\times \\
&(\frac{(1+\text{SIR}_0/\text{SIR}_\text{t})}{m^2(r-1)P_{\min}\text{SIR}_0}t),\sigma_i\cos(\theta_i)),\forall i\}. \qquad (4.33)
\end{aligned}
$$

Assuming that the log normal fading (between a mobile and several base stations) is correlated with correlation coefficient, $c$, i.e.,

$$\text{E}\{10\log(L_{k_1,i})10\log(L_{k,i})\} = c\sigma_\text{L}^2, \qquad (4.34)$$

the path gains $G_{k,i}$ can be written

$$
\begin{aligned}
G_{k,i} &= (\frac{1}{r_{k,i}})^\gamma L_{k,i}\cos^2(\theta_{k,i}) && (4.35)\\
&= (\frac{1}{r_{k,i}})^\gamma 10^{0.1(\sqrt{c}\xi_i+\sqrt{1-c}\xi_{k,i})}\cos^2(\theta_{k,i}) && (4.36)\\
&= 10^{0.1(\sqrt{c}\xi_i+\sqrt{1-c}\xi_{k,i}+m_{k,i})} && (4.37)
\end{aligned}
$$

where $\xi_{k,i}$ are independent, normally distributed random variables with mean zero and standard deviation $\sigma_L$. The mean $m_{k,i}$ is given by

$$m_{k,i} = -10\gamma\log(r_{k,i}) + 20\log(\cos(\theta_{k,i})). \qquad (4.38)$$

Conditioning on the position of the user, we obtain

$$1 - \Pr\{\text{Outage}|r_{i,i}, \theta_{i,i}\}$$
$$= \int_{x=0}^{\infty} f_{\xi_{i,i}}(x) \prod_{k \neq i} \Pr\{\xi_{k,i} \leq x + 10\log((r-1)P_{\min}) + \frac{1}{\sqrt{1-c}} \times (m_{i,i} - m_{k,i} + 10\log(g(\frac{\tilde{\mathbf{a}}^*(\theta_{i,i})\mathbf{R}(\theta_{i,i}, \sigma_{i,i})\tilde{\mathbf{a}}(\theta_{i,i})(\text{DTX})^{-1}(1 + \text{SIR}_0/\text{SIR}_\text{t})}{m^2(r-1)P_{\min}\text{SIR}_0}t, \sigma_{k,i}\cos(\theta_{k,i}))))\}. \quad (4.39)$$

Using the fact that $\xi_{k,i}$ is normally distributed with mean zero and variance $\sigma_\text{L}^2$ we obtain

$$\Pr\{\text{Outage}|r_{i,i}, \theta_{i,i}\} = 1 - \frac{1}{\sqrt{2\pi(1-c)}\sigma_L} \int_{x=0}^{\infty} \exp(\frac{-x^2}{2\sigma_\text{L}^2(1-c)}) \times \prod_{k \neq i} Q(y_0)\text{d}x, \quad (4.40)$$

where $y_0$ and $Q(y_0)$ are given by

$$\sigma_L(\sqrt{1-c})y_0 = m_{k,i} - m_{i,i} - x - 10\log((r-1)m^2P_{\min}) - 10\log(g(\tilde{\mathbf{a}}^*(\theta_{i,i})\mathbf{R}(\theta_{i,i}, \sigma_{i,i})\tilde{\mathbf{a}}(\theta_{i,i})\text{DTX}^{-1} (\text{SIR}_0^{-1} + \text{SIR}_\text{t}^{-1})(r-1)^{-1}P_{\min}^{-1}t, \sigma_{k,i}\cos(\theta_{k,i}))) \quad (4.41)$$

and

$$Q(y_0) = \frac{1}{\sqrt{2\pi}} \int_{y=y_0}^{\infty} e^{-y^2/2}\text{d}y. \quad (4.42)$$

respectively. When (4.40) is applied in this chapter, only the first tier of interfering base stations are taken into account. Furthermore, only the sector directed most closely towards the mobile of each cell is considered, since overly pessimistic results would otherwise be obtained. This is because (4.40) does not assume fully correlated log-normal fading between a mobile and the three sectors of a base station site, which is the case in the simulations.

### 4.C.2 SICR-RCS-WON ($e$ independent analysis)

We assume that the $k$th base transmits with the weighting vector

$$\mathbf{w}_k = \frac{1}{m}\tilde{\mathbf{a}}(\theta_{k,k}), \tag{4.43}$$

independently of the angular spread of the desired user $\sigma_{k,k}$. This is an approximation since the true solution involves the angular spread of the desired mobile. With this choice of weighting vector the results of the previous section can be used by letting the matrices $\mathbf{M}$, $\mathbf{D}_{k,i}$, and $\breve{\mathbf{D}}(x,y)$ all be equal to the identity matrix i.e.,

$$\mathbf{M} = \mathbf{D}_{k,i} = \breve{\mathbf{D}}(x,y) = \mathbf{I}. \tag{4.44}$$

Using (4.44) in (4.29) yields

$$f(x,y) = x/m, \tag{4.45}$$

which in turn implies

$$g(z,y) = m \times z. \tag{4.46}$$

Using (4.25) and (4.46) in (4.40) yields

$$\Pr\{\text{Outage}|r_{i,i},\theta_{i,i}\} = 1 - \frac{1}{\sqrt{2\pi}}\int_{x=0}^{\infty}\exp\left(\frac{-x^2}{2\sigma_{\text{L}}^2(1-c)}\right)\prod_{k\neq i}Q(y_0)\mathrm{d}x, \tag{4.47}$$

where $y_0$ and $Q(y_0)$ are given by

$$\sigma_L(\sqrt{1-c})y_0 = m_{k,i} - m_{i,i} - x - 10\log(t(m\text{DTX})^{-1}(\text{SIR}_{\text{t}}^{-1} + \text{SIR}_0^{-1})\tilde{\mathbf{a}}^*(0)\mathbf{R}(0,\sigma\cos(\theta_{i,i}))\tilde{\mathbf{a}}(0)), \tag{4.48}$$

and (4.42), respectively. When (4.47) is applied in this chapter, only the first tier of interfering base stations are taken into account. Furthermore, only the sector directed most closely towards the mobile of each cell is considered, since overly pessimistic results would otherwise be obtained. This is because (4.40) does not assume fully correlated log-normal fading between a mobile and the three sectors of a base station site, which is the case in the simulations.

### 4.C.3 SICR-SSFR

Without of loss of generality we will consider the transmission quality experienced by user 1. The spread in terms of the beamwidth, $\tilde{\sigma}$, (see (2.27)) within annular element $i_1$ (seen from the desired base) is bounded by

$$\tilde{\sigma} \leq \frac{\pi^2\sqrt{3}}{270^o}\sigma(0.05 i_1 R(\frac{\cos(\theta)}{\cos(30^o)})^{2/\gamma}), \tag{4.49}$$

where the function $\sigma(r)$ is defined in (2.36). It is assumed that the base erroneously believes that all users inside the annular element $i_1$, have their $\tilde{\sigma}$ equal to the bound in (4.49) or equivalently

$$\sigma = \frac{\breve{\sigma}}{\cos(\theta_{i,i})}, \tag{4.50}$$

where $\breve{\sigma}$ is given by

$$\breve{\sigma} = \sigma(0.05 i_1 R(\frac{\cos(\theta)}{\cos(30^o)})^{2/\gamma}). \tag{4.51}$$

Introduce the transformed angle $\tilde{\theta}$ defined by

$$\tilde{\theta} = (\frac{2\pi}{\sqrt{3}}\sin(\theta))_{2\pi}. \tag{4.52}$$

The results of Appendix 4.E, yield that the transformed azimuth angle $\tilde{\theta}_{i,i}$, for the users within an annular element are uniformly distributed $[0, 2\pi]$. When the channel allocator described in Section 3.3.1.1 is applied to the group, it follows (proof in Section 4.F) that the transformed angles $\tilde{\boldsymbol{\theta}} = [\tilde{\theta}_1, \ldots, \tilde{\theta}_d]$ of the same sector co-channel mobiles (seen from their desired base) converge to

$$\tilde{\theta}_1 = \text{Uniform}[0, 2\pi] \tag{4.53}$$

$$(\tilde{\theta}_k - \tilde{\theta}_1)_{2\pi} = \frac{2\pi}{D}(k-1), \tag{4.54}$$

as the number of users tends to infinity. Assume that the vector of transformed angles is $\tilde{\boldsymbol{\theta}}$ at the desired base and $\tilde{\boldsymbol{\theta}}^k$ at the $k$th interfering base. Assume further that the mobiles in the interfering cells belong to the annular element $i_1$ with respect to their base. Let $G_{k,1}, \theta_{k,1}, \sigma_{k,1}$, and $G_{1,1}, \theta_{1,1}, \sigma_{1,1}$ be the propagation parameters of user 1 seen from the

$k$th interfering base desired and the base 1 respectively. The situation is depicted in Figure 4.17.

Then the interference to signal ratio (averaged over fading) at user 1 (with transformed azimuth angle $\tilde{\theta}_1$) is given by

$$\begin{aligned}\mathrm{CIR}^{-1} = &\frac{1}{P_\mathrm{d}} \sum_{n=2}^{d} \eta_n \tilde{\mathbf{w}}_n^*(\tilde{\boldsymbol{\theta}}, \breve{\sigma}) \mathbf{R}(\theta_{1,1}, \sigma_{1,1}) \tilde{\mathbf{w}}_n(\tilde{\boldsymbol{\theta}}, \breve{\sigma}) \\ &+ \sum_k \frac{G_{k,1}}{G_{1,1} P_\mathrm{d}} \sum_{n=1}^{d} \eta_n^k \tilde{\mathbf{w}}_n^*(\tilde{\boldsymbol{\theta}}^k, \breve{\sigma}) \mathbf{R}(\theta_{k,1}, \sigma_{k,1}) \tilde{\mathbf{w}}_n(\tilde{\boldsymbol{\theta}}^k, \breve{\sigma}), \quad (4.55)\end{aligned}$$

where

$$P_\mathrm{d} = \tilde{\mathbf{w}}_1^*(\tilde{\boldsymbol{\theta}}, \breve{\sigma}) \mathbf{R}(\theta_{1,1}, \sigma_{1,1}) \tilde{\mathbf{w}}_1(\tilde{\boldsymbol{\theta}}, \breve{\sigma}), \quad (4.56)$$

$\eta$ is the voice activity factor ($\eta = 1$ when the user is active and $\eta = 0$ when the user is inactive $\Pr\{\eta = 1\} = \mathrm{DTX}$), and the *functions* $\tilde{\mathbf{w}}_n(\tilde{\boldsymbol{\theta}}, \breve{\sigma})$, $n = 1, \ldots, D$ are introduced in Section 4.C.4. Using (4.54),(4.78-4.79), (4.84-4.85 ), in (4.55) and (4.56) yields

$$\begin{aligned}\mathrm{CIR}^{-1} = &\frac{1}{P_\mathrm{d}} \sum_{n=2}^{d} \eta_n \tilde{\mathbf{w}}_n^*(\breve{\boldsymbol{\theta}}, \breve{\sigma}) \mathbf{R}(0, \sigma_{1,1} cos(\theta_{1,1})) \tilde{\mathbf{w}}_n(\breve{\boldsymbol{\theta}}, \breve{\sigma}) + \\ &\sum_k \frac{G_{k,1}}{G_{1,1} P_\mathrm{d}} \sum_{n=1}^{d} \eta_n^k \tilde{\mathbf{w}}_n^*(\breve{\boldsymbol{\theta}}, \breve{\sigma}) \mathbf{B}(\tilde{\alpha}_k) \mathbf{R}(0, \breve{\sigma}) \mathbf{B}^*(\tilde{\alpha}_k) \tilde{\mathbf{w}}_n(\breve{\boldsymbol{\theta}}, \breve{\sigma}), \quad (4.57)\end{aligned}$$

and

$$P_\mathrm{d} = \tilde{\mathbf{w}}_1^*(\breve{\boldsymbol{\theta}}, \breve{\sigma}) \mathbf{R}(0, \sigma_1 \cos(\theta_{1,1})) \tilde{\mathbf{w}}_1(\breve{\boldsymbol{\theta}}, \breve{\sigma}), \quad (4.58)$$

where

$$\breve{\boldsymbol{\theta}} = [0, \frac{2\pi}{D}, \ldots, (D-1)\frac{2\pi}{D}] \quad (4.59)$$

$$\tilde{\alpha}_k = (\tilde{\theta}_l^k - \frac{2\pi}{\sqrt{3}} \sin(\theta_{k,1})])_{2\pi} \quad (4.60)$$

and $\mathbf{B}(x)$ is defined in (4.72). From Appendix 4.D we have the approximation

$$\Pr\{\mathrm{SIR}_{\mathrm{instantaneous}} \leq \mathrm{SIR}_{\mathrm{t}}\} = \frac{\mathrm{SIR}_0}{(1+\mathrm{SIR}_0/\mathrm{SIR}_{\mathrm{t}})\mathrm{SIR}}. \tag{4.61}$$

The impact of frequency hopping and discontinuous transmission (assuming large number of users) is now appropriately modeled by averaging over $\eta_n^k$ and $\tilde{\alpha}_k$. For safety we assume that $\eta_n = 1$ i.e., same sector co-channel users are always active. It follows from the results of Appendix 4.E that $\tilde{\alpha}_k$ is uniform distributed $[0, 2\pi]$ and independent of $\theta_{k,1}$. We thus obtain

$$\Pr\{\mathrm{SIR}_{\mathrm{instantaneous}} \leq \mathrm{SIR}_t\} = \frac{\mathrm{SIR}_0}{(1+\mathrm{SIR}_0/\mathrm{SIR}_{\mathrm{t}})}(c_1 + c_2 d(\sum_k \frac{G_{k,1}}{G_{1,1}})) \tag{4.62}$$

where

$$c_1 = \frac{1}{P_{\mathrm{d}}} \sum_{n=2}^{d} \tilde{\mathbf{w}}_n^*(\breve{\boldsymbol{\theta}}, \breve{\sigma}) \mathbf{R}(0, \sigma_{1,1}\cos(\theta_{1,1})) \tilde{\mathbf{w}}_n(\breve{\boldsymbol{\theta}}, \breve{\sigma}) \tag{4.63}$$

$$c_2 = \frac{\mathrm{DTX}}{P_{\mathrm{d}}} \tilde{\mathbf{w}}_n^*(\breve{\boldsymbol{\theta}}, \breve{\sigma})(\frac{1}{2\pi} \int_{\tilde{\alpha}=0}^{2\pi} \mathbf{B}(\tilde{\alpha}) \mathbf{R}(0, \breve{\sigma}) \mathbf{B}^*(\tilde{\alpha})) \tilde{\mathbf{w}}_n(\breve{\boldsymbol{\theta}}, \breve{\sigma}) \tag{4.64}$$

$$= \frac{\mathrm{DTX}}{P_{\mathrm{d}}} \tilde{\mathbf{w}}_1^*(\breve{\boldsymbol{\theta}}, \breve{\sigma}) \tilde{\mathbf{w}}_1(\breve{\boldsymbol{\theta}}, \breve{\sigma}). \tag{4.65}$$

Assume that adequate speech quality is obtained if the instantaneous signal to interference ratio is larger than $\mathrm{SIR}_t$ in at least a fraction $t$ of time slots. Then the probability of outage (inadequate speech quality) can be approximated as

$$\Pr\{\mathrm{Outage}\} = \Pr\{(\sum_i \frac{G_{k,1}}{G_{1,1}}) \geq \frac{t(\mathrm{SIR}_t + \mathrm{SIR}_0) - c_1 \mathrm{SIR}_0 \mathrm{SIR}_{\mathrm{t}}}{\mathrm{SIR}_{\mathrm{t}} \mathrm{SIR}_0 D c_2}\}. \tag{4.66}$$

Combining (4.66), and (4.37) yields

$$\Pr\{\mathrm{Outage}\} = \begin{cases} 1 & \text{if } t \leq c_1((\mathrm{SIR}_0)^{-1} + (\mathrm{SIR}_t)^{-1})^{-1}, \\ \Pr\{\beta - \sqrt{1-c}\xi_{1,1} - m_{1,1} \geq \rho\} & \text{if } t > c_1((\mathrm{SIR}_0)^{-1} + (\mathrm{SIR}_t)^{-1})^{-1}. \end{cases} \tag{4.67}$$

where

$$\beta = 10\log(\sum_k 10^{0.1(\sqrt{1-c}\xi_{k,1}+m_{k,1})}). \tag{4.68}$$

$$\rho = 10\log(\frac{t(\mathrm{SIR}_t+\mathrm{SIR}_0)-c_1\mathrm{SIR}_0\mathrm{SIR}_\mathrm{t}}{\mathrm{SIR}_\mathrm{t}\mathrm{SIR}_0 Dc_2}) \tag{4.69}$$

and $\xi_k$ is $\mathrm{N}(0,\sigma_L)$ and $m_{k,i}$ is given by (4.38). Previous results, [SY81], have shown that a sum of log-normal random variables is closely approximated by another log-normal random variable. Thus conditioning on the position of user 1, $\beta$ defined in (4.68) is approximately normal. We use the procedure described in [SY81] to obtain the mean $m_\beta$ and standard deviation $\sigma_\beta$ of $\beta$. Given the position of the user 1, we calculate the probability of outage as

$$\Pr\{\mathrm{Outage}|r_{1,1},\theta_{1,1}\} = \begin{cases} 1 & \text{if } t \geq c_1\mathrm{SIR}_0, \\ Q(\frac{\rho+m_{1,1}-m_\beta}{\sqrt{\sigma_\beta^2+(1-c)\sigma_{\mathrm{dB}}^2}}) & \text{if } t > c_1\mathrm{SIR}_0. \end{cases} \tag{4.70}$$

where $Q(x_0)$ is defined as

$$Q(x_0) = \frac{1}{\sqrt{2\pi}}\int_{x=x_0}^{\infty} e^{-x^2/2}\mathrm{d}x. \tag{4.71}$$

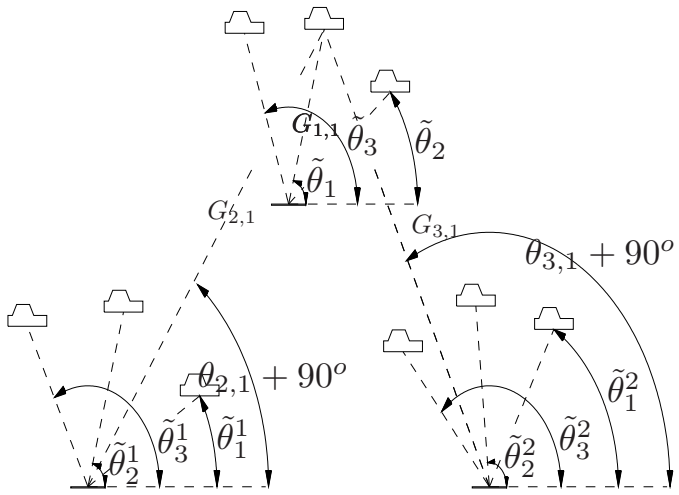


Figure 4.17: *The entities involved in reception at the user* 1.

### 4.C.4 Lemmas to Section 4.C.3

Define B($x$) as

$$\mathbf{B}(x) = \text{diag}(1, \exp(-jx), \ldots, \exp(-j(m-1)x)). \tag{4.72}$$

From the definition of $\mathbf{B}(x)$ in (4.72) we immediately obtain,

$$\mathbf{B}^{-1}(x) = \mathbf{B}^*(x) \tag{4.73}$$
$$= \mathbf{B}(-x) \tag{4.74}$$

and

$$\mathbf{B}(x + \Delta x) = \mathbf{B}(\Delta x)\mathbf{B}(x). \tag{4.75}$$

Using (2.26), (2.27), (4.8) and (4.72) we obtain

$$\mathbf{R}(\theta, \breve{\sigma}/cos(\theta)) = \mathbf{B}(\frac{2\pi}{\sqrt{3}}\sin(\theta))\mathbf{R}(0, \breve{\sigma})\mathbf{B}^*(\frac{2\pi}{\sqrt{3}}\sin(\theta)). \tag{4.76}$$

Define $\tilde{\mathbf{R}}(\tilde{\theta}, \breve{\sigma})$ as

$$\tilde{\mathbf{R}}(\tilde{\theta},\breve{\sigma}) = \mathbf{B}(\tilde{\theta})\mathbf{R}(0,\breve{\sigma})\mathbf{B}^{*}(\tilde{\theta}). \tag{4.77}$$

From (4.76) and (4.77) we obtain,

$$\mathbf{R}(\theta,\breve{\sigma}/cos(\theta)) = \tilde{\mathbf{R}}(\frac{2\pi}{\sqrt{3}}\sin(\theta),\breve{\sigma}). \tag{4.78}$$

Using (4.75) and (4.77) we arrive at,

$$\tilde{\mathbf{R}}(\tilde{\theta}+\Delta\tilde{\theta},\breve{\sigma}) = \mathbf{B}(\Delta\tilde{\theta})\tilde{\mathbf{R}}(\tilde{\theta},\breve{\sigma})\mathbf{B}^{*}(\Delta\tilde{\theta}). \tag{4.79}$$

Define $\tilde{\mathbf{w}}_k(\tilde{\boldsymbol{\theta}},\sigma)$ as

$$\tilde{\mathbf{w}}_k(\tilde{\boldsymbol{\theta}},\sigma) = \arg\min_{\mathbf{x}^{*}\tilde{\mathbf{M}}_1\mathbf{x}=1} \mathbf{x}^{*}\tilde{\mathbf{M}}\mathbf{x}, \tag{4.80}$$

where

$$\tilde{\mathbf{M}}_1 = \tilde{\mathbf{R}}(\tilde{\theta}_k,\sigma) \tag{4.81}$$

$$\tilde{\mathbf{M}} = \sum_{n=1,n\neq k}^{d} \tilde{\mathbf{R}}(\tilde{\theta}_n,\breve{\sigma}) + (R/D)ld\mathbf{I}. \tag{4.82}$$

Assuming that users $1,\ldots,d$ are same sector co-channel mobiles and that their angular spread seen from the desired base are given by $\sigma_{i,i} = \breve{\sigma}/\cos(\theta_{i,i})$, we obtain from (3.4), (3.7), (3.13), (4.78) and (4.80-4.82) that

$$\mathbf{w}_l = \tilde{\mathbf{w}}_l(\frac{2\pi}{\sqrt{3}}\sin(\theta_{1,1}),\ldots,\frac{2\pi}{\sqrt{3}}\sin(\theta_{D,D}),\breve{\sigma}). \tag{4.83}$$

Since $\mathbf{B}(x)$ and $\tilde{\mathbf{R}}(x,\breve{\sigma})$ are periodic with periodicity $2\pi$ in $x$ (from (4.72) and (4.79)) we obtain

$$\tilde{\mathbf{w}}_l(\tilde{\theta},\breve{\sigma}) = \tilde{\mathbf{w}}_l(\tilde{\theta}_1+k_1 2\pi,\ldots,\tilde{\theta}_d+k_D 2\pi,\sigma_0), \tag{4.84}$$

where $k_1,\ldots,k_d$ are integers.

**Theorem 1** The following angle invariance property for the weighting vectors holds

$$\tilde{\mathbf{w}}_k(\tilde{\theta},\breve{\sigma}) = \mathbf{B}^{*}(\Delta)\tilde{\mathbf{w}}_k(\tilde{\theta_1}+\Delta,\ldots,\tilde{\theta}_d+\Delta,\breve{\sigma}). \tag{4.85}$$

**Proof:**

Using (4.79) and (4.80)-(4.82) we obtain that $\tilde{\mathbf{w}}_k(\tilde{\theta}_1 + \Delta, \ldots, \tilde{\theta}_d + \Delta, \breve{\sigma}) = \tilde{\mathbf{w}}_k(\tilde{\theta} + \Delta, \breve{\sigma})$ is given by,

$$\tilde{\mathbf{w}}_k(\tilde{\theta} + \Delta, \breve{\sigma}) = \arg\min_{\mathbf{x}} \begin{cases} \mathbf{x}^* \mathbf{B}(\Delta) \tilde{\mathbf{M}} \mathbf{B}^*(\Delta) \mathbf{x} \\ \text{s. to } \mathbf{x}^* \mathbf{B}(\Delta) \tilde{\mathbf{M}}_1 \mathbf{B}^*(\Delta) \mathbf{x} = 1. \end{cases} \tag{4.86}$$

Introducing $\mathbf{y} = \mathbf{B}^*(\Delta)\mathbf{x}$ yields

$$\tilde{\mathbf{w}}_k(\tilde{\theta} + \Delta, \breve{\sigma}) = \arg\max_{\mathbf{x}} \begin{cases} \mathbf{y}^* \tilde{\mathbf{M}} \mathbf{y} \\ \text{s. to } \mathbf{y}^* \tilde{\mathbf{M}}_1 \mathbf{y} = 1 \\ \text{where } \mathbf{y} = \mathbf{B}^*(\Delta)\mathbf{x} \end{cases} . \tag{4.87}$$

From (4.80-4.82) and (4.87) it is obvious that

$$\tilde{\mathbf{w}}_k(\tilde{\theta}, \breve{\sigma}) = \mathbf{B}^*(\Delta) \tilde{\mathbf{w}}_k(\tilde{\theta}_1 + \Delta, \ldots, \tilde{\theta}_d + \Delta, \breve{\sigma}). \tag{4.88}$$

# Appendix 4.D Instantaneous Outage Probability

In appendix 4.C, analytical approximations of the outage probability are derived. In these derivations the following approximation of (4.4) is used

$$\Pr\{\mathrm{CIR}_{\mathrm{instantaneous}} \leq \mathrm{CIR}_{\mathrm{t}}\} = \frac{\mathrm{CIR}_0}{(1 + \mathrm{CIR}_0/\mathrm{CIR}_{\mathrm{t}})\mathrm{CIR}}, \tag{4.89}$$

which is a "linearization" of (4.4) around $\mathrm{CIR} = \mathrm{CIR}_0$. Using the parameters $\mathrm{CIR}_0 = 10^{0.9}$ and $\mathrm{CIR}_t = 10^{0.3}$, yields, at most, an underestimation of $\Pr\{\mathrm{CIR}_{\mathrm{instantaneous}} \leq \mathrm{CIR}_{\mathrm{t}}\}$ by 1.1%.

## Appendix 4.E Distribution of $\theta_{i,i}$

It follows from (4.9) that the distribution of $\theta_{i,i}$ inside an annular element (defined given in the text of Section 4.C.3) or in the entire coverage area is given by

$$f_{\theta_{i,i}}(\nu) = \frac{2\pi}{360^o\sqrt{3}}\cos(\nu), -60^o \leq \nu \leq 60^o. \tag{4.90}$$

This result implies in turn that $(2\pi/\sqrt{3})\sin(\theta_{i,i})$ is uniformly distributed $[-\pi, \pi]$.

# Appendix 4.F Proof of (4.54)

In this section equation (4.54) is proved. Let $\tilde{\theta}_1,\ldots,\tilde{\theta}_D$, be the same sector co-channel mobiles. The result of previous section yield that the distribution of $\tilde{\theta}_1,\ldots,\tilde{\theta}_D$ are uniform distributed $[0,2\pi]$, when they are taken separately (unconditioned). In Section 4.F.1, below it is shown that the joint distribution function of $\tilde{\theta}_1,\ldots,\tilde{\theta}_D$, is given by

$$\begin{aligned}
&\Pr\{(\tilde{\theta}_k-\tilde{\theta}_1)_{2\pi}\le\Delta x_k|\tilde{\theta}_1=x_1,(\tilde{\theta}_2-\tilde{\theta}_1)_{2\pi}=\Delta x_2,\ldots,\\
&\qquad\qquad(\tilde{\theta}_{k-1}-\tilde{\theta}_1)_{2\pi}=\Delta x_{k-1}\}\\
&=(2\pi-\Delta x_{k-1})^{-N_k}\sum_{n=0}^{(D-k+1)n_c-1}\binom{N_k}{n}(2\pi-\Delta x_k)^n(\Delta x_k-\Delta x_{k-1})^{N_k-n}\\
&\qquad\text{where } N_k=(D-k+2)n_c-1 \text{ and } \Delta x_{k-1}\le\Delta x_k\le 2\pi, \quad (4.91)
\end{aligned}$$

where $n_c$ is the number of channels used for the power-group. Using (4.91) it is shown in Sections 4.F.2 and 4.G, that

$$\begin{aligned}
&\mathrm{E}\{(\tilde{\theta}_k-\tilde{\theta}_1)_{2\pi}|\tilde{\theta}_1=x_1,(\tilde{\theta}_2-\tilde{\theta}_1)_{2\pi}=\Delta x_2,\ldots,\\
&\qquad\qquad(\tilde{\theta}_{k-1}-\tilde{\theta}_1)_{2\pi}=\Delta x_{k-1}\}\\
&\qquad\qquad=\Delta x_{k-1}+(2\pi-\Delta x_{k-1})/(D-k+2), \quad (4.92)
\end{aligned}$$

and

$$\begin{aligned}
&\mathrm{VAR}\{(\tilde{\theta}_k-\tilde{\theta}_1)_{2\pi}|\tilde{\theta}_1=x_1,(\tilde{\theta}_2-\tilde{\theta}_1)_{2\pi}=\Delta x_2,\ldots,\\
&\qquad\qquad(\tilde{\theta}_{k-1}-\tilde{\theta}_1)_{2\pi}=\Delta x_{k-1}\}\\
&\quad=(d-k+1)(2\pi-\Delta x_{k-1})^2/(((D-k+2)n_c+1)(D-k+2)^2), \quad (4.93)
\end{aligned}$$

respectively (VAR denotes variance). From (4.92) and (4.93), it follows that $(\tilde{\theta}_k-\tilde{\theta}_1)$ converges to $(k-1)\frac{2\pi}{D}$, in second mean [GS92], as the number of channels in the group, $n_c$, goes to infinity.

## 4.F.1 Derivation of (4.91)

Assume that $\tilde{\theta}_1=x_1,(\tilde{\theta}_2-\tilde{\theta}_1)_{2\pi}=\Delta x_2,\ldots,(\tilde{\theta}_{k-1}-\tilde{\theta}_1)_{2\pi}=\Delta x_{k-1}$ as depicted in Figure 4.18.

Divide the mobiles (within the same power group) into three disjunctive sets A, B and C with the properties

$$\begin{aligned} A &: (\tilde{\theta} - x_1)_{2\pi} \leq \Delta x_{k-1} \\ B &: \Delta x_{k-1} < (\tilde{\theta} - x_1)_{2\pi} \leq \Delta x_k \\ C &: \Delta x_k < (\tilde{\theta} - x_1)_{2\pi}, \end{aligned} \quad , \tag{4.94}$$

where $\tilde{\theta}$ is transformed angle of the mobiles. A close investigation of the procedure described in Section 3.3.1.1, yields that the number of mobiles in set A, No($A$), is given by

$$\mathrm{No}(A) = 1 + (k-2)n_c. \tag{4.95}$$

Since all $D \times n_c$ mobiles are contained in $A \cup B \cup C$ the number of mobiles in $B \cup C$ is,

$$\mathrm{No}(B \cup C) = N_k = (D - k + 2)n_c - 1. \tag{4.96}$$

The angle $(\tilde{\theta} - x_1)_{2\pi}$ of the mobiles in $B \cup C$ is independently and uniformly distributed between $\Delta x_{k-1}$ and $2\pi$. Thus the number of mobiles in $C$ will be binomially distributed according to

$$\mathrm{No}(C) \in \mathrm{Bi}(N_k, \frac{2\pi - \Delta x_k}{2\pi - \Delta x_{k-1}}). \tag{4.97}$$

Now, from (4.94)

$$(\mathrm{No}(B) \geq n_c) \Leftrightarrow ((\tilde{\theta}_k - \tilde{\theta}_1)_{2\pi} \leq \Delta x_k) \tag{4.98}$$

but

$$\mathrm{No}(B) \geq n_c \Leftrightarrow \mathrm{No}(C) \leq (D - k + 1)n_c - 1. \tag{4.99}$$

Thus from equation (4.98), (4.99) and (4.97) we finally obtain (4.91)

### 4.F.2 Derivation of Equation (4.92)

Differentiation of expression (4.91) with respect to $\Delta x_k$ yields

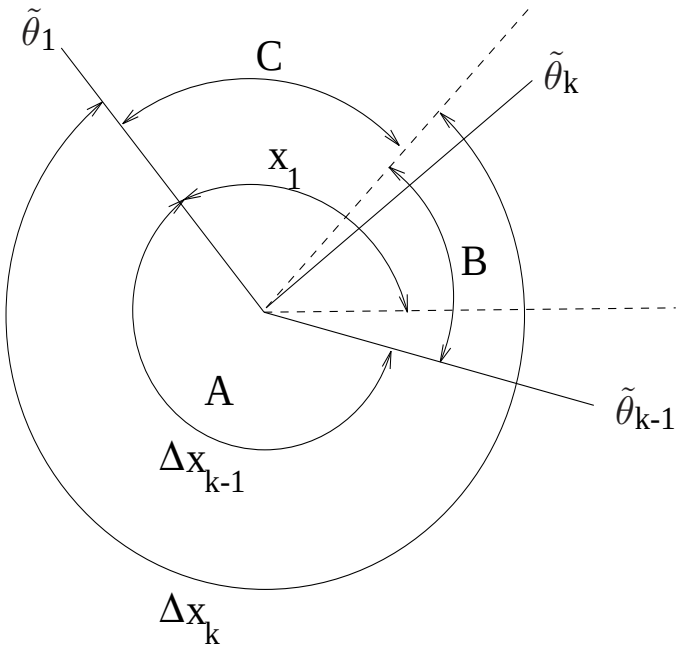


Figure 4.18: Illustration to Appendix 4.F.1

$$\frac{\partial}{\partial \Delta x_k}\Pr\{(\tilde{\theta}_k - \tilde{\theta}_1)_{2\pi} \le \Delta x_k | \tilde{\theta}_1 = x_1, (\tilde{\theta}_2 - \tilde{\theta}_1)_{2\pi} = \Delta x_2, \ldots , (\tilde{\theta}_{k-1} - \tilde{\theta}_1)_{2\pi} = \Delta x_{k-1}\} = (2\pi - \Delta x_{k-1})^{-N_k} \times \sum_{n=0}^{(d-k+1)n_c-1} (N_k - n)\binom{N_k}{n}(2\pi - \Delta x_k)^n (\Delta x_k - \Delta x_{k-1})^{N_k-n-1} - (2\pi - \Delta x_{k-1})^{-N_k} \times \sum_{n=1}^{(d-k+1)n_c-1} n\binom{N_k}{n}(2\pi - \Delta x_k)^{n-1}(\Delta x_k - \Delta x_{k-1})^{N_k-n}. \quad (4.100)$$

Since

$$\mathrm{E}\{(\tilde{\theta}_k-\tilde{\theta}_1)_{2\pi}|\tilde{\theta}_1=x_1,(\tilde{\theta}_2-\tilde{\theta}_1)_{2\pi}=\Delta x_2,\ldots \\ ,(\tilde{\theta}_{k-1}-\tilde{\theta}_1)_{2\pi}=\Delta x_{k-1}\}\Delta x_{k-1} \\ +\int_{\Delta x_k=\Delta x_{k-1}}^{2\pi}(\Delta x_k-\Delta x_{k-1})\,\frac{\partial}{\partial\Delta x_k}\mathrm{Pr}\{(\theta_k-\theta_1)_{2\pi}\le\Delta x_k|\ldots\}\mathrm{d}\Delta x_k,$$

we obtain

$$\mathrm{E}\{(\tilde{\theta}_k-\tilde{\theta}_1)_{2\pi}|\tilde{\theta}_1=x_1,(\tilde{\theta}_2-\tilde{\theta}_1)_{2\pi}=\Delta x_2,\ldots \\ ,(\tilde{\theta}_{k-1}-\tilde{\theta}_1)_{2\pi}=\Delta x_{k-1}\}=\Delta x_{k-1}+(2\pi-\Delta x_{k-1})^{-N_k}\times \\ \sum_{n=0}^{(d-k+1)n_c-1}(N_k-n)\binom{N_k}{n}h(n,N_k-n)-(2\pi-\Delta x_{k-1})^{-N_k}\times \\ \sum_{n=1}^{(d-k+1)n_c-1}n\binom{N_k}{n}h(n-1,N_k-n+1) \quad (4.101)$$

where $h(p,q)$ is given by

$$h(p,q)=\int_{\Delta x_k=\Delta x_{k-1}}^{2\pi}(2\pi-\Delta x_k)^p(\Delta x_k-\Delta x_{k-1})^q\mathrm{d}\Delta x_k \quad (4.102)$$

$$=((q+p+1)\binom{q+p}{p})^{-1}(2\pi-\Delta x_{k-1})^{q+p+1}. \quad (4.103)$$

The equality in (4.103) is easily shown if $q=0$, in this case we obtain

$$h(p,0)=\int_{\Delta x_k=\Delta x_{k-1}}^{2\pi}(2\pi-\Delta x_k)^p\mathrm{d}\Delta x_k \quad (4.104)$$

$$=|-(p+1)^{-1}(2\pi-\Delta x_k)^{p+1}|_{\Delta x_k=\Delta x_{k-1}}^{\Delta x_k=2\pi} \quad (4.105)$$

$$=(p+1)^{-1}(2\pi-\Delta x_{k-1})^{p+1}. \quad (4.106)$$

For general (p,q) equality (4.103) is shown by induction. Thus, assume that the expression (4.103) is valid for $h(p,q)$ when $q\le q_0$ . For $q=q_o+1$ we obtain

$$
\begin{aligned}
h(p,q_0+1) &= \int_{\Delta x_k=\Delta x_{k-1}}^{2\pi} (2\pi-\Delta x_k)^p(\Delta x_k-\Delta x_{k-1})^{q_0+1}\mathrm{d}\Delta x_k \\
&= |-(p+1)^{-1}(2\pi-\Delta x_k)^{p+1}(\Delta x_k-\Delta x_{k-1})^{q_0+1}|_{\Delta x_k=\Delta x_{k-1}}^{\Delta x_k=2\pi} \\
&+ (q_0+1)(p+1)^{-1}\int_{\Delta x_k=\Delta x_{k-1}}^{2\pi}(2\pi-\Delta x_k)^{p+1}(\Delta x_k-\Delta x_{k-1})^{q_0} \\
&= 0+(q_0+1)(p+1)^{-1}h(p+1,q_0) \\
&= \{\text{by assumption}\} \\
&= ((q_0+p+2)(q_0+1)^{-1}(p+1)\binom{q_0+p+1}{p+1})^{-1}(2\pi-\Delta x_{k-1})^{q_0+p+2} \\
&= ((q_0+1)+p+1)\binom{(q_0+1)+p}{p})^{-1}(2\pi-\Delta x_{k-1})^{(q_0+1)+p+1}
\end{aligned}
$$

We now continue by inserting the equality (4.103) in (4.101) which yields

$$
\begin{aligned}
\mathrm{E}\{(\theta_k-\theta_1)_{2\pi}|\ldots\} &= \Delta x_{k-1}+ \\
(2\pi-\Delta x_{k-1}) &\sum_{n=0}^{(d-k+1)n_c-1}(N_k-n)\binom{N_k}{n}((N_k+1)\binom{N_k}{n})^{-1} \\
-(2\pi-\Delta x_{k-1}) &\sum_{n=1}^{(d-k+1)n_c-1} n\binom{N_k}{n}((N_k+1)\binom{N_k}{n-1})^{-1} \\
&= \Delta x_{k-1}+\frac{2\pi-\Delta x_{k-1}}{N_k+1}(N_k-\sum_{n=1}^{(d-k+1)n_c-1}1) \\
&= \Delta x_{k-1}+\frac{2\pi-\Delta x_{k-1}}{d-k+2}. \quad (4.107)
\end{aligned}
$$

## Appendix 4.G Derivation of Equation (4.93)

Obviously,

$$\begin{aligned}&\mathrm{VAR}\{(\theta_k-\theta_1)_{2\pi}|\tilde{\theta}_1=x_1,(\tilde{\theta}_2-\tilde{\theta}_1)_{2\pi}=\Delta x_2\ldots\\&(\tilde{\theta}_{k-1}-\tilde{\theta}_1)_{2\pi}=\Delta x_{k-1}\}=\mathrm{VAR}\{((\theta_k-\theta_1)_{2\pi}-\Delta x_{k-1})|\ldots\}.\end{aligned}\tag{4.108}$$

and

$$\begin{aligned}&\mathrm{E}\{((\theta_k-\theta_1)_{2\pi}-\Delta x_{k-1})^2|\ldots\}\\&\qquad=\int_{\Delta x_k=\Delta x_{k-1}}^{2\pi}(\Delta x_k-\Delta x_{k-1})^2\times\\&\qquad\quad\frac{\partial}{\partial\Delta x_k}\mathrm{Pr}\{(\theta_k-\theta_1)_{2\pi}\le\Delta x_k|\ldots\}\mathrm{d}\Delta x_k.\end{aligned}\tag{4.109}$$

Using (4.100) and (4.102) we obtain

$$\begin{aligned}&\mathrm{E}\{((\theta_k-\theta_1)_{2\pi}-\Delta x_{k-1})^2|\ldots\}\\&=(2\pi-\Delta x_{k-1})^{-N_k}\textstyle\sum_{n=0}^{(d-k+1)n_c-1}(N_k-n)\binom{N_k}{n}h(n,N_k-n+1)\\&-(2\pi-\Delta x_{k-1})^{-N_k}\textstyle\sum_{n=1}^{(d-k+1)n_c-1}n\binom{N_k}{n}h(n-1,N_k-n+2)\\&=((2\pi-\Delta x_{k-1})^2(n_c^2+n_c))/((d-k+2)n_c+1)(d-k+2)n_c.\end{aligned}\tag{4.110}$$

Combining (4.108),(4.110) and (4.92) yields

$$\begin{aligned}\mathrm{VAR}\{(\theta_k-\theta_1)_{2\pi}|\ldots\}&=\mathrm{E}\{((\theta_k-\theta_1)_{2\pi}-\Delta x_{k-1})^2|\ldots\}\\&\quad-(\mathrm{E}\{((\theta_k-\theta_1)_{2\pi}-\Delta x_{k-1})|\ldots\})^2\\&=\frac{(d-k+1)(2\pi-\Delta x_{k-1})^2}{((d-k+2)n_c+1)(d-k+2)^2}.\end{aligned}\tag{4.111}$$

# Chapter 5

# The Generalized SICR Beamformer

The SICR beamformer is derived in Section 3.2.1 assuming that the channels between all mobiles and all base stations are given by the GAAO model introduced in Section 2.3.1 (i.e a GAA model with $d = 1$ ). This means that the energy received at the base from a mobile is impinging from the location of the mobile but with some spreading in azimuth around the nominal direction. In this chapter we extend the SICR beamformer to the more general GWSSUS propagation model, Section 2.2. Furthermore, an arbitrary number of clusters, $d_{k,i}$, between the $k$th base and $i$th mobile is assumed. The obtained approach is referred to as the generalized SICR beamformer.

As was mentioned in the introduction of Chapter 3, the beamforming algorithms of [FN95, GP96, RDJP95] resembles the SICR beamformer introduced herein. The algorithm most similar to the approach herein is the "subspace beamformer" introduced in [GP96] (in particular if a single iteration is used and $p_j = \text{Trace}\{\mathbf{R}_j\}$) which tries to maximize the sum of the inverse signal to interference ratio of the mobiles in the cell. The major difference between the two algorithms is that users in other cells are taken into account in the one used herein.

In comparison with the "co-operative algorithm" introduced in [RDJP95], the main differences are that no hard bounds on transmitted energy, generated interference, and desired signal power are imposed (if these can not be met, the paper [RDJP95] suggests a channel re-

allocation). The approach here is instead based on minimizing the sum of the inverse interference to carrier ratio at the co-channel users (as the subspace beamformer of [GP96]), subject to a constraint on the array gain towards the desired mobile.

The SICR beamformer introduced in Chapter 3 applies a more restrictive propagation model than the papers [FN95, GP96, RDJP95] do. However, a generalization of the proposed beamformer to the general GWSSUS model is provided in this chapter.

It is estimated in Example 7.4 of Chapter 7 that the average downlink interference level in the direction of an identified interfered user is reduced 11.9dB as using the generalized SICR beamformer and an eight antenna linear array (as compared with the use of a single antenna).

## 5.1 Some Notations and Assumptions

A cellular network of $Q$ co-channel base stations is assumed. The derivations are made from the viewpoint of transmission from the $k$th base station to the $k$th mobile. Entities describing the propagation from the $k$th base to the $i$th mobile are given the indices $k, i$.

Propagation according to the GWSSUS model introduced in Section 2.2 is assumed The number of clusters in the propagation between the $k$th base and $i$th mobile is denoted by $d_{k,i}$. In the GWSSUS model, the downlink multipath covariance matrix associated with the $r$th cluster of the base $k$, to mobile $i$ propagation, is denoted $\mathbf{R}_{k,i}^r$. Thus, the cluster index, $r$, which is a subscript in Chapter 2, is now a superscript. The summed covariance matrix introduced in Section 2.5 is denoted $\mathbf{R}_{k,i}$ i.e.,

$$\mathbf{R}_{k,i} = \sum_{r=1}^{d_{k,i}} \mathbf{R}_{k,i}^r. \tag{5.1}$$

## 5.2 Derivation

When generalizing the SICR beamformer of Section 3.2.1, the first step is to find the mean energy (averaged over the fast fast fading) received at the $i$th mobile from base $k$, assuming that base $k$ transmits with weighting vector $\mathbf{w}_k$. Since the effective steering vectors of the clusters are independent (see Section 2.2), the received energy averaged over the fast fading from the clusters is the sum of the energy from each individual cluster. Thus (2.42) generalizes to

$$P_{k,i} = \sum_{r=1}^{d_{k,i}} \mathbf{w}_k^* \mathbf{R}_{k,i}^r \mathbf{w}_k \tag{5.2}$$

$$= \mathbf{w}_k^* \mathbf{R}_{k,i} \mathbf{w}_k \tag{5.3}$$

where $\mathbf{R}_{k,i}^r$ is the multipath covariance matrix of the $r$th cluster in the connection between the $k$th base and $i$th mobile. The ad-hoc restriction (3.4) is generalized to

$$P_{k,k} = \mathbf{w}_k^* \mathbf{R}_{k,k} \mathbf{w}_k = \frac{\text{Trace}\{\mathbf{R}_{k,k}\}}{m}. \tag{5.4}$$

Equation (5.4) is equivalent to (3.4) in the special case of GAA model with $d_{k,k} = 1$ (GAAO). In order to get some understanding of what (5.4) means, consider transmission using $\mathbf{w}_k = [1, 0, \ldots, 0]^T$. Then from (5.3) the power received at mobile $k$ is $P_{k,k} = [\mathbf{R}_{k,k}]_{1,1}$. If $\mathbf{w}_k = [0, 1, \ldots, 0]^T$ then $P_{k,k} = [\mathbf{R}_{k,k}]_{2,2}$, and so on. Thus the right hand side of (5.4) is the energy received at the $k$th mobile assuming transmission using a single antenna and unit energy, averaged over the $m$ antennas of the array. The carrier to interference ratio at the $i$th mobile, neglecting interference from all other base stations than the $k$th base station, $\widetilde{\text{CIR}}_i$, is obtained from (5.3) and (5.4) as

$$\begin{aligned} \widetilde{\text{CIR}}_i &= \frac{P_{i,i}}{P_{k,i}} \\ &= \frac{\mathbf{w}_i^* \mathbf{R}_{i,i} \mathbf{w}_i}{\mathbf{w}_k^* \mathbf{R}_{k,i} \mathbf{w}_k} \\ &= \frac{\text{Trace}\{\mathbf{R}_{i,i}\}}{m \mathbf{w}_k^* \mathbf{R}_{k,i} \mathbf{w}_k}. \end{aligned} \tag{5.5}$$

The criterion function is chosen in the same way as in Section 3.2.1, i.e.,

$$\mathbf{w}_k = \arg_{\mathbf{w}} \min\{ \sum_{i=1,\neq k}^{Q} \widetilde{\text{CIR}}_i^{-1} \}, \tag{5.6}$$

subject to (5.4). Thus, in a sense, $\mathbf{w}_k$ is chosen to minimize *the sum of the inverse carrier to interference ratio of the mobiles in the system. This is the reason for referring to the algorithm introduced here and the algorithm in Section 3.2.1 as the summed interference to carrier ratio*

*minimizing(SICR) beamformer*. The word "generalized" stems from the more general propagation model used here versus Section 3.2.1. Combining (5.5) and (5.6) yields

$$\mathbf{w}_k = \arg_{\mathbf{w}} \min\{\mathbf{w}_k^* \mathbf{M} \mathbf{w}_k\}, \tag{5.7}$$

where the matrix, $\mathbf{M}$, is given by

$$\mathbf{M} = \sum_{i=1,\neq k}^{Q} \frac{m}{\text{Trace}\{\mathbf{R}_{i,i}\}} \mathbf{R}_{k,i}. \tag{5.8}$$

As in Section 3.2.1 the $Q$ users are divided into two categories: identified and unidentified. The matrix $\frac{m}{\text{Trace}\{\mathbf{R}_{i,i}\}}\mathbf{R}_{k,i}$ is assumed known for the identified mobiles, say $i = 1, \ldots, p$. In order to account for the unidentified mobiles the approximation

$$\sum_{i=p+1,\neq k}^{Q} \frac{m}{\text{Trace}\{\mathbf{R}_{i,i}\}} \mathbf{R}_{k,i}. \approx \text{constant} \times \mathbf{I}, \tag{5.9}$$

is made. This assumption is reasonable if the azimuth angles of the received wavefields are well spread, as seen from the $k$th base. The constant in (5.9) may be selected using loose reasoning as in Section 3.3.1.2 and 3.3.2.3. In the SSFR case, see Section 3.1.2, the identified interfered mobiles are served by the same base. This implies that $\mathbf{R}_{i,i} = \mathbf{R}_{k,i}$ using the framework here.

Finally, $\mathbf{w}_k$ is obtained as

$$\mathbf{w}_k = \sqrt{\frac{\text{Trace}\{\mathbf{R}_{k,k}\}}{m\mathbf{e}^* \mathbf{R}_{k,k} \mathbf{e}}} \mathbf{e}, \tag{5.10}$$

where $\mathbf{e}$ is the dominating generalized eigenvector associated with the matrix pair $(\mathbf{R}_{k,k}, \mathbf{M})$. In the RCS-WON case, i.e., capacity enhancement by reducing the cluster size without steering nulls in the direction of cochannel signals $\mathbf{e}$ is simply the dominating eigenvector of the matrix $\mathbf{R}_{k,k}$. In the special case of a GAA model with $d_{k,i} = 1$ for all $k$ and $i$ (GAAO), the SICR beamformer and the generalized SICR beamformer are equivalent.

# Chapter 6

# A Downlink Beam-Steering Algorithm for GSM

In this chapter we propose a technique for downlink beam steering in GSM/DCS1800/PCS1900[1], [MP92], using antenna array base stations. The objective is to find an algorithm which has performance close to that of the generalized-SICR beamformer introduced in Chapter 5, under the RCS-WON capacity enhancement approach. In the RCS-WON approach, the capacity is enhanced by increasing the fraction of the total available spectrum used in a cell, without pointing nulls in the direction of co-channel users, see Section 3.1.3. The basic principle of the proposed algorithm is to transmit in the direction which maximizes the desired power averaged over the fast fading. For this reason, the introduced technique is referred to as the maximum desired power (MDP) beamformer.

The analysis in the chapter differs from the references cited in Section 1.3.2, in that it investigates the impact on the uplink interference on the downlink performance, and applies the proposed solution to simulated as well as measured data. Furthermore, the proposed solution does not place nulls towards co-channel users, which all the techniques cited in Section 1.3.2 do. The reason for this choice follows from some practical considerations:

[1] from now on simply referred to as GSM collectively

Conventional GSM networks typically employ $K = 3, S = 3$ frequency reuse [2], [CJL+94] . If a more aggressive frequency reuse than $K = 1$, $S = 3$ is applied[3], a combination of dynamic channel allocation and power control has to be employed to avoid that the near-far ratios of the desired signal power to the power of the strongest co and adjacent channel signal, averaged over the fast fading (see Example 4.1 and 4.2) to exceed 25dB. The speed of the channel allocation and power control must be fast enough to follow the slow-fading. This may be impossible to implement within the specification of GSM. The threefold capacity enhancement achieved by decreasing the frequency reuse to $K = 1, S = 3$ can be obtained with the RCS-WON approach, see Example 4.5. The fact that the threefold capacity enhancement can be achieved without nulling does not imply that it is a bad idea to employ nulling to achieve the same capacity enhancement. For instance, the number of required antenna elements may be reduced. However, approaches without nulling are generally very robust with respect to calibration errors, and propagation conditions. In addition, some approaches with nulling, such as the SICR-RCS-WIN beamformer of Chapter 3, require base station time-slot synchronization, and tracking of users in other cells [4], which may difficult to achieve. Thus there is motivation for a study of approaches without nulling.

The analysis in the chapter assumes a GSM system and investigates the impact of frequency hopping as well as base station synchronization (synchronization of the TDMA frames of the base stations), on the performance of the proposed solution. The results indicate that the proposed technique generates less than 0.9dB more interference than the substantially more complex generalized SICR algorithm (under the RCS-WON approach), if some conditions are fulfilled. One of the requirements is that the mean uplink C/I is better than a certain threshold. This threshold is $-8$dB,$-8$dB,$+3$dB and $-2$ dB in the frequency hopping-synchronized (FHS), frequency hopping-unsynchronized (FHU), fixed frequency-unsynchronized (FFU) and fixed frequency-synchronized (FFS) case respectively. The performance of the proposed algorithm using measured data is estimated and found to be similar to the perfor-

[2]By $K = 3$, $S = 3$ reuse is meant that a third of total available spectrum is allocated per cell and a third of that spectrum, in turn, per 120-degree sector, see Section 3.1.1.

[3]By $K = 1$, $S = 3$ is meant that all the available spectrum is used in all cells, but only a third of the spectrum per 120-degree sector.

[4]Tracking here means estimation of angle of arrival, angular spread, and power of these users.

mance obtained using propagation models.

The chapter is organized as follows: In Section 6.1 some new notations and assumptions are introduced. Then Section 6.2 introduces the MDP beamformer. The treatment in Section 6.2 assumes a GWSSUS model with an arbitrary number of clusters of scatterers. However, some approximations are motivated using the more restrictive GAA model, which is a special case of the GWSSUS model. The impact of uplink interference is analyzed in Section 6.2.4. In Section 6.3 the MDP beamformer is simulated using the TU and BU models (Section 2.4) and measurement data ( Section 7.1). A comparison of the performance of the generalized SICR and MDP beamformers is also made in Section 6.3. This comparison uses a mixture of GAA and TU/BU models. Finally, some conclusions are drawn in Section 6.4.

## 6.1 Some Notations and Assumptions

A cellular network of $Q$ co-channel base stations is assumed. The derivations are made from the viewpoint of transmission from the $k$th base station to the $k$th mobile. Entities describing the propagation from the $k$th base to the $i$th mobile are given the indices $k, i$. In Section 2.1, basic propagation assumptions are made assuming a linear modulation. GSM applies a nonlinear GMSK modulation [GSM92]. However, investigations we have made have shown that the error of approximating the GMSK modulation with a linear modulation is less than $-23$dB[5]. Thus the basic assumptions may be considered to hold with reasonable accuracy. We now generalize the notation in Section 2.1 to the case of multiple interfering users and a burst mode transmission: Let $\mathbf{x}_{q,b}^{\mathrm{RX}}$ be the $q$th uplink sample in burst $b$ at base $k$. Next let $\mathbf{h}_{l,b}^{\mathrm{RX},i}$ be the $l$th tap of the multidimensional impulse response of the $i$th user as seen from the $k$th base station in burst $b$. The special notation $\mathbf{h}_{l,b}^{\mathrm{RX}} = \mathbf{h}_{l,b}^{\mathrm{RX},k}$ is introduced for the desired user. Assuming linearity (2.2) of Section 2.1, generalizes to

$$\mathbf{x}_{q,b}^{\mathrm{RX}} = \sum_{l\geq 0} \mathbf{h}_{l,b}^{\mathrm{RX}} I_{q-l,b} + \sum_{i=1,\neq k}^{Q} \sum_{l\geq 0} \mathbf{h}_{l,b}^{\mathrm{RX},i} I_{q-l,b}^{i} + \mathbf{n}_{q,b}, \tag{6.1}$$

[5] by this is meant that the GMSK signal can be decomposed into a linear modulated term and an approximation error term. The linear term is more than 23dB stronger than the error term.

where circularly symmetric, zero mean, spatially white Gaussian additive noise, $\mathbf{n}_{q,b}$, has been added. Thus

$$\mathrm{E}\{\mathbf{n}_{q,b}\} = \mathbf{0} \tag{6.2}$$

$$\mathrm{E}\{\mathbf{n}_{q,b}\mathbf{n}_{q,b}^T\} = \mathbf{0} \tag{6.3}$$

$$\mathrm{E}\{\mathbf{n}_{q,b}\mathbf{n}_{q,b}^*\} = \sigma_n^2\mathbf{I}. \tag{6.4}$$

The noise generated by the receiver amplifiers is assumed white. However, the receiver noise is filtered before sampling. The noise process, $\mathbf{n}_{q,b}$, is therefore temporally correlated. As in Section 2.3.1, the pulse $\mathrm{pr}(\tau)$ is assumed normalized according to

$$\int_{\tau=0}^{\infty} |\,\mathrm{pr}(\tau)|^2 \mathrm{d}\tau = 1. \tag{6.5}$$

The following discrete time version of (6.5) is also assumed

$$\sum_{l=0}^{\infty} |\,\mathrm{pr}(lT + \Delta\tau)|^2 = 1, \text{ for } 0 \leq \Delta \leq T. \tag{6.6}$$

Equation (6.6) follows from (6.5) if $\mathrm{pr}(\tau)$ is band limited $f \leq \frac{1}{2T}$. Calculations we have made using the pulse-shape of the linear approximation of the GSM waveform, and a 4th order Butterworth receiver filter with cut-off frequency 100kHz, have shown that the left hand side of (6.6) varies between 0.9993 and 1.002 using different $\Delta\tau$.

When the GWSSUS or GAA model is assumed (see Sections 2.2 and 2.3 respectively) the number of clusters in the propagation between the $k$th base and $i$th mobile is denoted by $d_{k,i}$. In the GWSSUS model the downlink multipath covariance matrix associated with the $r$th cluster of the base $k$, mobile $i$ connection, is denoted $\mathbf{R}_{k,i}^r$. Thus, the cluster index, $r$, which is a subscript in Chapter 2, is now a superscript. For simplicity the summed multipath covariance matrix defined as

$$\mathbf{R}_{k,i} = \sum_{r=1}^{d_{k,i}} \mathbf{R}_{k,i}^r, \tag{6.7}$$

is also introduced. When the GAA model and linear base station arrays are assumed, Section 2.3, the received power, angle of arrival, and angular spreading of the $r$th cluster $r = 1, \ldots, d_{k,i}$ are denoted by $G_{k,i}^r$, $\theta_{k,i}^r$ and

$\sigma^r_{k,i}$ respectively. In this special case, the multipath covariance matrices can be expressed as

$$\mathbf{R}^r_{k,i} = G^r_{k,i}\mathbf{R}(\theta^r_{k,i}, \sigma^r_{k,i}), \tag{6.8}$$

where $\mathbf{R}(\theta, \sigma)$ is a complex-matrix valued *function* of $\theta$ and $\sigma$, defined in (2.33). The realization of the $r$th effective downlink steering vector, Section 2.2, of the base $k$ mobile $k$ connection, in burst $b$, is denoted $\mathbf{v}^{\mathrm{TX}}_{r,b}$. The corresponding uplink variable is $\mathbf{v}^{\mathrm{RX}}_{r,b}$.

For convenience the normalized manifold vectors, $\tilde{\mathbf{a}}^{\mathrm{RX}}(\theta)$ and $\tilde{\mathbf{a}}^{\mathrm{RX}}(\theta)$ are introduced. They are defined as

$$\tilde{\mathbf{a}}^{\mathrm{RX}}(\theta) = \frac{\mathbf{a}^{\mathrm{RX}}(\theta, f^{\mathrm{RX}})}{\|\mathbf{a}^{\mathrm{RX}}(\theta, f^{\mathrm{RX}})\|} \tag{6.9}$$

and

$$\tilde{\mathbf{a}}^{\mathrm{TX}}(\theta) = \frac{\mathbf{a}^{\mathrm{TX}}(\theta, f^{\mathrm{TX}})}{\|\mathbf{a}^{\mathrm{TX}}(\theta, f^{\mathrm{TX}})\|} \tag{6.10}$$

respectively.

## 6.2 The MDP Beamformer

In the following three sections the maximum desired power (MDP) beamformer is derived, and analyzed. In Section 6.2.1 the main idea and basis of the proposed approach is introduced. In Second 6.2.2 the criterion function is rewritten such that it is easily applied in TDMA systems with training sequences. A detailed description of how the algorithm may be implemented in a GSM system is given in Section 6.2.3. The probability of transmission towards an interferer rather than the desired mobile is analyzed in Section 6.2.4. Finally, Section 6.2.5 motivates why the power is averaged in logarithmic scale rather than linear scale.

### 6.2.1 Basic Approach

As was mentioned in the introduction, the objective of the chapter is to design an algorithm which has performance similar to the generalized SICR beamformer in its RCS-WON form. The transmit vector $\mathbf{w}_k$ of the generalized-SICR beamformer is given by (5.10), which is the solution to the minimization (5.7) with $\mathbf{M} = \mathbf{I}$ subject to the constraint (5.4) over

all possible complex weighting vectors $\mathbf{w}_k$. An alternative would be to confine the search to weighting vectors of the form

$$\mathbf{w}_k = g\tilde{\mathbf{a}}^{\mathrm{TX}}(\theta_0), \tag{6.11}$$

with arbitrary $g$ and $\theta_0$. The solution to this minimization is

$$\theta_0 = \arg\max_{\theta} \tilde{f}(\theta) \tag{6.12}$$

$$g^2 = \frac{\mathrm{Trace}\{\mathbf{R}_{k,k}\}}{m(\tilde{\mathbf{a}}^{\mathrm{TX},*}(\theta_0)\mathbf{R}_{k,k}\tilde{\mathbf{a}}^{\mathrm{TX}}(\theta_0))} \tag{6.13}$$

where $\tilde{f}(\theta)$ is given by

$$\tilde{f}(\theta) = \tilde{\mathbf{a}}^{\mathrm{TX},*}(\theta)\mathbf{R}_{k,k}\tilde{\mathbf{a}}^{\mathrm{TX}}(\theta). \tag{6.14}$$

The disadvantage of applying the restriction (6.11) is an increased level of emitted interference, as compared to the generalized SICR beamformer. Due to the constraint (5.4), the power delivered at the desired mobile is, however, the same. Extensive calculations we have made with eight element linear arrays, a GAA propagation model with one to four Gaussian clusters i.e. , $d_{k,k} = 1, \ldots, 4$ and various angular spreads $\sigma^r_{k,k}$, gave a maximum increase of 0.65dB in $\|\mathbf{w}\|^2$ by introducing the constraint (6.11). This performance loss is judged to be small, and therefore the constraint (6.11) is imposed, in order to reduce complexity. In the following development we will concentrate on estimating $\theta_0$ defined by (6.12), and assume that $g$ is selected according to (6.13) by some independent power control algorithm. It should be noted that the solution (6.13) is due to the ad-hoc restriction (5.4). Our experience is that SICR-RCS-WIN and SICR-SSFR both are sensitive to this power normalization, while RCS-WON approach is not (Chapter 3). Thus, how to estimate $\theta_0$ is thus the important issue. *From (5.4),(6.11-6.12), and (6.14) we observe that $\theta_0$ is the direction which maximizes the mean desired power received through a (normalized) beam steered towards $\theta_0$. This is the motivation for referring to the approach derived as: the maximum desired power (MDP) beamformer.* In the sections following a sequence of approximates of $\theta_0$ denoted as $\tilde{\theta}_0$, $\breve{\theta}_0$, and $\grave{\theta}_0$ are derived. Finally an estimator of $\grave{\theta}_0$, denoted $\hat{\theta}_0$ is introduced. This estimate is used to form an estimate of $\mathbf{w}_k$ as

$$\hat{\mathbf{w}}_k = \hat{g}\tilde{\mathbf{a}}^{\mathrm{TX}}(\hat{\theta}_0), \tag{6.15}$$

where $\hat{g}$ is an estimate of $g$.

### 6.2.2 Some Manipulations of the Criterion Function

It follows from (2.11), (2.20) and (6.6) that the matrix $\mathbf{R}_{k,k}$, can be expressed as

$$\mathbf{R}_{k,k} = \mathrm{E}\{\sum_{l\geq 0} \mathbf{h}_{l,b}^{\mathrm{TX}} \mathbf{h}_{l,b}^{\mathrm{TX},*}\}. \tag{6.16}$$

Using (6.16) the criterion function, (6.14), can be rewritten as

$$\tilde{f}(\theta) = \mathrm{E}\{\xi(\theta)\}, \tag{6.17}$$

where $\xi(\theta)$ is given by

$$\xi(\theta) = \sum_{l\geq 0} \tilde{\mathbf{a}}^{\mathrm{TX},*}(\theta) \mathbf{h}_{l,b}^{\mathrm{TX}} \mathbf{h}_{l,b}^{\mathrm{TX},*} \tilde{\mathbf{a}}^{\mathrm{TX}}(\theta). \tag{6.18}$$

If the $d_{k,k}$ clusters are well separated in azimuth, $\theta$, the following approximation can be made

$$\xi(\theta) \approx \tilde{\mathbf{a}}^{\mathrm{TX},*}(\theta) \mathbf{v}_{r(\theta),b}^{\mathrm{TX}} \mathbf{v}_{r(\theta),b}^{\mathrm{TX},*} \tilde{\mathbf{a}}^{\mathrm{TX}}(\theta)\}, \tag{6.19}$$

where the integer-valued function $r(\theta)$ is given by

$$r(\theta) = \arg_{r=1,\ldots,d_{k,k}} \max |\tilde{\mathbf{a}}^{\mathrm{TX},*}(\theta_r) \tilde{\mathbf{a}}^{\mathrm{TX},*}(\theta)|^2, \tag{6.20}$$

and $\theta_r$ is some angle within the $r$th cluster. Thus for each $\theta$, the integer $r(\theta)$, is the number of the cluster which receives the most energy if a beam is steered towards $\theta$. Since $\mathbf{v}_{r(\theta),b}^{\mathrm{TX}}$ is Gaussian, circular symmetric and zero mean, see Section 2.2, it follows that $\xi(\theta)$ is approximately exponentially distributed. Thus $\theta_0$ is found by maximizing the mean of the approximately exponentially distributed random variable $\xi(\theta)$. Since $\xi(\theta)$ is approximately exponential distributed, an approximation of $\theta_0$ is obtained by maximizing the mean of $\log(\xi(\theta))$ i.e.

$$\begin{aligned} \theta_0 &= \arg_\theta \max\{\mathrm{E}\{\xi(\theta)\} && (6.21)\\ &\approx \arg_\theta \max\{\mathrm{E}\{10\log(\xi(\theta))\}\} && (6.22)\\ &= \tilde{\theta}_0. && (6.23) \end{aligned}$$

If $\xi(\theta)$ had been exactly exponential distributed then the two entities had been equivalent i.e. $\tilde{\theta_0} = \theta_0$. *Equation (6.23) is interpreted as $\tilde{\theta}_0$ being the maximizing argument of the mean of $\xi(\theta)$ in decibel (dB) scale.* The

following derivations are in fact based on (6.23). Section 6.2.5 is devoted to a motivation of why this choice is made. Combining (6.23) and (6.18) yields

$$\tilde{\theta}_0 = \arg_\theta \max\{\mathrm{E}\{10\log(\sum_{l\geq 0} |\tilde{\mathbf{a}}^{\mathrm{TX},*}(\theta)\mathbf{h}_{l,b}^{\mathrm{TX}}|^2)\}\}. \tag{6.24}$$

A natural step would be to obtain an estimate of $\theta_0$ by simply replacing $\mathbf{h}_{l,b}^{\mathrm{TX}}$ by an estimate thereof. Unfortunately it is impossible to estimate the downlink impulse response $\mathbf{h}_{l,b}^{\mathrm{TX}}$, see Section 2.5. To resolve this problem all downlink entities in (6.24) are replaced by the corresponding uplink entities yielding

$$\breve{\theta}_0 = \arg_\theta \max\{\mathrm{E}\{10\log(\sum_{l\geq 0} |\tilde{\mathbf{a}}^{\mathrm{RX},*}(\theta)\mathbf{h}_{l,b}^{\mathrm{RX}}|^2)\}\}. \tag{6.25}$$

If the statistical distribution of $\sum_{l\geq 0} |\tilde{\mathbf{a}}^{\mathrm{TX},*}(\theta)\mathbf{h}_{l,b}^{\mathrm{RX}}|^2$ and $\sum_{l\geq 0} |\tilde{\mathbf{a}}^{\mathrm{RX},*}(\theta)\mathbf{h}_{l,b}^{\mathrm{RX}}|^2$ are the same, then $\breve{\theta}_0 = \tilde{\theta}_0$. This is the case if

$$\tilde{\mathbf{a}}^{\mathrm{TX},*}(\theta_1)\mathbf{a}^{\mathrm{TX}}(\theta_2, f^{\mathrm{TX}}) = \tilde{\mathbf{a}}^{\mathrm{RX},*}(\theta_1)\mathbf{a}^{\mathrm{RX}}(\theta_2, f^{\mathrm{RX}}) \tag{6.26}$$

and (6.19) are valid for all $\theta_1$ and $\theta_2$. Equations (6.19) and (6.26) are typically good approximations and therefore $\breve{\theta}_0$ and $\tilde{\theta}_0$, for practical purposes, equivalent.

### 6.2.3 Implementation

In GSM it is usually assumed that all the desired signal energy is kept within five taps in a span of eleven taps say $l \in \{\lambda_0, \ldots, \lambda_0 + 4\}$ where $\lambda_0 = 1, \ldots, 7$. However, in order to reduce the impact of interference it is here assumed that all the energy in the desired direction $\theta_0$ is kept within three taps. In order to decrease computational complexity, the scan in $\theta$ is also limited to a discrete set of values $\Theta$. With these restrictions the algorithm

$$(\grave{\theta}_0, \lambda_0) = \arg_{\theta\in\Theta,\lambda\in[1,\ldots,7]} \max\{\mathrm{E}\{10\log(\sum_{l=\lambda}^{\lambda+2} |\tilde{\mathbf{a}}^{\mathrm{RX},*}(\theta)\mathbf{h}_{l,b}^{\mathrm{RX}}|^2)\}\} \tag{6.27}$$

is obtained. Note that (6.27) constitutes a search over two parameters, but where only $\grave{\theta}_0$ is of interest. The traffic bursts in GSM includes a

training sequence of 26 known symbols $I^{\mathrm{RX}}_{q,b}$ in the mid amble [MP92], say $q = 0, \ldots, 25$. Thus the tap estimates $\hat{\mathbf{h}}^{\mathrm{RX}}_{l,b}$ can be obtained by cross correlating the known training sequence with the received bursts. Mathematically this appears as

$$\hat{\mathbf{h}}^{\mathrm{RX}}_{l,b} = \sum_{q=l}^{l+25} \frac{1}{26} \mathbf{x}^{\mathrm{RX}}_{l,b} I^{*}_{q-l,b}. \tag{6.28}$$

Given $\hat{\mathbf{h}}^{\mathrm{RX}}_{l,b}$ for $l = 1, \ldots, 11, b = 1, \ldots, B$, the following approximation of (6.27), is obtained

$$(\hat{\theta}_0, \hat{\lambda}_0) = \arg_{\theta \in \Theta, \lambda \in [1,\ldots,7]} \max f(\theta, \lambda) \tag{6.29}$$

where

$$f(\theta, \lambda) = \sum_{b=1}^{B} \frac{1}{B} (10 \log(\sum_{l=\lambda}^{\lambda+2} |\tilde{\mathbf{a}}^{\mathrm{RX},*}(\theta) \hat{\mathbf{h}}^{\mathrm{RX}}_{l,b}|^2)). \tag{6.30}$$

In the case of a uniform linear array with eight antenna elements for 120 degree coverage, the search in the azimuth is confined to the values $\theta \in \Theta = [-72.7^o, -59.4^o, -49.8^o, -41.9^o, -35.0^o, -28.5^o, -22.6^o, -16.6^o, -11.0^o, -5.5^o, 0^o, 5.5^o, 11.0^o, 16.6^o, 22.6^o, 28.5^o, 35.0^o, 41.9^o, 49.9^o, 59.4^o, 72.7^o, 88.2^o]$, loosing at most 1dB in comparison with a continuous scan. With $k = \{1, \ldots, 9\}$ this yields a total of $9 \times 22 = 198$ points to search the criterion (6.30). An efficient way of computing these 198 values is to compute $|\tilde{\mathbf{a}}^{\mathrm{RX},*}(\theta) \hat{\mathbf{h}}^{\mathrm{RX}}_{l,b}|^2$ for all $s = 1, \ldots, 11, b = 1, \ldots, B, \theta \in \Theta$ and then "sum and log". The computational requirements for the outlined algorithm becomes $B \times 8 \times 11 \times 26 \times 4$ real valued multiplications for the calculation of $\hat{\mathbf{h}}^{\mathrm{RX}}_{l,b}$, and $B \times 8 \times 11 \times 4 \times 22$ real valued multiplications for the estimation of $|\mathbf{a}^{\mathrm{RX},*}(\theta, f^{\mathrm{RX}}) \hat{\mathbf{h}}^{\mathrm{RX}}_{l,b}|^2$. Both tasks also require equally many additions. The "sum and log" step requires $B \times 9 \times 9 \times 3$ additions and $B \times 9 \times 9$ logarithms. Finally the largest value among the all the 198 values has to be found. The total computational requirements are: $16896B$ multiplications, $17139B$ additions, $81B$ logarithms and 198 comparisons. This yields a computational load of 8.5Mflops since the time between two consecutive bursts is 4.6ms. The larger number of bursts $B$ that is used in the algorithm, the more accurate estimate of $\theta_0$, is obtained in principle. In practice however, the azimuth angles of the arriving wave fields $\theta_n$ (see Section 2.1), may be considered fixed only during a limited number of bursts. And therefore $\theta_0$ becomes a function

of time. Based on simulations we have found $B = 21$ to be a reasonable tradeoff. However, $B$ can be made larger if noise and interference is a major problem and smaller if the algorithm is to slow to track the changes in the environment.

When the desired mobile is in discontinuous transmission (DTX) mode it transmits in twelve bursts out of 104 bursts[6], [MP92]. Because of the relatively large averaging window, $B = 21$, an impulse response estimate with a very large error may make $\hat{\theta}_0$ point in the direction an interferer, for a whole second. We believe that the highest acceptable probability for such an outage should be 0.1%, i.e. a second out of three hours. The results of the next section indicates that that a mean uplink C/I of $-8$,$-13$,$-4$dB and 0 to 3dB is required to achieve the 0.1% target in the frequency hopping-synchronized (FHS), fixed frequency hopping-unsynchronized (FHU), fixed frequency-unsynchronized (FFU) and fixed frequency-synchronized (FFS) case respectively.

When the mobile is active (not in DTX mode) new $\theta_0$ estimates are received at a much higher rate than in DTX mode. Thus if a large channel estimation error occurs, $\hat{\theta}_0$, will typically point in an erroneous direction only for 0.1 seconds. This does not result in a considerable loss of speech quality. Another advantage of active mobiles is that the proposed algorithm will become more capable of tracking fast varying propagation scenarios. These considerations suggests that it may be favorable to disable the possibility for the mobiles to go into DTX mode in uplink. The obvious drawback of this being an increased uplink interference level. However, a higher performance improvement (by introducing the antenna arrays) may be achieved in uplink than in downlink, and therefore the degradation compensated.

### 6.2.4 Analysis of the Impact of Interference

This section analyzes the probability that the algorithm described in the previous section selects a completely wrong transmit direction due to interference. The impact of DTX on the uplink interference is not considered. The propagation conditions for the desired and interfering users is assumed to be flat Rayleigh fading with superimposed slow log-normal fading. Furthermore the azimuth power distribution of the desired and interfering signals are assumed to be narrow in comparison with

[6] In a conversation, one person is typically speaking while the other is listening. In order to reduce interference and power consumption, the transmission from the silent user enters DTX mode

the beam-width of the transmit beams formed by the antenna array. Mathematically this may be expressed as

$$\mathbf{h}_{l,b}^{\mathrm{RX},i} = \tilde{\mathbf{a}}^{\mathrm{RX}}(\theta_b^i)\sqrt{G_b^i} f_b^i \,\mathrm{pr}(lT + \Delta T_b^i - T - \tau_b^i), \tag{6.31}$$

where $\theta_b^i$, $G_b^i$, $f_b^i$, $\Delta T_b^i$, and $\tau_b^i$ are the direction of arrival, path gain, fast-fading, sampling-phase, and delay of the mobile in the $i$th cell in the $b$th burst as seen from the $k$th base. The variable $f_b^i$ is a Gaussian circular symmetric zero-mean complex random variable with variance 1, which is assumed independent from burst to burst. Of the four factors in (6.31) only $\tilde{\mathbf{a}}^{\mathrm{RX}}(\theta_b^i)$, is a vector. The path gain $G_b^i$ is given by

$$G_b^i = \frac{|p(\theta_b^i)|^2}{(r_b^i)^\gamma} L_b^i, \tag{6.32}$$

where $|p(\theta_b^i)|^2$ is the element pattern gain, $r_b^i$ is the distance from the $k$th base to the $i$th mobile, $\gamma$ is the propagation path-loss and $L_b^i$ is a log-normally distributed such that $10\log(L_b^i)$ is normally distributed with mean zero and standard deviation 8dB. The random variable $L_b^i$ is modeled as independent from burst to burst, i.e. a large number of carriers in the frequency hopping pattern, is assumed. This model is in fact the same model as the one introduced in Section 2.3.1, if $\sigma_{k,i}$ is set to zero for all $k$ and $i$, and $\theta_b^i$, $G_b^i$, $\Delta T_b^i$, $\tau_b^i$, $r_b^i$, $L_b^i$ are interpreted as the realization of $\theta_{i,k}$, $G_{i,k}$, $\Delta T_{i,k}$, $\tau_{i,k}$, $r_{i,k}$, $L_{i,k}$ in burst $b$. For the desired user ($i = k$) the propagation parameters $\theta_b^i$, $G_b^i$ $\Delta T_b^i$ and $\tau_b^i$ are assumed constant, i.e. independent of $b$. In the frequency hopping case, the corresponding entities for the interferers ($i \neq k$), change between time slots since different interferers are "met". In the fixed frequency case the parameters are assumed fixed also for the interfering users since the same co-channel users are "met" in each timeslot. When the entities are independent of $b$, the subscript $b$ is dropped.

The algorithm described in the previous section will select the correct direction in $\Theta$ provided that

$$f(\theta_0, \lambda_0) > \max_{\lambda} f(\theta, \lambda), \text{ for all } \theta \neq \theta_0. \tag{6.33}$$

The probability that the direction of a strong interferer is selected rather than the desired direction will now be analyzed. The interference enters the algorithm described in the previous section through errors in the tap estimates. Inserting (6.1) in (6.28) yields

$$\hat{\mathbf{h}}_{l,b}^{\mathrm{RX}} = \mathbf{h}_{l,b}^{\mathrm{RX}} + \sum_{i=1,\neq k}^{Q} \sum_{\tilde{l}} \mathbf{h}_{\tilde{l},b}^{\mathrm{RX},i} \gamma_{l-\tilde{l},b}^{i} + \sum_{q=l}^{l+25} \frac{1}{26} \mathbf{n}_{q,b} I_{q-l,b}^{*}. \tag{6.34}$$

where

$$\gamma_{p,b}^{i} = \frac{1}{26} \sum_{\tilde{q}=0}^{25} I_{\tilde{q}+p}^{i} I_{\tilde{q},b}^{*}, \tag{6.35}$$

and the correlation between the training sequence and undesired time-shifts of the desired bit stream has been neglected. We assume further that the manifold vectors $\tilde{\mathbf{a}}^{\mathrm{RX}}(\theta^i)$ of the interferers are orthogonal to each other and to the steering vector of the desired user. This assumption is reasonable if the users are separated more than a beamwidth in azimuth, otherwise it is pessimistic. Neglecting noise, (6.30) (6.34) yields that the value of $f(\theta^i, \lambda)$, where $\theta^i$ is in the direction of the $i$th cell, is limited by

$$\begin{aligned} f(\theta^i, \lambda) \leq \max_{\lambda} f(\theta^i, \lambda) = \sum_{b=1}^{B} \frac{1}{B} (10 \log(|\tilde{\mathbf{a}}^{\mathrm{RX},*}(\theta^i) \tilde{\mathbf{a}}(\theta_b^i)|^2) \\ + 10 \log(\frac{|p(\theta_b^i)|^2}{(r_b^i)^\gamma}) + 10 \log(L_b^i) + 10 \log(|f_b^i|^2)) \\ + \max_{\lambda} \{ \sum_{b=1}^{B} \frac{1}{B} (10 \log(\sum_{l=\lambda}^{\lambda+2} |\sum_{\tilde{l}} \mathrm{pr}(\tilde{l}T + \Delta T_b^i - T - \tau_b^i) \gamma_{l-\tilde{l},b}^{i}|^2))\}. \end{aligned} \tag{6.36}$$

In the worst case, $\theta_b^i = \theta^i$, for all $b$. Inserting this in (6.36) and using (6.9) yields

$$\begin{aligned} f(\theta^i, \lambda) \leq \sum_{b=1}^{B} \frac{1}{B} (10 \log(\frac{|p(\theta_b^i)|^2}{(r_b^i)^\gamma}) + 10 \log(L_b^i) + 10 \log(|f_b^i|^2)) \\ + \max_{k} \{ \sum_{b=1}^{B} \frac{1}{B} (10 \log(\sum_{l=\lambda}^{\lambda+2} |\sum_{\tilde{l}} \mathrm{pr}(\tilde{l}T + \Delta T_b^i - T - \tau_b^i) \gamma_{l-\tilde{l},b}^{i}|^2))\}. \end{aligned} \tag{6.37}$$

Neglecting noise $f(\theta_0, \lambda_0)$ is given by

$$f(\theta_0, \lambda_0) = \sum_{b=1}^{B} \frac{1}{B}(10\log(G^k) + 10\log(|f_b^k|^2)), \tag{6.38}$$

where it has been assumed that all the energy of the desired mobile is confined to the taps $\lambda, \ldots, \lambda + 2$. The probability $p_{\text{failure}}$ that the algorithm points the beam in the direction of an interferer rather than the desired mobile can now be expressed as

$$p_{\text{failure}} = \Pr\{f(\theta_0, \lambda_0) \leq \max_{i,\lambda} f(\theta^i, \lambda)\}. \tag{6.39}$$

**Example 6.1**

Simulations are performed to find $p_{\text{failure}}$ defined in (6.39). In the frequency hopping case it is assumed that there are three major interfering cells, while in the fixed frequency case we assume that the interference is dominated by a single interferer. For the three cells in the hopping case, say $i = 1, 2, 3$, it is assumed that

$$\frac{|p(\theta_b^1)|^2}{(r_b^1)^\gamma} = \frac{|p(\theta_b^2)|^2}{(r_b^2)^\gamma} = \frac{|p(\theta_b^3)|^2}{(r_b^2)^\gamma} = P_{\text{I}}, \tag{6.40}$$

where $P_{\text{I}}$ is a constant, independent of $b$. A fourth order Butterworth filter with $-3$dB attenuation at 100kHz is used as receiver filter $\text{pr}(t)$. In the unsynchronized cases the interfering bit streams are random. In the synchronized-frequency hopping case the interfering mobiles randomly selects a training sequence among number $1-7$ in each burst (the training sequences are defined in [GSM94]). In the synchronized-fixed frequency case a fixed training sequence is chosen for the interference. The mean signal to interference is naturally defined as

$$\Gamma^{\text{FH}} = 10\log(G^k) - 10\log(3P_{\text{I}}) \tag{6.41}$$

in the frequency hopping case and

$$\Gamma^{\text{FF}} = 10\log(G^k) - 10\log(G^1), \tag{6.42}$$

in the fixed frequency case, where $\Gamma^{\text{FH}}$ and $\Gamma^{\text{FF}}$ are in dB scale. Note that $\Gamma^{\text{FH}}$ and $\Gamma^{\text{FF}}$ represent the mean uplink signal to interference ratio, averaged over the fast fading and frequency hopping. In Figure 6.1 $p_{\text{failure}}$, is plotted as a function of $\Gamma$. As was discussed in previous section

the probability of selecting a strong interferer rather than the desired user should not exceed 0.1% when the desired user is in DTX mode. From Figure 6.1 we deduce that a minimum (mean) uplink signal to interference ratio of −13dB, −8dB and −4dB are needed in the frequency hopping-unsynchronized (FHU), frequency hopping-synchronized (FHS), and fixed frequency-unsynchronized (FHU) case to achieve the 0.1% target respectively. In the fixed frequency-synchronized case (FFS), a minimum C/I of +0dB,+1dB and +3dB is required if the interfering mobile uses training sequence 0,1 and 2 respectively (the training sequences are defined in [GSM94]). This indicates that the performance of the downlink beam-steering in a cellular system may be optimized by distributing the training sequences among the base stations in an intelligent fashion.

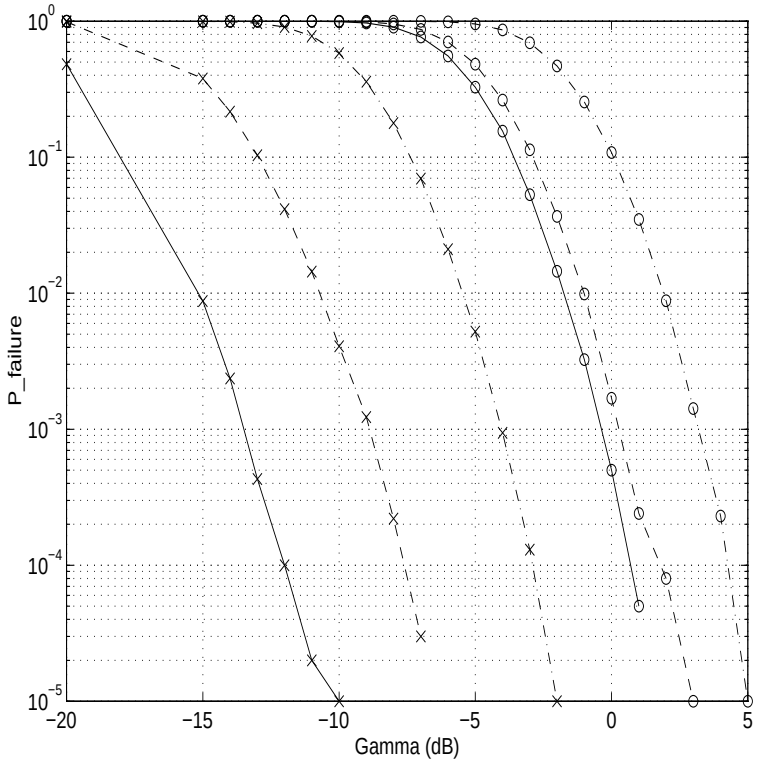


Figure 6.1: *Probability of selecting the direction of an interferer rather than the desired direction.*

—X——X——X— Frequency hopping unsynchronized

– X– – X– – X– Frequency hopping synchronized

- X— - X — - X— Fixed frequency unsynchronized

—O——O——O— Fixed frequency synchronized, interf train seq. 2

– O– – O– – O– Fixed frequency synchronized, interf train seq. 3

- O— - O — - O— Fixed frequency synchronized, interf train seq. 1

(The desired user always uses training sequence 0.)

### 6.2.5 Why Maximize The Desired Power on a Logarithmic Scale ?

In Section 6.2.2 we promised to motivate why the derivations were based on $\tilde{\theta}_0$ defined by (6.23) rather than $\theta_0$ which is defined by (6.21). This is done in this section, under the same propagation assumptions as previous section. If the derivations corresponding to (6.24) to (6.30) are based on $\theta_0$ rather than $\tilde{\theta}_0$, the following criterion function is obtained

$$f_{\text{linear}}(\theta,\lambda) = 10\log(\sum_{b=1}^{B}\frac{1}{B}(\sum_{l=\lambda}^{\lambda+2}|\tilde{\mathbf{a}}^{\text{RX},*}(\theta)\hat{\mathbf{h}}_{l,b}^{\text{RX}}|^2)), \tag{6.43}$$

where the subscript "linear" emphasizes that this estimator attempts to find the direction which maximizes the received desired power in linear scale rather than in logarithmic scale. Let us define the entities $\Delta f^i$ and $\Delta f^i_{\text{linear}}$ as

$$\Delta f^i = f(\theta_0,\lambda_0) - \max_{\lambda}\{f(\theta^i,\lambda)\} \tag{6.44}$$

and

$$\Delta f^i_{\text{linear}} = f_{\text{linear}}(\theta_0,\lambda_0) - \max_{\lambda}\{f_{\text{linear}}(\theta^i,\lambda)\} \tag{6.45}$$

respectively. Obviously $\max_i\{\Delta f^i\} > 0$ and $\max_i\{\Delta f^i_{\text{linear}}\} > 0$ is required for successful estimation (compare with (6.39)) in the two cases. Using the upper bounds of the previous section, and letting $B$ tend to infinity yields

$$\begin{aligned}\lim_{B\to\infty}\Delta f = 10\log(G^k) - 10\log(\frac{|p(\theta_b^i)|^2}{(r_b^i)^\gamma}) \\ - \mathrm{E}\{10\log(\eta)\} - \mathrm{E}\{10\log(L_b^i)\},\end{aligned} \tag{6.46}$$

where $\eta$ is defined by

$$\eta = \sum_{l=\lambda}^{\lambda+2}|\sum_{\tilde{l}}\text{pr}(\tilde{l}T + \Delta T_b^i - T - \tau_b^i)\gamma^i_{l-\tilde{l},b}|^2. \tag{6.47}$$

Using the same bounds in the linear case yields

$$\lim_{B\to\infty}\Delta f^i_{\text{linear}} = 10\log(G^k) - 10\log(\frac{|p(\theta^i_b)|^2}{(r^i_b)^\gamma}) - 10\log(\mathrm{E}\{\eta\}) - 10\log(\mathrm{E}\{L^i_b\}). \quad (6.48)$$

First note that $10\log(G^k) - 10\log(\frac{|p(\theta^i_b)|^2}{(r^i_b)^\gamma})$, is the mean power of the desired user to the mean power from the $i$th cell in logarithmic scale (frequency hopping is assumed and $L^i_b$ is modeled as independent from burst to burst). Since the right-hand sides of (6.46) and (6.48) are deterministic, $p_{\text{failure}}$, defined in (6.39) is either 1 or 0 as $B$ becomes large. The terms $\mathrm{E}\{10\log(\eta)\}$ and $10\log(\mathrm{E}\{\eta\})$ differ by approximately 1dB to the advantage of the logarithmic-scale averaging. A more important difference between (6.46) and (6.48) is in the terms involving $L^i_b$. From the assumptions $\mathrm{E}\{10\log(L^i_b)\} = 0$. However, the corresponding term in the linear case, is given by $10\log(\mathrm{E}\{L^i_b\}) \approx 7.3$dB. In total this gives an advantage of around 8dB using log-scale rather than linear scale averaging. In fixed frequency networks the advantage is very small.

## 6.3 Simulation and Measurement Results

Already the previous section presented some simulation results. However, these results were obtained assuming no angular or temporal spread, no DTX, and assuming at most three interfering cells. In the following sections, more realistic simulation results will be presented. In particular, some simulations are "semi-experimental." By this is meant that the desired signal is obtained by convolving random user data with impulse responses that have been obtained from channel sounding campaigns. The first and second section deal with the simulation assumptions and the performance measures respectively. The simulation and the experimental results are presented in Section 6.3.2.

### 6.3.1 Performance Measures

In the simulations of this section we use the total energy employed when transmitting i.e. $\|\mathbf{w}_k\|^2$ as a measure of the generated interference. However, for this to make sense, the power transmitted to the delivered at the desired mobile must also be taken into account.

Some of the simulations in this section assume that the desired mobile is propagating on the TU or BU model. As mentioned in Section 2.3 and shown in Appendix 2.D.5, the TU and BU models are well approximated by the GAA model using the appropriate parameters. Thus, in simulations using these models the constraint (5.4) can be employed to determine the transmission power, $\|\hat{g}\|^2$. This makes $\frac{1}{\|\mathbf{w}_k\|^2}$ a relevant measure of the factor with which the interference is reduced in comparison with a single antenna (per sector) system, since the energy at the desired mobile is the same as in the case $\mathbf{w} = [1, 0, \ldots, 0]^T$.

When the simulations are made using measured impulse responses (5.4) cannot be applied directly since there are no well defined $\mathbf{R}_{k,k}$ matrix. However, in the spirit of (5.4) it is postulated that the desired energy (averaged over the fast fading) received from the antenna array, should be the same as the energy received using a single antenna in the array. In the single antenna case, the desired energy in burst $b$, is given by

$$\sum_{l \geq 0} \|\mathbf{w}^*_{\text{single}} \mathbf{h}^{\text{TX}}_{l,b}\|^2 \tag{6.49}$$

where $\mathbf{w}^*_{\text{single}} = [1, 0, \ldots, 0]^T$ if element number one is used, $\mathbf{w}^*_{\text{single}} = [0, 1, \ldots, 0]^T$ if element number two is used, and so on. To get the best estimate of the performance using a single antenna element, we average (6.49) over the antenna elements of the array yielding

$$\sum_{l \geq 0} \|\mathbf{h}^{\text{TX}}_{l,b}\|^2 / m, \tag{6.50}$$

where $m$ is the number of antenna elements. Let $\hat{\theta}_{0,b}$ be the estimate of $\theta_0$ obtained from (6.30) in burst $b$. Then using (6.15) the desired energy received in burst $b$, assuming transmission with all antennas of the array, is given by

$$\sum_{l \geq 0} |(\hat{g}\tilde{\mathbf{a}}^{\text{TX}}(\hat{\theta}_{k,b}))^* \mathbf{h}^{\text{TX}}_{l,b}|^2. \tag{6.51}$$

The desired energy (averaged over the fast fading) received from the antenna array should be the same as the energy received using a single antenna in the array. Using (6.50) and (6.51) this may be formulated mathematically as

$$\sum_{b=b_0}^{b_0+\Delta b-1}\sum_{l\geq 0}|(\hat{g}\tilde{\mathbf{a}}^{\mathrm{TX}}(\hat{\theta}_{k,b}))^*\mathbf{h}_{l,b}^{\mathrm{TX}}|^2=\sum_{b=b_0}^{b_0+\Delta b-1}\sum_{l\geq 0}\|\mathbf{h}_{l,b}^{\mathrm{TX}}\|^2/m, \qquad (6.52)$$

where $\Delta b$ should be chosen large enough to eliminate the fast fading. In the simulations the desired mobile runs along some route. This route is divided into sections of $\Delta b = 8$ bursts, for which the constant $|\hat{g}|^2$ is determined from (6.52). With this restriction it may be anticipated that the interference transmitted by the $k$th base is reduced with a factor $\frac{1}{\|\hat{\mathbf{w}}_k\|^2}=\frac{1}{|\hat{g}|^2}$. The determination of $|\hat{g}|^2$ using (6.52) or (5.4) requires an exact knowledge of desired users channel. This is the case in the simulations but not in practice. However, as have been mentioned earlier, our experience is that the constraint (5.4) or its counterpart for general channels (6.52), is not important for the overall system performance. However the restriction (6.52) serves to make $\frac{1}{\|\hat{\mathbf{w}}_k\|^2}=\frac{1}{|\hat{g}|^2}$ a relevant measure of the interference reduction, achieved by the antenna array. This is the primary reason for employing it in these investigations. The obtained $|\hat{g}|^2$ estimates along the route are averaged according to

$$\bar{g}^2=\frac{1}{N}\sum_{n}^{N}|\hat{g}_n|^2, \qquad (6.53)$$

where $|\hat{g_n}|^2$ is the estimate obtained in the $n$th section (consisting of $\Delta b = 8$ bursts) and $N$ is the number of sections. Thus $\frac{1}{\bar{g}^2}$ is the factor with which the interference is reduced on average, if all mobiles in the cell are allocated along the simulated/measured route.

From a network perspective the beam steering yields an on-off effect on the interference: on if the interfering base stations beam is directed towards the considered mobile and off otherwise. This means that the effect of introducing the antenna array will be similar to a reduction of the load (fraction of number of channels used to the number of channels available) in the system with a factor $\frac{1}{\bar{g}^2}$.

In some cases it is illustrative to look at the performance improvement, $PI_{k,i}$, at a certain mobile say the $i$th mobile, by employing the MDP beam former at base $k$. Such an improvement is estimated as

$$PI_{k,i}=\frac{\sum_{b=b_0}^{b_0+\Delta b-1}\sum_{l\geq 0}|(\hat{g}\mathbf{a}^{\mathrm{TX}}(\hat{\theta}_{k,b}))^*\mathbf{h}_{l,b}^{\mathrm{TX},i}|^2}{\sum_{b=b_0}^{b_0+\Delta b-1}\sum_{l\geq 0}\|\mathbf{h}_{l,b}^{\mathrm{TX},i}\|^2/m}, \qquad (6.54)$$

for each section, where $\hat{g}$ and $\hat{\theta}_{k,b}$ are estimated as described above.

### 6.3.2 Simulations

**Example 6.2**

Simulations are performed as described in Appendix 6.A. This means that a network based on $K = 1$, $S = 3$ cell planning is simulated, see Section 3.1.1, from the viewpoint of one base station. This base station employs an eight element linear array of sector elements. The site to site distance is 3km, and nine interferers are modeled in the uplink. In Figure 6.2 results using the TU model described in Section 2.3, are shown. As mentioned in Section 2.4, the energy distribution in azimuth is approximately Gaussian with standard deviation 5 degrees in this model. The desired mobile is assumed to be in DTX mode during the whole simulation. The network is synchronized and employs frequency hopping. The user activity factor is 0.5. The base to mobile distance is 2km, and the mobile speed is approximately 30km/h. The upper plot show an estimate of the performance improvement (as defined in (6.54)) at the downlink co-channel user in cell 1 (a cell in front of the considered base). The middle plot shows the azimuth position of the desired and interfering mobile and the estimated transmit direction $\hat{\theta}_0$. The lower plot shows an estimate of the uplink mean signal to interference ratio during the $B = 21$ consecutive active bursts in a block of 104 bursts. The mean interference reduction i.e. $1/(\bar{g}^2)$. (defined in 6.53) is estimated to be 8.3dB.

**Example 6.3**

Simulations are performed as described in Example 6.2, using the TU and BU propagation models for the desired user, and a mobile speed of approximately 30km/h. The mean interference reduction i.e. $1/(\bar{g}^2)$ is estimated using the GAA approximation as described in Section 6.3.1 above. The generalized-SICR beamformer weights are also calculated using (5.10), and the GAA approximation of the TU and BU models, Section 2.4 (assuming perfect estimation of the $\mathbf{R}_{k,k}$ matrix. The interference reduction is estimated for the MDP as well as the generalized SICR-beamformer (in its RCS-WON form). The average performance improvement $1/(\bar{g}^2)$ defined by (6.53) for sections with certain mean uplink C/I ranges, is listed in Tables 6.1 - 6.6, below.

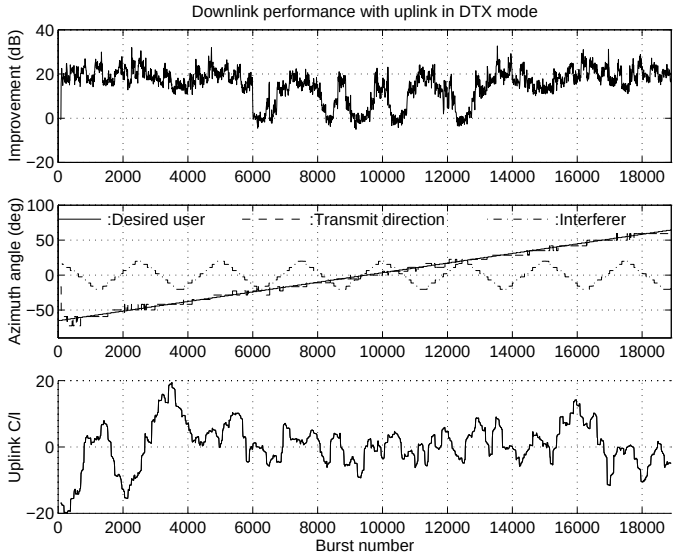


Figure 6.2: *Simulation of proposed algorithm on a TU model*

The performance obtained using the MDP beamformer is listed under "Actual". The performance of the generalized SICR beamformer minus the performance of the MDP beamformer is listed under "Loss." From the tables it is deduced that the MDP beamformer generates less than 0.9dB more interference, than the generalized SICR beamformer, provided that the uplink (mean) C/I is better than −8dB,−8dB,0dB and −6 dB in the frequency hopping-synchronized (FHS), fixed frequency hopping-unsynchronized (FHU), fixed frequency-unsynchronized (FFU) and fixed frequency-synchronized (FFS) cases respectively.

---

**Example 6.4**

Simulations are performed as described in Appendix 6.A. However, this time desired signal is propagating on impulse responses obtained from measurements collected in the city center of Aalborg[7]. Some details of the measurement environment and equipment are described in Section 7.1.

[7]The measurements were made by Aalborg University within the framework of TSUNAMI(II).

The measurements are divided into four routes. In route 0, the mobile is approximately at broadside at a 2.5km distance. In route 1, the mobile drives from $\theta = +30$ to $\theta = -100$ degrees, at a 2.5km distance. In route 2, the mobile drives away from the base starting at a 300 meter distance, and ending at a 1200 meter distance, all at approximately $\theta = -40$ degrees. In route 3 finally, the base starts at a 200 meter distance, and stops at 4km. The angle of the start is $\theta = +45$ degrees and of the end $\theta = 0$ degrees. The mean interference reduction i.e. $\frac{1}{\bar{g}^2}$. (as defined in equation 6.53) is estimated to be 6.2dB, 7.7dB, 7.8dB and 7.6dB in routes 0-3, respectively. No data was discarded. The worst uplink C/I during the simulation was $-8$dB.

## 6.4 Conclusions

A computationally simple downlink beam steering algorithm has been developed. This algorithm steers a beam towards the desired user in the downlink of a GSM/DCS1800/PCS1900 system. There is no attempt to track and avoid transmission towards co-channel users. The algorithm and approach are fully capable of handling multipath scenarios (Example 6.2, 6.3 and 6.4). Compiling the analytical (Section 6.2.4) and simulation results (Section 6.3.2), we conclude that the performance of the proposed algorithm is close to that of the generalized-SICR beamformer (without nulling) provided that the uplink mean C/I (the downlink transmission is based on uplink data) is better than a certain threshold. This threshold is conservatively estimated to be $-8$dB,$-8$dB,$+3$dB and $-2$ dB in the frequency hopping-synchronized (FHS), fixed frequency hopping-unsynchronized (FHU), fixed frequency-unsynchronized (FFU) and fixed frequency-synchronized (FFS) case respectively. The simulations as well as the analytical results also show that the algorithm is capable of reducing the downlink interference level approximately $6 - 8$dB using linear arrays of eight antenna elements per sector (as compared of using a single antenna element per sector).

| C/I (from)-(to) | BU2km,FHS | | BU2km,FHU | |
|---|---|---|---|---|
| | Actual | Loss | Actual | Loss |
| (-∞)-(-10) | 5.9 | 0.057 | 5.9 | 0.057 |
| (-10)-(-8) | 5.8 | 1 | 5.7 | 1.1 |
| (-8)-(-6) | 6.0 | 0.71 | 5.9 | 0.82 |
| (-6)-(-4) | 5.9 | 0.57 | 6.0 | 0.41 |
| (-4)-(-2) | 6.3 | 0.49 | 6.3 | 0.47 |
| (-2)-(0) | 6.6 | 0.5 | 6.6 | 0.49 |
| (0)-(+2) | 6.7 | 0.43 | 6.7 | 0.4 |
| (+2)-(+4) | 6.1 | 0.71 | 6.2 | 0.59 |
| (+4)-(+6) | 7.1 | 0.21 | 7.1 | 0.23 |
| (+6)-(+8) | 7.0 | 0.25 | 7.0 | 0.25 |
| (+8)-(+10) | 7.5 | 0.24 | 7.5 | 0.27 |
| (+10)-(∞) | 7.5 | 0.28 | 7.5 | 0.28 |
| (+4)-(∞) | 7.2 | 0.24 | 7.2 | 0.25 |

Table 6.1: *Comparison of the performance of the generalized-SICR beamformer (without estimation errors) and actually obtained performance using the BU propagation model and 2km base-mobile distance. FHS = frequency hopping-synchronized, FFU = frequency hopping-unsynchronized.*

| C/I (from)-(to) | BU2km,FFS | | BU2km,FFU | |
|---|---|---|---|---|
| | Actual | Loss | Actual | Loss |
| (-∞)-(-10) | -4.5 | 11 | -3.2 | 9.8 |
| (-10)-(-8) | -4.6 | 11 | -2.1 | 8.8 |
| (-8)-(-6) | -3.3 | 9.9 | 1.9 | 4.8 |
| (-6)-(-4) | -0.36 | 7.2 | 6.1 | 0.8 |
| (-4)-(-2) | 4.8 | 2.3 | 6.4 | 0.6 |
| (-2)-(0) | 5.9 | 1.0 | 6.4 | 0.62 |
| (0)-(+2) | 6.3 | 0.51 | 6.3 | 0.61 |
| (+2)-(+4) | 6.7 | 0.57 | 6.7 | 0.49 |
| (+4)-(+6) | 7.2 | 0.25 | 7.2 | 0.21 |
| (+6)-(+8) | 7.3 | 0.24 | 7.0 | 0.38 |
| (+8)-(+10) | 6.6 | 0.65 | 7.4 | 0.28 |
| (+10)-(∞) | 7.5 | 0.29 | 7.5 | 0.31 |

Table 6.2: *Comparison of the performance of the generalized-SICR beamformer (without estimation errors) and actually obtained performance using the BU propagation model and 2km base-mobile distance. FFS = fixed frequency-synchronized, FFU = fixed frequency-unsynchronized.*

| C/I (from)-(to) | TU2km,FHS | | TU2km,FHU | |
|---|---|---|---|---|
| | Actual | Loss | Actual | Loss |
| (-∞)-(-10) | -3.5 | 12 | -2.2 | 11 |
| (-10)-(-8) | 8.1 | 0.16 | 8.1 | 0.28 |
| (-8)-(-6) | 7.9 | 0.25 | 8.0 | 0.17 |
| (-6)-(-4) | 7.8 | 0.26 | 7.6 | 0.41 |
| (-4)-(-2) | 7.7 | 0.29 | 7.6 | 0.40 |
| (-2)-(0) | 7.8 | 0.21 | 7.8 | 0.20 |
| (0)-(+2) | 7.9 | 0.18 | 7.8 | 0.32 |
| (+2)-(+4) | 7.8 | 0.18 | 7.7 | 0.27 |
| (+4)-(+6) | 7.9 | 0.12 | 7.8 | 0.20 |
| (+6)-(+8) | 7.9 | 0.2 | 7.9 | 0.26 |
| (+8)-(+10) | 7.9 | 0.28 | 8.0 | 0.18 |
| (+10)-(∞) | 8.0 | 0.17 | 8.0 | 0.23 |
| (+4)-(∞) | 7.9 | 0.19 | 7.9 | 0.22 |

Table 6.3: *Comparison of the performance of the generalized-SICR beamformer (without estimation errors) and actually obtained performance using the TU propagation model and 2km base-mobile distance. FHS = frequency hopping-synchronized, FHU = frequency hopping-unsynchronized .*

| C/I (from)-(to) | TU2km,FFS | | TU2km,FFU | |
|---|---|---|---|---|
| | Actual | Loss | Actual | Loss |
| $(-\infty)$-(-10) | -10 | 19 | -7.5 | 16 |
| (-10)-(-8) | -3.8 | 12.0 | -5.6 | 14 |
| (-8)-(-6) | -3.3 | 11.0 | -2.6 | 11 |
| (-6)-(-4) | -0.69 | 8.7 | 2.8 | 5.2 |
| (-4)-(-2) | 7.3 | 0.81 | 5.8 | 2.1 |
| (-2)-(0) | 7.6 | 0.38 | 7.7 | 0.37 |
| (0)-(+2) | 7.7 | 0.32 | 7.8 | 0.3 |
| (+2)-(+4) | 7.6 | 0.42 | 7.9 | 0.24 |
| (+4)-(+6) | 8.0 | 0.13 | 7.8 | 0.28 |
| (+6)-(+8) | 7.9 | 0.27 | 8.0 | 0.19 |
| (+8)-(+10) | 8.0 | 0.083 | 7.9 | 0.22 |
| (+10)-$(\infty)$ | 7.9 | 0.29 | 8.1 | 0.17 |

Table 6.4: *Comparison of the performance of the generalized-SICR beamformer (without estimation errors) and actually obtained performance using the TU propagation model and 2km base-mobile distance. FFS = fixed frequency-synchronized, FFU = fixed frequency-unsynchronized.*

| C/I (from)-(to) | TU1km,FHS | | TU1km,FHU | |
|---|---|---|---|---|
| | Actual | Loss | Actual | Loss |
| (-∞)-(-10) | 5.6 | 0.37 | 5.7 | 0.23 |
| (-10)-(-8) | 6.5 | 0.25 | 6.3 | 0.31 |
| (-8)-(-6) | 5.8 | 0.35 | 5.9 | 0.35 |
| (-6)-(-4) | 6.4 | 0.31 | 6.4 | 0.31 |
| (-4)-(-2) | 6.4 | 0.39 | 6.4 | 0.43 |
| (-2)-(0) | 6.5 | 0.49 | 6.6 | 0.45 |
| (0)-(+2) | 6.1 | 0.41 | 6.2 | 0.32 |
| (+2)-(+4) | 6.0 | 0.60 | 6.0 | 0.59 |
| (+4)-(+6) | 5.8 | 0.63 | 5.8 | 0.59 |
| (+6)-(+8) | 5.9 | 0.28 | 5.9 | 0.29 |
| (+8)-(+10) | 6.6 | 0.19 | 6.2 | 0.43 |
| (+10)-(∞) | 6.2 | 0.50 | 6.2 | 0.49 |
| (+4)-(∞) | 6.0 | 0.45 | 6.0 | 0.45 |

Table 6.5: *Comparison of the performance of the generalized-SICR beamformer (without estimation errors) and actually obtained performance using the TU propagation model and 1km base-mobile distance. FHS = frequency hopping-synchronized, FHU = frequency hopping-unsynchronized.*

| | TU1km,FFS | | TU1km,FFU | |
|---|---|---|---|---|
| C/I (from)-(to) | Actual | Loss | Actual | Loss |
| $(-\infty)$-(-10) | -8.5 | 16 | -8.1 | 15.0 |
| (-10)-(-8) | -6.3 | 14 | -8.4 | 15.0 |
| (-8)-(-6) | -6.2 | 14 | -6.0 | 13.0 |
| (-6)-(-4) | -3.2 | 11 | -2.1 | 8.8 |
| (-4)-(-2) | -1.1 | 8.6 | 1.1 | 5.4 |
| (-2)-(0) | 6.9 | 0.46 | 6.2 | 0.41 |
| (0)-(+2) | 6.7 | 0.76 | 6.2 | 0.39 |
| (+2)-(+4) | 6.7 | 0.56 | 5.9 | 0.34 |
| (+4)-(+6) | 7.0 | 0.28 | 6.1 | 0.24 |
| (+6)-(+8) | 7.3 | 0.38 | 6.2 | 0.34 |
| (+8)-(+10) | 7.2 | 0.62 | 6.9 | 0.27 |
| (+10)-$(\infty)$ | 7.1 | 0.21 | 6.1 | 0.25 |

Table 6.6: *Comparison of the performance of the generalized-SICR beamformer (without estimation errors) and actually obtained performance using the TU propagation model and 1km base-mobile distance. FFS = fixed frequency-synchronized, FFU = fixed frequency-unsynchronized.*

# Appendix 6.A Simulations Using the "Beamlink" Package

This section describes the "Beamlink" software for simulation of base station antenna array systems, in particular GSM based. This package is employed in the detailed simulations of the MDP beamformer in this chapter. The appendix is divided into two sections. Section 6.A.1 describes the software package and the possibilities that it offers while Section 6.A.2 describes the configuration of Beamlink when it is employed in this chapter.

## 6.A.1 In General

The developed simulator is implemented such that it can be reconfigured to accommodate different transmission formats, cellular geometries, propagation models, and measured impulse responses.

As input to the simulator the geometry of a considered and a number of co-channel cells is specified. It is assumed that all channels can

be considered fixed for the duration of a burst (approximately 0.5ms in GSM). An impulse responses *file* is assigned to each cell. An impulse response file consists of a list of mobile positions (distance and angle with respect to a base) and multidimensional impulse responses from the single mobile antenna to the multiple base antennas i.e. $\mathbf{h}_l^{\mathrm{RX}}$, $l = 1, 2, \ldots$ in the framework of Chapter 2. There may also be a downlink impulse response, $\mathbf{h}_l^{\mathrm{RX}}$,$l = 1, 2, \ldots$ associated with each position. The impulse responses associated with a cell are defined as the impulse responses with positions within that cells geometrical area.

Beamlink runs a main loop where for each revolution it: reads the impulse response of the desired and interfering users, convolves with correctly formatted bit streams, adds the signals and noise, applied algorithms and saves performance results. Each burst is processed using an uplink combining and downlink beam steering algorithm. The performance of the uplink combining algorithm is obtained by estimating the instantaneous carrier to interference ratio off the combined signal and post-processes that information using the look-up tables of [WM96]. The downlink beam steering uses the uplink signals as input and produces a vector of transmission weights, $\mathbf{w}$ (see Section 2.1.2). Beamlink logs the downlink performance by calculating the power delivered at the desired and co-channel mobiles. In order to do this, the downlink impulse response to these mobiles are needed. If the impulse response files doesn't contain any downlink impulse responses the uplink impulse responses are used *but with a displacement in mobile position of a couple of wavelengths.* The justification for this procedure is given in Section 6.A.1.1 below. The downlink performance using transmision with just a single element in the array, is also logged in order to enable comparison. The impulse response files are produced either by propagation models or by measurements, see Appendix 2.C.3 and Section 7.1 respectively. Since the scaling of impulse responses may be incompatible, Beamlink starts by estimating the path loss slope and scaling of each file. The impulse responses are then forced to the same scaling and path-loss slope according to the method described in Appendix 2.E. The simulator also estimates the average signal strength for sections of a few wavelengths. Thus an estimate of the mean signal strength averaged over the fast fading (see Section 2.1) is available for each burst. This makes it simple to generate FER versus mean signal to interference rate curves, using the output of Beamlink. The signal strength is also utilized when the noise is added.

The noise level is specified by the Eb/N0 quotient, where Eb is the energy per bit averaged over fast fading and N0 is the spectrum density

of the flat noise spectrum. Thus the noise level follows the slow fading.

The simulator is capable of simulating (slow) random frequency hopping as follows: The interfering co-channel user positions are drawn throughout the whole interfering cell, in each burst. If the impulse response file for the desired user is generated (or measured) with frequency hopping then its impulse response file is read sequentially. Otherwise it is read with some random dithering around the nominal position in order to emulate frequency hopping. In the downlink, the performance is measured in terms of reduction of emitted interference compared with transmission using a single antenna element. The downlink beamforming approach of this Chapter, does not track and "null" in the direction of interfering users in other cells, see Chapter 3. Thus the uplink and downlink position of the co-channel users in other cells need not coincide. Thus when the frequency hopping option is selected, it is actually applied only in uplink and not in downlink. This enables the downlink interference level at a co-channel user at a co-channel user to be logged burst by burst. Furthermore, the fast fading is easily removed by averaging the signal strength over consequtive bursts. In order to simulate approaches with nulling such as the SSFR and RCS-WIN approaches introduced in Chapter 3, some reprogramming of Beamlink is necessary.

In the frequency hopping case the interfering users are in DTX mode with probability 50%, whereas with fixed frequency they are always active. DTX mode means that the user is silent and the mobile therefore only uses 12 out of 104 bursts (in GSM). The DTX feature is modeled in the frequency hopping case by multiplying the interfering users with a factor $\eta$ where $\Pr\{\eta = 0\} = \Pr\{\eta = 1\} = 0.5$. This factor is randomized independently from mobile to mobile and burst to burst. The desired user is either in DTX mode or active during all the simulation.

When fixed frequency is employed, all impulse response files are read sequentially, and DTX is not modelled for the interfering user.

Beamlink is capable of simulating TDMA systems with unsynchronized TDMA frames. This is made by using two co-channel users per interfering cell when generated one time-slot for the desired user. The two time-slots arrive contiguously in time with the transition in accordance with the frame-offset between the two cells. When a synchronized network is considered only one user per cell is modeled. However, the timing of that user takes the propagation delay and time-advancing into account, [MP92].

#### 6.A.1.1 Emulation of Downlink Using Uplink

If downlink impulse responses are not available it is assumed that

$$\mathbf{a}^{\mathrm{RX}}(\theta, f^{\mathrm{RX}}) = \mathbf{a}^{\mathrm{TX}}(\theta, f^{\mathrm{TX}}). \tag{6.55}$$

This is the case if two separate antenna arrays are employed for up and downlink and these arrays have the same geometrical configuration but with scaling according to their respective wavelength. Then $\mathbf{R}^{\mathrm{RX}} = \mathbf{R}^{\mathrm{TX}}$ from (2.20) assuming the GWSSUS model. If $\tau_k^{\mathrm{RX}} = \tau_k^{\mathrm{TX}}$ then from (2.11) the statistical distribution of the up and downlink channels are the same. However if $\tau_k^{\mathrm{RX}} \neq \tau_k^{\mathrm{TX}}$ all important statistical properties are still the same. Thus under these assumptions, a sample of the uplink channel can also be seen as a sample of the downlink channel. However, since a FDD system is assumed, the up and downlink channels are uncorrelated and therefore independent, see Section 2.5. Thus if sample $p$ is used as uplink channel in a certain burst, sample $p - d$ of the uplink channel may be used to emulate the downlink channel in burst where $d$ should be chosen large enough for the gain and position of the effective scatters to be considered constant, see Chapter 2. In the simulations a separation of two wavelengths is employed.

### 6.A.2 Configuration of Beamlink in this Thesis

All simulations using Beamlink in this Thesis are based on a $K = 1, S = 3$ frequency allocation, see Section 3.1.1. This geometry is illustrated in Figure 6.3 below, using slightly different sector shapes than in Section 3.1.1. The symbol 'o' in Figure 6.3 represents the location of the base stations, and the dotted lines illustrate the shape of the co-channel sectors. The "considered" base is labeled "0" in the figure. The site to site distance is 3km. The burst formats and frequencies are those of DCS1800, [MP92]. All channels and all time slots are utilized i.e. the network is fully loaded. A fourth order Butterworth filter with 100khz cut-off frequency is applied as receiver filter. All interfering mobiles are generated using the TU model introduced in Section 2.4. The speed of all interfering mobile is 30km/h, thus the distance traveled between two consecutive bursts is 0.04 meter. The impulse responses for the desired user are either generated using the TU or BU (see Section 2.4) propagation model or obtained from the measurements described in Section 7.1. The TU and BU impulse response files are generated as described in Section 2.C.3. This implementation assumes that the mobile is moving

circumferentially. Figure 6.3 illustrates how these circumferential routes are used to emulate the different cells using arcs. When a unsynchronized network is simulated, the TDMA frames of the cells are offset as listed in Table 6.7 below as compared with cell 0. As a reference, the length of a TDMA frame in GSM or DCS1800, is 156.25 bits including guard time. Table 6.7 also lists the training sequence employed by the cells. For a definition of the training sequences see [GSM94]. The Eb/N0 value employed in all simulations is 10dB.

The considered base station is assumed to employ two eight element linear arrays to cover a 120 degree sector. One is used in the uplink and the other in downlink. The element spacing is half a wavelength at the respective carrier frequency. The reason for assuming two different arrays is that the available impulse response measurement only consider uplink, see Section 7.1. When generating impulse responses using the TU and BU propagation models the antenna element patterns, $p(\theta, f)$, are assumed to be given by

$$p(\theta, f) = \begin{cases} \sin(\frac{\pi}{2}\cos(\theta)) & \text{when } |\theta| \leq 70^o \\ 10^{0.1(-5-30\frac{|\theta|-70^o}{70})} & \text{when } 70^o < |\theta| \leq 140^o \\ 10^{-3.5} & \text{when } |\theta| > 140^o. \end{cases} \tag{6.56}$$

Thus $\mathbf{a}^{\mathrm{RX}}(\theta, f)$ is given by (2.4) with $p(\theta, f)$ given by (6.56).

| Cell | Number of bits offset with respect to cell 0 in unsynchronized mode. | Training sequence number. |
|---|---|---|
| 0 | 0 | 0 |
| 1 | 114.8 | 1 |
| 2 | 48.8 | 2 |
| 3 | 120.1 | 3 |
| 4 | 136.1 | 4 |
| 5 | 122.5 | 5 |
| 6 | 45.5 | 6 |
| 7 | 108.3 | 5 |
| 8 | 34.0 | 7 |
| 9 | 114.9 | 3 |

Table 6.7: *TDMA frame offsets in unsynchronized mode and the distribution of the training sequences*

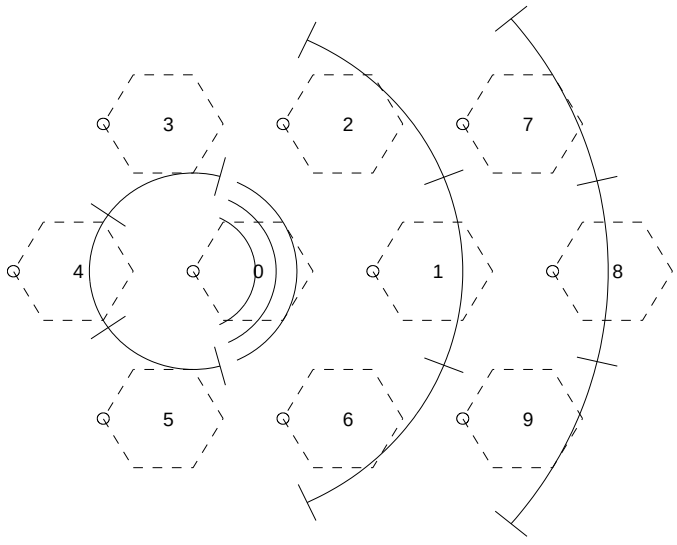


Figure 6.3: *The cellular geometry involved in the simulations.*

# Chapter 7

# Experimental Performance Results

Previous multiple antenna related measurement results presented in the literature, e.g. [AFWP86, Egg95a, Mar96], have focused on describing the propagation in terms of quantitative measures or by estimating model parameters. These characterizations are very useful for algorithm development and understanding of systems. However, they do not provide sufficient information to asses the performance of downlink beam steering with nulling, such as the SICR and generalized-SICR beam formers introduced in Section 3.2.1 and Chapter 5, respectively. Herein, experimental data[1] is used to adapt the model parameters of the GAAO model introduced in Section 2.3.1, such that reasonable performance predictions are obtained from the model. This model assumes that the energy received at the base from a given mobile is Gaussian distributed in azimuth, with mean in the direction of the mobile, and a standard deviation which is a function of base-mobile distance.

In this chapter, the SICR and the generalized-SICR beamformer, introduced in Section 3.2.1 and Chapter 5 respectively, are applied to the experimental data and to the GAAO model. Under the GAAO model the two beamformers are equivalent, if no errors in the input parameters are assumed. The results show that the *average* nulling performance estimated from the experimental data, agrees well with that predicted

[1]The experimental data were collected by Aalborg University in December 1996, within the framework of the European commission ACTS-TSUNAMI(II) project

using the GAAO model, for the SICR beamformer, if the parameters $\sigma_0 = 6^o$, $r_0 = \infty$ are applied (implies $\sigma = \sigma_0 = 6^o$ at all distances $r$). The average performance of the generalized-SICR beamformer is significantly higher, and corresponds to $\sigma_0 = 3^0$, $r_0 = \infty$. In both cases, the performance deviates substantially from that predicted by the model, in particular cases. The influence of these deviation on the system simulations such as those in Chapter 4, has to be evaluated in the future (see "Semi-experimental simulations" in Section 8.2). However, the results show that $\sigma_0 = 3^o$ to $6^o$, $r_0 = \infty$ is a realistic model, and that there is good hope that the performance predicted in Chapter 4, using these parameters, can be obtained in reality using techniques such as the SICR and generalized-SICR beamformer. The chapter is organized as follows: Section 7.1 describes the measurements in terms of the environment and equipment. Section 7.2 describes how the SICR and generalized-SICR beamformers are implemented, and defines several nulling performance estimates. The defined performance estimates are applied to the measured data in Section 7.3. Finally conclusions are drawn in Section 7.4.

## 7.1 Experimental Setup

The measurements were performed in downtown Aalborg city, a typical European city characterized by an irregular street layout and mostly 3-5 story buildings with only a few higher buildings. The base station antenna array was installed on a 41 meter high roof of a power plant. The base antenna consists of an ten by four planar array of vertically polarized dipole elements, in front of a ground plane. The four vertical elements are passively combined to achieve high elevation gain. The eight inner columns are connected to the receiver chains, while the outermost columns are passively loaded. The array is assumed to be an ideal linear array in the processing i.e., $\mathbf{a}(\theta, f)$ is given by (2.4), where $\theta$ is with reference to broadside, see Figure 2.2. The measurements are divided into four routes. In route 0, the mobile is approximately at broadside at a 2.5km distance. In route 1, the mobile drives from $\theta = +30$ to $\theta = -100$ degrees, at a 2.5km distance. In route 2, the mobile drives away from the base starting at 300 meter distance, and ending at a 1200meter distance, all at approximately $\theta = -40$ degrees. In route 3 finally, mobile starts at a 200 meter distance, and stops at 4km. The angle in the start is $\theta = +45$ degrees and in the stop $\theta = 0$ degrees.

The total distance traveled by the mobile during the experiments is

approximately 13km. The uplink channel impulse response is estimated repeatedly during the measurements with a distance of 0.051 meters between consecutive estimates. The channel impulse responses includes the effect of the receiver filters and the modulation pulse shape and extends over ten bits. The receiver filter employed is a fourth-order Butterworth filter with 3dB bandwidth at 100kHz. The sampling frequency is four times the bit-rate. However since the framework of Chapter 2, assumes sampling at bit-rate, the data is decimated by a factor of four before further analysis. Since the bit-rate is close to the Nyquist sampling-rate, very little information is lost in the decimation process. In the framework of Chapter 2, the thus obtained entity is $\mathbf{h}_l$ for, say, $l = l_0, \ldots, l_0 + 9$.

The mobile is transmitting signals with the modulation, frequency and TDMA structure of the DCS-1800 uplink, [MP92]. Five types of TDMA frames are transmitted: pseudo-random bit sequence, traffic, synchronization, calibration, and frequency correction. The synchronization and frequency correction bursts are inserted to enable the base to find the timing and frequency of the mobile. The pseudo-random bit sequence consists of 63 pre-defined bits which are employed to enable the base to form a highly accurate estimate of the channel. In the calibration burst the mobile is silent and a calibration tone is injected in each receiver branch in order to estimate and compensate for the phase, gain, and bias of each receiver branch including cables.

The mobile is equipped with a GPS positioning system (without differential correction), and continuously transmits its position to the base. Thus the mobile position is considered known. The base uses eight parallel receivers i.e., $m = 8$ in the framework of Chapter 2. Each receiver is physically separated into a mast and base unit. The mast unit is placed near the antenna array. The signals are down-converted to 300MHz in the mast unit. A four to one RF-switch is inserted before each front end filter. During the measurements the RF-switch is employed to switch between the antenna array outputs and a calibration signal.

## 7.2 Analysis Method

The statistic

$$\hat{\mathbf{v}}_b = \sum_{l=0}^{9} \hat{\mathbf{h}}_{l,b}, \tag{7.1}$$

is estimated for each estimated impulse response where $\hat{\mathbf{h}}_{l,b}$ denotes the estimate of the $l$th tap in the $b$th bursts. Propagation according to the GWSSUS model introduced in Section 2.2 is assumed. Note that this model does not impose any restrictions on the spatial properties of the propagation. If the transmitted signal is narrow-band a single cluster of scatters i.e., $d = 1$, is sufficient in the GWSSUS model. The estimate $\hat{\mathbf{v}}_b$ is seen as an estimate of the effective steering vector in the $b$th burst, for the case that a narrow-band signal (with the same center frequency as the actual signal) had been applied. Thus in a sense, the bandwidth is reduced, and therefore some spatio-temporal information is lost. However, our goal is to characterize the spatial propagation characteristics only. The measured routes are divided into consecutive sections of fifty bursts extending over two and a half meters of mobile motion. On the $i$th route, the multipath covariance matrix estimate , $\hat{\mathbf{R}}_s^i$ of the $s$th section is defined as

$$\hat{\mathbf{R}}_s^i = \sum_{b \in \{\text{the bursts of the } s\text{th section of the } i\text{th route}\}} \mathbf{v}_b \mathbf{v}_b^*. \tag{7.2}$$

From each section a GAA $d = 1$ model is adapted. More precisely, the $\hat{\mathbf{R}}_s^i$ matrix is used as input to the weighted least squares method in [TO96]. This method produces an estimate of the mean angel, $\hat{\theta}_s^i$, angular spreading, $\hat{\sigma}^i$, and power $\hat{G}_s^i$ of the cluster (a noise variance estimate is also obtained but that is not used). These estimates can be seen as an approximation of $\hat{\mathbf{R}}_s^i$ namely

$$\hat{\mathbf{R}}_s^i \approx \hat{G}_s^i \mathbf{R}(\hat{\theta}_s^i, \hat{\sigma}_s^i), \tag{7.3}$$

where the complex-matrix valued function $\mathbf{R}(\theta, \sigma)$ is defined in (2.33-2.34). In order to estimate the "error" in the model implied by $\hat{\theta}_s^i, \hat{\sigma}_s^i$ the performance of the SICR beamformer introduced in Section 3.2.1 is investigated (this beamformer assumes a GAA, $d = 1$ model). The performance is assessed as follows: The $\hat{\theta}_s^0$ and $\hat{\sigma}_s^0$ estimates obtained on route 0, are used as the mean angle and angular spread for a desired user . The parameters of an identified interfered user are taken from one of the remaining routes i.e., $i = 1, 2, 3$ (other combinations have also been tried, e.g the third route for the desired user, however the results are similar to those below). The SICR beamformer is applied in its SSFR version described in Section 3.3.1.2. This means that the matrix $\mathbf{M}$ defined in (3.13), is given by

$$\mathbf{M} = \mathbf{R}(\hat{\theta}_s^i, \hat{\sigma}_s^i) + 1.3161\mathbf{I}, \tag{7.4}$$

where $i = 1, 2$ or 3. Thus using the $s$th section for the desired and interfering user a weighting vector $\hat{\mathbf{w}}_s$ is obtained. In order to investigate the performance of the obtained weighting vectors, the power at the desired and interfering mobile in section $s$ is estimated as

$$\widehat{\mathrm{PD}}_s = \hat{\mathbf{w}}_{s-1}^* \hat{\mathbf{R}}_s^0 \hat{\mathbf{w}}_{s-1}, \tag{7.5}$$

and

$$\widehat{\mathrm{PI}}_s = \hat{\mathbf{w}}_{s-1}^* \hat{\mathbf{R}}_s^i \hat{\mathbf{w}}_{s-1} \tag{7.6}$$

respectively. Note that the "one section old" weighting vector estimates are applied. This is because, unlike the uplink, the downlink beamforming vectors must be based on past data. Note that although the $\hat{\mathbf{w}}_{s-1}$ vectors are based on the GAA $d = 1$ model, the estimates in (7.6) and (7.5) are not, since they apply unstructured estimates of the desired and interfering mobile multipath covariance matrices. The performance estimate of the obtained beamforming weights, $\widehat{\mathrm{PE}}_s$ is defined as

$$\widehat{\mathrm{PE}}_s = \frac{\widehat{\mathrm{PD}}_s}{\widehat{\mathrm{PI}}_s} \tag{7.7}$$

$$= \frac{\hat{\mathbf{w}}_{s-1}^* \hat{\mathbf{R}}_s^0 \hat{\mathbf{w}}_{s-1}}{\hat{\mathbf{w}}_{s-1}^* \hat{\mathbf{R}}_s^i \hat{\mathbf{w}}_{s-1}}. \tag{7.8}$$

In order to obtain an estimate of the nulling performance, normalization of $\widehat{\mathrm{PE}}_s$ with respect to the performance using a single antenna is desirable. The single antenna performance is derived as follows: Consider transmission using $\hat{\mathbf{w}}_k = [1, 0, \ldots, 0]^T$. Then from (7.8) the $\widehat{\mathrm{PE}}_s$ is given by $[\hat{\mathbf{R}}_s^0]_{1,1}/[\hat{\mathbf{R}}_s^i]_{1,1}$ while if $\mathbf{w}_k = [0, 1, \ldots, 0]^T$ it is given by $[\hat{\mathbf{R}}_s^0]_{2,2}/[\hat{\mathbf{R}}_s^i]_{2,2}$ . From this discussion it is clear that an estimate of the performance using transmission with a single element, $\widehat{\mathrm{SEP}}_s$ is obtained as

$$\widehat{\mathrm{SEP}}_s = \frac{\mathrm{Trace}\{\hat{\mathbf{R}}_s^0\}}{\mathrm{Trace}\{\hat{\mathbf{R}}_s^i\}}, \tag{7.9}$$

which, in a sense, is an average over the antenna elements. The nulling performance of the SICR beamformer, may now be defined as

$$\widehat{\mathrm{NP}}_s^{\mathrm{SICR}} = \widehat{\mathrm{PE}}_s(\widehat{\mathrm{SEP}}_s)^{-1} \tag{7.10}$$

Combining (7.8-7.10) yields

$$\widehat{\mathrm{NP}}_s^{\mathrm{SICR}} = \frac{\hat{\mathbf{w}}_{s-1}^* \hat{\mathbf{R}}_s^0 \hat{\mathbf{w}}_{s-1} \mathrm{Trace}\{\hat{\mathbf{R}}_s^i\}}{\hat{\mathbf{w}}_{s-1}^* \hat{\mathbf{R}}_s^i \hat{\mathbf{w}}_{s-1} \mathrm{Trace}\{\hat{\mathbf{R}}_s^0\}}. \tag{7.11}$$

A reasonable measure of the interference reduction factor $\bar{g}^2_{\mathrm{SICR}}$, using the SICR beamformer, is

$$\bar{g}^2_{\mathrm{SICR}} = \mathrm{E}\{(\widehat{\mathrm{NP}}_s^{\mathrm{SICR}})^{-1}\}, \tag{7.12}$$

where the average is over the sections. In order to evaluate the relevance of the model obtained from the parameters $\hat{\theta}_s^0$, $\hat{\sigma}_s^0$ $\hat{\theta}_s^i$ and $\hat{\sigma}_s^i$, a structured nulling performance estimate is defined as

$$\widehat{\mathrm{NP}}_s^{\mathrm{SICR,struct}} = \frac{\hat{\mathbf{w}}_{s-1}^* \mathbf{R}(\hat{\theta}_s^0, \hat{\sigma}_s^0) \hat{\mathbf{w}}_{s-1}}{\hat{\mathbf{w}}_{s-1}^* \mathbf{R}(\hat{\theta}_s^i, \hat{\sigma}_s^i) \hat{\mathbf{w}}_{s-1}}, \tag{7.13}$$

where the word "struct" is shorthand for "structured" and emphasizes that this is the performance obtained if the model implied by the parameters $\hat{\theta}_s^0$, $\hat{\sigma}_s^0$ $\hat{\theta}_s^i$, and $\hat{\sigma}_s^i$ is true. In Chapter 5 a generalized version of the the SICR beamformer is introduced. This beamformer is generalized to the case of arbitrary GWSSUS models. This beamformer is also applied to the data. This is done by using the unstructured multipath covariance matrices $\hat{\mathbf{R}}_{s-1}^0$ and $\hat{\mathbf{R}}_{s-1}^i$ as input to the algorithm. In a real implementation of the algorithm, these matrices may have to be transformed from the receive to the transmit frequency, before being applied in the beamformer. Since the measurements are performed only at a single frequency, this problem is ignored. This can be interpreted as if case 2 in the enumeration in Section 2.5 applies. Thus, the generalized-SICR beamforming vectors $\hat{\tilde{\mathbf{w}}}_{\mathbf{s}}$ are obtained as

$$\hat{\tilde{\mathbf{w}}}_{\mathbf{s}} = \sqrt{\frac{\mathrm{Trace}\{\hat{\mathbf{R}}_{\mathbf{s}}^{\mathbf{0}}\}}{\mathbf{m}\mathbf{e}^* \hat{\mathbf{R}}_{\mathbf{s}}^{\mathbf{i}} \mathbf{e}}}\mathbf{e} \tag{7.14}$$

where $\mathbf{e}$ is the dominant generalized eigenvector associated with the matrix pair

$$(\hat{\mathbf{R}}_s^0, \frac{m}{\mathrm{Trace}\{\hat{\mathbf{R}}_s^i\}} \hat{\mathbf{R}}_s^i + \mathrm{constant} \times \mathbf{I}), \tag{7.15}$$

where again constant = 1.3161 is applied. The nulling performance, and the mean interference reduction factor, of the generalized SICR beamformer is obtained as

$$\widehat{\mathrm{NP}}_s^{\text{gen-SICR}} = \frac{\hat{\tilde{\mathbf{w}}}^*_{\mathbf{s-1}} \hat{\mathbf{R}}^{\mathbf{0}}_{\mathbf{s}} \hat{\tilde{\mathbf{w}}}_{\mathbf{s-1}} \mathrm{Trace}\{\hat{\mathbf{R}}^{\mathbf{i}}_{\mathbf{s}}\}}{\hat{\tilde{\mathbf{w}}}^*_{\mathbf{s-1}} \hat{\mathbf{R}}^{\mathbf{i}}_{\mathbf{s}} \hat{\tilde{\mathbf{w}}}_{\mathbf{s-1}} \mathrm{Trace}\{\hat{\mathbf{R}}^{\mathbf{0}}_{\mathbf{s}}\}}. \tag{7.16}$$

and

$$\bar{g}^2_{\text{gen-SICR}} = \mathrm{E}\{(\widehat{\mathrm{NP}}_s^{\text{gen-SICR}})^{-1}\} \tag{7.17}$$

respectively. In order to compare the nulling performance of the SICR and generalized-SICR beamformer on the real data with the nulling performance implicitly assumed in Chapter 4, the performance of the SICR on the GAAO model of Section 2.3.1 (which is assumed in Chapter 4) is also investigated. The GAAO model is basically a GAA, $d = 1$ model (Gaussian angular spreading, single cluster) with a $\sigma$ which varies with distance as

$$\sigma(r) = \begin{cases} \frac{r_0}{r}\sigma_0, \text{ when } r > r_0 \\ \sigma_0 \text{ when } r < r_0 \end{cases} \tag{7.18}$$

where $\sigma_0$ and $r_0$ are parameters. The nulling performance estimate for the SICR beamformer on this channel is defined by

$$\widehat{\mathrm{NP}}_s^{\text{model}} = \frac{\breve{\mathbf{w}}^*_s \mathbf{R}(\theta^o_s, \sigma(r^0_s))\breve{\mathbf{w}}_s}{\breve{\mathbf{w}}^*_s \mathbf{R}(\theta^i_s, \sigma(r^i_s))\breve{\mathbf{w}}_s}, \tag{7.19}$$

where $r^s_0$ and $r^i_s$ are the distance to the desired and interfering user respectively, and the weighting vector $\breve{\mathbf{w}}_s$ is obtained from the SICR beamformer assuming perfect estimation of the parameters. The angle and distance to the desired and interfered users are obtained from the GPS positioning system. The mean interference reduction using on the model is defined as

$$\bar{g}^2_{\text{model}} = \mathrm{E}\{(\widehat{\mathrm{NP}}_s^{\text{model}})^{-1}\}. \tag{7.20}$$

Note that on the GAAO model, the SICR and generalized-SICR beamformers are equivalent, and therefore the performance estimates (7.19) and (7.20) also pertains to the generalized-SICR beamformer.

In the following, the wording "the $\sigma_0 = 6^o$, $r_0 = \infty$ model" will be used as shorthand for "the GAAO model of Section 2.3.1, using the parameter setting $\sigma_0 = 6^o$, $r_0 = \infty$".

### 7.2.1 Details

A practical problem involved with the calculation of the nulling performance estimates is that the number of sections are different in all routes. This problem is solved by reading route 0, which is for the desired user, from the beginning to the end, and then start from the first section again. The interfering routes are read one after another sequentially. This implies that both the desired and interfering user sometimes make instantaneous jumps of several kilometers. The performance statistics from sections immediately after the jump become irrelevant. These sections are therefore discarded.

The weighted least squares method in [TO96], which is employed to estimate $\hat{\theta}_s^i$ and $\hat{\sigma}_s^i$, is initialized, with respect to $\hat{\theta}_s^i$, using a conventional beamforming method. The criterion function is evaluated on a grid of points, centered around the initial $\hat{\theta}_s^i$ estimate.

## 7.3 Results

**Example 7.1**

**Plots**

In Figures 7.1 the 30%, 50%, and 70% levels of the cumulative distribution function the $\hat{\sigma}_s^i$ estimates obtained using the least squares method of [TO96], are shown as a function of base-mobile distance. The plot was generated in the following way: The $\hat{\sigma}_s^i$ estimates were divided into 14 groups. The $\hat{\sigma}_s^i$ estimates corresponding to sections with base-mobile distances in the range from $300 \times (g-1)$ meter to $300 \times g$ meter, were put in the $g$th group ($g = 1, \ldots, 14$). Then the 30%, 50%, and 70% levels of the cumulative distribution of $\hat{\sigma}_s^i$ is determined, for each group. The obtained levels are plotted in Figure 7.1 where the x-value $300 \times g - 150$ (meter) is used for the $g$th group.

**Observations**

The angular spreading does *not* seem to be decreasing with distance. At a 3km distance, very high levels of angular spreading are obtained. The 50% percentile is typically 6 degrees. This is a *weak* indication that $\sigma_0 = 6^o$, $r_0 = \infty$ is a reasonable model.

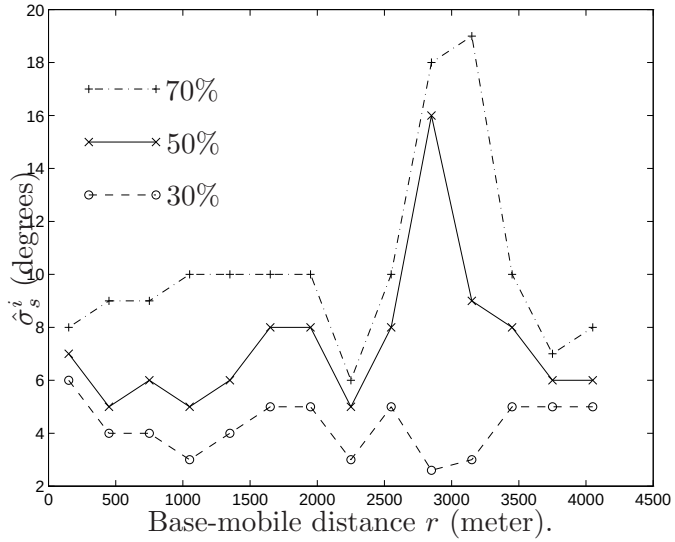


Figure 7.1: *The* 70%, 50% *and* 30% *levels of the cumulative distribution of* $\hat{\sigma}_s$.

**Example 7.2**

In order to do downlink nulling successfully the transmit vector $\mathbf{w}_k$ should be basically orthogonal to the dominant subspace of the multi-path covariance matrix of the nulled user, in this case $\hat{\mathbf{R}}_s^i$. The higher dimension of this subspace, the more difficult the downlink beamforming becomes. Two measures $m_1$ and $m_2$ are introduced to determine the degree to which $\hat{\mathbf{R}}_s^i$, can be approximated by a rank one and a rank two matrix respectively. The measures $m_1$ and $m_2$ are defined by

$$m_1 = \frac{\lambda_1}{\sum_{n=1}^{m} \lambda_n} \tag{7.21}$$

and

$$m_2 = \frac{\lambda_1 + \lambda_2}{\sum_{n=1}^{m} \lambda_n}, \tag{7.22}$$

respectively, where $\lambda_1 \geq \lambda_2, \ldots, \geq, \lambda_m$ are the eigenvalues of the matrix $\hat{\mathbf{R}}_s^i$. If $m_1$ and $m_2$ are close to one $\hat{\mathbf{R}}_s^i$ is well approximated by a a rank one matrix. If $m_2$ is close to one, while $m_2$ is not, a rank-two approximation of $\hat{\mathbf{R}}_s^i$ is appropriate.

**Plots**

The sections are divided into groups as in Example 7.1. The 10%, 50%, and 90% levels of the commutative distribution of the obtained $m_1$ and $m_2$ values for the different groups are plotted in the upper and lower part of Figure 7.2. As a reference, some $m_1$ and $m_2$ values for the matrix, $\mathbf{R}(\theta, \sigma)$ are listed in Table 7.1 below.

**Observations**

The measures $m_1$ and $m_2$ generally do not decrease with distance. Thus downlink nulling does not become easier with increasing distance. A reasonable value for the $r_0$ parameter in the GAAO model is thus $r_0 = \infty$, which implies a distance independent angular spreading. An angular spread, $\sigma_0$, in the range from $\sigma_0 = 3^o$ to $\sigma_0 = 6^o$ seems to be realistic.

| $\theta$ | $\sigma$ | $m_1$ | $m_2$ |
|---|---|---|---|
| $0^o$ | $6^o$ | 0.68 | 0.94 |
| $60^o$ | $6^o$ | 0.88 | 0.9935 |
| $0^o$ | $3^o$ | 0.88 | 0.9935 |
| $60^o$ | $3^o$ | 0.9661 | 0.9995 |

Table 7.1: *The measures of* $m_1$ *and* $m_2$ *applied to the matrix,* $\mathbf{R}(\theta, \sigma)$.

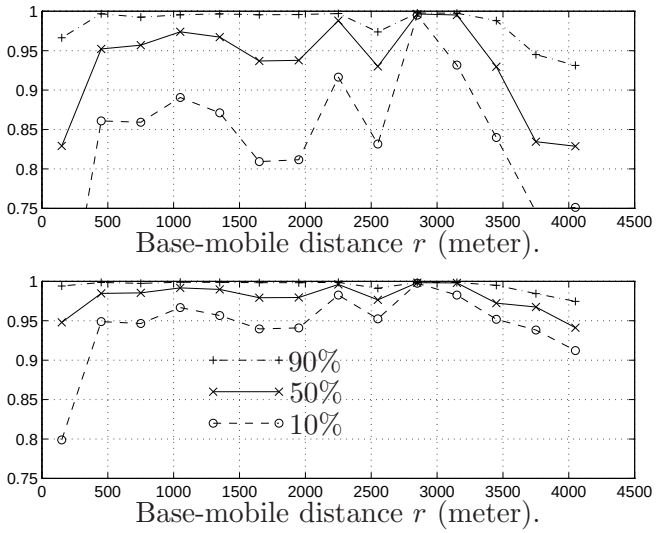


Figure 7.2: *The* 90%, 50% *and* 10% *level of the cumulative distribution of* $m_1$ *upper and* $m_2$ *lower*

**Example 7.3**

**Plots**

The structured and unstructured nulling performance estimates, for the SICR beamformer, corresponding to the same desired and interfering section, are marked with an 'x' in Figure 7.3. The x-axis indicates the structured estimate obtained from (7.13), and the y-axis the unstructured estimate (7.11). The dotted line in the figure shows the line $y = x$. The number of 'x's below the dotted line is 43.5%. The mean and standard deviation of $10\log(\widehat{\mathrm{NP}}_s^{\mathrm{SICR}}) - 10\log(\widehat{\mathrm{NP}}_s^{\mathrm{SICR,struct}})$, is 1.7(dB) and

6.5(dB) respectively. The mean interference reduction factor for SICR beamformer is estimated to be $\bar{g}^2_{\text{SICR}} = 0.1369$ i.e., an improvement of 8.6dB.

In Figure 7.4, a similar plot as Figure 7.3 is shown, with the difference being that the performance of the SICR beamformer using the $\sigma_0 = 6^o$, $r_0 = \infty$ model, defined by (7.19), is on the x-axis. The dotted line in Figure 7.4 is again $y = x$. The number of 'x's below the dotted line is 50.0%. The mean and standard deviation of $10\log 10(\widehat{\text{NP}}_s^{\text{SICR}}) - 10\log(\widehat{\text{NP}}_s^{\text{model}})$, is -0.12dB and 6.6dB respectively. The mean interference reduction factor on the $\sigma_0 = 6^o$ , $r_0 = \infty$ model is estimated to be $\bar{g}^2_{\text{model}} = 0.1328$ i.e., an improvement of 8.8dB.

**Observations** The model obtained through the $\hat{\theta}^i_s$ and $\hat{\sigma}^i_s$ estimates does not predict the performance of the SICR beamformer better that the $\sigma_0 = 6^o$, $r_0 = \infty$ model. Thus the $\hat{\sigma}^i_s$ estimates should not be taken too seriously. The average performance of the SICR beamformer obtained on the real data, and on the $\sigma_0 = 6^o$,$r_0 = \infty$ model are very similar.

---

**Example 7.4**

**Plots**

In Figure 7.5, the performance of the SICR beamformer on the $\sigma_0 = 6^o$,$r_0 = \infty$ model is again on the x-axis. However, the performance of the generalized SICR beamformer estimated using (7.16) is on the y-axis. The dotted line in Figure 7.5 is $y = x$. The number of 'x's below the dotted line is 22.7%. The mean and standard deviation of $10\log(\widehat{\text{NP}}_s^{\text{gen-SICR}}) - 10\log(\widehat{\text{NP}}_s^{\text{model}})$, is 3.8dB and 6.4dB respectively. The interference reduction factor for generalized-SICR beamformer is estimated to be $\bar{g}^2_{\text{gen-SICR}} = 0.0639$ i.e., an improvement of 11.9dB.

**Observations**

The performance of the generalized-SICR beamformer is in the order of 3dB better than the SICR beamformer.

---

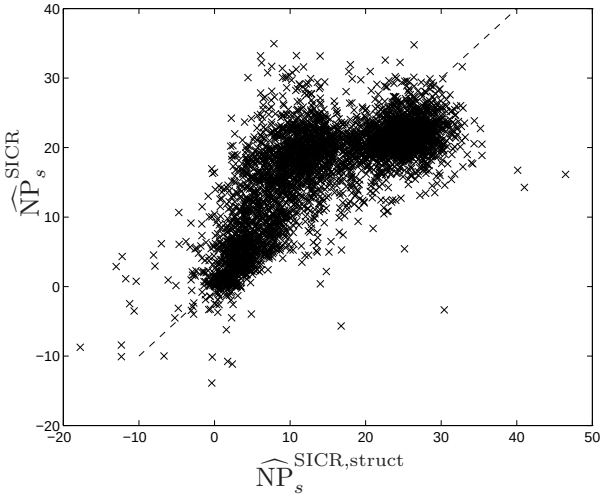


Figure 7.3: *Relationship between the structured and unstructured estimate of the performance of the SICR beamformer.*

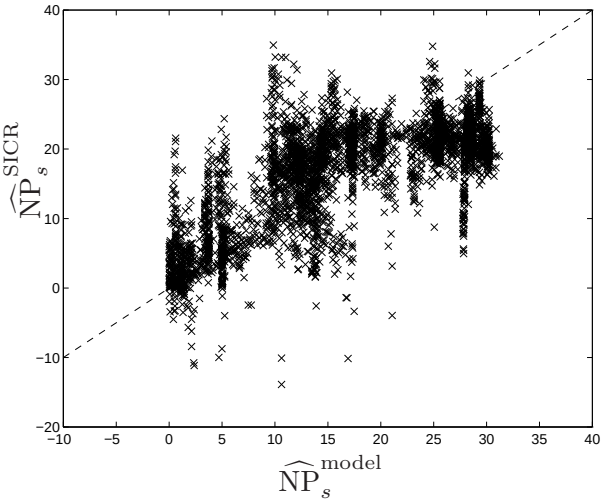


Figure 7.4: *Relationship between the performance of SICR beamformer on the $\sigma = 6^o$,$r_0 = \infty$ model and the actual performance of the SICR beamformer estimated from the data.*

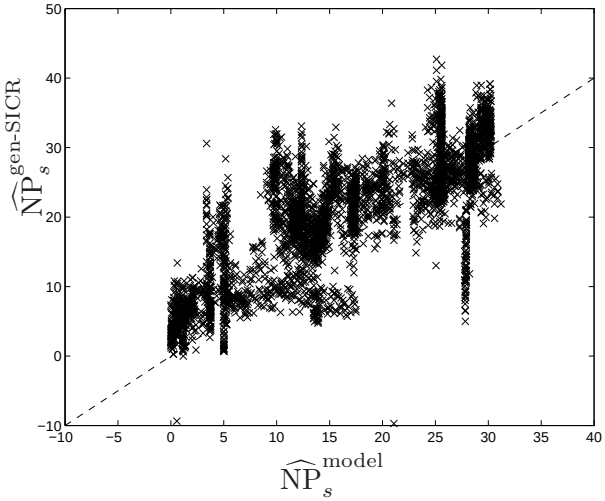


Figure 7.5: *Relationship between the performance of generalized SICR beamformer on the $\sigma = 6^o$,$r_0 = \infty$ model and the actual performance of the SICR beamformer estimated from the data.*

**Example 7.5**

**Plots**

Figure 7.6 is identical to Figure 7.5 except that the model performance obtained using $\sigma_0 = 3^0$, $r_0 = \infty$ is on the x-axis rather than $\sigma_0 = 6^0$, $r_0 = \infty$ as in Figure 7.5. As usual the dotted line in Figure 7.6 is $y = x$. The number of 'x's below the dotted line is 51.0%. The mean and standard deviation of $10\log(\widehat{\mathrm{NP}}_s^{\text{gen-SICR}}) - 10\log(\widehat{\mathrm{NP}}_s^{\text{model}})$, are 0.036dB and 6.1dB respectively. The mean interference reduction factor using the $\sigma_0 = 3^o$ , $r_0 = \infty$ model is estimated to be $\bar{g}^2_{\text{model}} = 0.0866$ i.e., an improvement of 10.6dB.

**Observations**

The average performance of the generalized SICR beamformer on the measured data is similar to that obtained on the $\sigma_0 = 3^o, r_0 = \infty$ model.

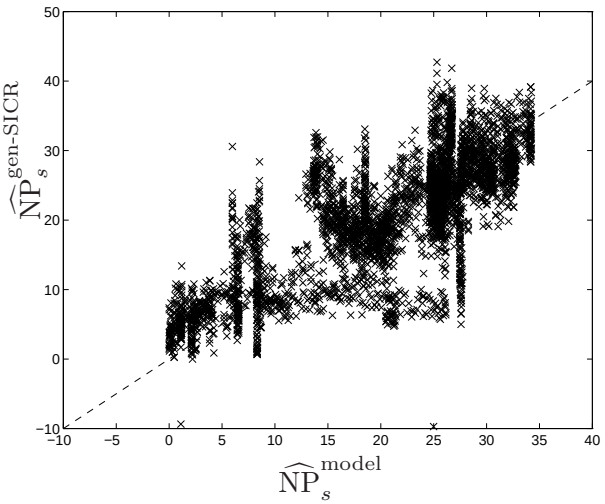


Figure 7.6: *em Relationship between the nulling performance of the generalized SICR beamformer on the* $\sigma = 3^o$,$r_0 = \infty$ *model and the performance estimated from the data.*

## 7.4 Conclusions

In Chapter 3 and 4 the GAAO model was assumed and the SICR beamformer applied. Under the GAAO model, and assuming perfect estimation of the required parameters, the SICR and the generalized-SICR beamformer are identical. Thus the results of Chapter 3 and 4 may be interpreted in two ways : as the performance of the SICR beamformer, or as the performance of the generalized-SICR beamformer. The results of this chapter indicate that $\sigma_0 = 6^0, r_0 = \infty$ is the appropriate parameter setting in the former case and $\sigma_0 = 3^0, r_0 = \infty$, in the latter, for the considered urban macro-cellular environment, see Examples 7.3 and 7.4.

However it should be noted that the translation from the RX to the TX frequency, see Section 2.5, involved in the generalized-SICR beamformer has been ignored in the chapter. This translation will lead to some degradation of the performance of the generalized-SICR beamformer, due to calibration and other errors. The analysis of the SICR beamformer is however influenced by such errors through the parameterization of the multipath covariance matrix using $\theta$ and $\sigma$.

The fact that $\sigma_0 = 3^o$ to $6^o$ with $r_0 = \infty$ is a good model for the

average performance obtained using the measurement results does not prove that the results of Chapter 4, using this parameter setting, are correct, since there are large deviations for particular sections. However, it seems unlikely that these deviations should affect the performance of the RCS based approaches (capacity is increased by increasing the fraction of the available spectrum used in a cell), since the RCS approaches do not apply a channel allocation which attempts to separate the desired and interfering users angular power distribution (as seen from the base). Detailed simulations involving several base stations and mobiles, using a mixture of measured and model-generated signals could be employed to fully assess the influence of the deviations.

The paper [MPLE$^+$97] uses the same data as used here to estimate angular spreads, $\sigma$, ranging from 0 to 5 degrees (fluctuations depending on mobile location). This seems to be consistent with the results for the generalized-SICR beamformer obtained in this chapter. The reason for the much worse performance in the SICR case, could be that small calibration and model errors cause large errors in the $\theta$ and $\sigma$ estimates $(\hat{\theta}_s^i, \hat{\sigma}_s^i)$ employed by the algorithm.

In summary, we conclude that $\sigma_0 = 3^o$ to $6^o$ with $r_0 = \infty$, is a reasonable model for predicting the performance of techniques such as the SICR or generalized-SICR beamformer in urban environments, with elevated base stations.

# Chapter 8

# Thesis Summary and Future Research Issues

## 8.1 Summary

This thesis deals with the problem of increasing the capacity of cellular communication systems by the use of antenna array base stations. Within this field, we have focused on how and how much the downlink capacity can be enhanced in FDD systems with macro-cells In Chapter 1 the following four critical issues, involved in answering these questions were identified

- propagation modeling, i.e., finding a mathematical relation between the signals transmitted and the signals received,
- beamforming, i.e., how the transmitted signals should be distributed over the antenna elements of the array in order to maximize performance,
- channel allocation, i.e., how to distribute the available spectrum among the mobiles in order to maximize the performance gain of the antenna array,
- capacity estimation, i.e., estimating the achieved spectrum efficiency as a function of the number of antennas employed in the arrays, and other critical parameters.

The following list describes the main contributions and conclusions of the chapters of the thesis

**Chapter 2** Five propagation models are derived: Gaussian Wide Sense Stationary Uncorrelated Scattering (GWSSUS), Gaussian Angle of Arrival (GAA), Gaussian Angle of Arrival One Cluster (GAAO), Typical Urban (TU) and Bad Urban (BU).

The GWSSUS model is a generalization of the well-known wideband statistical multipath model [PB82, Pro89] to the multiple antenna case. The GAAO model assumes that all energy received at the base from a certain mobile is Gaussian distributed in azimuth, with a certain (optionally distance dependent) angular spreading $\sigma$. The results of Chapter 7 indicate that such a model yields realistic performance predictions using $\sigma = 3^o$ to $6^o$.

The new model which has almost the same temporal-domain power distribution as the frequently used typical urban model of [GSM92], is introduced i.e., an exponentially decaying power delay profile with an rms-delay spread of $1\mu s$. The azimuthal power distribution of the model is Gaussian with a standard deviation of $\sigma = 10^o/r$ where $r$ is the base to mobile distance in kilometers (as seen from the bases).

**Chapter 3 and 4** Three capacity enhancement approaches are introduced: same sector frequency reuse (SSFR), reduced cluster size without nulling (RCS-WON), and reduced cluster size with nulling (RCS-WIN). The two variants of RCS distinguishes weather nulls are steered in the direction of strong users in adjacent cells or not. A beamformer called SICR is derived from the GAAO model introduced in Section 2.3.1. Channel allocation and uplink power control algorithms to take care of the inter-cell cross-talk and dynamic range problems for the three systems are proposed. The thus systems obtained are referred to as SICR-RCS-WIN, SICR-RCS-WON and SICR-SSFR. The main findings of the chapters are

- A large *uplink* power control range is necessary to make the *downlink* inter-cell nulling feature of the SICR-RCS-WIN system effective.
- The uplink near-far ratio, defined as the ratio of the power of the strongest user to the weakest desired user (averaged over fast fading), allocated to the same timeslot (but sometimes

different carrier), is typically less than 25dB, for all investigated systems. For the SICR-RCS system with $e = 1$ and fast handover, it is typically less than 4dB.

- The SICR-SSFR system requires around 16 channels (per power group and sector) in order to be able to allocate channels with spatially well separated users.
- The SICR-SSFR system increases capacity more than SICR-RCS-WIN and SICR-RCS-WON systems in most of the investigated cases.
- The capacity enhancement achieved using SICR-RCS-WIN is larger than or equal to that obtained using SICR-RCS-WON.
- The experimental results of Chapter 7 suggest that $\sigma_0 = 3^o$ to $6^o$, $r_0 = \infty$ (the framework is introduced in Section 2.3.1) is a realistic model. Combining this information with the results of Chapter 4, yields the following capacity predictions in the more optimistic case $\sigma_0 = 3^o$: Threefold capacity enhancement is achieved using the SICR-RCS-WIN and SICR-RCS-WON systems with three and five antenna elements per 120-degree sector, respectively (in comparison with a reference system employing a single element per 120-degree sector). Four and tenfold capacity enhancement is achieved with SICR-SSFR using five and eighteen antenna elements respectively. Using SICR-RCS-WIN or SICR-SSFR, eight antenna elements per sector, and an improved handover, a ninefold capacity enhancement is obtained. However, it is unclear how much of the ninefold capacity enhancement should be attributed to the improved handover in this case.
- The derived analytical expression for the outage probability agrees well with simulation results in the SICR-SSFR case if sixteen (or more) channels per group are employed, in the SICR-RCS-WIN case if $e = 1$ is employed, and in the SICR-RCS-WON case if slow handover is assumed.

**Chapter 5** In this chapter the beamformer of Chapter 3 is generalized to more general propagation models. The results of Chapter 7 indicate that this generalization improves the interference suppression approximately 3dB (see Examples 7.3 and 7.4). The beamformer introduced herein also forms the starting point for the derivation of the less complex beamformer of Chapter 6.

**Chapter 6** In this chapter a simple beamforming algorithm for implementation of the RCS-WON approach in GSM is proposed. Consideration of approaches without nulling is motivated by their less demanding requirements on channel allocation, power control, synchronization, and hardware. Furthermore, approaches without nulling are generally very robust with respect to angular dispersion and calibration errors.

The simulation results indicate that the proposed technique generates less than 0.9dB more interference than the generalized-SICR algorithm, under some assumptions. In the case of frequency hopping, this result is obtained even at a $-8$dB uplink signal to interference ratio. Simulation results using the TU and BU model, as well as using the data collected in downtown Aalborg (Section 7.1), indicate that the algorithm is capable of reducing the downlink interference level approximately $6-8$dB in urban environments using linear arrays of eight antenna elements per sector (as compared to using a single antenna element per sector).

**Chapter 7** The nulling performance of the SICR and generalized-SICR beamformers, are estimated by applying them to data measured in a macro-cellular environment. The parameters needed in the SICR beamformer are estimated using the least-squares algorithm introduced in [TO96], while the input matrices needed in the generalized-SICR algorithm are estimated directly from the data. It is concluded that the angular dispersion is basically independent of the base-mobile distance in the available data. The performance of the SICR and generalized-SICR beamformer is estimated from the measurement data and compared with that obtained from the GAAO model introduced in Section 2.3.1. It is found that average performance of the SICR and generalized-SICR beamformer is close to that obtained on the on the GAAO model using $\sigma_0 = 6^o$,$r_0 = \infty$ and $\sigma_0 = 3^o$, $r_0 = \infty$ respectively. From this result the conclusion is drawn, that $\sigma_0 = 3^o$ to $6^o$ is a good first assumption for predicting the performance of downlink beamforming approaches involving nulling. However, further investigations are needed to evaluate the system impact of the deviation between the actual and predicted performance in particular situations.

## 8.2 Future Research Issues

The following issues need further study:

**RX to TX translation** The generalized-SICR beamformer requires the summed multipath covariance matrix for the desired and co-channel users as input, see Section 2.5 and Chapter 5. This matrix can be estimated from the uplink data at the uplink (RX) frequency. In order to do the translation to downlink (TX) frequency, one of the methods listed in Section 2.5 can be used. No analysis, known to the author, has been made to identify the performance of these different methods. This is an issue that needs investigation.

**Semi-experimental simulations** In Chapter 7 we found that the GAAO model with $r_0 = \infty$ and $\sigma_0 = 3^o$ to $6^o$ yields reasonable performance predictions (i.e., a Gaussian angular power distribution with a fixed standard deviation 3 to 6 degrees, independently of base-mobile distance). However, in particular cases, the actual performance is sometimes much worse or much better. The influence of these deviations has to be investigated. This could be done by "semi-experimental simulations". By this is meant that a mixture of measured and model generated data is used to simulate a cellular system consisting of several base stations.

**Reduced degrees of freedom** The SICR and generalized-SICR algorithm of Section 3.2.1 and Chapter 5, respectively, maximize their criterion function over all possible complex transmission vectors. By reducing the degrees of freedom in the weight vectors, it may be possible to reduce the computational complexity and improve the robustness against uplink noise and interference. The RX to TX translation problem mentioned above may also be simplified.

**Channel allocation and handover** The channel allocation algorithms in Chapter 3 assume that all channels are occupied and that any allocation is possible. In practice, an algorithm is required which successively allocates mobiles which enter and leave the system. A trade-off between the performance of the allocation and the number of re-allocations should be made for this algorithm. It is probably also necessary to put hard bounds on the cross-talk and angular separation of the users allocated to the same and neighboring channels. The blocking probability imposed by these hard bounds should also be analyzed.

**Propagation, measurements and performance** The spatial distribution of power received at the base should to be investigated further to enable more accurate modeling and a better understanding of systems. Performance assessments of downlink beam-steering, such as in Chapter 6 and 7, also need to be made for other environments and base locations.

# Bibliography


[AFWP86] F Adachi, M.T Feeney, A.G Williamson, and J.D Parsons. "Crosscorrelation between the envelopes of 900Mhz signals received at a mobile radio base station site". *IEE Proceedings, Pt. F*, 133(6), October 1986.

[Ake91] A Akeyama. "UHF Band Spatial Correlation Characteristics of Mobile Base Station Antennas". *Electronics and Communications in Japan, Part 1*, 74(7):107–113, 1991.

[AMVW91] S Anderson, M Millnert, M Viberg, and B Wahlberg. "An Adaptive Array for Mobile Communication Systems". *IEEE Transactions on Vehicular Technology*, 40:230–236, February 1991.

[Ber82] D.P Bertsekas. *Constraint Optimization and Lagrange Multiplier Methods*. Academic Press, 1982.

[BM86] Y Bresler and A Mocovski. "Exact Maximum Likelihood Parameter Estimation of Superimposed Exponential Signals in Noise". *IEEE Transactions on Acoustics, Speech, and Signal Processing*, 34:1081–1089, October 1986.

[BS92] P Balaban and J Salz. "Optimum Diversity Combining and Equalization in Digital Data Transmission with Applications to Cellular Mobile Radio Radio". *IEEE Transactions on Communications*, 40(5):865–907, May 1992.

[Cal96] M.H Callendar. "IMT-2000 (FPLMTS) Standardization". In *ACTS Mobile Communications Summit*, Grenada, Spain, November 1996. Annex pp. 8-12.

[CJL+94] C Carneheim, S.O Jonsson, M Ljungberg, M Madfors, and J Näslund. "FH-GSM Frequency Hopping GSM". In *Proceedings IEEE Vehicular Technology Conference*, pages 1155–1159, Stockholm, Sweden, June 1994.

[Cla68] R.H Clarke. "A Statistical Theory of Mobile Radio Reception". *The Bell System Technical Journal*, 47:957–1000, 1968.

[Cox75] D.C Cox. "Correlation Bandwidth and Delay Spread Multipath Propagation for 910MHz Urban Mobile Radio Channels". *IEEE Transactions on Communications*, COM-23:1271–1280, November 1975.

[CTK94] I Chiba, T Takahashi, and Y Karasava. "Transmitting null Beam Forming with Beam Space Adaptive Array Antennas". In *Proceedings IEEE Vehicular Technology Conference*, pages 1498–1502, 1994.

[Ebi91] Y Ebi. "A Study of Vertical Space Diversity for a Land Mobile Radio". *Electronics and Communications in Japan, Part 1*, 74(1):68–76, 1991.

[Egg95a] P.C.F Eggers. "Angular Dispersive Mobile Radio Environments Sensed by Highly Directive Base Station Antennas". In *IEEE International Symposium on Personal, Indoor and Mobile Radio Communications*, September 1995.

[Egg95b] P.C.F Eggers. "Quantitative Descriptions of Radio Environment Spreading Relevant to Adaptive Antenna Arrays". In *European Personal and Mobile Communications Conference*, pages 68–73, Bologna, Italy, November 1995.

[Egg96] P.C.F Eggers. "Angular - Temporal Domain Analogies of the Short-term Mobile Radio Propagation Channel at the Base Station". In *IEEE International Symposium on Personal, Indoor and Mobile Radio Communications*, pages 742–746, October 1996.

[Fai89] M Failli. *COST 207, Final report (14 March 1984 - 13 Sept. 1988).* Commission of the European Communities, Directorate-General Telecommunications, Information Industries and Innovation, L-2920 Luxembourg, 1989. pp. 135-147.

[FG97] G.J. Foschini and M.J. Gans. "Capacity When Using Diversity at Transmit and Receive Sites and the Rayleigh-Faded Matrix Channel is Unknown at the Transmitter". In *Sixth Winlab Workshop on Third Generation Wireless Information Networks*, pages 217–227, March 1997.

[FJK+94] U Forssén, B Johannisson, J Karlsson, F Kronestedt, F Lotse, and M Almgren. "Adaptive Antenna Arrays for TDMA Systems". Technical report, Ericsson Radio Systems AB, september 1994.

[FN95] C Farsakh and J.A Nossek. "Channel Allocation and Downlink Beamforming in an SDMA Mobile Radio System". In *IEEE International Symposium on Personal, Indoor and Mobile Radio Communications*, pages 687–691, September 1995.

[FN96] C Farsakh and J.A Nossek. "A Real Time Downlink Channel Allocation Scheme for an SDMA Mobile Radio System". In *IEEE International Symposium on Personal, Indoor and Mobile Radio Communications*, pages 1216–1220, October 1996.

[Ger95] D Gerlach. *Adaptive Transmitting Antenna Arrays at the Base Station in Mobile Radio Networks*. PhD thesis, Information Systems Laboratory, Stanford University, Stanford CA 94305 , USA, 1995.

[GF96] J Goldberg and J.R Fonollosa. "Downlink Beamforming for Spatially Distributed Sources in Cellular Mobile Communications". In *ACTS Mobile Communications Summit*, pages 510–516, November 1996.

[GL83] G.H Golub and C.F Van Loan. *Matrix Computations*. The Johns Hopkins University Press, Baltimore, 1983.

[GP94] D Gerlach and A Paulraj. "Adaptive Transmitting Antenna Arrays with Feedback". *IEEE Signal Processing Letters*, 1(10):150–152, October 1994.

[GP96] D Gerlach and A Paulraj. "Base Station Transmitting Antenna Arrays for Multipath Environments". *Signal Processing*, 54(1):59–73, 1996.

[GS92] G.R Grimmet and D.R Stirzaker. *Probability and Random Processes*. Clarendon Press, Oxford, 1992.

[GSM92] "GSM 05.05 Radio Transmission and Reception". Technical report, European Telecommunications Standards Institute, ETSI Secretariat: B.P.152. F-06561 Valbonne Cedex. France, TP. +33 92 94 42 00, TF + 33 93 65 47 16, April 1992.

[GSM94] "GSM 05.02 Multiplexing and Multiple Access on the Radio Path". Technical report, European Telecommunications Standards Institute, ETSI Secretariat: B.P.152. F-06561 Valbonne Cedex. France, TP. +33 92 94 42 00, TF + 33 93 65 47 16, September 1994.

[Hoy95] G Hoyt. "TDMA with a Direct Sequence Spread Spectrum (DS/SS) Overlay Provides a Cost Effective PCS Multiple Access System". In *IEEE Wireless Communications Systems Symposium*, pages 203–207, November 1995.

[JLXV95] S.S Jeng, H.P Lin, G Xu, and W.J Vogel. "Measurements of Spatial Signature of an Antenna Array". In *IEEE International Symposium on Personal, Indoor and Mobile Radio Communications*, pages 669–672, 1995.

[Joh95] B Johannison. "Planar Antenna Array for Adaptive Beamforming". In *Nordic Radio Symposium*, pages 177–180, Saltsjöbaden Sweden, April 1995.

[Kle75] K.L Kleinrock. *Queueing Systems*. John Wiley & Sons Inc., New York, 1975.

[KMT+96] A Klein, W Mohr, R Thomas, P Weber, and B Wirth. "Direction of Arrival of Partial Waves in Wideband Mobile Radio Channels for Intelligent Antenna Concepts". In *Proceedings IEEE Vehicular Technology Conference*, November 1996.

[Lee73] W.C.Y Lee. "Effects of Correlation Between Two Mobile Radio Base-Station Antennas". *IEEE Transactions on Communications*, 21(11):1214–1224, November 1973.

[Lee93] W.C.Y Lee. *Mobile Communications Design Fundamentals*. Wiley, New York, 1993.

[LP95] J Liang and A Paulraj. "On Optimizing Base Station Antenna Array Topology for Coverage Extension in Cellular Radio Networks". In *IEEE International Symposium on Personal, Indoor and Mobile Radio Communications*, pages 866–870, September 1995.

[LR96] J.C Liberti and T.S Rappaport. "A Geometrically Based Model for Line of Sight Multipath Radio Channels". In *Proceedings IEEE Vehicular Technology Conference*, May 1996.

[Mac79] V.H MacDonald. "The cellular concept". *Bell Syst. Tech. J.,vol 58*, 58:15–41, January 1979.

[Mar96] U Martin. "Statistical Mobile Radio Channel Simulator for Multiple Antenna Reception". In *International Symposium on Antennas and Propagation*, September 1996.

[Mat95] A Matthews. "Application of IS-136 to Personal Communication Services". In *IEEE Wireless Communications Systems Symposium*, pages 181–187, November 1995.

[Maw92] A Mawira. "Models for the Spatial Correlation Functions of the (Log)-Normal Component of the Variability of VHF-UHF Field Strength in Urban Environment". In *IEEE International Symposium on Personal, Indoor and Mobile Radio Communications*, pages 436–440, 1992.

[Mit95] J Mitola. "The Software Radio Architecture". *IEEE Communications Magazine*, 33(5):26–38, May 1995.

[MP92] M Mouly and M.B Pautet. *The GSM System for Mobile Communications*. Michel Mouly and Marie-Bernadette Pautet, 49 rue Louise Bruneau, F-91120 Palaiseau France, 1992. ISBN 2-9507190-0-7.

[MPLE+97] P.E Mogensen, K.I Pedersen, P Leth-Espensen, B Fleury, F Frederiksen, K Olesen, and S Leth-Espensen. "Preliminary Measurements Results from an Adaptive Antenna Array Testbed for GSM/UMTS". In *Proceedings IEEE Vehicular Technology Conference*, May 1997.

[MW96] P.E Mogensen and J Wigard. "On Antenna and Frequency Diversity in GSM Related Systems (GSM-900, DCS-1800,

PCS-1900)". In *IEEE International Symposium on Personal, Indoor and Mobile Radio Communications*, Taipei, Taiwan, October 1996.

[MZD+96] P.E Mogensen, P Zetterberg, H Dam, P Leth Espensen, S Leth Larsen, and K Olesen. "Algorithms and Antenna Array Recommendations (part 1)". Technical Report A020/AUC/A1.2/DR/P/005/a1, Tsunami(II), Contact pm@cpk.auc.dk or perz@s3.kth.se for a copy and information, September 1996.

[NEA95] O Norklit, P.C.F Eggers, and J.B Andersen. "Jitter Diversity in Multipath Environments". In *Proceedings IEEE Vehicular Technology Conference*, 1995.

[NM96] A.M Negrat and R.C.V Macario. "Cordless Telephones in Transition". In *Proceedings IEEE Vehicular Technology Conference*, pages 456–461, November 1996.

[NMT85] "Automatic Cellular Mobile Telephone System: Nordic NMT-900, System Description". Technical report, The Telecommunications Administrations of Denmark, Finland, Norway and Sweden, January 1985.

[Ohg94] T Ohgane. "Spectral Efficiency Evaluation of Adaptive Base Station for Land Mobile Cellular Systems". In *Proceedings IEEE Vehicular Technology Conference*, pages 1470–1474, 1994.

[Oja96] T Ojanpera. "Comparative Study of Hybrid Multiple Access Schemes for UMTS". In *ACTS Mobile Communications Summit*, pages 124–130, Grenada, Spain, November 1996.

[Orf90] S.J Orfanidis. *Optimum Signal Processing, an introduction*. McGraw-Hill, Singapore, 1990.

[ORK89] B Ottersten, R Roy, and T Kailath. "Signal Waveform Estimation in Sensor Array Processing". In *Asilomar Conference on Signals, Systems and Computers*, 1989.

[OVK92] B Ottersten, M Viberg, and T Kailath. "Analysis of Subspace Fitting and ML Techniques for Parameter Estimation from Sensor Array Data". *IEEE Transactions on Signal Processing*, 40(3):590–600, March 1992.

[Par80] B Parlett. *The Symmetric Eigenvalue Problem*. Prentice Hall, 1980.

[PB82] J.D Parsons and A.S Bajwa. "Wideband Characterization of Fading Mobile Radio Channels". *IEE Proceedings,Pt. F*, pages 95–101, 1982.

[PK91] R Prasad and A Kegel. "Improved Assessment of Interference Limits in Cellular Radio Performance". *IEEE Transactions on Vehicular Technology*, 40(2):412–419, May 1991.

[Pow78] M.J.D Powell. "Algorithms for Nonlinear Constraints that use Lagrangian Functions". *Mathematical Programming*, (14):224–248, 1978.

[Pro89] J.G Proakis. *Digital Communications*. McGrawHill Co., Singapore, 2nd edition, 1989.

[RDJP95] G Raleigh, S.N. Diggavi, V.K Jones, and A Paulraj. "A Blind Adaptive Transmit Antenna Algorithm for Wireless Communication". In *Proceedings IEEE International Conference on Communications*, 1995.

[RDNP94] G Raleigh, S.N. Diggavi, A Naguib, and A Paulraj. "Characterization of Fast Fading Vector Channels for Multi-Antenna Communication Systems,.". Technical report, Information Systems Laboratory, Stanford University, Stanford CA 94305 , USA, October 1994.

[RPK86] R Roy, A Paulraj, and T Kailath. "ESPRIT- A Subspace Rotation Approach to Estimation of Parameters of Cisoids in Noise". *IEEE Transactions on Acoustics, Speech, and Signal Processing*, (34):1340, 1986.

[RU91] K Raith and J Uddenfeldt. "Capacity of Digital Cellular TDMA Systems". *IEEE Transactions on Vehicular Technology*, 40:323–332, May 1991.

[Sas96] A Sasaki. "A Perspective of Third Generation Mobile Systems in Japan". In *ACTS Mobile Communications Summit*, Grenada, Spain, November 1996. Annex pp. 1-7.

[SBEM90] S.C Swales, M.A Beach, D.J Edwards, and J.P McGeehan. "The Performance Enhancement of Multibeam Adaptive Base-Station Antennas for Cellular Land Mobile Radio Systems". *IEEE Transactions on Vehicular Technology*, 39:56–67, February 1990.

[Sch79] R.O Schmidt. "Multiple Emitter Location and Signal Parameter Estimation". In *RADC Spectral Estimation Workshop, Griffiths AFB, NY*, pages 243–258, reprinted in IEEE Trans. Antennas Propagat., vol. AP–34, no. 3, pp. 281–290, Mar. 1986., 1979.

[Sch87] M Schwartz. *Telecommunication Networks Protocols, Modeling and Analysis*. Reading MA: Addison Wesley, 1987.

[SJD94] E.S Sousa, V.M Jovanović, and C Daigneault. "Delay Spread Measurements for the Digital Cellular Channel in Toronto". *IEEE Transactions on Vehicular Technology*, 43(4):837–847, November 1994.

[Spi90] M.R Spiegel. *Mathematical Handbook*. McGraw-Hill, Inc., 1990.

[SS90] P Stoica and K Sharman. "Maximum Likelihood Methods for Direction of Arrival Estimation". *IEEE Transactions on Acoustics, Speech, and Signal Processing*, ASSP-38:1132–1143, July 1990.

[Ste92] R Steele, editor. *Mobile Radio Communications*. Pentech Press, London, 1992.

[SW94] J Salz and J.H Winters. "Effect of Fading Correlation on Adaptive Arrays in Digital Mobile Radio". *IEEE Transactions on Vehicular Technology*, 43(4):1049–1057, November 1994.

[SY81] S.C Schwartz and Y.S Yech. "On the Distribution Function and Moments of Power Sums With Log -Normal Components". *The Bell System Technical Journal*, 61:1441–1462, September 1981.

[Tan94] M Tangemann. "Near-Far Effects in Adaptive SDMA Systems". In *IEEE International Symposium on Personal, Indoor and Mobile Radio Communications*, pages 745–749, 1994.

[Tan95] M Tangemann. "Near-Far Effects in Adaptive SDMA Systems". In *IEEE International Symposium on Personal, Indoor and Mobile Radio Communications*, pages 1293–1297, 1995.

[Tie95] E.G Tiedemann. "An Overview of the CDMA PCS System". In *IEEE Wireless Communications Systems Symposium*, pages 189–194, November 1995.

[TO96] T Trump and B Ottersten. "Maximum Likelihood Estimation of Nomina direction of Arrival and Angular Spread Using an Array of Sensors". *Signal Processing*, 50(1-2):57–69, April 1996.

[TVP94] S Talwar, M Viberg, and A Paulraj. "Blind Estimation of Multiple Co-Channel Digital Signals Using an Antenna Array". *IEEE Signal Processing Letters*, 1(2):29–31, February 1994.

[Vau87] R.G Vaughan. "Antenna Diversity in Mobile Communications". *IEEE Transactions on Vehicular Technology*, 36(4):149–172, November 1987.

[Wep95] J.A Wepman. "Analog-to-Digital Converters and Their Applications in Radio Receivers". *IEEE Communications Magazine*, 33(5):39–45, May 1995.

[Wig95] J. Wigard. "GSM Link Simulation on a Static Channel". *Unpublished Results*, 1995.

[Win84] J.H Winters. "Optimum Combining in Digital Mobile Radio with Cochannel Interference". *IEEE Transactions on Vehicular Technology*, 33(3):144–155, August 1984.

[Win94] J.H Winters. "The Diversity Gain of Transmit Diversity in Wireless Systems with Rayleigh Fading". In *Proceedings IEEE International Conference on Communications*, pages 1121–1125, 1994.

[WM96] J. Wigard and P Mogensen. "A Simple Mapping from C/I to FER and BER for a GSM type of air Interface". In *IEEE International Symposium on Personal, Indoor and Mobile Radio Communications*, pages 78–82, Taipei, Taiwan, October 1996.

[WMFN95] J Wigard, P Mogensen, F Frederiksen, and O Nørklit. "Evaluation of Optimum Diversity Combining in DECT". In *IEEE International Symposium on Personal, Indoor and Mobile Radio Communications*, pages 507–511, Toronto, Canada, September 1995.

[YKT91] Y Yamada, K Kagoshima, and K Tsunekawa. "Diversity Antennas for Base and Mobile Stations in Land Mobile Communications Systems". *IEICE Transactions*, E 74(10):3202–3209, October 1991.

[You79] W.R Young. "Advanced Mobile Phone Service: Introduction Background, and Objectives". *Bell Syst. Tech. J.,vol 58*, 58:1–14, January 1979.

[ZDF+96] P Zetterberg, H. Dam, F. Fredreksen, S. Leth Larsen, P. Leth Espensen, P. Mogensen, and K. Olesen. "Experimental Investigation of Capacity and Quality Enhancement of GSM using Adaptive Beamforming". In *Nordic Radio Symposium*, pages 535–539, Lund, Sweden, August 1996.

[ZE96] P Zetterberg and P Leth Espensen. "A Downlink Beam Steering Technique for GSM/DCS1800/PCS1900". In *IEEE International Symposium on Personal, Indoor and Mobile Radio Communications*, Taipei, Taiwan, October 1996.

[ZEM96] P Zetterberg, P Leth Espensen, and P. Mogensen. "Propagation Model, Direction of Arrival and Uplink Combining Algorithms for use in Mobile Communications". In *ACTS Mobile Communications Summit*, Grenada, Spain, November 1996.

[Zet95a] P Zetterberg. "A Comparison of two Systems for Down Link Communication with Antenna Arrays at the Base". Technical report, Signal Processing, Royal Institute of Technology, Sweden, Available by WWW, document URL:

http://www2.e.kth.se/s3/signal/INDEX.html or by anonymous ftp to: ftp.e.kth.se directory /pub/signal/reports., 1995. Submitted to IEEE Transactions on Vehicular Technology.

[Zet95b] P Zetterberg. "A Comparison of two Systems for Down Link Communication with Antenna Arrays at the Base". In *IEEE Wireless Communications Systems Symposium*, pages 15–20, November 1995.

[Zet95c] P Zetterberg. "Mobile Communication with Base Station Antenna Arrays: Propagation Modeling and System Capacity". Technical Report IR-S3-SB-9502, Available by WWW, document URL: http://www2.e.kth.se/s3/signal/INDEX.html or by anonymous ftp to: ftp.e.kth.se directory /pub/signal/reports., February 1995. Licentiate Thesis.

[Zet97] P Zetterberg. "An Advanced Base Station Antenna Array System For Future Mobile Radio". In *Proceedings IEEE Vehicular Technology Conference*, Phoenix, Arizona, USA, May 1997.

[ZO94] P Zetterberg and B Ottersten. "Experiments Using an Antenna Array in a Mobile Communications Environment". In *Proc. 7th SP Workshop on Statistical Signal & Array Processing*, June 1994. Also registred as technical report IR-S3-SB-9412.

[ZO95] P Zetterberg and B Ottersten. "The Spectrum Efficiency of a Basestation Antenna Array System for Spatially Selective Transmission". *IEEE Transactions on Vehicular Technology*, 44(3):651–660, August 1995.